2007-03-13

# Human Erythrocyte Glucose Transporter (GLUT1) Structure, Function, and Regulation: A Dissertation

David M. Blodgett
*University of Massachusetts Medical School*

# HUMAN ERYTHROCYTE GLUCOSE TRANSPORTER (GLUT1) STRUCTURE, FUNCTION, AND REGULATION

A Dissertation Presented

By

David M. Blodgett

Submitted to the Faculty of the University of Massachusetts

Graduate School of Biomedical Sciences, Worcester

in partial fulfillment of the requirements for the degree of

Doctor of Philosophy

13-March-2007

Department of Biochemistry & Molecular Pharmacology

HUMAN ERYTHROCYTE GLUCOSE TRANSPORTER (GLUT1)
STRUCTURE, FUNCTION, AND REGULATION

A Dissertation Presented

By

David M. Blodgett

Approved as to style and content by:

_____
Dr. William Kobertz, Chair of Committee

_____
James Evans, Member of Committee

_____
Dr. C. Robert Matthews, Member of Committee

_____
Dr. Ann Rittenhouse, Member of Committee

_____
Dr. Ian Simpson, Member of Committee

_____
Dr. Anthony Carruthers, Thesis Advisor

_____
Dr. Anthony Carruthers
Dean of the Graduate School of Biomedical Sciences

Department of Biochemistry & Molecular Pharmacology
13-March-2007

***ACKNOWLEDGEMENTS***

First, I would like to thank my mentor Dr. Anthony Carruthers for his unending support, encouragement, confidence, and patience. I am most appreciative that he gave me the freedom to pursue my research independently, but was always available to discuss ideas and answer the millions of questions I must have asked while working in his lab. I would also like to thank the members of the Carruthers laboratory and particularly single out Dr. Kara Levine and Dr. Julie DeZutter. Their enthusiasm and willingness to help guide me through every step of the graduate school process is much appreciated, as is their shared obsession with the Boston Red Sox. I would also like to acknowledge my effervescent bay mate Tabitha Kramarz for keeping it real. I would like to thank Dr. William Kobertz for his scientific advice as well has his general enthusiasm for life, specifically on ski trails and putting greens. I also must acknowledge Jim Evans and the Mass Spectrometry Facility and Staff, especially Karin Green and Barbara Evans. I would not have been able to do much of this work without their guidance and the mass spectrometry lessons and troubleshooting with which they provided me during my time in the lab.

I also am greatly appreciative of the love and support my family has given me while I have been in graduate school. I am indescribably indebted to my parents David and Joan for their continued encouragement and belief in their son. I also must acknowledge my sister Melissa and her prowess in and around the kitchen to keep me well fed. I will always be thankful that my family took the time to ask how school was going, when I

would be done, and what I was going to do next. They kept me on my toes and helped me to reach my goals.

Finally, I have to thank my friends for being a constant source of entertainment during the course of my graduate school career. Sharing the graduate school experience with my friends Joe and Dirk encouraged me to work hard and finish up school so I could keep up with them. Steve has been a great distraction from science as an outlet for discussing all things Boston sports and I cannot thank my friend Liz enough for putting up with and taking part in our shenanigans and for introducing us to the Pohly girls.

I owe a tremendous amount to everyone who has been a part of my life and made this whole experience both possible and worthwhile.

## *ABSTRACT*

The structure-function relationship explains how the human erythrocyte glucose transport protein (GLUT1) catalyzes sugar transport across the plasma membrane. This work investigates the glucose transport mechanism, the structural arrangement and dynamics of GLUT1 membrane-spanning α-helices, the molecular basis for glucose transport regulation by ATP, and how cysteine accessibility contributes to GLUT1 structure.

A rapid kinetics approach was applied to examine the conformational changes GLUT1 undergoes during the transport cycle. To transition from a global to molecular focus, a novel mass spectrometry technique was developed to resolve GLUT1 sequence that is associated either with membrane embedded GLUT1 subdomains or with water exposed domains. By studying accessibility changes of specific amino acids to covalent modification by a Sulfo-NHS-LC-Biotin probe, specific protein regions associated with glucose transport modulation by ATP were identified. Finally, mass spectrometry was applied to examine cysteine residue accessibility under native and reducing conditions.

This thesis presents data supporting the isolation of an intermediate, occluded GLUT1 conformational state that temporally bridges import and export configurations during glucose translocation. Our results confirm that amphipathic α-helices line the translocation pathway and promote interactions with the aqueous environment and substrate. In addition, we show that GLUT1 is conformationally dynamic, undergoes reorganization in the cytoplasmic region in response to ATP modulation, and that GLUT1 contains differentially exposed cysteine residues that affect its folding.

***TABLE OF CONTENTS***

## *LIST OF TABLES*

## *LIST OF FIGURES*

## *ABBREVIATIONS*

| | |
|---|---|
| 2DOG | 2-Deoxyglucose |
| 3MG | 3-*O*-methyl-D-glucose |
| 4HCCA | α-cyano-4- hydroxycinaminic acid |
| ABC | ATP-binding cassette Superfamily |
| ATP | adenosine 5′-triphosphate |
| BR | bacteriorhodopsin |
| C-Ab | rabbit polyclonal antiserum raised against a synthetic peptide comprised of GLUT1 residues 480-492 |
| CCB | cytochalasin B |
| CCD | cytochalasin D |
| CD | Circular Dichroism |
| CHO | Chinese hamster ovary |
| δ-Ab | rabbit polyclonal antiserum raised against non-denatured, non-reduced GLUT1 proteoliposomes |
| DTT | dithiothreitol |
| EDTA | ethylenediaminetetraacetic acid |
| EGTA | ethylene glycol bis (P-aminoethyl ether)-N, N-tetraacetic acid |
| ELISA | enzyme-linked immunosorbent assay |
| FITC | fluorescein isothiocyanate |
| GLUT1 | human erythrocyte glucose transport protein |
| HEPES | (N–[2–Hydroxyethyl]piperazine–N'–[2–ethanesulfonic acid]) |

| | |
|---|---|
| HPLC-ESI-MS | high performance liquid chromatography electrospray ionization mass spectrometry |
| HRP | horseradish peroxidase |
| iTRAQ | isobaric tags for relative and absolute quantitation |
| L6-7-Ab | rabbit polyclonal antiserum raised against a synthetic peptide comprised of GLUT1 residues 217-231 |
| L7-8-Ab | rabbit polyclonal antiserum raised against a synthetic peptide comprised of GLUT1 residues 299-311 |
| MALDI-TOF | Matrix-Assisted, Laser Desorption/Ionization Time-Of-Flight |
| MFS | Major Facilitator Superfamily |
| MS | mass spectrometry |
| N-Ab | rabbit polyclonal antiserum raised against a synthetic peptide comprised of GLUT1 residues 1-13 |
| OG | n-octyl-β-glucoside |
| PBS-T | phosphate-buffered saline containing Tween |
| pCMBS | p-chloromercuribenzene sulfonate |
| PNGaseF | N-Glycosidase F |
| RBC | red blood cell |
| SDS-PAGE | sodium dodecyl sulfate-polyacrylamide gel electrophoresis |
| Tris–HCl | tris(hydroxymethyl)aminomethane hydrochloride |

# CHAPTER I

## INTRODUCTION:

## CARRIER-MEDIATED TRANSPORT AND GLUT1 LITERATURE REVIEW

### *WHY STUDYING CARRIER-MEDIATED TRANSPORT IS IMPORTANT*

The human body maintains its internal environment at a steady state in which flux and demand are balanced, a process known as homeostasis. Cells utilize integral membrane proteins to monitor and regulate interactions with the surrounding environment to maintain homeostasis. Virtually every cell system requires integral membrane proteins to catalyze necessary biological processes such as metabolism, cell signal recognition, and ion transport to maintain optimum conditions for cell survival [1]. Examining the fundamental properties and functions of this important protein class and the structure-function relationships that govern and regulate their activity, therefore, is vital to understanding the mechanism of numerous biological processes. This thesis will focus primarily on the type I facilitative glucose transporter (GLUT1), a member of the Major Facilitator Superfamily (MFS), one of the largest groups of integral membrane transport proteins. By studying and examining how integral membrane proteins operate at the molecular level, we can appreciate the biological process from the standpoint of cells and organisms.

### *THE PLASMA MEMBRANE*

All prokaryotic and eukaryotic cells are surrounded by a plasma membrane composed of amphipathic phospholipids and cholesterol. Phospholipid molecules combine a hydrophilic head group, which interacts with the external interstitial fluid or internal cytoplasm, with a hydrophobic tail of uncharged, nonpolar long chain fatty acids that associate with one another to form a tightly packed phospholipid bilayer [2]. The plasma

membrane, therefore, effectively seals the cell from its external environment and, owing to its intrinsically impermeant nature, controls and maintains intracellular volume and cellular composition.

In addition to lipids, various classes of proteins are associated with the plasma membrane. Peripheral membrane proteins are noncovalently attached to the bilayer surface (predominantly cytoplasmic surface). Integral membrane proteins penetrate the bilayer and are permanently associated with the plasma membrane. Monotopic integral membrane proteins reside within the bilayer, bitopic proteins cross the membrane once and have one extracellular and one intracellular terminal end. Finally, transmembrane proteins, such as GLUT1, span the bilayer multiple times. The fluid mosaic model describes the plasma membrane as a discontinuous lipoprotein bilayer in which integral membrane proteins are partitioned at the surface and buried within the hydrophobic core due to the amphipathic nature of the protein regions [2,3]. The plasma membrane and its associated proteins control the passage of molecules into and out of the cell.

### *TYPES OF DIFFUSION*

Small, uncharged, hydrophobic molecules such as gases (e.g. carbon dioxide and oxygen), unionized drugs (e.g. anesthetics), and endogenous compounds (e.g. steroids, ethanol, urea) are lipid soluble and pass through the membrane by simple diffusion. The rate of entry into or exit from the cell is modulated by hydrophobicity, molecular permeability, membrane thickness, and the concentration gradient. Smaller, more hydrophobic molecules display the most rapid rates of penetration and diffusion across

the bilayer [2]. In contrast to these small, nonpolar molecules, large, charged, and polar molecules such as nutrients, amino acids, and ions cannot pass through the membrane via simple diffusion. These molecules cross the membrane by facilitated diffusion, a process that requires integral membrane proteins to mediate passage into the cell (Figure 1.1).

### *INTEGRAL MEMBRANE PROTEINS*

Integral membrane proteins such as pores, channels, and carriers all mediate facilitated diffusion, however, they differ in permeation pathway, transport mechanism, and solute movement. Pore proteins form cross membrane pathways that are always open and present simultaneous access to both sides of the plasma membrane. Aquaporin (AQP1), a tetrameric pore protein that spans the lipid bilayer, facilitates the simple diffusion of water across the membrane in single file motion [4]. Channels are more closely regulated, and structured in such a way that a terminal end acts as the gate that controls whether the channel is closed or open. A selectivity filter controls what class (positive or negative) and type of ions can pass through the open-channel pore [2]. Sodium, potassium, calcium, and chloride are the most common charged ions that enter and exit the cell. Channel transport rates are governed by open probability, the number of channels expressed at the cell surface, single channel conductance capability, and are saturable [2]. Sensors on the channel respond to changes in membrane potential, second messengers, and ligands to govern this described opening and closing process.

Unlike pores and channels, carriers never present simultaneous access to both the intra- and extracellular environments. Instead, carrier-proteins must undergo a dynamic cycle of

**Figure 1.1 Diffusion across the plasma membrane.** A lipid bilayer is shown providing a barrier between the extracellular environment (above) and intracellular space (below). The substrate, represented by the yellow circles, has a higher extracellular concentration, which creates a concentration gradient. Passive diffusion processes (simple or facilitated diffusion by pores, channels, and carriers) mediates substrate transport down its concentration gradient while active transport carriers use energy to transport substrate against its concentration gradient. The substrate represents a molecule that must cross the plasma membrane, and is not universally transported by all mechanisms. Small, uncharged, hydrophobic molecules can pass through the plasma membrane by simple diffusion. Larger, charged, and polar molecules require proteins to mediate passage into the cell. Protein channels and carriers are generally specific to one type of class of molecules.

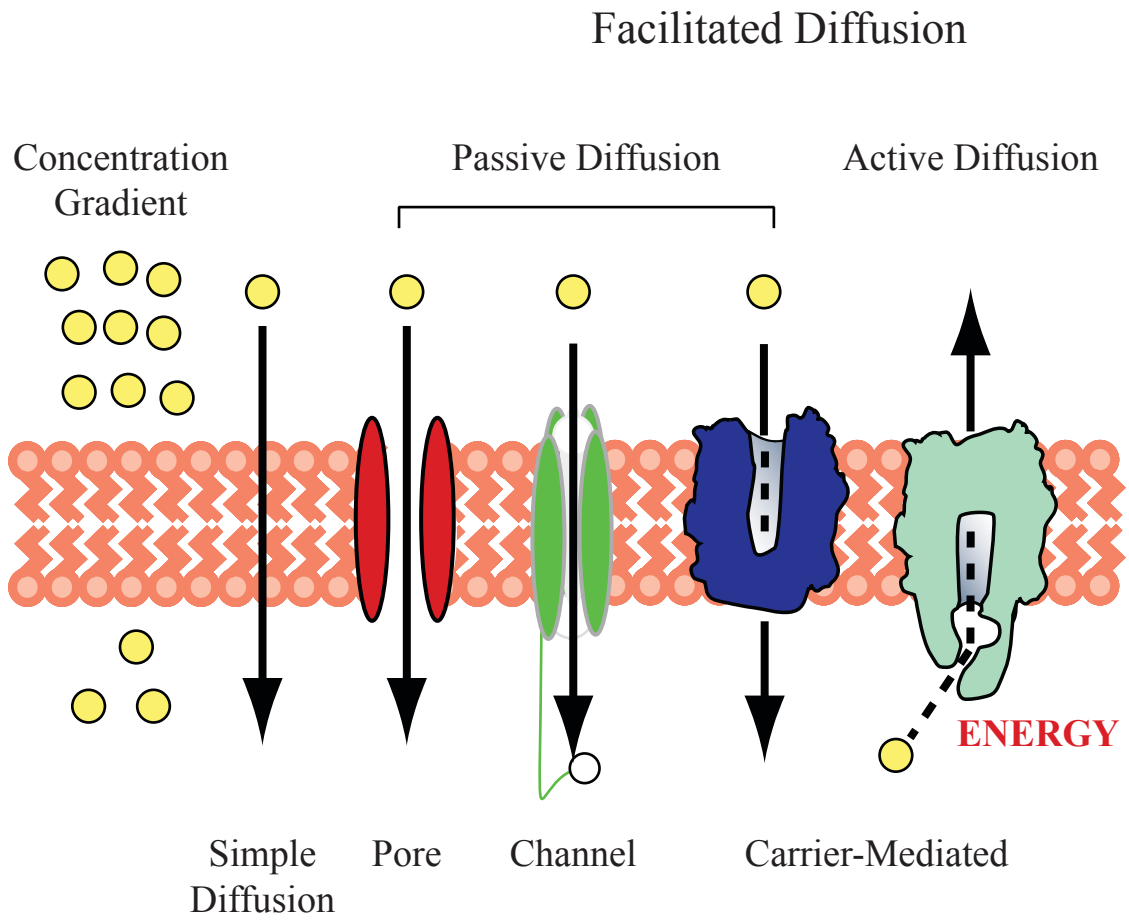
Facilitated Diffusion
Concentration Gradient
Passive Diffusion
Active Diffusion
ENERGY
Simple Diffusion
Pore
Channel
Carrier-Mediated

Figure 1.1

conformational changes to facilitate translocation [2]. Carrier-mediated transport, therefore, is a saturable process, which limits the respective rate and quantity of molecules transported per event. Substrate binding within the transmembrane domain initiates cycling between binding site exposure to the inside or outside of the cell, thus marking the inception of the transport process. Cytoplasmic transporter domains, however, often control and regulate this process based upon interactions with intracellular factors, such as nucleotides.

A second difference between pores and channels versus carriers is the driving force for solute movement. Pores and channels exclusively facilitate the passage of molecules down an electrochemical gradient without an additional energy source. Two factors contribute to regulating this passive transport process. First, the chemical potential difference is based upon the solute concentration gradient inside versus outside of the cell. Second, the electrical potential difference across the plasma membrane becomes a factor if the solute is charged. Together, the electrochemical potential difference determines net flux of a single solute into or out of a cell. Passive transporters generally catalyze uniport, a transport process that facilitates the uncoupled passage of a single substrate across the membrane.

Carrier-proteins, such as GLUT1, mediate passive transport, but transporters are also capable of catalyzing active transport. In primary active transport, a solute is moved against its electrochemical gradient by utilizing the energy released by a coupled favorable process, such as ATP hydrolysis. In secondary active transport, energy

generated from the favorable movement of one solute down its electrochemical gradient is coupled to movement of another solute against its electrochemical gradient. Secondary active transporters generate the energy needed to mediate transport via antiport, where two substrates are transported in opposite directions, one into and one out of the cell, or via symport, where the coupled transport of two substrates proceeds in the same direction [5]. Active transport, regardless of the mechanism used to produce it, requires energy input to overcome the electrochemical gradient, thus providing the driving force for carrier-mediated net-solute flux.

### *CARRIER-MEDIATED TRANSPORT PHYSIOLOGY*

The recent sequencing of the human genome indicates that at least 20% of identified proteins are polytopic integral membrane proteins and 3% are transport proteins [6-9]. The importance of carrier-mediated transport systems to cells and organisms is most evident when considering the pathophysiology of improperly functioning systems.

Mutations within the type I facilitative glucose transport protein (GLUT1) impair glucose passage into the brain, a condition known as GLUT1-deficiency syndrome. These heterozygous mutations reduce glucose transport across the blood brain barrier by up to 50%, which deprives neuronal cells of their primary energy source, causing seizures, developmental delay, and ataxia within affected patients [10]. The only known treatment for this disease is a high fat, low carbohydrate ketogenic diet. The Monocarboxylate Transporter (MCT1) is responsible for ketone delivery to the brain, thereby providing an alternative fuel source to glucose [11].

Similarly, in cystic fibrosis, a much more common and fatal hereditary disease, specific point mutations within the cystic fibrosis transmembrane conductance regulator protein (CFTR) cause improper folding of its transmembrane and cytosolic domains resulting in protein degradation [12]. In the absence of CFTR, negatively charged chloride ions can no longer cross the plasma membrane. Chloride accumulation outside of epithelial cells disrupts the intracellular electrochemical gradient resulting in the formation of thick, dehydrated mucus that blocks narrow passages within the lungs, pancreas, and intestines causing infection and organ damage.

GLUT4 is the insulin-sensitive glucose transporter found within intracellular pools of heart, skeletal muscle, and adipose tissue. Upon insulin binding to its receptor, a complex signaling cascade results in GLUT4-vesicle translocation to the cell surface. This insulin-sensitive response promotes a 10-20-fold increase above basal glucose transport levels, thereby controlling the postprandial rise in blood glucose concentration [13,14]. In patients suffering from Type II diabetes, insulin resistance causes higher than normal blood glucose levels. Unlike in type I diabetes, the Islets of Langerhans found in the pancreas still produce and release the insulin hormone, however, patients demonstrate resistance to insulin action, and the GLUT4-vesicle translocation response is stunted. Currently, GLUT4 and the insulin-signaling pathway are under extensive study to determine how insulin resistance develops, why it is linked with obesity, and how to overcome it.

Furthermore, integral membrane proteins such as drug receptors and transport proteins are increasingly being studied as targets for therapeutic agents. Chemotherapy agents are designed to diffuse or be transported across the plasma membrane of target cells, killing them and stopping further growth. Tumor cells that express the multidrug resistance transport proteins (MDR1, for example) are able to export these compounds from the cell rendering them ineffective as treatments. Mammalian MDR proteins are primary active transporters belonging to the ATP-binding cassette (ABC) Superfamily [15]. As the name implies, MDR proteins can transport multiple cytotoxic compounds with very little structural or charge similarity. Understanding the transport process from substrate recognition to conformational changes that mediate passage is crucial to improving drug treatment methods.

Addictive drugs such as cocaine and heroin affect the ability to regulate neurotransmitter release or recycling by transport proteins. Cocaine specifically blocks and inhibits dopamine transporters, resulting in dopamine accumulation at the synapse, which stimulates pleasure [16,17]. Heroin, or its morphine metabolite, prevents the release of pain signals, subsequently enhancing the feeling of pleasure [18].

It is abundantly clear that transport proteins play a crucial role in ensuring cellular survival. Current studies focus upon the fundamental basis of how the structure-function relationship governs the role carrier-transport processes play in maintaining properly functioning biological processes. The findings of these works will lead to new and improved therapeutic strategies for the successful treatment of human disease.

### *GLUCOSE METABOLISM*

Glucose is the primary metabolite utilized by living cells to produce energy. In fact, the brain requires continuous GLUT1-mediated sugar transport across the blood brain barrier (BBB). Neurons rely almost exclusively on glucose as the requisite energy source for maintaining communication and connection with the rest of the body [19]. Following digestion of dietary polysaccharides or hepatic metabolic processes, the circulatory system absorbs the produced glucose and delivers it to target cells. Various environmental factors, such as energy demand and oxygen availability determine how glucose is broken down. Glucose can be metabolized in rapid or efficient manners to produce ATP by anaerobic or aerobic glycolysis, respectively. Anaerobic metabolism produces the maximum amount of ATP in the shortest amount of time, providing the cell with sufficient energy for muscle contractions. This process is 100x faster than the slower, but more efficient aerobic glycolysis pathway that subjects pyruvate from the initial glycolysis reaction to the citric acid cycle and oxidative phosphorylation [20]. Aerobic glycolysis produces significant quantities of ATP per molecule of glucose by increasing the thermodynamic efficiency of the process at the expense of time. These two processes may be coupled in different cell types in the brain. According to the Astrocyte Neuron Lactate Shuttle (ANLS) hypothesis [21], astrocytes import glucose and process the glucose through lactate. The lactate is subsequently exported via the MCT transporter family into the interstitium, from which it is imported by neurons and processed aerobically.

### *GLUCOSE TRANSPORTERS*

Hexose metabolism is the primary source by which mammalian cells generate energy, but hydrophilic sugar molecules do not readily diffuse into the cell in a physiologically efficient manner. Glucose, therefore, must be transported across the cell membrane by carrier-proteins. Two different families of glucose transport proteins mediate sugar transport into the cell. Sodium/glucose cotransport proteins (SGLT) are expressed in the luminal membrane of absorptive tissue epithelial cells lining the small intestine and kidneys. These transporters use the electrochemical sodium gradient generated by the sodium-potassium ATPase pump to couple favorable sodium ion import with glucose uptake against its concentration gradient [22]. In contrast, the GLUT family of passive sugar transporters is distributed throughout all cell types in a tissue specific manner [22,23]. The facilitative glucose transporter family contains thirteen individual protein species named GLUT1-12 and HMIT (proton-coupled myo-inositol transporter). These proteins are subdivided into three classes based upon multiple sequence alignments. Within the entire family, the proteins display sequence identity ranging from 28 to 65% and share specific sugar transporter signature motifs [22,23].

Class I isoforms of the facilitative glucose transporters, comprised of GLUT1 through GLUT4, have been studied most extensively in terms of their structure, function, substrate specificity, and tissue distribution. GLUT1 is the most ubiquitous of all glucose transporters, expressed in almost all cell types [24]. GLUT2 is found in the liver, kidney, intestine, and pancreatic islets and has a low affinity, but high capacity for dietary sugars

such as glucose, fructose and galactose [25]. In addition to being responsible for glucose transport from absorptive tissues into the bloodstream, GLUT2 also serves as a glucose sensing protein. Within the various tissue systems, it releases signals that regulate intestinal absorption, control insulin release, and trigger the transcription of glucose sensitive genes. GLUT3 primarily resides within sperm, platelets, the placenta, and the brain, specifically on the surface of neuronal cells, and has a characteristically high glucose affinity and high catalytic activity [19]. Finally, GLUT4 is the insulin sensitive glucose transporter found in heart, skeletal muscle, and adipose tissue.

Classes II and III of the facilitative glucose transporters are less well understood than class I, and some of the members have only recently been identified by homology searches. Class II contains GLUT5, GLUT7, and GLUT11, which transport fructose as the primary substrate and GLUT9, a glucose transporter. Finally class III contains the remaining GLUT6, GLUT8, GLUT10, GLUT12, and HMIT, for which substrate specificity, trafficking, and potential role in diabetes have yet to be completely elucidated [22,23].

This thesis specifically examines how the structural design of GLUT1 contributes to its physiological function. Furthermore, the similarities observed among polytopic integral membrane protein carriers will allow us to use GLUT1 as a model for studying other transport proteins. In this capacity, we address questions regarding the membrane transport process, structural organization of transport proteins within the plasma membrane, and provide new methods for the study of integral membrane proteins.

### *A MODEL TRANSPORT SYSTEM: THE HUMAN ERYTHROCYTE AND GLUT1*

The human erythrocyte serves as an ideal model system for studying transport. The red blood cell maintains homeostasis by using carrier-mediated transport to regulate proper pH, maintain a stable volume, and ensure proper gas-transport. Integral membrane proteins that complete these and other processes found within the red cell membrane include a $Na^{+}$-$K^{+}$ pump, a $Ca^{2+}$-pump, an anion exchange protein, and the glucose transport protein GLUT1 [2,26].

The mature, hemoglobin-containing erythrocyte is responsible for oxygen transport throughout the body [27]. During erythropoiesis, reticulocytes extrude all internal organelles, including the nucleus and DNA, such that only integral membrane proteins within the plasma membrane, the hemoglobin protein, and glycolytic enzymes remain in mature red blood cells. As a result, human red cells have a 120-day lifespan during which their biconcave shape and flexible nature, attributed to the cytoskeletal composition, allows them to circulate to all tissue systems within the body releasing hemoglobin bound oxygen to keep cells alive. In addition, since erythrocytes comprise 50% of the bloodstream, they effectively double the sugar carrying capacity of the blood using GLUT1-mediated transport of glucose to fill free space within the red cell. In this way, the red blood cells maximize the efficiency of the human circulatory system rapidly delivering and maintaining high levels of oxygen and sugar where they are needed most.

In particular, the facilitative glucose transport protein GLUT1 expressed at the red blood cell surface provides an excellent cellular and protein model system for studying the

carrier-mediated transport process and mechanism. First, an established purification protocol has been developed that produces an ample amount of greater than 90% pure functional GLUT1 reconstituted in native erythrocyte lipids; 10 milligrams of GLUT1 is routinely purified from one unit of human blood [28]. Second, GLUT1 is membrane resident within the red blood cell plasma membrane. Unlike GLUT4, which must be trafficked to the plasma membrane by the insulin-signaling pathway, GLUT1 expressed in red blood cells serves as the paradigm example of carrier-mediated transport. Third, a large body of research exists describing GLUT1 substrate specificity, kinetics of transport, and tissue distribution, making it one of the most characterized eukaryotic transport proteins [14].

### *GLUT1 Physiology*

GLUT1, the most ubiquitous of all glucose transporters, is primarily expressed in red blood cells and the endothelial cells of the blood brain barrier (BBB) [24]. In addition, GLUT1 has been shown to be responsible for basal glucose transport in almost all other cell types including cardiomyocyte, muscle, and adipose tissue. Since glucose transport across the plasma membrane is the rate-limiting step of glycolysis and metabolism, GLUT1-mediated transport is vital to initiating energy production within these cells [29]. GLUT1 plays a fundamental role in delivering glucose to the brain to keep the central nervous system (CNS) functioning at maximum capacity. The BBB is made up of endothelial cells connected by tight junctions that effectively isolate the CNS from the rest of the extracellular environment found in the human body. In order to enter the CNS,

nutrients such as amino acids and glucose or drugs must pass through the transport systems expressed on both the luminal (blood-side) and abluminal (brain-side) membranes of the blood brain barrier [30]. In this way, the BBB and associated carrier-proteins, such as GLUT1, serve to maintain homeostasis by regulating the import of required molecules and the export of unwanted drugs or secondary metabolites [19,30]. Within the endothelial cells of the BBB, GLUT1 is expressed at high levels. In this way, it catalyzes the rapid transport of glucose from the bloodstream, across the plasma membrane of the endothelial cells, and through the BBB into the interstitial fluid of the CNS [19,31]. Once in the CNS, glucose can be transported into neurons by the high-affinity GLUT3 isoform, which is expressed at the neuronal plasma membrane. Since the brain cannot store glucose, the transfer across the BBB into the CNS must be rapid and efficient to keep the brain running at an optimized level.

By governing GLUT1 expression levels at the plasma membrane, cells regulate glucose uptake rates to directly control metabolism. GLUT1 overexpression has been detected in many cancers including hepatic, pancreatic, breast, renal, brain, ovarian, lung, and cervical carcinomas [32]. The upregulation of high affinity GLUT1 results in increased glucose transport and energy generation from increased glycolytic flux. This increased energy generation enhances the biosynthesis of nucleotides, phospholipids, and other components necessary for new cell development [32]. GLUT1-mediated transport, therefore, supports angiogenesis and rapid cell division resulting in the propagation of cancer cells.

### *IMPORTANCE OF THE CARRIER-PROTEIN STRUCTURE-FUNCTION RELATIONSHIP*

Understanding the relationship by which the structure of a particular protein enables its subsequent function has long dominated the transporter research field. The most vexing question: how does the structure of membrane spanning amphipathic proteins catalyze substrate specific translocation across the plasma membrane? For GLUT1, early clues were provided by glucose transport kinetic studies performed by Widdas, Jung, and colleagues that established the carrier-mediated transport hypothesis [5,33-39]. Over the next thirty years, researchers intensively studied transport structure-function relationships using traditional techniques such as ligand binding and kinetic transport studies, computer simulations, peptide mapping, glycosylation and cysteine scanning mutagenesis, and hydropathy analysis [24,40-51]. These methods encompassed the fields of biochemistry, molecular biology, and bioinformatics and provided the raw data to develop, revise, refute, and explain the transport process.

Following the crystallization of the KcsA potassium channel in 1998 [52], researchers succeeded in crystallizing the first transport protein when *Toyoshima et al.* published the structure of the P-type ATPase Superfamily calcium pump two years later [52,53]. Generally speaking, MFS transporters have proven refractory to crystallization because they are conformationally dynamic, exist in multiple states, are highly hydrophobic, and are difficult to overexpress in cellular systems [7]. In the last four years, however, the three-dimensional crystal structures for four MFS transport proteins have been obtained: oxalate transporter (OxlT; formate for oxalate; antiport; [5,34]), lactose permease (LacY;

galactoside/proton: symport; [33]), the glycerol-3-phosphate/phosphate antiporter (GlpT; phosphate for glycerol-3-phosphate: antiport; [35]), and an E. coli multidrug transporter (EmrD; proton for drugs that uncouple oxidative phosphorylation: antiport; [39]). The crystal structures reflect LacY and GlpT in an inward facing conformation (e1) and OxlT and EmrD in an intermediate or closed state (possibly the e2/e1 intermediate configuration). Although the sequence identity amongst these transporters is less than 20%, they share a similar folding pattern and arrangement of transmembrane domains.

Given that transporters are remarkably dynamic and undergo extensive conformational changes to catalyze substrate translocation, visualizing the static structure alone is not sufficient for answering all biological questions concerning the transport process. Crystal structures, however, do provide important information regarding the number of transmembrane helices, the helix packing motif, helical tilts, substrate binding sites, the flexibility or rigidity of peri- and cytoplasmic loops, and, in some instances, the breadth of different transporter conformations that exist in the presence or absence of substrates, inhibitors, or modulators. Additionally, crystal structures and subsequent homology modeling provide opportunity for the development of specific hypotheses that can be subject to experimental testing. Combining traditional biochemical techniques with three-dimensional crystallography will produce the largest data set for analysis in terms of understanding the structure-function relationship that governs membrane transport proteins.

### *MAJOR FACILITATOR SUPERFAMILY*

Members of the Major Facilitator Superfamily (MFS) of transport proteins are ubiquitously expressed across all three domains of living organisms: Archaea, Bacteria, and Eukaryota. These proteins are responsible for the passive or secondary active transport of simple sugars, complex oligosaccharides, drugs, amino acids, ions, neurotransmitters, nucleosides, and other molecules catalyzing substrate translocation via uniport, antiport, or symport [54]. As an integral membrane protein responsible for facilitating sugar flux across cell membranes via uniport, GLUT1 belongs to the Major Facilitator Superfamily (MFS) of transport proteins [55]. Bioinformatics tools, such as sequence alignments and hydropathy plots, indicate that MFS proteins likely share very similar secondary structure properties, the majority of which contain 12 membrane spanning $\alpha$-helices with the amino and carboxy termini exposed to the cytoplasm. MFS transport proteins average 400 to 600 amino acids in length and have two six-helix halves connected by a large intracellular loop (see the putative GLUT1 topography in Figure 1.2) [6,33,35,56]. Although the two bundles display apparent structural symmetry, the sequence identity is quite low.

The crystal structures reveal that these four distinct MFS transport proteins share several structural features. The N- and C-terminal halves display a striking pseudo two-fold symmetry in helical arrangement, tilt, and organization within the lipid membrane, consistent with the gene duplication hypothesis [57]. Within the plasma membrane, each adjacent helix is inserted into the membrane in the opposite direction of its partner. For

**Figure 1.2 GLUT1 primary amino acid sequence and putative membrane topology from GlpT homology based structure** [64]. Several key properties should be noted. Group 1 TMs are highlighted in pink. Group 2 and Group 3 TMs are highlighted in blue and green respectively. Some helices that span the bilayer extend beyond the boundaries of the bilayer (shown by horizontal lines). The bilayer-embedded region of each membrane spanning helix (TMs 1 through 12) comprise amino acids 17 - 39, 64 - 86, 93 - 112, 120 - 141, 157 - 178, 187 - 207, 267 - 291, 305 - 325, 335 - 356, 362 - 385, 401 - 421 and 431 - 452 respectively. GLUT1 is heterogeneously glycosylated at Asn45. TMs 6 and 7 are linked by a large cytoplasmic loop (L6-7). The N- and C-termini are exposed to cytoplasm. Several conserved residues and signature sequences found among GLUT proteins are also noted. Conserved glycine, tryptophan, and tyrosine residues are boxed. Numerous symmetrical sequence motifs are shown using colored filled circles RXGRR (red), $EX_6R$ (olive), and PESPR/PETKGR (sky blue). Signature motifs found in most GLUT proteins that surprisingly do not confer substrate specificity include the QLS and STSIF sequences (orange) as well as a conserved proline-rich region thought to impart conformational flexibility on the molecule (yellow).

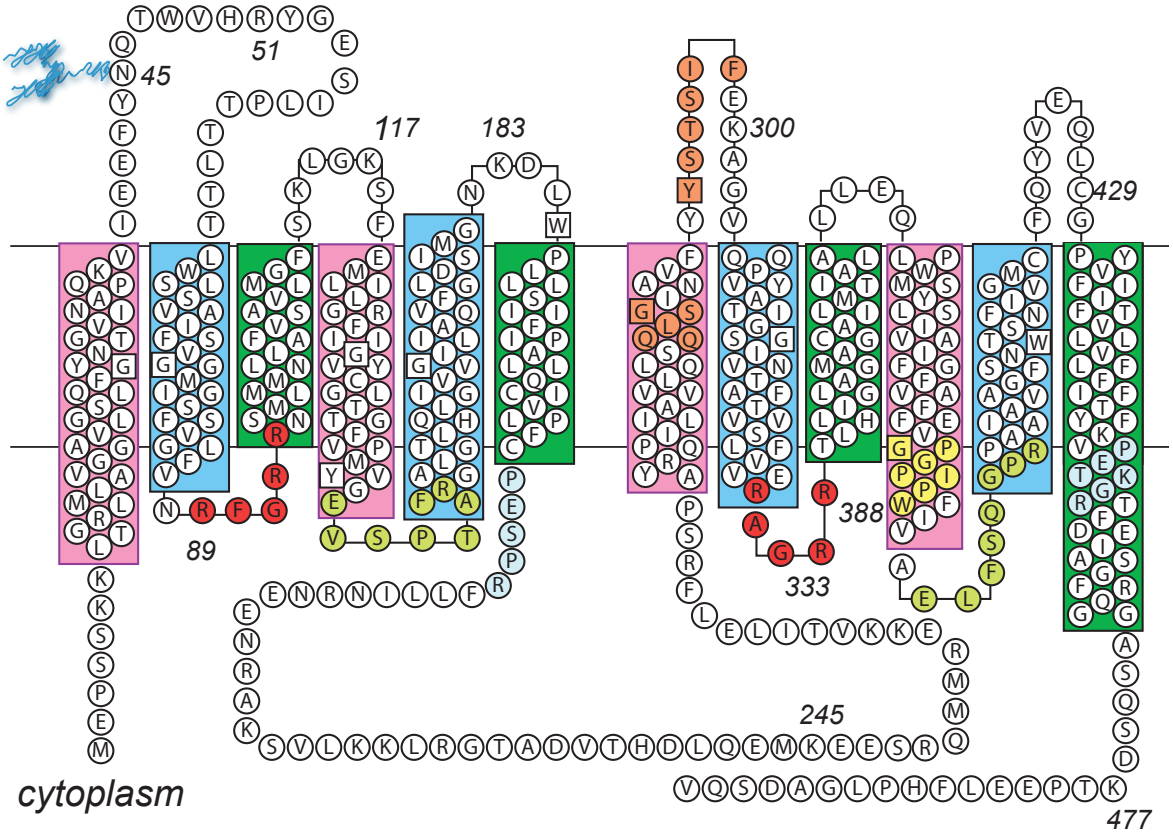


Figure 1.2

example, the N-terminal regions of helices 1 and 7 are oriented toward the cytoplasm while the C-terminal region faces the periplasm. Conversely, the N-terminal halves of helices 2 and 8 are oriented toward the periplasmic face whereas the C-terminal halves interface with the cytoplasm. The crystallized MFS structures suggest that the TM helices can be separated into three groups based upon their helix packing arrangements and associations with the lipid bilayer. Group 1, comprised of α-helices 1, 4, 7, and 10 and Group 2, composed of α-helices 2, 5, 8, and 11 appear to contribute to the aqueous pore. Group 3 transmembrane domains, including α-helices 3, 6, 9, and 12 serve as the scaffolding helices, which provide support for the eight substrate translocation cavity helices. Figure 1.3 shows the crystallized GlpT structure and illustrates the emergent MFS transport protein helix-packing model.

Helical orientation can be described by studying the arrangement of each helix within the LacY and GlpT crystal structures that represent the endofacial e1 conformation. The group 1 TM domains form the most interior region of the aqueous translocation pathway [35]. TM1 and TM7 are inserted into the membrane from the cytoplasm and approach as they tilt toward each other until they come within close contact in the middle of the bundle formed by exofacial hemi-leaflet domains of TM2-TM5-TM-8-TM11. Helices 4 and 10 are on opposite sides of the narrow cavity and do not come close to contacting one another. Group 2 TM domains form the outer portion of the cavity [35]. The N- and C-terminal pairs are tilted at a 20° angle from the membrane normal, but in opposite directions, thus displaying a square peak-like orientation within the membrane, and presenting an opening within the cytoplasm. The placement and orientation of

**Figure 1.3 MFS crystal structure and helix packing model. (A)** The three-dimensional model of GLUT1 α-helix arrangement within the membrane as presented by *Salas-Burgos et al* [64]. The GLUT1 primary sequence was homology modeled using the GlpT crystal structure template. **(B)** The putative MFS helix packing arrangement viewed from the cytoplasmic surface. TMs are colored and numbered as in Figure 1.2. The internal symmetry between N- and C-terminal halves of GLUT1 is evident from the helical tilts and may have resulted from a gene-duplication event. Adapted from [33,35].

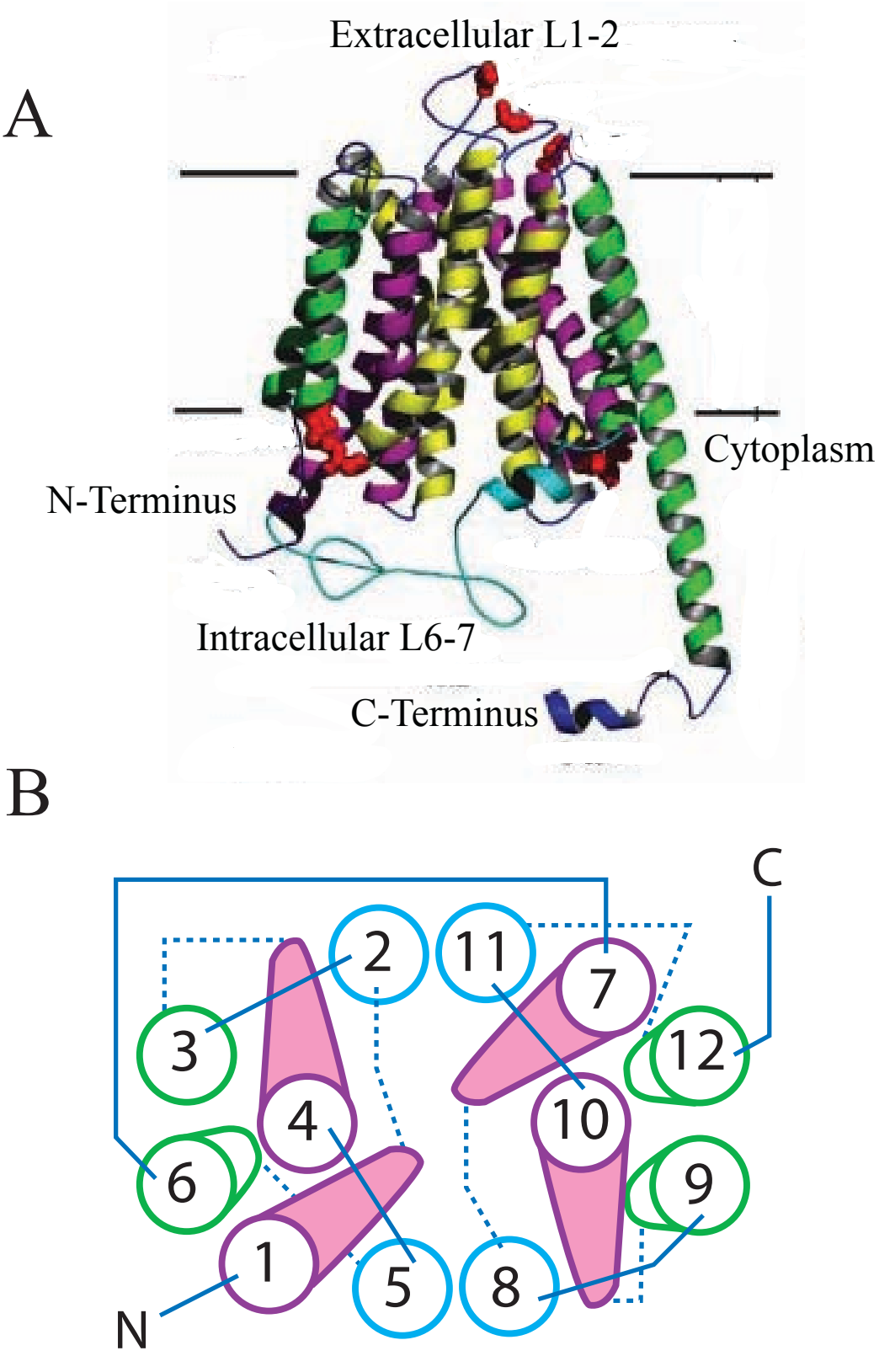
A
Extracellular L1-2
Cytoplasm
N-Terminus
Intracellular L6-7
C-Terminus
B
C
2
11
7
3
12
4
10
6
9
1
5
8
N

Figure 1.3

transmembrane group 3 helices with respect to the transport pore represent a striking synonymous characteristic amongst the four crystallized transporters [5,33-35,39]. Each of these helices faces away from the internal pore structure, is completely embedded within the lipid bilayer, and presents absolutely no side chain accessibility to solvent. These qualities explain why group 3 helices serve as such an effective support system for the eight cavity-forming helices.

The shortest three helices, TM3, TM6, and TM9, define the boundaries of the membrane bilayer, indicating which protein domains are embedded within the plasma membrane [35]. As a result, in the e1 conformation, the majority of the periplasmic loops do not protrude very far from the membrane surface. In contrast, however, many of the α-helices and the large intracellular loops and C-terminus protrude into the cytoplasm, away from the plasma membrane. Loop 6-7, which connects the amino and carboxy-terminal halves of the protein, appears to be a long, flexible structure with minimal helical secondary structure [35].

### *THE GLUT1 STRUCTURE-FUNCTION RELATIONSHIP*

Researchers have employed a vast range of biochemical and biophysical techniques to understand the molecular basis of GLUT1 function. Over 50 years ago, several researchers studying the absorption of glucose in the intestine, its entry into erythrocytes, and its transfer from mother to fetus using sheep placenta found that glucose accumulation data could not be modeled by simple diffusion kinetics [58,59]. Widdas observed, rather, that sugar transport displayed saturation kinetics, i.e. a finite number of

carriers present themselves for sugar transport, and that this process could be modeled by the Michaelis-Menten equation routinely used to characterize enzyme activity [38]. Widdas further determined that the carrier was glucose specific, was presented at the cell surface, and likely exhibited a wide range of tissue distributions.

The fluid-mosaic model was developed twenty years later and it described the plasma membrane as a discontinuous lipid bilayer with transmembrane spanning proteins embedded within it. Jung and colleagues provided strong evidence that membrane bound erythrocyte proteins catalyzed glucose transport into red blood cells. Jung showed that lysed and resealed erythrocyte ghosts, lacking internal cellular components, retained the glucose transport properties of red blood cells [37]. Additionally, transport capability was not observed when erythrocyte lipids alone were reconstituted into resealed bilayers [36]. Taking the observations of Widdas, Jung, and Singer together, researchers hypothesized that glucose transport in these systems was a saturable passive transport process mediated by substrate specific integral membrane proteins [14].

Mueckler and colleagues first cloned GLUT1 from HepG2 cells in 1985, over thirty years after Widdas initially hypothesized that a glucose carrier protein existed [24]. The primary sequence contains 492 amino acid residues with a calculated molecular weight of 54,117 Daltons. GLUT1 contains a single, heterologous, N-linked glycosylation site (NQT) at asparagine 45, which causes the protein to resolve as a broad, diffuse band when visualized by gel electrophoresis. The amino acid sequence indicates that over 60% of the residues are hydrophobic in nature. Fourier transform infrared spectroscopy studies

of proteolyzed, membrane-retained GLUT1 indicate a predominance of α-helices in the transmembrane region [60]. Circular dichroism and polarized Fourier transform studies confirmed this result and showed that the transmembrane α-helices are generally organized in an orientation perpendicular to the lipid bilayer [61,62].

Hydropathy plot predictions, N-linked glycosylation mutagenesis, and homology modeling simulations indicate that GLUT1 is comprised of 12 α-helical transmembrane spanning domains embedded within the lipid bilayer (Figure 1.2) [24,45,63,64]. Consistent with the organization for MFS transport proteins, proteolysis and antibody binding studies have revealed that the N and C-termini are cytoplasmic. A large intracellular loop between transmembrane domains 6 and 7 links the seemingly symmetric N- and C-terminal halves of the protein, an arrangement thought to have resulted from a gene duplication of the 6 transmembrane domain precursor [57]. The external loop connecting TMs 1 and 2, containing the N-linked glycosylation site, the large intracellular loop, and the C-terminal are the largest, most flexible non-membrane embedded protein segments. Additionally, covalent labeling with membrane-impermeant probes has shown that lysine 300 between TMs 7 and 8 and cysteine 429 between TMs 11 and 12 are exposed to the interstitium adding further evidence for the proposed topographical arrangement of this membrane spanning transport protein [61,65,66].

Currently, a high-resolution three-dimensional GLUT1 crystal structure does not exist. *Salas-Burgos et al.* and *Holyoake et al.* have recently modeled the GLUT1 helix packing arrangement using the alignment from fellow MFS transport protein GlpT [63,64]. This

helix-packing model is consistent with hydrogen-deuterium exchange studies showing that approximately 80% of GLUT1 amide protons freely exchange with a deuterated aqueous environment, indicating that a majority of the protein is exposed to solvent [67].

Mueckler and colleagues have studied virtually all of the GLUT1 TM helices to further understand the three-dimensional structure and helix packing arrangement of GLUT1. This method systematically scans through each proposed TM and adds back single cysteine mutations to a cysteine-less construct expressed in a *Xenopus laevis* oocyte expression system. The mutant protein is then assayed for p-chloromercuribenzene sulfonate (pCMBS) sensitivity by monitoring glucose transport rates compared to the cysteine-less mutant. Since pCMBS is a membrane impermeant cysteine reactive probe, it is proposed that transport inhibition in the presence of pCMBS is due to the exposure of the mutated residue to the aqueous environment, and by extension, said residue is predicted to line the permeation pathway. TM domains 1, 2, 5, 7, 8, 10, 11, and 12 have been found to contain residues that are pCMBS sensitive [48,68-74], while mutations within TMs 3 and 4 seemingly do not affect transport rates in the presence of pCMBS [49,50]. TMs 6 and 9 have yet to be studied via this technique. The observations are consistent with the proposed MFS helix-packing model, with the exception of TMs 4 (pCMBS-insensitive) and 12 (pCMBS-sensitive).

Bioinformatics analyses and sequence alignments of all facilitative glucose transport family members have revealed multiple signature sequences and invariable residues highly conserved among each GLUT family member (Figure 1.2) [23,61]. Although

many of these residues and signature sequences are required for transporter function, their respective contribution to substrate specificity is ambiguous at best. First, GLUT1 contains two conserved tyrosine and tryptophan residues that fall within helix pairs 4 and 7 and 6 and 11 respectively. Of these four conserved residues, W412 has proven to be functionally important for transport activity and ligand binding. Second, seven conserved glycine residues can be found within the membrane embedded region and are proposed to maintain the structural flexibility of these respective transmembrane α-helices [23]. The location of the conserved glycine residues is particularly interesting because they illustrate the trend of symmetrically conserved areas of the primary structure. Six of these residues are found in TM helices 1, 2, and 4, which correspond to TMs 7, 8, and 10 according to the gene duplication hypothesis [56].

Third, two even more striking displays of symmetry in the primary structure can be found in transporter signature motifs located at the cytoplasm-lipid bilayer interface at corresponding locations on the N- and C-terminal halves of the protein. Both the RXGRR and $EX_6R$ motifs are highly charged and are found in the intracellular loops connecting TMs 2-3 and 8-9 and TMs 4-5 and 10-11, respectively. Mutational analysis has shown the RXGRR motif to play a pivotal role in anchoring and properly orienting the protein within the lipid bilayer [75]. Additionally, the presence of numerous conserved charged residues at the meeting point between the lipid bilayer and intra- or extracellular space may also play a role in substrate induced conformational changes [75]. Finally, the most N-terminal residues of L6-7 and the cytoplasm exposed C-terminus contain GLUT family conserved PESPR and PETKGR motifs, respectively.

A characteristic sequence motif found within TM10, which includes W388, is both proline and glycine rich (GPGPIPW). Mutational studies indicate that although the individual residues do not appear to be crucial in maintaining transport activity, the side chains likely confer conformational flexibility to the transporter, facilitating the isomerization between the e2 (exofacial) and e1 (endofacial) orientations [76]. The QLS (QQLSG) and STSIF (YSTSIF) motifs found in TM7 and L7-8, respectively were initially characterized as glucose specificity sequences. [23,61,76-78]. When GLUT family members in addition to GLUT1-4 were found, however, this idea became less likely. The HMIT protein, which does not transport glucose, possesses the conserved QLS motif. Furthermore GLUT8 displays glucose specificity, however, it lacks the STSIF motif. It therefore appears that these conserved and symmetric residues play key roles in maintaining transport ability, transmembrane integrity, and in facilitating the required conformational changes, but do not confer substrate specificity [23].

In the absence of a GLUT1 crystal structure, affinity-labeling and mutagenesis experiments have provided significant information regarding how GLUT1 structure relates to its function. These experiments used two well know endofacial transport inhibitors, cytochalasin B (CCB) and forskolin, to identify cytoplasmic regions of the protein critical for both substrate and inhibitor binding. CCB and forskolin are both inhibitors of glucose binding and transport, with CCB serving as a competitive inhibitor that binds at the glucose-binding site [61]. Regions of the protein affinity labeled by these two molecules correspond to the cytoplasmic loop that links TMs 10 and 11 as well as the endofacial halves of these two transmembrane domains. Within TM10, W388 has been

directly identified in forming one of the bonds with the forskolin molecule. When both W388 (of TM10) and W412 (of TM11) are mutated, the CCB binding and glucose transport capability are absolutely abolished [79]. The sequence alignments, identification of signature motifs, affinity-labeling observations, and mutagenesis studies have clearly implicated that the cytoplasmic portions of TMs 10 and 11 including the linker region are highly dynamic. Given how important these regions are in mediating CCB and forskolin binding, this region clearly plays a vital role in establishing a cytoplasmic glucose-binding pocket.

The final structural characteristic that contributes to GLUT1 function is its oligomeric state. Like other MFS transporters, GLUT1 is active as a functional monomer. Kinetic observations measured in erythrocytes, however, are inconsistent with a physiologically relevant monomeric carrier. Rather, these studies suggest that GLUT1 is a complex oligomer, either a dimer or a tetramer in the plasma membrane. *Carruthers et al.* have measured the hydrodynamic radii of GLUT1 molecules in proteoliposomes and examined freeze-fractured electron microscope images to conclude that the functional transporter exists as a homotetramer [80]. Exposure to a reducing environment, however, supports the dimeric form. The tetramer is assembled as a dimer of dimers. Each monomeric subunit can transport glucose independently, but this arrangement pairs the two subunits in an obligate, anti-parallel fashion, such that as one subunit isomerizes from the e2 conformation to the e1, its partner isomerizes in the opposite direction, regardless as to whether substrate has bound to both subunits [81]. This arrangement supports the simultaneous presentation of import and export sites within the complete oligomer.

### *KINETICS-DERIVED GLUT1 TRANSPORT MODEL*

Since we currently lack a GLUT1 crystal structure, the majority of transport models describing GLUT1 behavior have been developed using kinetic measurements. Widdas and Naftalin used these data to develop the two most predominant models that explain carrier-mediated transport: the alternating conformer model and the fixed-site carrier model.

Widdas initially proposed the mobile carrier hypothesis where a glucose specific molecule bound glucose on one side of the membrane, moved across the lipid bilayer, and subsequently deposited the translocated glucose molecule on the other side of the membrane [38]. Although this model would prove incorrect, the glucose transport protein does not physically shuttle from one side of the membrane to the other, it spawned the alternating conformer model, see Figure 1.4. Here, the single GLUT1 transport subunits alternately present sugar import (e1) and export sites (e2). Glucose binding to the e1 site catalyzes a conformational change that results in its translocation across the plasma membrane. Multiple rounds of transport proceed by reconversion of the e1 conformation to the e2 arrangement either by simple isomerization or substrate binding and translocation. At any one time, however, the GLUT1 monomer presents only one site, either e1 or e2 [14].

Conversely, the fixed-site carrier model predicts that ligands bind the e2 and e1 sites simultaneously, see Figure 1.5 [14,82]. Here, the transporter exists as an oligomer within the membrane where one subunit presents an import site and the other an export site.

**Figure 1.4 The simple carrier model. (A)** King-Altman diagram showing the GLUT1 carrier in either the e1 (inward facing) or e2 (outward facing) state. The carrier can either bind to extracellular sugar (e2.S2) or intracellular sugar (e1.S1). As described, the simple carrier model indicates that the transporter can only be bound to one molecule at a time. $k_0$, $k_{-0}$, $k_1$, $k_{-1}$, $b_{-1}$, and $b_{-2}$ are the first-order rate constants describing the rates of conformational changes or sugar dissociation. $b_1$ and $b_2$ are second order rate constants describing the rate of carrier interaction with S1 and S2, respectively [43]. **(B)** Graphical representation of the sugar transport process through a single GLUT1 subunit. Glucose binds to the e2 orientation, the transporter-sugar complex converts to the e1 conformation as the sugar is translocated across the cell membrane, the sugar is released into the cell, and finally the carrier relaxes or is converted back to the e2 conformation for another round of transport.

A

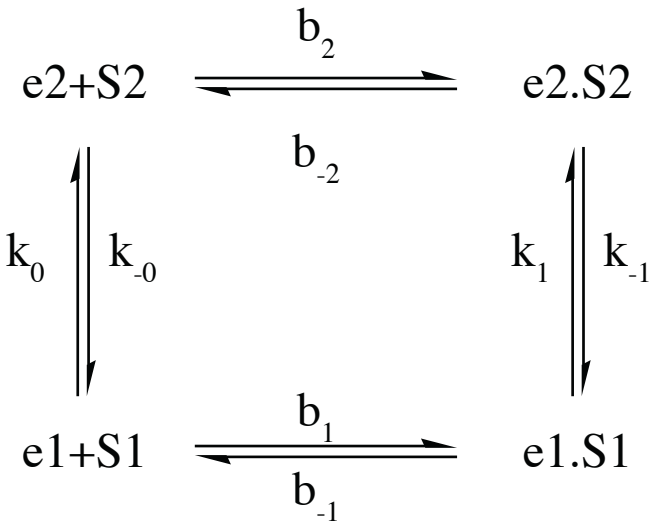
e2+S2
e2.S2
e1+S1
e1.S1
b2
b-2
k0
k-0
k1
k-1
b1
b-1

B

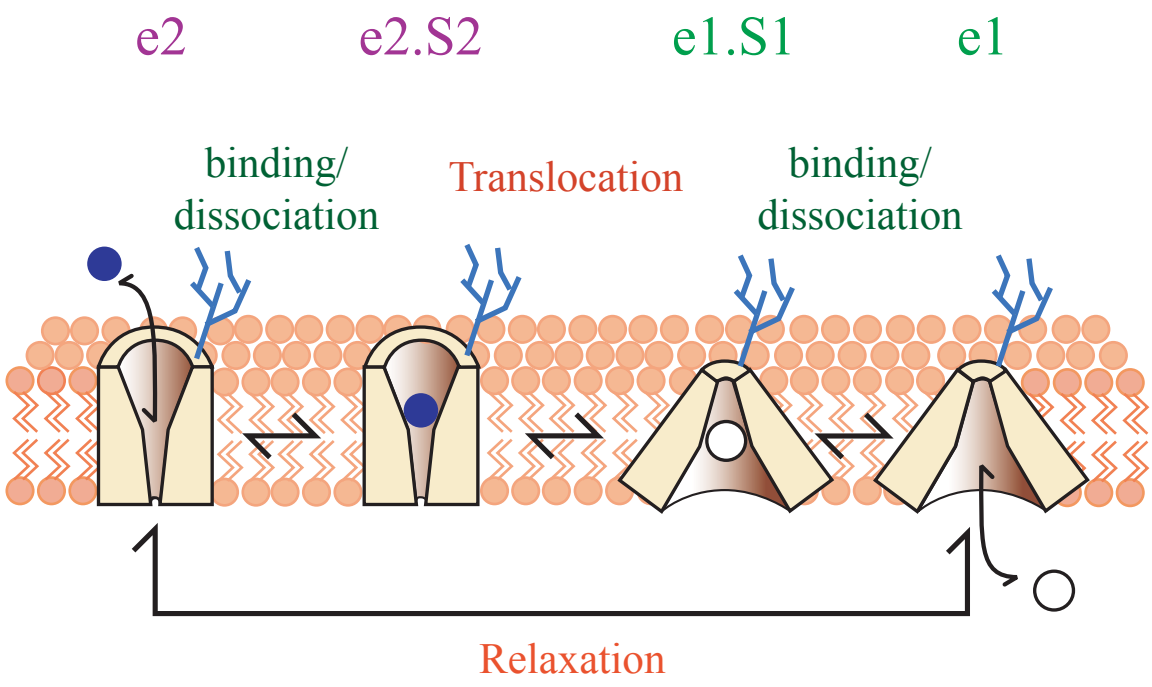
e2
e2.S2
e1.S1
e1
binding/
dissociation
Translocation
binding/
dissociation
Relaxation

Figure 1.4

**Figure 1.5 The fixed-site carrier model. (A)** King-Altman diagram shows the carrier simultaneously presenting the e2 and e1 sugar binding sites. The carrier can be complexed with extracellular sugar (e.S2), intracellular sugar (e.S1), or both sugars (S2.e.S1). $\alpha$ represents the cooperativity constant for when the carrier is occupied at both binding sites. K1 and K2 are the dissociation constants between the sugar and the carrier [43]. **(B)** Graphical representation of the sugar transport process showing the movement of each subunit within a GLUT1 tetramer. The steps of this process (sugar binding, translocation, and release) are the same as described for the simple-carrier hypothesis. When one subunit undergoes a conformational change (e2→e1) its partner undergoes the reverse conformational change. In this way, the tetramer serves as a dimer of dimers paired in an obligate antiparallel arrangement that works in concert to catalyze glucose transport [86].

A

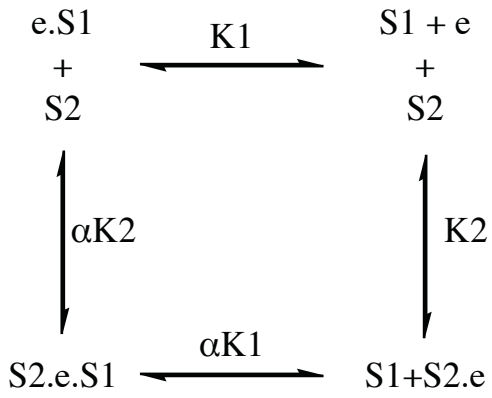
e.S1
+
S2
K1
S1 + e
+
S2
αK2
K2
αK1
S2.e.S1
S1+S2.e

B

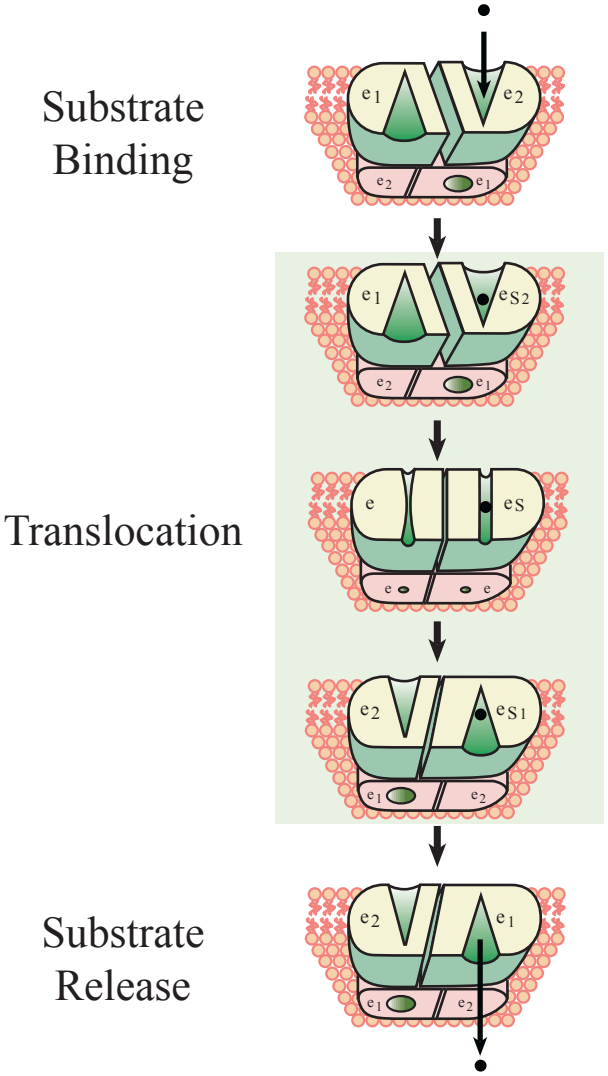
Substrate
Binding
Translocation
Substrate
Release

Figure 1.5

*Carruthers et al.* observed that the rate of CCB binding to the endofacial e2 binding site was affected by the presence of exofacial e1-site-reactive sugars [83]. This observation is consistent with a hypothesis that predicts the simultaneous presentation of import and export sites and it resulted in a revised transport model. When sugar binds to an e2 site, it undergoes a conformational change resulting in sugar transport to the cytoplasm. At the same time, the other subunit, either with or without substrate bound, converts from the e1 to e2 orientation. In this way, the two subunits present an obligate antiparallel arrangement, and account for the simultaneous presentation of the e2 and e1 sites across a dimeric subunit [81].

The recent MFS transporters crystal structures are strongly supportive of the biochemical evidence suggesting that the transport process is catalyzed by an individual transporter protein subunit [33,35]. Many transporters are believed to function as complex oligomers, however, and communication between the subunits confounds our understanding of the true transport mechanism. In fact, kinetic studies measuring glucose transport in red cells suggest that GLUT1 displays a higher order tetrameric structure within the cell membrane. Glucose transport regulation by intracellular nucleotides is dependent upon GLUT1 oligomeric state and it appears as if intramolecular disulfide bonds are responsible for this tertiary structure [28,81,84-86].

Respecting the complexity of GLUT1 oligomeric structure, the examination of glucose translocation through a single, independent subunit is most useful in our efforts to illustrate how each domain and the total protein mediate transport. The simple carrier

hypothesis, therefore, appears to adequately describe individual subunit conformational changes. Specifically, a substrate recognizes and binds to a carrier protein oriented outside of the cell (e2→eS2). This binding results in a conformational change where the substrate becomes completely occluded within the transport protein in the form e(S) [5,87]. Another conformational change results in the exposure and release of the substrate into the cytoplasm of the cell (eS1→e1). The external facing conformation is then regenerated for another round of transport via the following mechanism: (e1→e( )→e2).

### *How MFS Structure-Function Relationships Compare to other Transporters*

In addition to MFS transporters, members from five additional families and superfamilies have recently been crystallized: 1.) P-type ATPase ($H^+$-ATPase and $Ca^{2+}$-ATPase) [53,88-90]; 2.) ATP Binding Cassette (ABC) Transporter (BtuCD and Sav1866) [91-95]; 3.) Monovalent Cation/Proton Antiporter (CPA) ($Na^+/H^+$ Antiporter) [96]; 4.) Resistance-Nodulation-Cell Division (RND) (AcrB) [97-99]; 5.) Mitochondrial Carrier (MCF) (ADP/ATP Carrier) [100].

This literature review provides a structural basis for carrier-mediated transport mechanisms employed by transmembrane proteins. Thus far, we have focused predominantly on the structure-function relationship governing GLUT1 and fellow MFS transporters. It is interesting to note that many other transporters utilize the cytoplasmic domains to coordinate the conformational changes facilitating substrate translocation. Furthermore, ATP hydrolysis by the cytoplasmic domains of carriers is frequently exploited to power the transport machinery. In this regard, the transmembrane regions

appear to merely provide the transport pathway, but the regulatory factors are intracellular and not embedded in the plasma membrane. Carrier helix packing models, numbers of helices, helical tilts and interactions, propensity for and dependence upon homo- and hetero-oligomerization in structural and or functional mechanisms differ to varying degrees for passive, primary, or secondary active transporters [81]. Even though each transporter shares a common goal - the transport of substrate across the plasma membrane - the mechanisms employed to accomplish this objective differ greatly. We will review each mechanism, therefore, by focusing on how these processes compare and contrast to the MFS carrier-mediated transport phenomenon.

### *P-TYPE ATPASE AND ABC SUPERFAMILIES*

Proteins belonging to the P-type ATPase and ABC superfamilies are integral membrane proteins in which a large portion of the primary structure resides in the cytoplasm. The majority of MFS transporter structure is typically embedded within the membrane bilayer. P-type ATPase proteins are primary active cation transporters, which create an electrochemical gradient inside the cell that helps to maintain intracellular pH and membrane potential by providing energy for nutrient uptake and ion exchange by secondary active transporters. ATP Binding Cassette (ABC) Transporters catalyze the unidirectional transport of substrates (such as drugs, vitamins, and waste products) across the membrane bilayer [93]. Recent crystallizations of the $Ca^{2+}$-ATPase [53,88-90], the Sav1866 homodimer (each subunit contains a transmembrane and nucleotide binding domain (TMD; NBD) [91]), and the BtuCD heterotetramer (comprised of TMD and NBD

homodimers) [92,94,95]have provided a better understanding of how the membrane-bound and cytoplasmic domains interact to catalyze transport.

$Ca^{2+}$-ATPase transporters have four major domains: an actuator (A; L2-3), nucleotide binding (N), and phosphorylation (P; L4-5) domains found in the cytoplasm and a transmembrane domain (M) containing ten α-helices embedded in the lipid bilayer. The two calcium ion-binding sites are formed by transmembrane helices M4, M5, M6, and M8 [88]. This packing model does not appear to display the structural symmetry observed for MFS carriers. ATP binding causes the N- and P-domains to approach and thereby produces profound conformational changes within cytoplasmic domains resulting in a more tightly packed overall structure. Consequently, the A-domain tilts causing the M-domain, to respond by occluding calcium ions within the transmembrane region.

ABC transporters are comprised of two domains: the membrane embedded transmembrane domain (TMD) and the cytoplasmic nucleotide binding domain (NBD). The transmembrane domain subunits (TMD) reside within the lipid bilayer, contain 6-10 α-helices each, form a water-filled cavity, link to the NBD at the lipid-cytoplasm interface, and create the ligand binding site [93]. The recent Sav1866 structure even indicates that the TMD regions from each subunit physically intertwine. TM1-2 of one subunit and TM3-6 of the corresponding subunit form the two sides of the open conformation [91]. The dimeric nucleotide binding domain (NBD) is highly conserved. While the coupling of ATP hydrolysis to transport is similar across the superfamily, TMD regions vary in sequence composition, likely contributing to a wide-range of

substrate specificity [93]. Although substrate binding initiates the transport cycle, ATP hydrolysis, catalyzed by isomerization between the open and closed conformations of each NBD, provides the requisite free energy for TMD conformational changes and subsequent substrate translocation.

The transport cycle of each transporter superfamily follows a modified Albers-Post derived e2→e1 series of conformational changes resembling those utilized by MFS transporters. The requirement for nucleotide binding, autophosphorylation, and subsequent dephosphorylation (P-type ATPase) or nucleotide binding and ATP hydrolysis (ABC transporters) to catalyze cycling between the e2 and e1 conformations differs from the passive or secondary active MFS transporters. With the primary active carriers, ATP binding, rather than substrate interaction appears to choreograph TM helical movements that result in substrate translocation. This role explains the importance of the large cytoplasmic domains of primary active carriers, which distinguishes them from MFS transporters, which typically only have a relatively small cytoplasmic loop connecting TMs 6 and 7. P-type ATPase transporters transport cations both into and out from the cell, and in fact, cation binding is required for cycling between the e2 and e1 conformations [88,89,101]. MFS and P-type ATPase transporters share this substrate-induced reconversion cycling mechanism. This is not found in ABC transporters, which display only a unidirectional substrate transport pathway. Here, reconversion from trans to cis conformations following substrate release is dependent upon ATP hydrolysis, not substrate binding [93].

### *MONOVALENT CATION/PROTON ANTIPORTERS*

Monovalent Cation/Proton Antiporters (CPA) regulate, cation/proton concentrations, cell volume. The recently crystallized sodium proton antiporter NhaA of *Escherichia coli* appears to function as an intracellular pH sensor [96]. NhaA exists as a homodimer within the lipid bilayer, however, like many MFS transporters, the monomer serves as the functional unit. Like MFS transport proteins, NhaA contains twelve membrane embedded helices with the N- and C-termini oriented towards the cytoplasm. The organization and packing of these TM helices, however, are very different from those of MFS transporters and the secondary structures of TMs IV and XI are quite unique.

The TM region is organized into two tightly packed domains; domain A contains two oppositely oriented but structurally similar helix bundles and domain B contains 1 linear bundle. Helices IV and XI, which are oppositely oriented within the membrane, are especially noteworthy as they comprise a short helix, an unstructured chain, and another short helix; the helices are denoted as c or p, based upon proximity to the cytoplasm or periplasm, respectively. Two groups of TM helices, one containing TMIVc and the other TMXIp, form two distinct pockets facing the cytoplasm and interstitium, respectively. The extended chains of TM domains IV and XI block the link between the two pores.

This organization of helices and evidence for two incomplete pores, (envisioned as e1 and e2 oriented binding sites) plays a significant role in the functional mechanism employed by NhaA. $Na^+/H^+$ exchange is predicted to occur via an alternating access mechanism. Based upon the crystal structure, the authors suggest that a pH regulated

movement of the unstructured chains of TM domains IV and XI controls the accessibility of the binding pore to the intra- or extracellular environment [96]. Unlike the MFS transporters, the functional mechanism for NhaA only requires small conformational changes within a limited portion of the TM region, especially helices IV and XI. This functional mechanism may explain why NhaA [102] has a turnover number approximately 50-100 fold higher than LacY [103], the ADP/ATP antiporter [104], or GlpT [105].

### *MITOCHONDRIAL CARRIER PROTEINS*

A family of mitochondrial carrier proteins (MCF) transports nucleotides, phosphates, and other metabolites across the mitochondrial membrane. One such member of the MCF is the ADP/ATP antiporter, which imports spent ADP into the mitochondrial matrix and exports resynthesized ATP to the cytoplasm. The carrier has only six transmembrane α-helical domains, organized as three dual-helix repeats. All of the helices are tilted, with the odd helices demonstrating a kink to the arrangement caused by an internal proline residue [100]. Within the crystal structure, the helices form a cavity accessible to the interstitium. The helices are connected to one another by short internal α-helical stretches and external loops. The cavity within the transmembrane region is quite hydrophilic in nature. The design, degree of secondary structure, and helical arrangement of the transport pore are quite different than those observed in MFS transporters. The difference in structure, beginning with oligomeric state likely explains why the transport process varies significantly.

Unlike MFS transporters where the monomer dominates as the common functional subunit, the functional ADP/ATP carrier is a dimer. The subunit adopting an external conformation will bind ADP and the subunit adopting an internal conformation will bind ATP. Both binding sites must be occupied for the antiport cycle to be completed [100]. It is likely that the relative orientation of the subunit to the mitochondrial membrane determines its conformation and confers specificity for the correct substrate (ADP when facing the outside and ATP when facing the inside). The kinked helices likely play a role in opening the channel that permits substrate transfer, and the tilt degree may play a role in exposing specific regions within the cavities to confer higher affinity toward one of the two nucleotides [100].

### *RESISTANCE-NODULATION-CELL DIVISION*

The Resistance-Nodulation-Cell Division (RND) family of transporters exports numerous anionic, cationic, zwitterionic, and neutral toxic compounds from the periplasm of Gram-negative bacteria, thus granting multidrug resistance to the cells with high levels of RND protein expression. ArcB, a multidrug resistance transporter in *Escherichia coli*, is a member of the RND family. ArcB requires cooperation with TolC, an outer membrane channel, and ArcA, a membrane fusion protein to export molecules from the cell. The transporter itself is a functional trimer and each multi-domain subunit is referred to as a protomer. The protomer contains three major domains: the transmembrane domain, the porter domain, and the TolC docking domain. ArcB has been crystallized with each

protomer subunit in either the access, binding, or extrusion states of the transport mechanism [97-99].

The drug export mechanism displays little similarity with MFS or other transporter proteins. The porter domain of ArcB is located at the interface between the inner membrane and the periplasm. This domain undergoes the major substrate-induced conformational changes that extrude toxic drugs from the periplasm into the TolC channel, which exports them across the outer membrane and into extracellular space. The transport mechanism provides useful information regarding alternative ways to export drugs from cells and the breadth of conformational changes that can accomplish this process [97,99]. First, in the access stage, a periplasmic drug enters an open vestibule, that has restricted access to the binding site. Following an enlargement of the binding site, the drugs enter and bind within a large binding pocket. The exit site is blocked by the inclined central helix from the adjacent protomer, which is in the extrusion state. Finally, the access and binding vestibule is closed, the occluding helices are inclined away, and the substrate is pushed up, out of the binding pocket to TolC, rotating the protomer back to the access state, therefore readying for another round of transport. Each protomer is always in one of the three states and the rotation from access to binding to extrusion state is controlled by proton translocation that occurs in an entirely different domain within the transmembrane region. Unlike crystallized LacY and GlpT, the proton translocation pathway is completely separate and independent from the substrate pathway [97].

## *OVERALL CONCLUSIONS AND RESEARCH PURPOSE*

Carrier-mediated transport and the proteins that catalyze these reactions play an important physiological role in sustaining total body and cellular homeostasis. Using GLUT1 as a model transport system, the goals of this thesis focus on examining the integral membrane protein structure-function relationship. In particular, this work will investigate the glucose transport mechanism, the structural arrangement and dynamics of the 12 GLUT1 membrane-spanning α-helices, and the molecular mechanism for glucose transport regulation by ATP.

With regard to the glucose transport mechanism, we ask how does GLUT1 catalyze sugar translocation? Our goal is to further dissect the mechanism by which glucose is transported into or out of the cell. In particular, we would like to answer the following questions: How many glucose transport steps are required? Is each step protein–mediated? What kinetic constraints govern each step? How do regulatory agents such as ATP modulate each step? Using rapid kinetics studies, we were able to examine the series of conformational changes required for GLUT1 catalysis of a complete glucose transport cycle. These experiments isolated a previously unidentified rapid transport step. A number of experimental results are presented to support our proposal that the rapid step represents the intermediate step between the e2 to e1 uptake cycling event. Recent crystallographic evidence showing MFS transporters statically trapped in this arrangement have since been observed for OxlT and EmrD [5,39,87].

In light of the recent three-dimensional structures obtained for MFS transport proteins LacY, GlpT, OxlT, and EmrD, does the organization of GLUT1 α-helices within the lipid bilayer share a common fold or present a different and unique arrangement? Homology modeling has become a popular technique in creating structural models for proteins that continue to prove refractory to crystallization. Recent publications have used sequence alignment and homology threading to identify conserved residues within secondary active MFS transporters (LacY template) and homology-modeled GLUT1 using the GlpT structure as the template [7,63,64]. While both GlpT and GLUT1 belong to the MFS classification, GlpT is an antiporter that transports phosphate molecules, whereas GLUT1 is a uniporter that transports glucose molecules. Homology modeling, therefore, is an *a priori* exercise rather than an analysis supported by direct experimental evidence.

In order to test our hypothesis, we developed a novel mass spectrometry approach to resolve individual GLUT1 peptides encompassing all protein domains. Mass spectrometry of integral membrane proteins has been notoriously difficult [106,107]. Despite comprising greater than 20% of the proteins encoded by the human genome, integral membrane proteins are continually underrepresented in proteomics studies. The hydrophobic nature of the transmembrane domains, tendency of these peptides to aggregate during HPLC separation, presence of reactive reduced cysteine residues, and contamination by more soluble proteins in cellular samples contribute to this difficulty [107]. Furthermore, few mass spectrometry studies exist that exclusively focus on the structure-function relationship of single integral membrane proteins [108-113].

The development of this technique and the observed findings provide powerful insight into the GLUT1 structure-function relationship and will lay the groundwork for future studies examining this association. We therefore subjected native GLUT1 proteoliposomes to site-specific proteolytic digests and covalent modification with water-soluble probes for two reasons: first, to map the surface accessibility of GLUT1 domains and second, to study conformational dynamics and differential labeling in the presence of substrates, inhibitors, and modulators. Our findings directly support the hypothesis that GLUT1 shares the consensus MFS helix packing arrangement, implicate two transmembrane α-helices and the cytoplasmic regions in conformational dynamics, and support the existence of an aqueous accessible glucose translocation pore.

To further assess the arrangement of GLUT1 α-helices, we ask how sulfhydryl chemistry controls the native oligomeric structure and organization of GLUT1 within the lipid bilayer? The structure-function relationship for GLUT1-mediated transport has been thoroughly examined in two different systems. In human erythrocytes, a large body of biophysical and biochemical data describes GLUT1 transport kinetics, oligomeric state, and allosteric regulation [14,42,43,81,86,114]. GLUT1 expressed in a *Xenopus* oocyte system, however, has been employed in studies that examine the function and orientation of transmembrane helices [40,44,48-51]. The *Xenopus* expression system, however, does not display the same kinetic sensitivity to reductant (i.e. the breaking of potential disulfide bridges that cause an observed reduction in transport rates) or oligomerization properties observed for GLUT1 natively expressed in erythrocytes, CHO, HEK, and COS cells [86]. In particular, we wanted to analyze how sulfhydryl chemistry controls native

oligomeric structure and GLUT1 organization within the membrane. We examined the reductant sensitivity of cysteine residue accessibility to alkylating agents. After observing that deglycosylated GLUT1 resolves anomalously by gel electrophoresis, we show that GLUT1 cysteine residues are differentially alkylated in the presence of reductant. Thiol chemistry and disulfide formation, therefore, likely affect GLUT1 structure.

In summary, the data and analysis presented here will address questions regarding how the structural organization of GLUT1 within the plasma membrane contributes to the carrier-mediated transport process. In addition to furthering our understanding as to how GLUT1 functions on the molecular level, the methods developed in the process of obtaining these results can be broadly applied to studying the structure-function relationship in other integral membrane proteins.

# CHAPTER II

## QUENCH FLOW ANALYSIS REVEALS MULTIPLE PHASES OF GLUT1-MEDIATED SUGAR TRANSPORT

This chapter was published in the journal *Biochemistry* in 2005, and can be found using the following reference:

*Blodgett DM, Carruthers A (2005) Quench-flow analysis reveals multiple phases of GluT1-mediated sugar transport. Biochemistry 44: 2650-2660.*

Initial work was published in the journal *Blood Cells, Molecules, and Diseases* in 2004 as a result of a 2003 talk presented to the Red Cell Club held at Yale University School of Medicine:

*Blodgett DM, Carruthers A (2004) Conventional transport assays underestimate sugar transport rates in human red cells. Blood Cells Mol Dis 32: 401-407.*

**Research was supported by NIH Grant DK44888.**

***ABSTRACT***

Standard models for carrier-mediated nonelectrolyte transport across cell membranes do not explain sugar uptake by human red blood cells. Most measurements of red cell sugar transport have been made over intervals of 10 seconds or greater, a range which may be too long to measure transport accurately. In the present study, we examine the time course of sugar uptake over intervals as short as 5 milliseconds to periods as long as 8 hours. Using conditions where transport by a uniform population of cells is expected to be monophasic (use of subsaturating concentrations of a non-metabolizable but transported sugar, 3-*O*-methylglucose), our studies demonstrate that red cell sugar uptake is comprised of three sequential, protein-mediated events (rapid, fast and slow). The rapid phase is more strongly temperature-dependent than the fast and slow phases. All three phases are inhibited by extracellular (maltose or phloretin) or intracellular (cytochalasin B) sugar transport inhibitors. The rate constant for the rapid phase of uptake is independent of 3-*O*-methylglucose concentration. The magnitude (moles of sugar associated with cells) of the rapid phase increases in a saturable manner with [3-*O*-methylglucose], similar to both the amount of sugar retained by red cell membrane proteins upon addition of cytochalasin B and phloretin and the D-glucose inhibitable cytochalasin B binding capacity of red cell membranes. These data support a transport mechanism in which newly bound sugars are transiently sequestered within the translocation pathway where they become inaccessible to extra- and intracellular water.

## *INTRODUCTION*

A family of glucose transport proteins catalyzes the stereoselective, bidirectional, passive transport of sugar molecules across the cell membrane. One member of this family, GLUT1, mediates sugar transport across the human erythrocyte membrane [115].

Although extensively studied, the molecular mechanism of GLUT1-mediated sugar transport is unknown. In the absence of stable GLUT1-substrate intermediates for structural analysis, researchers have used biochemical and biophysical approaches to investigate transport. Their results suggest three possible transport mechanisms. The transporter may function as a simple, alternating carrier, sequentially presenting sugar import (e2) and export (e1) sites [2,38,41,116]. During uptake, extracellular sugar binding to the e2 site catalyzes a conformational change (e2→e1) that releases bound sugar into cytosol and exposes an e1 site. The e2 conformer is regenerated for additional cycles of sugar import via the inverse (e1→e2) conformational change resulting from either the binding and rapid export of intracellular sugar or from a slow, sugar independent relaxation to the initial state. An alternative hypothesis describes a simultaneous-carrier mechanism, where the transporter molecule simultaneously exhibits import and export configurations [117-119]. In this model, the transporter is proposed to be a complex of four GLUT1 proteins in which each subunit (GLUT1 protein) functions as a simple, alternating carrier. An obligate functional relationship between subunits is proposed to limit the conformational freedom of subunits within the transport complex. At any instant,

therefore, two subunits must exist as e2 conformers while the remaining two subunits must present e1 conformers [84]. A third model suggests that GLUT1-mediated sugar transport is inconsistent with the predictions of either of the preceding mechanisms. Imported sugars are proposed to interact with noncatalytic binding sites associated with the carrier or with internal red cell components [117,120,121]. This compromises the accuracy of transport determinations because intracellular $[sugar]_{total}$ > intracellular $[sugar]_{free}$.

The recent crystallization of lactose permease (LacY) in the e1 (export) configuration provides a clearer picture of a carrier substrate binding site [33]. Although not strictly a passive sugar carrier, this proton-disaccharide symporter is capable of passive transport in the absence of an electrochemical gradient for proton driven sugar transport [122]. LacY is also a member of the wider Major Facilitator Superfamily (MFS) of transporters that includes the GLUT family of carriers [23,57]. The LacY e1 crystal structure is characterized by a large internal hydrophilic cavity (25 Å by 15 Å) extending from the cytosol to deep within the core of the membrane-embedded portion of the carrier. The volume of the cavity is approximately $1.5 \times 10^{-24}$ L – a space large enough to contain as many as 3 - 5 hydrated glucose molecules assuming a self-diffusion coefficient of glucose of $4 \times 10^{-6}$ $cm^2.s^{-1}$ at 20°C [123]. It is proposed that following substrate binding to e1, the cavity closes to engulf the bound sugar molecule and then opens at the opposite or trans-side of the membrane to form a similar outward facing cavity into which the bound

substrate can dissociate and subsequently diffuse into the interstitium [33]. The e1 structure of a second MFS transporter – the bacterial glycerol-3-phosphate/Pi antiporter (GlpT) – provides additional support for the alternating conformer transport mechanism in prokaryotes [35,124]. The process by which the substrate binding event promotes conformational changes that result in substrate translocation is unknown [33,35,124] and e2 or intermediate forms of LacY and GlpT are unavailable for more detailed analysis.

While the alternating conformer model for carrier mediated transport gains strong support from the LacY and GlpT structures, it is also evident that this model does not quantitatively describe the sugar transport properties of human red blood cells [43,125]. Transport measurements obtained by conventional bench-top procedures indicate that the Haldane requirements for a passive transport mechanism ($Vmax/K_{m(app)}$) ratios for exchange and net entry and exit of sugars must be equal) are not satisfied [43,125-127]. More rapid sampling procedures (resolution less than 1 second) obtained by quench flow appear to result in transport parameters that satisfy the Haldane requirements [116]. This suggests that red cell sugar transport is very fast and requires rapid sampling procedures for accurate determination of initial rates. However, these more rigorously determined Michaelis and velocity parameters fail to predict the kinetics of red cell sugar transport over physiological time intervals (seconds to minutes; [43,125,128-130]).

The present study was conducted to examine the kinetics of sugar uptake by human red cells over intervals ranging from milliseconds to hours. To achieve this, we used a rapid

quench flow device (which provides subsecond temporal resolution) in conjunction with reduced reaction temperature to study the earliest events associated with glucose transport. These studies provide evidence for at least three phases of protein-mediated glucose translocation into the red cell, provide "$V_{max}$ and $K_m$" parameters for transport obtained during each of these phases, and suggest that it is possible to isolate an intermediate GLUT1 form, e(S), that bridges the e·S2→e·S1 transition.

## *MATERIALS AND METHODS*

***Materials*** [$^3$H]-3-*O*-Methylglucose and [$^3$H]-cytochalasin B were purchased from Amersham Biosciences (Piscataway, NJ); [$^3$H]-L-Glucose was purchased from Sigma-Aldrich. Rabbit antisera against amino acid residues 480-492 of the GLUT1 carboxy terminus (C-Ab) were prepared as described in and obtained from Animal Pharm Services, Inc. (Healdsburg, CA) [85]. Goat Anti-Rabbit (GAR) horseradish peroxidase (HRP) conjugate was purchased from Bio-Rad Laboratories (Hercules, CA). Washed red blood cells and whole blood stored in CPDII AS-1 preservative solution were obtained from Biological Specialties Corporation (Colmar, PA). All other reagents were purchased from Sigma-Aldrich (St. Louis, MO) unless otherwise noted.

***Solutions*** KCl saline (kaline) consisted of 150mM KCl, 6mM $MgCl_2$, 5mM HEPES, and 4mM EGTA, pH 7.4. Ice-cold lysis medium contained 10 mM Tris – HCl and 1 mM EGTA, pH 7.4. Stopper solution consisted of ice-cold kaline, 10 μM cytochalasin B

(CCB) and 100 μM phloretin; RQF stopper solution contained ice-cold kaline, 20 μM CCB, and 200 μM phloretin. Phosphate buffer saline (PB) consisted of 145 mM NaCl and 20 mM sodium phosphate. Sample buffer (2x) contained 125 mM Tris – HCl, pH 6.8, 4% SDS, 20% glycerol, and 50 mM DTT.

***Red Blood Cell Preparation*** Red cells were isolated from whole human blood by repeated wash/centrifugation cycles. One volume of whole blood was mixed with 20 volumes of ice-cold kaline and centrifuged at 5,443 x g for 10 minutes at 4°C. The serum and white buffy coat were aspirated and the cycle repeated until the supernatant was clear and the buffy coat was no longer visible. When depletion of endogenous intracellular sugar was required, cells were resuspended in 20 volumes of kaline and incubated for 30 minutes at 37°C.

***Red Cell Ghost Preparation*** Washed red cells were mixed with 50 volumes of ice-cold hypotonic lysis buffer, and the suspension gently stirred for 10 minutes at 4°C. Red cell membranes were harvested by centrifugation at 18,566 x g for 15 minutes, followed by two additional washes in lysis buffer and centrifugation steps. Membranes were resealed in 20 volumes of kaline medium for 30 minutes at 37°C, containing or lacking 4 mM ATP, pH 7.4. Resealed ghosts were harvested using the same centrifugation settings, and stored on ice for no more than 24 hours.

***Red cell integral membrane proteins (IMPs)*** Peripheral proteins were displaced from red cell membranes by exposing unsealed erythrocyte ghosts to 2 mM EDTA, 15.4 mM NaOH, pH 12 at a concentration of 0.8 mg protein/mL for 10 minutes at 4°C. Membranes were collected by centrifugation at 18,566 x g for 20 minutes at 4°C. The pH of the membrane suspension was restored by 3 wash/centrifugation cycles in 5 volumes of Tris – HCl medium. Final protein concentration of the membrane suspension was adjusted to 2 mg/mL in Tris – HCl and membranes were stored at -20°C (prior to use within 24 hr) or at -80°C (for longer storage intervals).

***Bench-top Sugar Transport Measurements*** The time course of [$^3$H]-3-*O*-methylglucose ([$^3$H]-3MG) uptake by red cells and red cell ghosts was measured at 4°, 12°, and 20°C as described previously [131]. Briefly, 50 or 100 μL of cells or ghosts were exposed to unlabeled sugar with trace amounts of [$^3$H]-labeled sugar. Uptake was allowed to proceed over intervals as short as 10 seconds to equilibrium intervals of up to 8 hours (at 4°C, with high concentrations of cold sugar). The addition of 10 volumes of ice-cold stopper solution to the reaction suspension was used to quench the transport reaction. Cells were pelleted by a one-minute centrifugation (Fisher-Scientific, Model 235C microcentrifuge; 14,000 x g), washed for a second time in stopper solution, and pelleted again via a second one-minute spin. The contents of the isolated cells were released upon addition of 1 mL 3% perchloric acid (PCA), clarified by centrifugation, and two 400 μL aliquots of

supernatant were transferred to scintillation vials, mixed with scintillation fluid, and counted in a Beckman Scintillation Spectrophotometer (LS6500).

***Rapid Quench Flow Sugar Transport Measurements*** The time course of [$^3$H]-3-*O*-methylglucose ([$^3$H]-3MG) uptake by red cells and red cell ghosts was measured at 4° and 20°C by the RQF-63 Rapid Quench Flow system (Hi-Tech Scientific), as described previously [132]. Briefly, this instrument permits precise control of the processes of reagent ***mixing*** (radiolabeled sugar and cells), ***delay*** (reagents sit in a reaction loop, where the length of the loop and reactant flow rate determine the total reaction time), and ***quenching*** (addition of stopper solution) to complete an uptake assay. Stopper solution was maintained at 4°C for all uptake experiments at all temperatures. The reaction sample is collected manually in 1 mL of stopper solution and processed as in conventional transport assays. The RQF was calibrated for temporal accuracy by monitoring the alkaline hydrolysis of dinitrophenolacetate (DNPA), a reaction that forms dinitrophenol and acetate. Using HCl (1 M) as the stopper solution, and DNPA (88 μM) and NaOH (0.5 M) as the reactants, half-lives of 38.5 ± 3.9 milliseconds and 178 ± 9 milliseconds were obtained for DNPA hydrolysis at 22°C and 4°C respectively. These results are consistent with an $E_a$ (activation energy) for DNPA hydrolysis of 14.7 kcal/mol/K and extrapolate to the expected $t_{1/2}$ for DNPA hydrolysis at 25°C of 25 msec [133].

***Equilibrium Sugar Spaces*** Washed red blood cells and resealed ghosts were incubated with 50 μM 3MG, with trace radiolabel for 2 hours at 4°C, at which point equilibrium

3MG distribution was reached. Incubation time was increased up to eight hours when 3MG stock concentrations exceeded 10 mM. The reaction was quenched and the samples processed as described for conventional transport assays.

Fractional equilibration at each time point ($FE_t$) was calculated using the following equation:

$$FE_t = \frac{dpm_t}{dpm_{equilibrium}}$$

where $dpm_t$ represents disintegrations per minute (amount of [$^3$H]-3MG) at time t, and $dpm_{equilibrium}$ describes disintegrations per minute (amount of [$^3$H]-3MG) when the reaction has attained equilibrium. This calculation normalizes results for variations in cell dilutions and radioisotope specific activity across multiple experiments.

***Sugar occlusion*** Washed red blood cells were lysed in the presence or absence of 4 mM MgATP. Cells were then incubated at 4°C in lysis medium with 50 μM 3MG plus trace radiolabel for sufficient time (> 2 hr) to ensure equilibrium 3MG binding with GLUT1. Reactions were stopped by addition of 50 volumes of ice-cold stopper and processed as per usual methods. In lysed ghost experiments, the reaction was stopped with lysis buffer containing or lacking 10 μM CCB and 100 μM phloretin. In experiments using IMPs, kaline buffer replaced lysis buffer and contained no inhibitors, CCB (10 μM), phloretin (100 μM) or CCB plus phloretin. IMPs were subject to trypsin digestion at a

1:30 trypsin:protein ratio for 15 minutes at 37°C, as described previously [134]. Proteolysis was stopped by addition of a complete EDTA-free protease inhibitor cocktail (Roche). Parallel null digestions received equivalent volumes of trypsin-free kaline and protease inhibitor.

***Equilibrium Cytochalasin B Binding*** CCB binding to red cells and stripped ghosts was measured as described previously [43]. Briefly, 50 μL of cells were mixed with 50 μL of radiolabeled CCB, in the presence of increasing concentrations of unlabeled CCB. Two 10 μL aliquots were removed for counting (totals). The suspension was incubated with rotation at 4°C for 30 minutes by which time equilibrium binding was achieved. The suspension was centrifuged for one minute, and two 10 μL aliquots of the supernatant were removed for counting (free) counts. Bound CCB is computed as total counts less free counts. Cytochalasin D (10 μM) was included in all solutions to inhibit CCB binding to non-GLUT1 sites.

***Analytical Procedures*** Protein concentrations were determined by the Pierce BCA procedure. Enzyme-linked immunosorbent assays (ELISA) confirmed that membrane suspensions contained equivalent amounts of GLUT1. C-Ab and goat anti-rabbit HRP conjugate antibodies served as the primary and secondary antibodies, respectively. ELISA reactions were developed with Pierce 1-Step ATBS developing solution and analyzed by using a Bio-Rad Laboratories Benchmark Microplate Reader. SDS-slab (10%) PAGE and Western blot analysis of proteins using C-Ab of membrane proteins were performed as

described previously [135]. Red cell counts were obtained by using a standard curve of cell suspension hemoglobin absorbance at 417 nm versus manual cell counts obtained using a hemocytometer. ATP was measured in neutralized perchloric acid extracts of cells and red cell ghosts using a luciferin-luciferase assay kit purchased from Molecular Probes (Eugene, OR).

***Calculation of Transport Constants*** Radiolabeled sugar uptake by cells and ghosts (time-course data) were fitted to a three-compartment (phase) equation:

$$S_t = C_r(1 - e^{-k_r t}) + C_f(1 - e^{-k_f t}) + C_s(1 - e^{-k_s t})$$

where $S_t$ = sugar associated with the cells at time t and $C_r$, $C_f$, and $C_s$ represent equilibrium sugar spaces associated with rapid, fast and slow cell compartments or transport phases respectively, and $k_r$, $k_f$, and $k_s$ are first-order rate constants describing the rate of equilibration of rapid, fast and slow compartments/phases respectively. $V_{max}$ and $K_{m(app)}$ for 3MG uptake were computed using direct, nonlinear regression analysis of the sugar concentration dependence of 3MG uptake assuming simple Michaelis-Menten kinetics. Arrhenius plots (ln k *versus* 1/T) were fitted by linear regression using the equation:

$$\ln k_n = \ln A + \frac{E_a}{RT}$$

where $k_n$ is the rate constant for rapid, fast or slow phases of uptake, A is the Arrhenius constant, R is the gas constant (1.987 cal. $K^{-1}$ $mole^{-1}$), $E_a$ is the activation energy (kcal $K^{-1}$

mole$^{-1}$). The slope ($E_a$/R) is obtained by linear regression analysis. The software program KaleidaGraph (version 3.6, Synergy Software) was used to plot all data and compute best fit parameters for each curve fit.

***RESULTS***

***Time Course of 3MG Uptake*** 3MG uptake by red blood cells has been reported to be a biphasic process [121]. With the extended temporal resolution provided by the RQF, it is now evident that curve fitting with a two exponent equation does not adequately describe the most rapid transport process. The time course of 3MG uptake by erythrocytes at 22°C (0.01 to 3600 seconds) is best described by a three exponent fit (Figure 2.1). This analysis describes net transport as the sum of either three parallel or three sequential processes. These processes are the rapid filling of a small compartment, a fast filling of a large compartment, and the slow filling of a large compartment.

The temperature dependence of 3MG net import by erythrocytes is summarized in Figure 2.2. The size of each compartment and the corresponding rates of compartment filling are significantly affected by reduced temperature. The rapid process is inhibited by 50-fold upon lowering temperature from 22° to 4°C, whereas the relative size of the slow process is increased with decreasing temperature. Only conventional assays could be performed at 12°C because the RQF was not easily adjusted to this temperature. Arrhenius analysis of the temperature dependence of the rate of each process is presented

**Figure 2.1 3-*O*-methylglucose uptake by human erythrocytes at 22°C.** Ordinate: 3MG uptake reported as fractional equilibration. Abscissa: time in seconds. The dashed and solid curves were computed by nonlinear regression and represent the time course of net 3MG uptake assuming that transport consists of a double or triple exponential process, respectively. The two exponent fit fails to account for the rapid phase. The following constants were obtained: for the double exponential: $C_r = 0.58$; $k_r = 0.17$ $sec^{-1}$; $C_f = 0.42$; $k_f = 0.0008$ $sec^{-1}$; Constants describing the triple exponential are: $C_r = 0.13$; $k_r = 22.6$ $sec^{-1}$; $C_f = 0.50$; $k_f = 0.086$ $sec^{-1}$; $C_s = 0.37$; $k_s = 0.0007$ $sec^{-1}$. Each data point represents the mean of triplicate measurements made in three separate experiments.

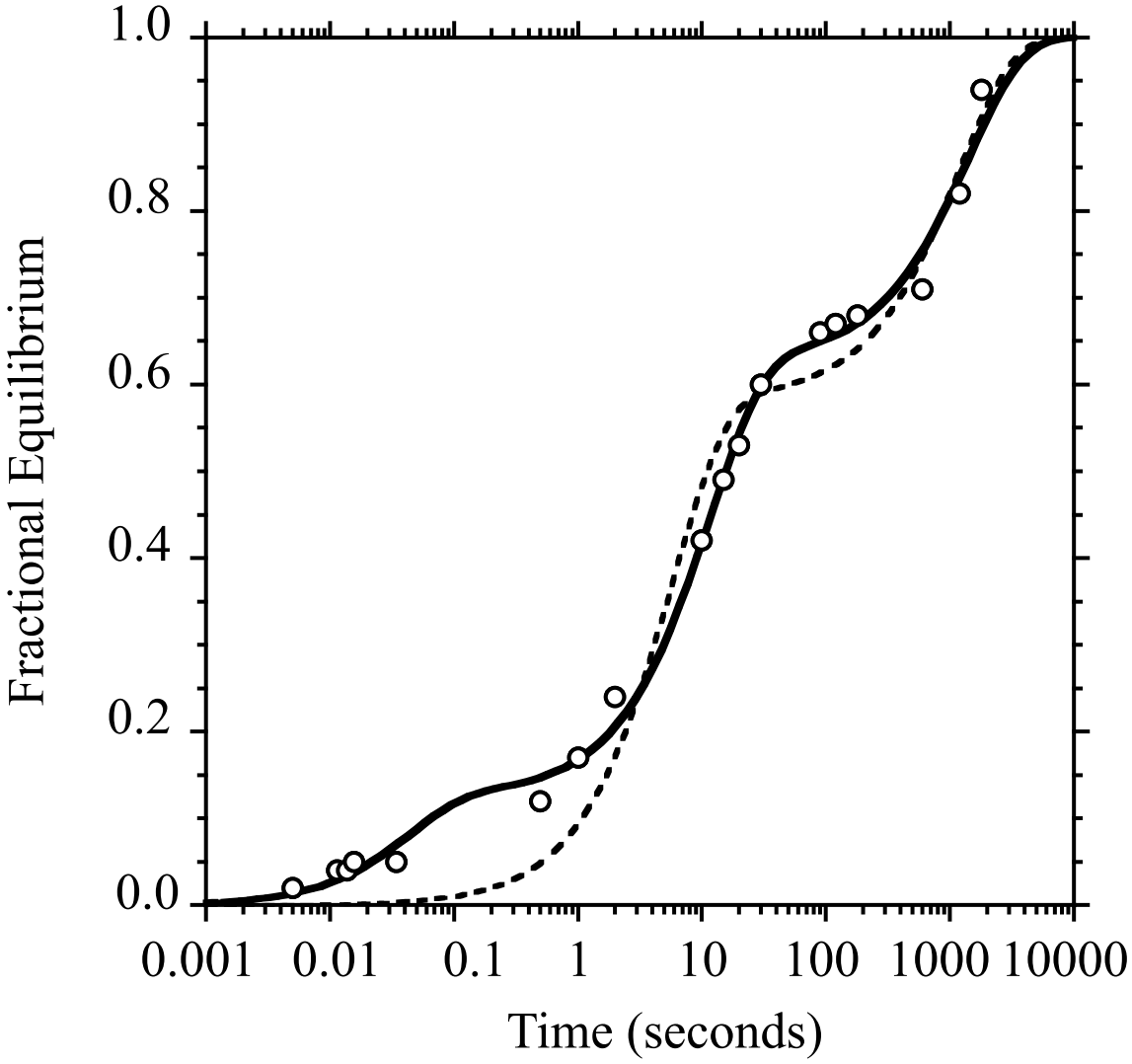
1.0
0.8
0.6
0.4
0.2
0.0
Fractional Equilibrium
0.001
0.01
0.1
1
10
100
1000
10000
Time (seconds)

Figure 2.1

**Figure 2.2 Temperature dependence of 3-*O*-methylglucose uptake by human erythrocytes:** at 4°C (●), 12°C (▲), and 22°C (○), respectively. Ordinate: 3MG uptake reported as fractional equilibrium. Abscissa: time in seconds. Uptake at 4°C and 22°C are fit with a three exponent curve, the 12°C data do not include the rapid (earliest) phase of 3MG uptake data. All data are superimposed on a background of 0.02. Each point represents the mean of three independent experiments. The following rate constants were obtained: ***4°C***: $C_r = 0.01$; $k_r = 0.277$ $sec^{-1}$; $C_f = 0.248$; $k_f = 0.0147$ $sec^{-1}$; $C_s = 0.742$; $k_s = 0.000236$ $sec^{-1}$; ***12°C***: $C_r = 0.03^{\S}$; $k_r = 6.8$ $sec^{-1\S}$; $C_f = 0.502$; $k_f = 0.0675$ $sec^{-1}$; $C_s = 0.468$; $k_s = 0.00121$ $sec^{-1}$; ***22°C***: $C_r = 0.03$; $k_r = 38.76$ $sec^{-1}$; $C_f = 0.562$; $k_f = 0.115$ $sec^{-1}$; $C_s = 0.408$; $k_s = 0.000687$ $sec^{-1}$. ($^{\S}$Represents values estimated from Arrhenius plot, not obtained directly.)

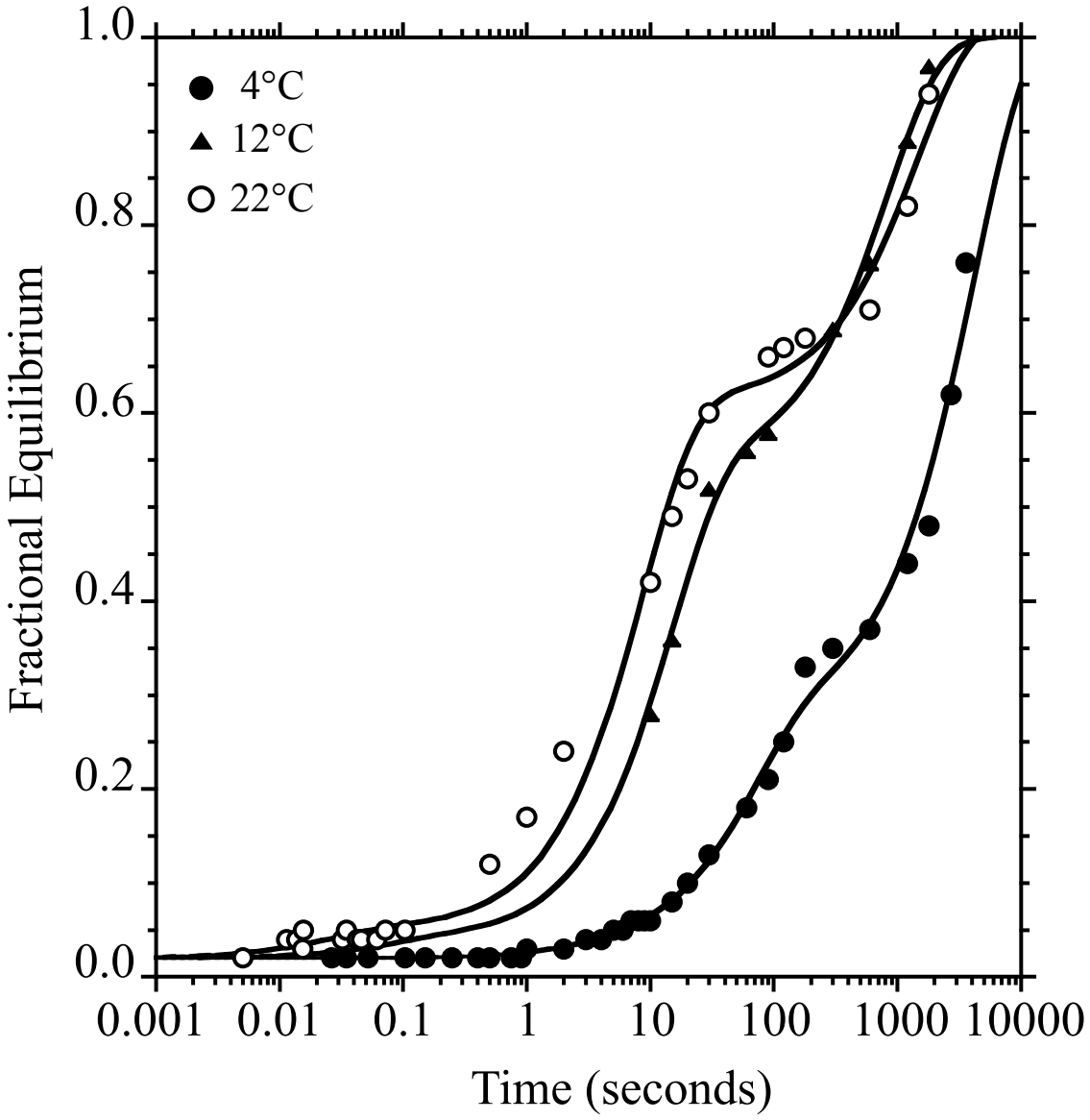
1.0
0.8
0.6
0.4
0.2
0.0
Fractional Equilibrium
4°C
12°C
22°C
0.001
0.01
0.1
1
10
100
1000
10000
Time (seconds)

Figure 2.2

in Figure 2.3. Rapid, fast, and slow phases are characterized by activation energies of 44.6 (two temperature points only), 20.9 ± 5.9, and 20.8 ± 6.7 kcal.mole$^{-1}$ respectively. By comparison, $E_A$ for the simple self-diffusion of glucose in aqueous solution is 5.1 kcal.mole$^{-1}$ [123]. This suggests that neither the rapid, fast or slow processes are diffusion-limited reactions.

***Time Course of 3MG Uptake in the Presence of Inhibitors*** Cytochalasin B interacts with the sugar exit site of GLUT1 serving as a competitive inhibitor of sugar exit, and as a noncompetitive inhibitor of sugar uptake [136,137]. Extracellular maltose is not transported by GLUT1, but interacts with the glucose import site to competitively inhibit sugar uptake [136]. The time course of 3MG uptake by red blood cells at 4°C is severely inhibited in the presence of 50 μM CCB (Figure 2.4A) and 50 mM maltose (Figure 2.4B). These results indicate that all three transport phases are subject to inhibition by specific inhibitors of carrier (protein)-mediated sugar transport. This result is expected if uptake were described by three, independent (parallel), carrier-mediated processes. This result would also be produced if net transport were described by three sequential (dependent) processes in which all three processes are carrier-mediated and inhibited by CCB. This result is not expected if only the first or second phases of three sequential processes are inhibited. Here only the inhibited phases should show reduced rates of progression.

Monophasic 3MG uptake by red cells in the presence of CCB also suggest that the population of cells employed in these studies is uniform with respect to surface

**Figure 2.3 Arrhenius plot examining temperature dependence of 3-*O*-methylglucose uptake rates.** Ordinate: natural log of rate constants from figure 2.2. Abscissa: 1/Temperature as $K^{-1}$. The straight lines drawn through the points were computed by linear regression. The activation energies of each of the three phases are obtained from the slope of each plot as described in *Materials and Methods*: rapid (□): 44.6 kcal kcal.mole$^{-1}$, fast (▲): 20.9±5.9 kcal.mole$^{-1}$, and slow (○): 20.8±6.7 kcal.mole$^{-1}$, respectively. Data are also shown for red blood cell ghosts lacking (small □, small △, and small ○) or containing 4 mM ATP during resealing (small ■, small ◢, and small ●). Ghost data summarize rate constants for rapid (squares), fast (triangles) and slow (circles) phases of uptake.

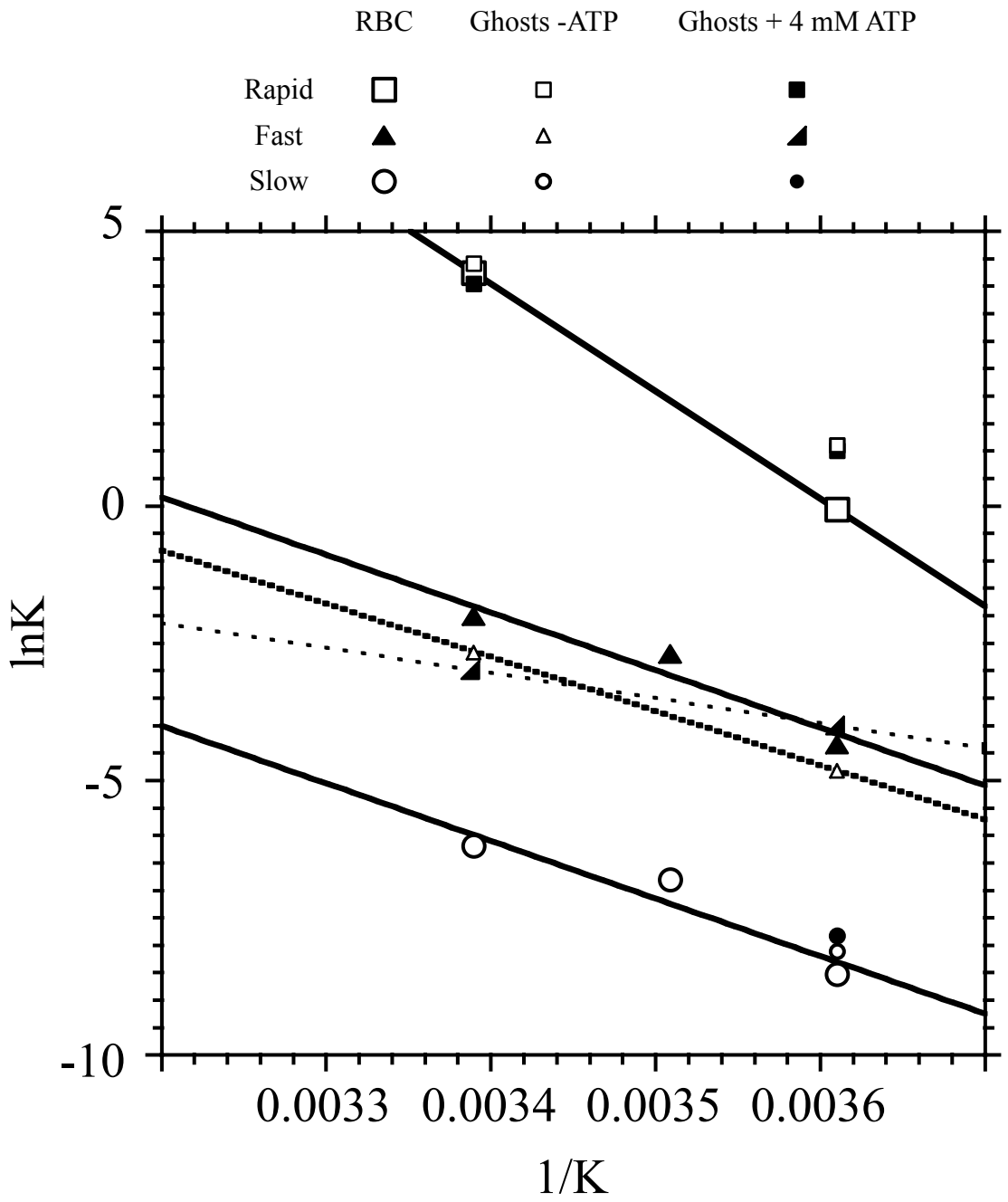
RBC
Ghosts -ATP
Ghosts + 4 mM ATP
Rapid
Fast
Slow
5
0
-5
-10
lnK
0.0033
0.0034
0.0035
0.0036
1/K

Figure 2.3

**Figure 2.4 A 3-*O*-methylglucose uptake by human erythrocytes in the presence of transport inhibitors: (A)** Cytochalasin B at 4°C. Ordinate: 3MG uptake reported as fractional equilibrium. Abscissa: time in seconds. Control uptake (●) in the absence of CCB differs greatly from uptake where the red cells and 3MG were previously exposed to 50 μM CCB (○). At all measured time points, a substantially higher fractional equilibrium is reached when uptake is uninhibited. The curves drawn though the points have the following constants: *control* $C_r = 0.05$; $k_r = 5$ $sec^{-1}$; $C_f = 0.45$, $k_f = 0.014$ $sec^{-1}$; $C_s = 0.5$, $k_s = 11.8 \times 10^{-5}$ $sec^{-1}$, $R^2 = 0.997$; *CCB* $C_s = 1$; $k_s = 0.0002$ $sec^{-1}$; background = 0.02, $R^2 = 0.567$. **(B)** 3-*O*-methylglucose uptake by human erythrocytes in the presence of competing sugar maltose at 4°C. Control uptake (●) proceeds more rapidly than uptake in the presence of 50mM (△) maltose. The curves drawn though the points have the following constants: *control* $C_r = 0.05$; $k_r = 2$ $sec^{-1}$; $C_f = 0.35$, $k_f = 0.009$ $sec^{-1}$; $C_s = 0.6$, $k_s = 7.3 \times 10^{-5}$ $sec^{-1}$, $R^2 = 0.989$; *50 mM Maltose* $C_r = 0.035$; $k_r = 1$ $sec^{-1}$; $C_f = 0.45$, $k_f = 0.0054$ $sec^{-1}$; $C_s = 0.515$, $k_s = 7.0 \times 10^{-5}$ $sec^{-1}$, $R^2 = 0.991$.

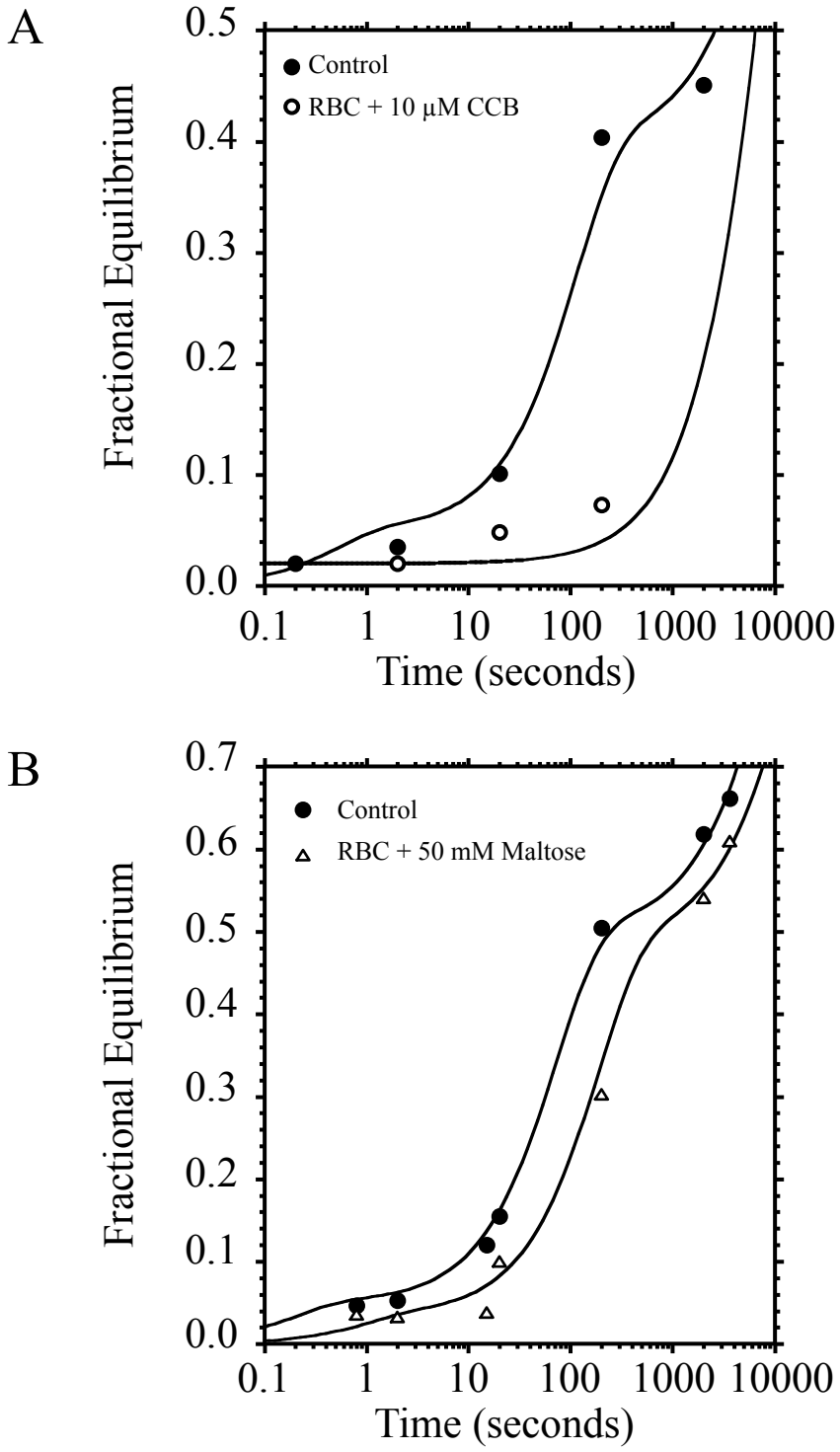
A
Control
RBC + 10 μM CCB
Fractional Equilibrium
0.0
0.1
0.2
0.3
0.4
0.5
0.1
1
10
100
1000
10000
Time (seconds)
B
Control
RBC + 50 mM Maltose
Fractional Equilibrium
0.0
0.1
0.2
0.3
0.4
0.5
0.6
0.7
0.1
1
10
100
1000
10000
Time (seconds)

Figure 2.4

area:volume ratio. The rate constant, ***k***, for trans-bilayer diffusion of a molecule into a cell of radius ***r*** is directly proportional to the product ***PA*** where ***P*** is the permeability coefficient ($cm.s^{-1}$) for transbilayer diffusion of the molecule and ***A*** is the surface area:volume ratio ($cm^{-1}$) of the cell [2]. Assuming ***P*** is constant for all red cell-derived, membrane bound vesicles, ***k*** is directly proportional to ***A***. For a spherical body, the surface area: volume ratio, ***A = 3/r*** (red cells are biconcave disks but membrane vesicles formed from red cells are predominantly spherical [138,139]). Thus for rapid, fast and slow rate constants of 69.7, 0.13 and 0.0021 per sec (22ºC, Table 2.1), the relative ***A*** values are $3.4 \times 10^3$, 66 and 1 respectively. If the slowest phase corresponds to the radius of an erythrocyte (3.5 μm), the rapid and fast phases would correspond to uptake by cells with radii of 0.1 nm and 45.7 nm respectively. Thus a mixture of three cell populations of these sizes is also expected to display rapid, fast and slow phases of transmembrane sugar diffusion.

***Time Course of 3MG Uptake in resealed, hypotonically lysed cells*** At 22ºC, the slowest phase of net sugar uptake is 32,000-fold slower than the most rapid phase of uptake. This raises the interesting possibility that the slow phase of sugar import may reflect some process other than sugar release into cytosolic water. 3MG, like D-glucose, can non-enzymatically glycate cellular proteins [140]. The slow phase may therefore represent 3MG interaction with cellular proteins to form glycated proteins or to form noncovalent precursors to glycated proteins [140]. If 3MG interaction with cytosolic

**Legend to Table 2.1 Kinetics of 3MG uptake in red cells and red cell ghosts.** [a]The time course of 50 μM 3MG uptake was measured in red cells and red cells ghosts containing or lacking 4 mM exogenous MgATP. Uptake data were analyzed assuming 3 phases of uptake – rapid, fast and slow (see Figures 2.1, 2.2 and 2.5). [b]k is the first-order rate constant describing the rate of compartment filling (per sec). [c]C is the compartment size as a fraction of the total cellular 3MG space. [d]Experiments made at 12ºC did not permit determination of the kinetics of filling of the rapid compartment. These numbers were obtained by extrapolation from Arrhenius analysis of the temperature dependence of transport (see Figure 2.3). [e]These analyses were made before we recognized that uptake was consistent with a three compartment model. Time points were not obtained over a sufficiently broad time-range to accurately determine $k_s$ and $C_s$. The data are therefore analyzed assuming only two components of uptake – rapid and fast. These data represent the mean ± SEM of at least 3 separate determinations made in triplicate.

| Table 2.1 3MG uptake kinetics in red cells and ghosts | | | | | | | |
|---|---|---|---|---|---|---|---|
| | | [a]Compartment | | | | | |
| | | Rapid | | Fast | | Slow | |
| Cells | Temperature ºC | [b]$k_{rapid}$ | [c]$C_{rapid}$ | [b]$k_{fast}$ | [c]$C_{fast}$ | [b]$k_{slow}$ | [c]$C_{slow}$ |
| | | *$s^{-1}$* | *fraction* | *$s^{-1}$* | *fraction* | *$s^{-1}$* | *fraction* |
| | | | | | | | |
| Intact Cells | 4 | 0.94 | 0.036 | 0.013 | 0.27 | 0.00020 | 0.71 |
| | | ± | ± | ± | ± | ± | ± |
| | | 0.26 | 0.006 | 0.001 | 0.03 | 0.00003 | 0.02 |
| | | | | | | | |
| | 12 | [d]6.76 | 0.03 | 0.067 | 0.502 | 0.0011 | 0.468 |
| | | | | ± | ± | ± | ± |
| | | | | 0.001 | 0.016 | 0.0001 | 0.016 |
| | | | | | | | |
| | 22 | 69.7 | 0.037 | 0.13 | 0.51 | 0.0021 | 0.45 |
| | | ± | ± | ± | ± | ± | ± |
| | | 17.5 | 0.004 | 0.01 | 0.08 | 0.0015 | 0.09 |
| | | | | | | | |
| Ghosts + ATP | 4 | 2.73 | 0.071 | 0.0183 | 0.594 | 0.0004 | 0.335 |
| | | ± | ± | ± | ± | ± | ± |
| | | 0.77 | 0.016 | 0.009 | 0.030 | 0.0001 | 0.046 |
| | | | | | | | |
| | 22 | [e]56.83 | [e]0.058 | [e]0.050 | [e]0.942 | | |
| | | ± | ± | ± | | | |
| | | 26.16 | 0.026 | 0.012 | | | |
| | | | | | | | |
| Ghosts 0 ATP | 4 | 3.02 | 0.122 | 0.008 | 0.3913 | 0.0003 | 0.4867 |
| | | ± | ± | ± | ± | ± | ± |
| | | 1.47 | 0.013 | 0.0023 | 0.022 | 0.00004 | 0.035 |
| | | | | | | | |
| | 22 | [e]82.80 | [e]0.043 | [e]0.069 | [e]0.958 | | |
| | | ± | ± | ± | | | |
| | | 25.96 | 0.017 | 0.017 | | | |

proteins accounts for the slow phase of net uptake, the use of resealed erythrocyte ghosts which lack more than 90% of cytosolic proteins should diminish this phase of transport.

The kinetics of 3MG net uptake by resealed red blood ghosts at 4ºC are not significantly different from those observed in intact cells (Table 2.1, Figure 2.5). This observation refutes the hypothesis that the slow phase of uptake results from 3MG interaction with cytosolic proteins. Sugar that is transported into the cell is also fully recoverable during sugar export [121,141] indicating that 3MG does not form a covalent complex with cellular molecules.

Experiments at 22ºC were performed before it was recognized that three phases of uptake exist. These data were analyzed assuming two phases of uptake and, because insufficient time points were collected at longer times (200 – 10,000 sec), the data do not permit accurate determination of constants for filling of the slow compartment. Compartment size and rates of compartment filling in red cell ghosts lacking exogenous ATP at 4ºC are not significantly different from those measured in intact red cells. The intact cells used in these specific measurements had been stored at 4ºC for a prolonged period (>14 days) suggesting that they may have become metabolically depleted. Exogenous, intracellular ATP (4 mM) increases the size of the fast compartment at the expense of the slow compartment in resealed cells (Figure 2.5). Analysis of cellular ATP content indicates that ATP-free ghosts are nominally ATP-free while intact cells contain significantly lower ATP levels (0.7 mM) than do ghosts containing exogenous ATP (3.8 mM). These data

**Figure 2.5 3-*O*-methylglucose uptake at 4°C by human erythrocyte ghosts containing (●) or lacking (○) 4 mM ATP respectively.** Ordinate: 3MG uptake reported as fractional equilibrium. Abscissa: time in seconds. Uptake is fitted with a three exponent curve. The following rate constants were obtained from averages of three independent experiments: ***4 mM ATP (dotted curve)***: $C_r = 0.01$; $k_r = 0.277$ $sec^{-1}$; $C_f = 0.248$; $k_f = 0.0147$ $sec^{-1}$; $C_s = 0.742$; $k_s = 0.000236$ $sec^{-1}$; ***0 ATP (dashed curve)***: $C_r = 0.03^{\S}$; $k_r = 13.1$ $sec^{-1\S}$; $C_f = 0.502$; $k_f = 0.0675$ $sec^{-1}$; $C_s = 0.468$; $k_s = 0.00121$ $sec^{-1}$. The time course of 3MG uptake in red cells at 4ºC (Figure 2.2) is also shown for comparison (solid line).

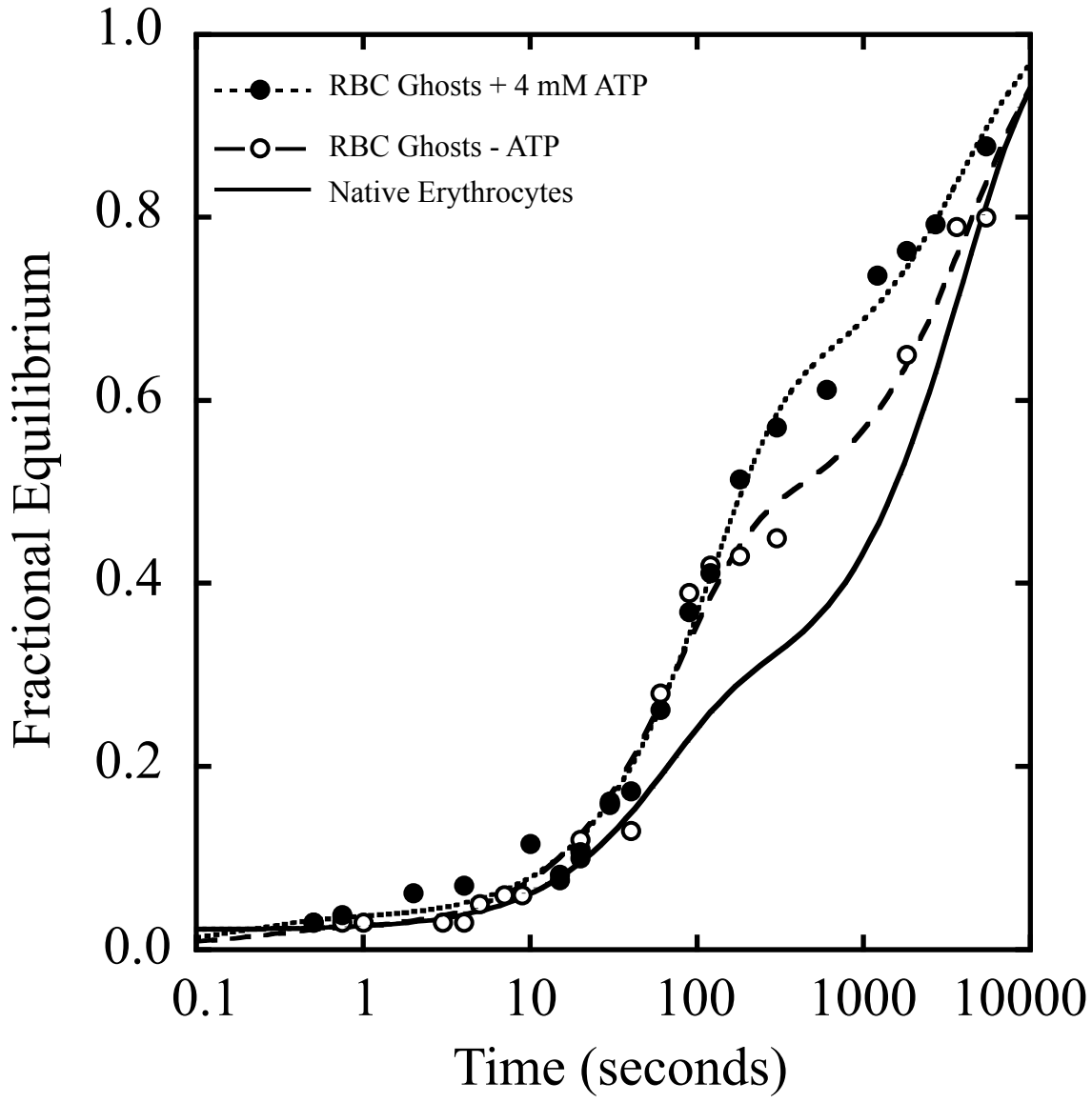
RBC Ghosts + 4 mM ATP
RBC Ghosts - ATP
Native Erythrocytes
Fractional Equilibrium
1.0
0.8
0.6
0.4
0.2
0.0
0.1
1
10
100
1000
10000
Time (seconds)

Figure 2.5

strongly suggest that prolonged cold storage of human blood results in significant depletion of intracellular ATP levels.

The temperature dependence (4 and 22°C) of 3MG net import by resealed erythrocyte ghosts is summarized in Figure 2.3 and Table 2.1. The rapid process ($k_r$) is indistinguishable from that of intact red cells. The fast process in ghosts appears to have somewhat reduced (2-fold) temperature sensitivity relative to the fast process in intact cells. This is manifest as indistinguishable $k_f$ in cells and ghosts at 4ºC but slightly lower $k_f$ in ghosts at 22ºC. At 4ºC, the slow processes ($k_s$) in intact cells and red cell ghosts are indistinguishable.

***Concentration-Dependence of Sugar Uptake*** $V_{max}$ and $K_{m(app)}$ parameters for sugar uptake are, in principle, computed by using initial rates of net sugar transport. RBC 3MG uptake at 4°C was measured during rapid (0.125 min), fast (0.5 min) and slow (30 min) phases of uptake (Figure 2.6). $V_{max}$ and $K_{m(app)}$ values computed for uptake during the rapid transport phase are 42.6 ± 4.2 mmol/L cell water/min and 26.5 ± 4.1 mM, respectively. $V_{max}$ and $K_{m(app)}$ for uptake during the fast phase are 2.5 ± 0.6 mmol/L cell water/min and 27.5 ± 10.7 mM respectively. $V_{max}$ and $K_{m(app)}$ for uptake during the slow transport phase are 1.97 ± 1.01 mmol/L cell water/min and 148.2 ± 84.5 mM, respectively. $V_{max}$ for sugar uptake is approximately 15-fold greater when computed using rapid time points rather than fast incubation intervals. $K_{m(app)}$ values are similar when

**Figure 2.6 [3MG]-dependence on $V_{max}$ and $K_m$ in human erythrocytes at 4°C.** Ordinate: Uptake rate of 3MG (moles $L^{-1}$ $minutes^{-1}$). Abscissa: 3MG concentration in uptake solution, measured in mM concentration units. 3MG uptake rates were measured at three time points corresponding to rapid (0.125 min), fast (0.5 min) and slow (30 min) phases of sugar transport. The transport parameters at each time point are reported as follows: rapid phase (●): $V_{max}$ = 40.3 ± 16.0 mmol/L cell water/min, $K_m$ = 22.6 ± 10 mM, $R^2$ = 0.998; fast phase (□): $V_{max}$ = 2.4 ± 0.5 mmol/L cell water/min, $K_m$ = 22.7 ± 6.2 mM, $R^2$ = 0.982; slow phase (Δ): $V_{max}$ = 1.33 ± 0.02 mmol/L cell water/min, $K_m$ = 94.2 ± 4.5 mM, $R^2$ = 0.997.

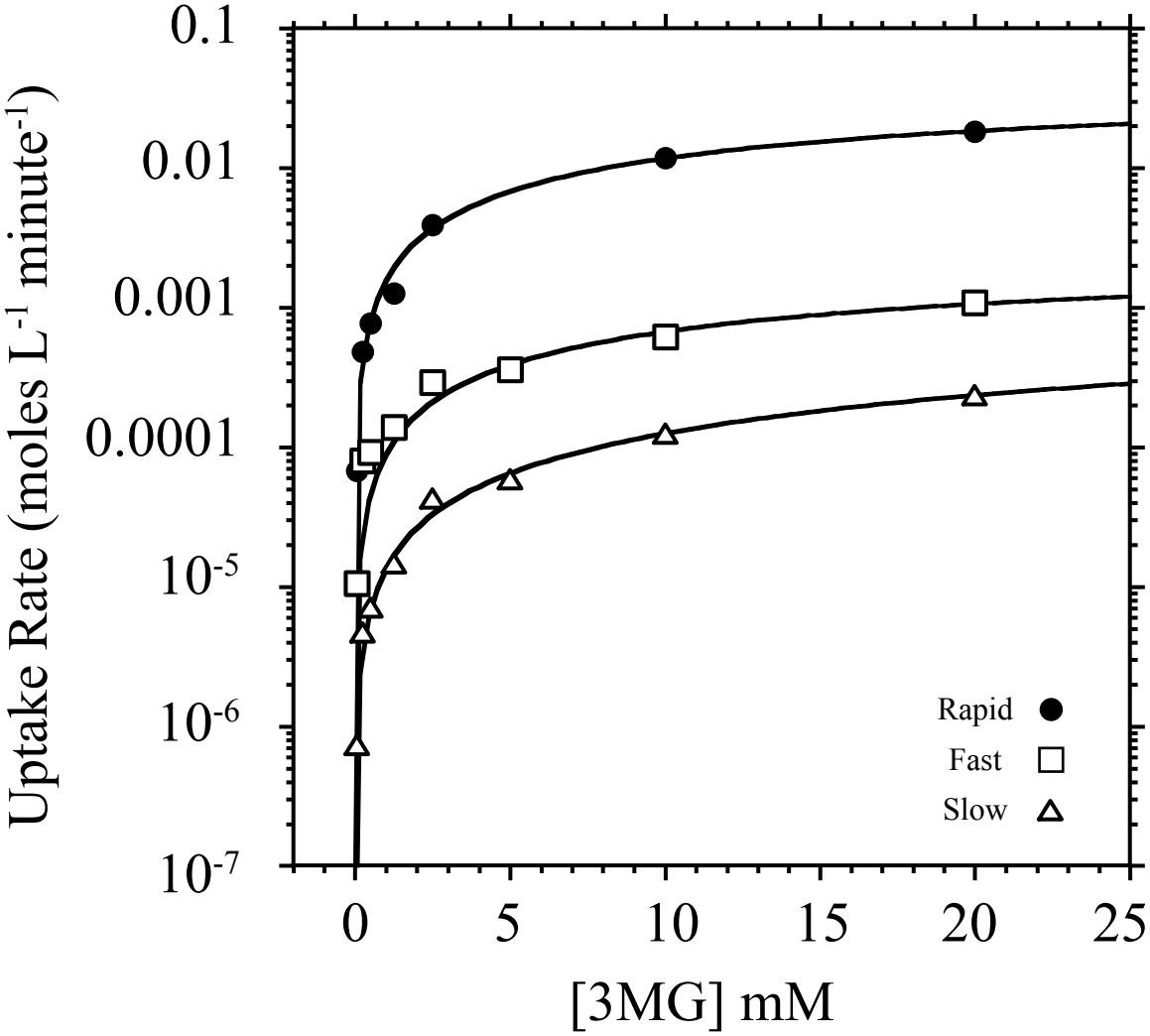
0.1
0.01
0.001
0.0001
10-5
10-6
10-7
Uptake Rate (moles L-1 minute-1)
0
5
10
15
20
25
[3MG] mM
Rapid
Fast
Slow

Figure 2.6

measured during rapid and fast phases and 6-fold higher when measured during the slow phase.

***3MG Concentration-Dependence of $k_r$*** Figure 2.7 summarizes the [3MG] dependence of $k_r$ and $C_r$. $k_r$ is independent of [3MG] but the size of the rapid compartment ($C_r$) increases in a saturable manner with [3MG]. The maximal size of $C_r$ is 1.94 nmol/mg membrane protein and the compartment is 50% filled at 340 μM 3MG.

***Is Sugar occluded by GLUT1?*** Previous equilibrium sugar binding experiments have demonstrated that 2 mol 3MG are bound per mol GLUT1 [131]. Only one of these sites is inhibited by CCB. In the present study, we considered the possibility that the rapid phase of net sugar uptake corresponds to CCB and phloretin-dependent sugar-occlusion within the translocation pathway. If correct, occlusion may be measurable in lysed (unsealed) ghosts and in IMPs as the ability of membranes to retain sugar following removal of unbound sugar by multiple ice-cold washes in the presence of the transport inhibitors CCB and phloretin.

Ghosts lysed in the presence of Mg or MgATP and incubated in lysis medium containing 3MG, retain more sugar upon washing in sugar-free stopper solution than do ghosts lysed in the absence of MgATP. MgATP containing ghosts, however, characteristically display higher absorbance at 417 nm and higher total protein amounts, despite ELISA analysis confirmation that all cells contain the same amount of GLUT1. It is possible, therefore,

**Figure 2.7 [3MG]-dependence of $k_r$ and $C_r$ at 4°C.** 3MG (50, 125, 250 and 625 μM) uptake was measured during the first 2 seconds following mixing. $k_r$ and $C_r$ were computed by nonlinear regression and are plotted as a function of [3MG]. **A** Dependence of $k_r$ on 3MG. Ordinate: $k_r$, per sec; Abscissa: [3MG] in μM. The results of two or more separate experiments made in triplicate are shown as mean ± SEM. The straight line drawn through the points was computed by nonlinear regression (assuming $k_r$ = intercept + constant* [3MG]) and weighted by the SEM of each data point. The results were: Intercept = (0.90 ± 0.12) per sec, constant = (0.00014 ± 0.00036) per μM per sec, $R^2$ = 0.074. **B** Dependence of $C_r$ on 3MG. Ordinate: [3MG] per pmol 3MG retained per 100 μg membrane protein (μM 3MG 100 μg membrane protein /pmol 3MG retained); Abscissa: [3MG] in μM. This is a Hanes-Woolf analysis of 3MG retention by red cell IMPs. The results of two or more separate experiments made in triplicate are shown as mean ± SEM. The straight line drawn through the points was computed by nonlinear regression (assuming $C_r$ = intercept + constant X [3MG]). The results are: Intercept = (1.74 ± 0.34) μM 3MG 100 μg membrane protein /pmol 3MG retained, constant = (0.0051 ± 0.0009) μM 3MG 100 μg protein per pmol 3MG retained, $R^2$ = 0.953.

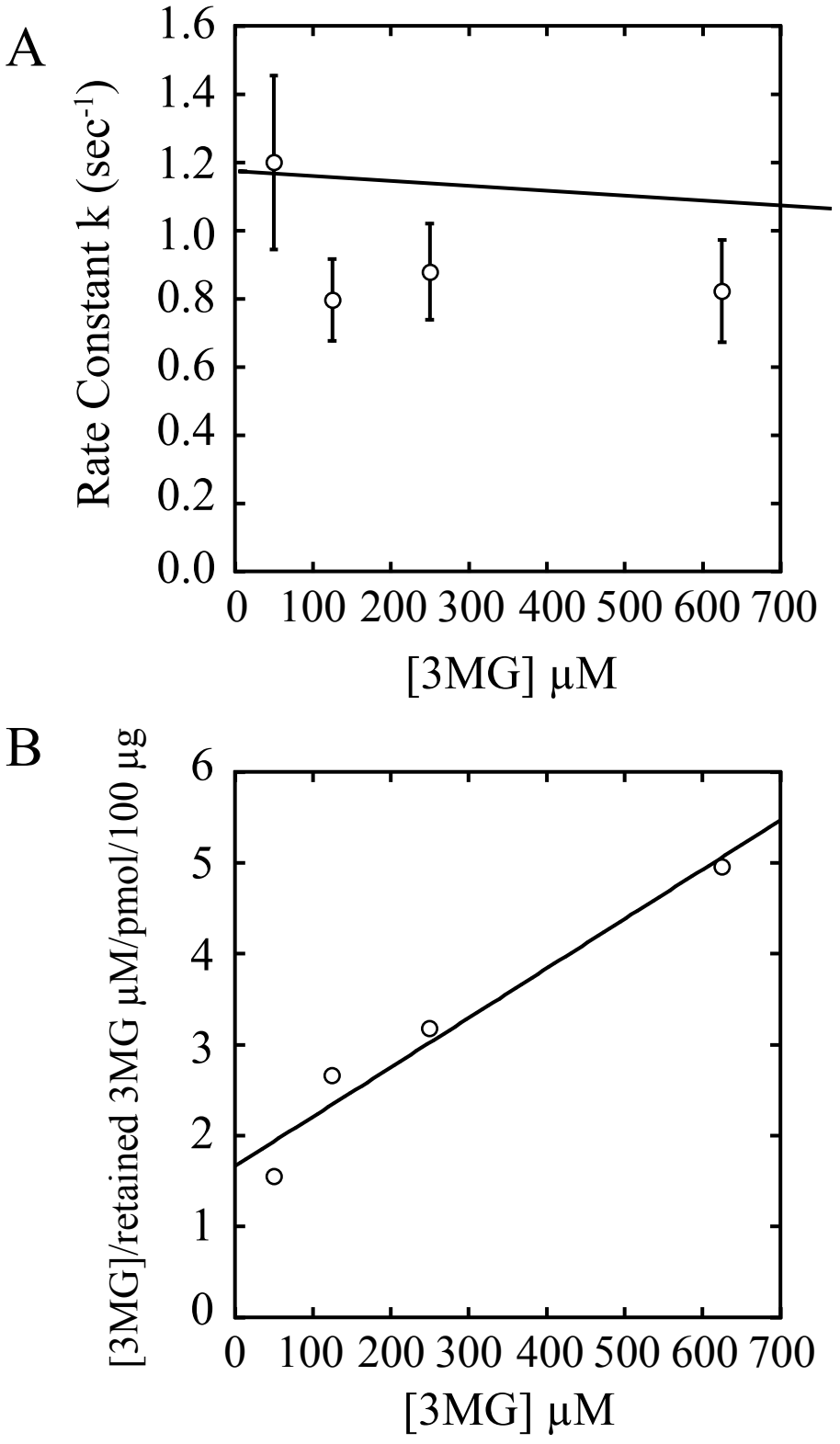
A
Rate Constant k (sec-1)
1.6
1.4
1.2
1.0
0.8
0.6
0.4
0.2
0.0
0 100 200 300 400 500 600 700
[3MG] µM
B
[3MG]/retained 3MG µM/pmol/100 µg
6
5
4
3
2
1
0
0 100 200 300 400 500 600 700
[3MG] µM

Figure 2.7

that this effect is due to decreased lysis efficiency in the presence of MgATP. To avoid this pitfall, sugar occlusion experiments were repeated using IMPs. These membranes are enriched in GLUT1 content, are osmotically inactive and both cytosolic and extracellular GLUT1 domains are quantitatively accessible to peptide-directed IgGs [84,142]. This confirms that IMPs do not form sealed proteoliposomes under these conditions. As with ghost membranes, the presence of transport inhibitors in the wash solution promotes sugar retention by IMPs (Figure 2.8).

GLUT1 digestion by intracellular trypsin is known to inhibit red cell sugar transport [143]. We hypothesized that trypsin would also inhibit 3MG occlusion by RBC IMPs due to proteolytic modification of sugar and inhibitor binding sites. 3MG retention at 4°C by native and trypsinized IMPs are not significantly different (Figure 2.8A). CCB binding by IMPs is not significantly altered by trypsinization (control: $B_{max}$ = 0.72 ± 0.19 nmol/mg membrane protein, $K_{d(app)}$ = 72 ± 30 nM; trypsin: $B_{max}$ = 1.01 ± 0.25 nmol/mg membrane protein, $K_{d(app)}$ = 177 ± 55 nM). A second round of exposure of control and trypsin treated IMPs to conditions that disrupt salt-bridges (alkaline wash medium) does not significantly diminish CCB binding to IMPs. Immunoblot analysis of IMPs using GLUT1 carboxy-terminal peptide-directed Abs (C-Abs) confirms that trypsin quantitatively cleaves GLUT1 carboxy-terminal domains (not shown).

Sugar retention appears to be enhanced by stopper solutions in trypsinized cells *versus* control cells. Retention measurements made using radiolabeled L-glucose (a nonreactive

**Figure 2.8 3MG Sugar Retention. (A)** 3-*O*-methylglucose retention by red cell integral membrane proteins at 4°C after arresting equilibrium reactions (50 μM 3MG or 50 μM L-glucose plus 100 μg IMPs) with buffer or buffer plus transport inhibitors. *Ordinate*: sugar retention measured in mol sugar per 100 μg membrane protein. Abscissa: equilibrium transport reaction stop conditions. In control non-trypsin treated cells (solid bar), stopping the reaction with complete CCB/Phloretin quench solution, results in the statistically significant increase of 3.3 pmol 3MG retained versus stopping the reaction with kaline buffer. In trypsin-treated IMPs (dashed bar), stopping the reaction with complete quench, CCB, and phloretin, results in the statistically significant increase of 4.4, 2.3, and 3.3 pmol of 3MG retained versus stopping the reaction with kaline buffer. Trypsinized membranes retain 3MG more effectively than do control membranes. L-Glucose retention ± quench (CCB and phloretin) were not significantly different from 3MG in the absence of quench. **B**. Quantitative comparison of 50 μM 3-*O*-methylglucose uptake by red cells and retention by red cell integral membrane proteins at 4°C. *Ordinate*: sugar uptake by red cells or retention measured in mol sugar per 100 μg membrane protein. Abscissa: time in minutes. The open circles show the time course of 3MG uptake by cells. The curve drawn through the points is a single exponential with the following constants: $C_r$ = (22.6 ± 8) pmol/100 μg protein; $k_r$ = 0.5 ± 0.2 per sec. The open bar represents the equilibrium (±SEM) 3MG retention space of IMPs when quenched with CCB and phloretin. The filled bar represents the equilibrium (±SEM) 3MG retention space of IMPs when quenched with inhibitor-free buffer.

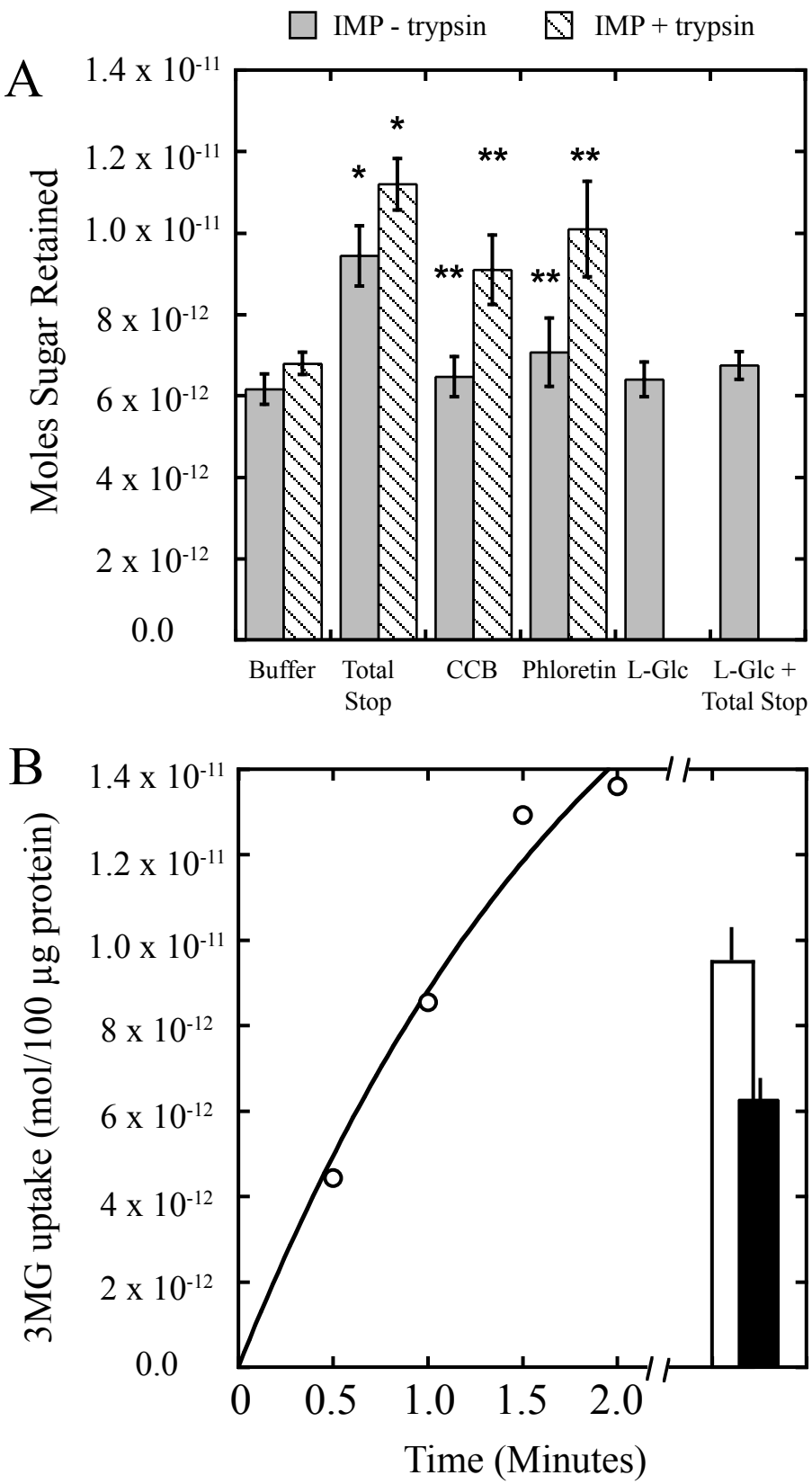
IMP - trypsin
IMP + trypsin
A
Moles Sugar Retained
1.4 x 10-11
1.2 x 10-11
1.0 x 10-11
8 x 10-12
6 x 10-12
4 x 10-12
2 x 10-12
0.0
*
*
**
**
**
Buffer
Total Stop
CCB
Phloretin
L-Glc
L-Glc + Total Stop
B
3MG uptake (mol/100 µg protein)
1.4 x 10-11
1.2 x 10-11
1.0 x 10-11
8 x 10-12
6 x 10-12
4 x 10-12
2 x 10-12
0.0
0
0.5
1.0
1.5
2.0
Time (Minutes)

Figure 2.8

substrate) indicate no enhancement of sugar retention in the presence of CCB and phloretin. L-glucose retention by IMPs is quantitatively indistinguishable from 3MG retention in the absence of CCB and phloretin (Figure 2.8A). These observations suggest that CCB and phloretin-dependent 3MG retention is a GLUT1-mediated event. Figure 2.8B compares the amount of 3MG retained by IMPs (± quench) to the rapid time course of 50 μM 3MG uptake by red cells at 4°C.

## *DISCUSSION*

***The Three Sequential Phases of Glucose Transport*** The experiments presented in this study indicate that monosaccharide import by erythrocytes is comprised of at least three phases. Multiphasic uptake is consistent with two possibilities. 1) There are three distinct populations of red cells characterized by different sizes or by different GLUT1 content. 2) There is a single cell population containing three serial compartments through which a sugar molecule must pass to equilibrate with total cellular space.

Several observations argue against the first hypothesis. These include: 1) Rejection of multiple cell sizes by the observation of monophasic 3MG uptake in cells when transport is inhibited by CCB (Figure 2.4A and [121]); 2) The extreme range of cell sizes (0.1 nm - 3.5 μm radii, see Results) that would be necessary to explain the findings. 3) Monophasic sugar exit from red cells over time courses corresponding to the fast and slow phases of uptake [[121,144,145]; Leitch and Carruthers, unpublished]. The latter observation

excludes the possibility that some red cells possess greater sugar transport capacity than other cells in the same population. We therefore conclude that the three phases of protein-mediated sugar import correspond to three processes that occur sequentially.

***What are the Three Measurable Glucose Transport Phases?*** Rapid, fast, and slow phases of 3MG uptake by red cells are retained in red cell ghosts. This indicates that all three phases are associated with the red cell membrane and are independent of sugar interaction with cytoplasmic proteins. This does not exclude the possibility that 3MG interacts with other membrane associated proteins following release from the glucose transporter.

***The rapid phase*** The 3MG uptake experiments presented in Figures 2.2 and 2.3 show that all phases of sugar translocation are temperature-sensitive. The high activation energy of the rapid phase indicates that this phase presents the greatest energy barrier to sugar import. Each transport phase is inhibited by specific inhibitors of GLUT1-mediated sugar transport. This result is expected if transport proceeds through serial steps and all three steps are sensitive to inhibitor. The CCB and phloretin-dependent 3MG space "occluded" in or retained by unsealed red cell ghosts and by integral membrane protein suspensions is quantitatively most similar to the smallest and most rapid phase of sugar uptake by cells. The sugar concentration dependence of the size of this phase indicates simple, saturable kinetics with a 3MG capacity of 1.94 nmol/mg membrane protein and $K_{d(app)}$ = 340 μM. This sugar binding capacity is indistinguishable from the sugar-inhibitable CCB binding capacity of human red cells (0.9 - 1.5 nmol/mg membrane protein

[131,146]) but is somewhat greater than the measured 3MG retention of red cell membrane integral membrane proteins at 50 μM 3MG (see Figure 2.8B).

The time-course of the rapid phase of 50 μM 3MG uptake at 4°C extrapolates to an equilibrium 3MG space of 22.6 ± 8.1 pmol 3MG per 100 μg membrane protein. The quench-dependent 3MG retention space of IMPs at 50 μM 3MG is 3.2 ± 1.3 pmol per 100 μg protein. Assuming the relative GLUT1 content of IMPs is 1.67-fold greater than that of intact red cell membranes and that the rapid phase of uptake and 3MG retention by membranes represent the same process, this represents a retention efficiency of 10%. Low efficiency sugar retention could result from two factors: 1) In red cell experiments, sugar associated with the rapid phase of uptake is released into the wash-inaccessible, intracellular water whereas in experiments with IMPs, the water content of the entire suspension is exchanged during washes; 2) The transient nature of carrier interaction with the quenching agents (CCB and phloretin) may lead to loss of carrier-sequestered sugars. CCB has an average dwell time on the e1 site of approximately 1 sec at 4-10°C ($1/k_{off}$; [83,147]). While equivalent data do not exist for phloretin interaction with the e2 site, $K_{i(app)}$ for phloretin inhibition of GLUT1 is approximately 10-fold greater than $K_{i(app)}$ for CCB inhibition of transport [136] suggesting that $k_{off}$ for phloretin dissociation from the e2.phloretin complex may be even greater than $k_{off}$ for CCB dissociation from e1.CCB. The lifetime of the rapid phase of 3MG import (0.3 - 1 second at 4°C) is similar to the

CCB dwell time on the carrier. It is probable, therefore, that a significant fraction of the sequestered 3MG is lost during multiple washes in the presence of CCB and phloretin.

$k_r$ is independent of [3MG] (Figure 2.7A) suggesting that this step does not represent the second order process of sugar binding to GLUT1 in which $k_r$ would be expected increase linearly with [3MG] [83]. We therefore propose that the rapid phase represents a conformational change subsequent to and promoted by 3MG binding to e2. This conclusion is also supported by estimates of the second order encounter rate constant for 3MG interaction with GLUT1 if the rapid phase of import were to represent the second-order reaction between 3MG and GLUT1. If this were true, the pseudo-first order rate constant ($k_r$) for this interaction at fixed [GLUT1] is given [83] by

$$k_r = k_{off} + k_e\,[3MG]$$

where the rate constants $k_{off}$ and $k_e$ describe the reaction:

$$\text{GluT1} + 3\text{MG} \underset{k_{off}}{\overset{k_e}{\rightleftharpoons}} \text{GluT1.3MG}$$

$k_e$ is therefore obtained as:

$$k_e = \frac{k_r - k_{off}}{[3MG]}$$

$k_{off}$ for simple carrier-mediated transport is estimated [2] as

$$k_{off} = \frac{V_{\max}^{exchange}}{[GLUT1]}$$

where $V_{\max}^{exchange}$ is the $V_{max}$ for unidirectional sugar fluxes when $[3MG]_i = [3MG]_o$. Previous measurements of $V_{\max}^{exchange}$ permit calculation of $k_{off}$ as 40 $s^{-1}$ at 4ºC and 275 $s^{-1}$ at 22ºC [43]. Measurements of $k_r$ reported here are 1 $s^{-1}$ at 4ºC and 70 $s^{-1}$ at 22ºC (Table 2.1). According to this analysis, $k_e$ would have a negative value if $k_r$ represents the second order interaction between 3MG and GLUT1. This is a physical impossibility. The pseudo first order rate constant describing 3MG interaction with GLUT1 must be at least 4 to 40-fold greater than the first-order rate constants measured for the rapid phase of transport.

We suggest that the occluded 3MG space and the rapid phase of 3MG uptake by cells represent sugar occlusion within the sugar translocation pathway. The occluded 3MG space cannot be the previously reported ATP-dependent 3MG binding to GLUT1 [131] because that reaction is inhibited by CCB and phloretin, is rapidly reversible and bound 3MG would therefore be lost during multiple washes to remove unbound sugars.

***The fast and slow phases*** The fast and slow phases have lower temperature sensitivities than the rapid phase of net import. The activation energy for GLUT1-mediated glucose transport in reconstituted proteoliposomes ranges between 5.1 and 23.7 kcal.$mole^{-1}$ (specific values are lipid composition-dependent; [148]). In human red cells, the activation energy for glucose transport is 18.4 kcal.$mole^{-1}$ [149,150]. This latter value

was obtained by measuring transport over intervals that correspond to the fast phase reported in the present study where $E_A$ is 20.9±5.9 kcal.mole$^{-1}$.

Previous studies from this laboratory have demonstrated the existence of a cytosolic 3MG occlusion mechanism in which an additional sugar binding site within the glucose transporter is exposed upon GLUT1 interaction with ATP [131]. We propose that this binding phenomenon is associated with the fast phase of transport reported in the present study because 3MG equilibrium binding to the cytosolic site and the fractional size of the fast phase of 3MG uptake by red cells and red cell ghosts are both increased by cytoplasmic ATP (see Figure 2.5, Table 2.1 and [131]). We propose that the slow phase of net sugar import corresponds to release of bound sugar from the GLUT1 cytoplasmic sugar binding site into bulk cytosol. It is also possible that the slow phase represents noncovalent 3MG interactions with red blood cell membrane proteins. Interactions with bulk cytosolic proteins are ruled out because the kinetics of slow compartment filling and the relative sizes of fast and slow compartments are retained in red cell ghosts.

***Model for Glucose Transport*** Resolution of the crystal structures of *E. coli* LacY and GlpT transport proteins in the e1 (inward-facing) conformation has prompted the development of a model for lactose-proton symport [33,35]. The model is a physical reinterpretation of the theoretical simple carrier, as proposed by Stein [2]. The monomeric transporter first presents an import (e2) site. Upon lactose and proton binding, LacY undergoes a conformational change to the export (e1) configuration where sugar

and proton are subsequently released. This mechanism presumes an intermediate conformation between e2 and e1 isomers in which the bound substrates are transiently sequestered within the closed translocation pathway and are neither accessible to interstitium nor cytosol. This translocation intermediate may resemble the occluded K and Na states of the Na,K-ATPase (an e1e2ATPase) in which Na-dependent, ATP-hydrolysis and K-binding induced dephosphorylation promote conformational changes that temporarily occlude bound substrate from the aqueous milieu [151,152].

As with these preceding transport systems, the glucose transporter undergoes an analogous e2↔e1 conformational change. This change, however, does not require ATP hydrolysis and can occur (although more slowly) in the absence of bound substrate. Sugar transport through a GLUT1 subunit may proceed as follows (see Figure 2.9): 1) sugar binds to the e2 or external configuration to form eS2; 2) this event promotes a conformational change forming the translocation intermediate e(S); 3) when the transporter proceeds through e(S) to the eS1 state, the sugar dissociates into an internal cavity formed by GLUT1 cytosolic domains where it may bind to an ATP-dependent, noncatalytic sugar binding site and thus remain within the confines of the protein; 4) the sugar is released from the noncatalytic binding site back into the internal cavity or is released directly from eS1 into the cavity from which it diffuses (slowly in the presence of ATP) into bulk cytosol. We propose that the present study has examined phases two, three, and four while phase one, the initial binding step, is refractory to the specific

**Figure 2.9 A King-Altman scheme for sugar transport.** The transporter, e, can exist in only one of 3 states in the absence of substrate (S) and ligands (I). e1 is the inward configuration of the carrier that presents a sugar binding site to cytosol. e2 is the outward configuration of the carrier that presents a sugar binding site to interstitium. The carrier isomerizes between e1 and e2 states via the e( ) conformer. The e( ) conformer can bind extracellular (I2) and intracellular (I1) inhibitors simultaneously. e2 can interact only with extracellular inhibitor I2 or extracellular sugar S2. e1 can interact only with intracellular inhibitor I1 or intracellular sugar S1. eS1 isomerizes to eS2 via the occluded e(S) complex in which the sugar is trapped within the translocation pathway. As with e( ), e(S) can interact with I1 and I2 simultaneously.

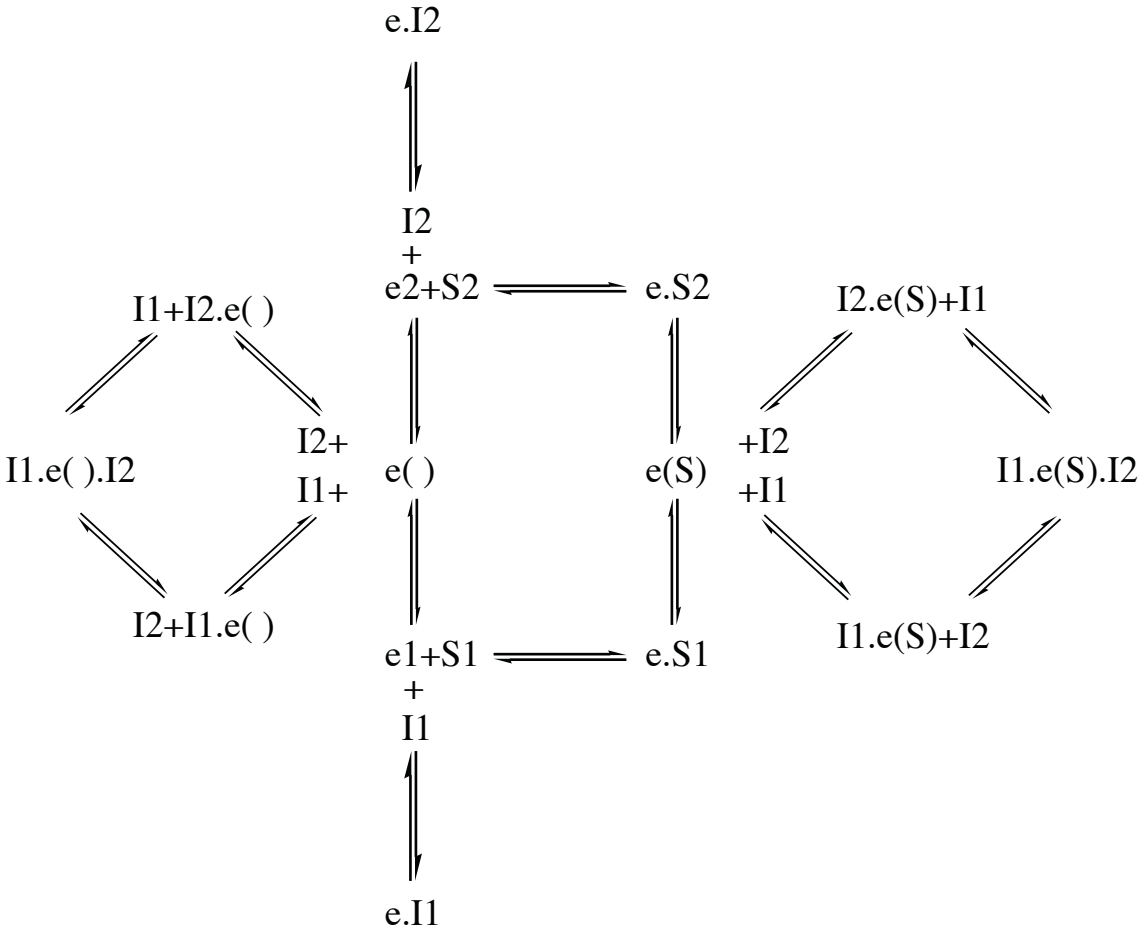
e.I2
I2
+
e2+S2
e.S2
I1+I2.e( )
I2.e(S)+I1
I1.e( ).I2
I2+
I1+
e( )
e(S)
+I2
+I1
I1.e(S).I2
I2+I1.e( )
I1.e(S)+I2
e1+S1
e.S1
+
I1
e.I1

Figure 2.9

techniques of measurement used. It should be noted that this hypothesis predicts that ATP removal (e.g. formation of ghosts ± $ATP_i$) should reduce the size of the fast compartment ($C_f$) and increase the rate of release of sugar from the fast to slow compartments (reduce $k_s$). The former prediction is observed (Figure 2.5 and Table 2.1) but the latter is not – in part, perhaps due to lack of precision in data. Future studies must address this prediction more closely.

If the rapid phase does indeed represent the formation of an e(S) state in which the sugar is occluded within the sugar transport pathway, this would mean that e(S) is capable of binding CCB and/or phloretin/extracellular maltose simultaneously. Indeed it is possible to measure e(S) only in the presence of these inhibitors. A fundamental tenet of the simple carrier hypothesis is that CCB and maltose cannot bind to a carrier that contains a complexed transport substrate [118]. However, we do know that GLUT1 does react simultaneously with CCB and phloretin [118]. If the simple carrier hypothesis is correct, the ability of e(S) to bind phloretin and CCB would explain the experimental observations. A recent theoretical model of GLUT1 structure [64] suggests that intracellular CCB and extracellular phloretin docking sites may be simultaneously presented by each GLUT1 subunit. A second possibility is that in multimeric GLUT1, 3MG can be occluded within one subunit while the second subunit is locked into a dead-end conformation with CCB or phloretin. This hypothesis suggests a molar stoichiometry of 1 mol CCB bound per mol e(S) - an assertion consistent with the results of this study.

It would be interesting to determine the effects of intracellular sugar on all three phases of unidirectional sugar uptake. Under infinite-trans uptake conditions (intracellular unlabelled [sugar] is high, extracellular radiolabeled sugar levels are varied), the simple carrier hypothesis predicts that more e2 sites are available for interaction with extracellular sugar (S1 drives the carrier back to e2 via the eS1→e(S)→eS2 export translocation pathway which is faster than the e1→e( )→e2 relaxation pathway; Figure 2.9). The simple carrier hypothesis, therefore, predicts that S1 will increase the amount of e(S) but not the rate of e(S) formation. The tetramer model predicts that the amount of e(S) formed is independent of S1 but that the rate of formation is increased by S1 due to allosteric interactions between subunits. In two exploratory experiments measuring uptake of 50 μM 3MG in intact cells, we observe that 1 mM unlabelled intracellular 3MG increases $C_{rapid}$ from 0.031±0.009 to 0.060±0.013 while $k_{rapid}$ is unchanged (68 ± 11 per sec). This suggests that the former rather than the latter model may be more consistent with the data. $k_{fast}$ was also increased from 0.043 ± 0.004 to 0.100 ± 0.008 per sec by $3MG_i$. This result is expected for simple competitive inhibition of a binding process ($k_{obs} = k_{off} + k_{on}([3MG_i] + [^{14}C\text{-}3MG_i])$ and is consistent with the hypothesis that imported radiolabeled extracellular sugar and unlabelled intracellular sugar compete for binding at a GLUT1 cytoplasmic site. More detailed analyses must be performed to confirm these findings and to examine the effects of intracellular ATP on these processes.

***Compartment Sizes*** Most of the experiments reported in the present study were carried out at [3MG] = 50 μM. It is useful to consider the compartment sizes that would result if the proposed transport mechanism were correct. The starting assumptions are as follows: 1) The free water space of a red cell is 60 fL [121]; 2) The GLUT1 content of a red cell is 600,000 copies per cell [131]; 3) $K_{d(app)}$ for 3MG binding to e2 is 340 μM (Figure 2.7B); 4) The number of ATP-dependent, noncatalytic 3MG binding sites in the "cage" is ***n***; 5) $K_{d(app)}$ for 3MG binding to these noncatalytic sites is extremely low and the sites are always occupied (1 molecule in the LacY e1 cavity ($1.5 \times 10^{-24}$ L; [33,35]) would produce a [3MG] of 1.1 M). With these starting assumptions, the relative amounts of cellular 3MG in the forms of e(S) (rapid compartment), $eS_{cage}$ (fast compartment) and cell water (slow compartment) at equilibrium are 3.5 : 24.1 : 72.4 (when ***n*** = 1); 2.8 : 38.9 : 58.3 (when ***n*** = 2) and 2.3 : 48.8 : 48.8 (when ***n*** = 3). These numbers are generally consistent with the available data and suggest that ***n*** lies between 2 and 3. The LacY e1 cavity is large enough to hold as many as 3-5 hydrated glucose molecules [33]. The slow rate of loss of sugar from the cage to cytosol may reflect the very significant probability of re-association of sugar in the cage with the noncatalytic binding sites. As [3MG] is increased, the relative contribution of $C_{rapid}$ and $C_{fast}$ to total cellular 3MG space should fall significantly. This has been observed previously [121].

## *CONCLUSIONS*

The present study demonstrates that the time-course of 3MG uptake at 4-22°C by human red blood cells is comprised of 3 sequential phases - rapid, fast and slow. Each phase is inhibited by carrier-mediated glucose transport inhibitors. The rapid phase is more strongly temperature dependent than the fast and slow phases. The rapid phase does not represent the reaction between sugar and carrier to form a carrier-sugar complex. Rather, it may represent the subsequent conversion of the carrier-substrate complex to the intermediate form e(S) where the bound sugar is occluded within the translocation pathway. This occluded form of carrier can be isolated (with 10% efficiency) in the presence of transport inhibitors thus rendering the occluded sugar inaccessible to interstitium and cytosol.

# CHAPTER III

## HUMAN ERYTHROCYTE GLUCOSE TRANSPORT PROTEIN TOPOLOGY AND HELIX PACKING

This chapter will be submitted as a manuscript in April of 2007.

**This work was supported by NIH grants DK 36081 and DK 44888 and by ADA grant ADA 1-06-IN-04 (Gail Patrick Innovation Award supported by a generous gift from the Estate of Gail Patrick)**

***ABSTRACT***

We present a study that examines whether the emergent bacterial MFS helical folding pattern adequately describes the structural organization of the mammalian facilitative glucose transporter GLUT1. Proteolytic enzymes trypsin and α-chymotrypsin and lysine specific covalent probes were used to examine GLUT1 membrane topology and accessibility of transmembrane α-helices to solvent. Peptide fragments were characterized by release into aqueous solvent or retention within the membrane following proteolysis and incubation with ligands. Unique elution conditions for each transmembrane α-helix provided relative hydrophobicity values. Putative pore-forming α-helices (1, 2, 4, 5, 7, 8, 10, and 11) are accessible to proteolysis and release peptide fragments into the aqueous solvent. The remaining α-helices (3, 6, 9, and 12) are completely resistant to proteolysis and do not interact with the aqueous environment. The lipid-embedded α-helices are significantly more hydrophobic than the pore lining α-helices. Transmembrane domain 1 is released from the membrane following trypsin proteolysis and cytochalasin B binding to the transporter promotes transmembrane domain 8 release into the aqueous environment. These results confirm that amphipathic α-helices line the translocation pore and promote interactions with the aqueous environment and substrate. The relative aqueous accessibility of each α-helix is fundamental to glucose-induced GLUT1 conformational changes and glucose translocation.

## *INTRODUCTION*

Major Facilitator Superfamily (MFS) transport proteins mediate passive and secondary active transmembrane transport of nutrients, drugs, amino acids, ions, neurotransmitters, and other molecules in organisms spanning bacteria to eukaryotes [56]. Of the more than 1,000 proteins belonging to the MFS classification, the facilitative glucose transporter family (GLUT1-12 and HMIT) is responsible for monosaccharide uniport [22,23]. GLUT proteins are expressed in a tissue- and organ-system specific manner allowing them to meet the metabolic needs of each cell type. For example, GLUT2 is found in the liver [25], GLUT3 is expressed in neuronal cells [19], and insulin-sensitive GLUT4 is found in muscle and adipose tissue [13]. GLUT1 is found in many tissues throughout the body but is expressed most highly in the circulatory system [23,153] and at blood-tissue barriers [31,154]. Glucose transfer at the blood-brain barrier (an epithelium comprising capillary endothelial cells connected by tight junctions) is mediated by GLUT1, which catalyzes transcellular glucose transport.

*Mueckler et al.* cloned GLUT1 from HepG2 cells in 1985 [24], more than thirty years after Widdas initially hypothesized that a glucose carrier protein existed [38]. GLUT1 primary sequence contains 492 amino acids, has a molecular weight of 54,117 Daltons, and contains a single, heterologous, exofacial N-linked glycosylation site (NQT) at asparagine 45. GLUT1 sequence indicates that over 60% of the residues are hydrophobic and Fourier transform infrared spectroscopy studies show that GLUT1 peptides retained by membranes following proteolysis are predominantly $\alpha$-helical in nature [60].

Hydropathy analysis [155], scanning glycosylation mutagenesis [45], proteolysis, antibody binding, and covalent modification studies indicate that GLUT1 contains 12 transmembrane (TM) α-helices, intracellular N- and C-termini, and a series of extra- and intracellular loops that connect each TM domain [61]. Amphipathic α-helices are proposed to form an aqueous translocation pathway through which glucose crosses the plasma membrane and enters the cell [64,74].

The structural basis of stereoselective substrate translocation across the plasma membrane, as reviewed by *Dahl et al*., has been greatly aided by the recent low and high-resolution crystal structures of membrane transport proteins [156]. Of particular interest are the structures solved for the lactose permease ((LacY [33]); a galactoside/proton symporter), the glycerol-3-phosphate antiporter (GlpT [35]) and a multidrug transporter (EmrD; proton/drug antiporter [39]) - each protein being native to and crystallized from *Escherichia coli*. An electronic density map for the oxalate transporter (OxlT; formate/oxalate antiporter [34]) of *Oxalobacter formigens* is also available. Although there is little sequence similarity between these four structures, they demonstrate a common folding pattern and helix arrangement that may be characteristic of all MFS transport proteins.

Mammalian membrane transporters, such as GLUT1, remain refractory to three-dimensional crystallization. The flexible, dynamic, and amphipathic nature of mammalian membrane carrier proteins, coupled with their low expression *in vivo* contribute to this complexity [7,156]. Transporter proteins with unsolved structures can

be homology modeled using the template provided by a crystallized homolog [156]. Models change as new and more homologous crystal structures are solved. In the past, GLUT proteins have been modeled using aquaporin [157], MscL, OxlT [158], and LacY [159] templates and low resolution modeling programs [160]. These attempts, however, have required manual manipulation and fitting to account for the differences between template and GLUT1 sequence alignments, number of transmembrane domains, and native folds.

*Salas-Burgos et al*. and *Holyoake et al*. have recently developed a three-dimensional GLUT1 model using the GlpT template [63,64]. This model fits GLUT1 to the emergent MFS helical fold and uses biochemical data to support the helix packing arrangement. Mueckler and colleagues have employed cysteine-scanning mutagenesis in a *Xenopus laevis* expression system to systematically examine the accessibility of each TM helix in accordance with this model [40,48-50,68-70,72,74]. There are, of course, striking differences between the GlpT template and the GLUT1 modeling target. GlpT is a secondary active phosphate antiporter, while GLUT1 is a passive glucose uniporter. GlpT and GLUT1 share less than 20% sequence similarity, and often times the larger extra- and intracellular loops found in mammalian proteins can complicate sequence alignment [156]. The most practical use of homology modeling, therefore, lies in cues it provides for devising further biochemical experiments to assess and examine the protein structure-function relationship.

We present a study that examines the accessibility of transmembrane α-helices within the native, membrane-resident GLUT1 protein using reverse phase high performance liquid chromatography in-line with electrospray ionization mass spectrometry (RP-HPLC-ESI-MS/MS). We characterize the relative accessibility of TM helices 1-12 to proteolytic digestion by water-soluble enzymes trypsin and α-chymotrypsin. We assess lysine residue topology by analysis of accessibility to covalent modification. We examine how proteolysis affects peptide partitioning between the aqueous environment and membrane bilayer, and we identify a TM α-helix that is released from the lipid bilayer in response to incubation with a transport inhibitor. We calculate the relative hydrophobicity of individual TM α-helices based upon their unique RP-HPLC elution profile. These results provide new insights into the physical properties of GLUT1 transmembrane α-helices and how they contribute to glucose transport function.

## *MATERIALS AND METHODS*

***Materials*** Fresh, de-identified human blood was purchased from Biological Specialties Corporation (Colmar, PA). Protein assays, Pro Blue coomassie stain, Sulfo-NHS-LC-Biotin and Supersignal chemiluminescence kits were from Pierce (Rockford, IL). Glycerol-free endoglycosidase peptide-N-glycosidase F (PNGaseF) was purchased from New England Biolabs (Ipswich, MA). Nitrocellulose and Immobilon-P were purchased from Fisher Scientific (Hampton, NH). Purified rabbit IgGs raised against a synthetic cytoplasmic carboxyl-terminal peptide of human GLUT1 (C-Ab, residues 480-492) were

obtained from Animal Pharm Services, Inc. (Healdsburg, CA). All other reagents were purchased from Sigma-Aldrich (St. Louis, MO).

***Solutions*** Saline consisted of 150 mM NaCl, 10 mM Tris-HCL, and 0.5 mM EDTA, pH 7.4. Lysis medium contained 10 mM Tris-HCl and 0.2 mM EDTA, pH 7.2. Stripping solution contained 2 mM EDTA, 15.2 mM NaOH, pH 12. Tris medium contained 50 mM Tris-HCL, pH 7.4. Kaline consisted of 150 mM KCl, 5 mM HEPES, 4 mM EGTA, and 5 mM $MgCl_2$. Phosphate-buffered saline containing Tween (PBS-T) comprised 140 mM NaCl, 10 mM $Na_2HPO_4$, 3.4 mM KCl, 1.84 mM $KH_2PO_4$, 0.1% Tween, pH 7.3.

***Human erythrocyte membranes and glucose transport protein*** Glucose transporter and endogenous lipids were purified from human erythrocyte membranes in the absence of reductant as described previously [84,161]. This produces osmotically inactive, unsealed GLUT1 proteoliposomes [83], which contain (by protein mass) 90% GLUT1, 8% RhD protein, 2% nucleoside transporter (ENT1) and have a lipid:total protein mass ratio of 1:1 [86].

***GLUT1 Deglycosylation*** GLUT1 (50 µL 1 mg GLUT1/mL in kaline buffer) was incubated with 3 µL (1,500 activity units) PNGaseF for 1 hr at 37ºC.

***Gel Electrophoresis and Western Blotting*** GLUT1 protein was resolved on 8% polyacrylamide gels as described by Laemmli [162]. Immunoblot analysis using C-Ab (at 1:10,000 dilution) was as previously described [86].

***GLUT1 covalent modification*** GLUT1 (25-100 μg) was incubated with freshly dissolved EZ-Link-Sulfo-NHS-LC-Biotin (10 mM; pH 7.4, 4ºC) at GLUT1:covalent probe molar ratios ranging from 1:0.2 to 1:2,000 for 1 minute to 1,800 minutes. Reactions were quenched with 50 mM TrisHCl or glycine and membranes were sedimented and washed several times with additional quench. The final pellet was resuspended in appropriate media for follow-up analysis (PBS, 2% Triton-X-100 in PBS, or Kaline for ELISA, solid state precipitation ELISA, and digestion/HPLC ESI-MS, respectively).

***ELISA Assays*** Biotin incorporation was quantitated using enzyme-linked immunosorbent assays (ELISA). Since GLUT1 purification results in 10% protein contamination, GLUT1 was immuno-absorbed onto 96-well polystyrene plates pre-coated with C-Ab (200 μL of a 1:5,000 dilution for 300 minutes at 37°C, followed by a blocking step with 3% bovine serum albumin for 120 minutes at 37°C). Following biotinylation, labeled GLUT1 proteoliposomes were solubilized in 2% Triton X-100 in PBS (60 minutes at 4°C). Solubilized GLUT1 (200 μL per well, in triplicate) was added to the plate, incubated for 2 hr at 4ºC then washed and blocked in 3% BSA (+2% Triton-X-100). Horseradish peroxidase (HRP) conjugated streptavidin (1 μg/mL; 1 hour; 20°C) served as the reporting probe with product development measured as absorbance at 415 nm using a Benchmark Microplate Reader (BioRad).

***Preparation of Tryptic and α-Chymotryptic Digested GLUT1 Peptides*** Unmodified or pretreated GLUT1 reconstituted into proteoliposomes and resuspended in Kaline (0.5 mg/mL, 55 μL total reaction volume) was digested with trypsin or α-chymotrypsin at a

1:10 ratio (proteolytic enzyme:GLUT1, by mass) for 0 to 2 hours at 30°C. Peptides were either subjected to HPLC-ESI-MS/MS immediately or processed further. The digested sample was separated into aqueous and membrane fractions by centrifugation for 30 minutes at 4°C in Beckman Air-Driven Ultracentrifuge (≈ 200,000 x g). The supernatant was collected and subjected to HPLC-ESI-MS/MS or stored at -20°C to prevent further proteolytic digestion. The membrane fraction (trypsin-digested GLUT1 pellet) was resuspended in kaline buffer plus ligands (0.2% DMSO, 10 μM CCB or CCD, or 50 mM D-glucose or maltose) and subjected to a second round of sedimentation and aqueous fraction isolation for storage at -20°C or direct processing by HPLC-ESI-MS/MS.

***HPLC Separation of GLUT1 Peptides*** Peptides were subjected to HPLC separation prior to in-line electrospray ionization mass spectrometry. The digested mixture (25 μg GLUT1 in 50 μL kaline) was resolved by reverse phase chromatography [111] using a polystyrene divinylbenzene copolymer column (5 μm, 300 Å, 150 x 2.1 mm; PLRP-S, Polymer Labs (Amherst, MA)) at 40°C. Peptides were eluted using one of two gradients with different rates of conversion from solvent A (5% 1:1 (v/v) acetonitrile:isopropanol (ACN:IPA) in HPLC Grade water) to solvent B (1:1 (v/v) ACN/IPA); both solvents contained 0.1% formic acid 0.01% trifluoroacetic acid (TFA) [108,111]. Resolution of supernatant fractions was achieved by using: 15 minute equilibration in 98% solvent A and 2% solvent B followed by raising the percentage of solvent B to 10% over 3 minutes, 45% over 37 minutes, and 95% over 2 minutes, where it was held for 10 minutes prior to re-equilibration. Flow rate was 200 μL/min. The gradient for resolution of membrane fraction peptides required longer exposure to organic solvents: after 15 minutes of

exposure to 95% solvent A and 5% solvent B, the percentage of solvent B was raised to 20% over 4 minutes, 95% over 56 minutes, where it was subsequently held for 10 minutes prior to re-equilibration. Gradients were controlled with Janeiro II software and a Rheos 2000 micro LC/MS pump (Flux Instruments AG Basel, Switzerland) when using the Thermo-Fisher LCQ ESI-MS and using the X-Calibur control software and Thermo-Fisher surveyor MS pump when using an LTQ ESI-MS.

***Electrospray Ionization Mass Spectrometry*** ESI-MS analysis was performed using either a Thermo Fisher LCQ or LTQ electrospray ionization mass spectrometer. Operational parameters include positive ion mode, spray voltage, 4.5 kV; capillary temperature, 225°C; scan range *m/z* 400-2,000. The linear ion trap measures the *m/z* ratio of each peptide (creating an MS spectrum), and ions exceeding the threshold intensity are isolated. MS/MS fragments of isolated peptide species were produced in the ion trap by collision induced dissociation (CID) with inert helium gas at 35 V. Acquisition methods were created using X-Calibur (version 1.2). MS/MS spectra were identified using the Bioworks Sequest version 3.2 database search program against the human red blood cell proteome database compiled by *Kakhniashvili et al*. [27].

### *RESULTS*

All experiments were performed using purified GLUT1 proteoliposomes reconstituted with co-purified, native erythrocyte lipids. These proteoliposomes are unsealed and simultaneously expose endo- and exofacial GLUT1 domains to exogenous ligands, proteolytic enzymes, and antibodies [83,147]. All RP-HPLC-ESI-MS/MS results were

obtained following a two hour digestion (30°C) of GLUT1 proteoliposomes with either trypsin or α-chymotrypsin at a 1:10 enzyme to protein ratio (by mass). The entire sample of digested GLUT1 peptides was subjected to chromatography and mass spectrometry to identify all amino acid residues accessible to proteolytic enzymes. The digested sample was sedimented to separate membrane-associated peptides from peptides released into the aqueous environment (supernatant fraction). Resuspension of the membrane-associated region with GLUT1 ligands followed by a second round of sedimentation permits analysis of the released peptides that respond to GLUT1-ligand interactions. As our frame of reference, GLUT1 residues comprising individual transmembrane α-helices, intra- and extracellular loops, and the N- and C-termini were assigned using the homology model developed by *Salas-Burgos et al*. in which the GLUT1 primary sequence was threaded through the GlpT crystal structure template (Figure 3.1A) [64]. This model establishes three groups of transmembrane α-helices organized by putative location and function: those forming the aqueous translocation pathway (Group 1 (TMs 1, 4, 7, and 10) and Group 2 (TMs 2, 5, 8, and 11)) or those comprising the membrane-embedded scaffolding region (Group 3 (TMs 3, 6, 9, and 12); Figure 3.1B) [33,35].

***GLUT1 Accessibility to Proteolytic Enzymes*** GLUT1 contains 16 lysine and 20 arginine residues that are potential TPCK-trypsin proteolysis sites [155]. These residues are systematically spread throughout the protein within proposed intra- and extracellular loops, the N- and C-termini, and at the membrane-solvent interface as shown by the putative topology. Our findings indicate that 33 sites are accessible to trypsin cleavage

**Figure 3.1 Putative GLUT1 topology and MFS helix-packing model. (A)** Putative GLUT1 topology adapted from the GlpT homology based structure [64]. Several key properties should be noted. Group 1 TMs are highlighted in pink. Group 2 and Group 3 TMs are highlighted in blue and green respectively. Some helices that span the bilayer extend beyond the boundaries of the bilayer (shown by horizontal lines). The bilayer-embedded region of each membrane spanning helix (TMs 1 through 12) comprise amino acids 17-39, 64-86, 93-112, 120-141, 157-178, 187-207, 267-291, 305-325, 335-356, 362-385, 401-421 and 431-452 respectively. GLUT1 is heterogeneously glycosylated at Asn45. TMs 6 and 7 are linked by a large cytoplasmic loop (L6-7). The N- and C-termini are exposed to cytoplasm. **(B)** Putative helix packing arrangement viewed from the cytoplasmic surface. TMs are numbered and colored as in Figure 3.1A. The internal symmetry between N- and C-terminal halves of GLUT1 is evident from the helical tilts and may have resulted from a gene-duplication event [56]. Adapted from [33,35].

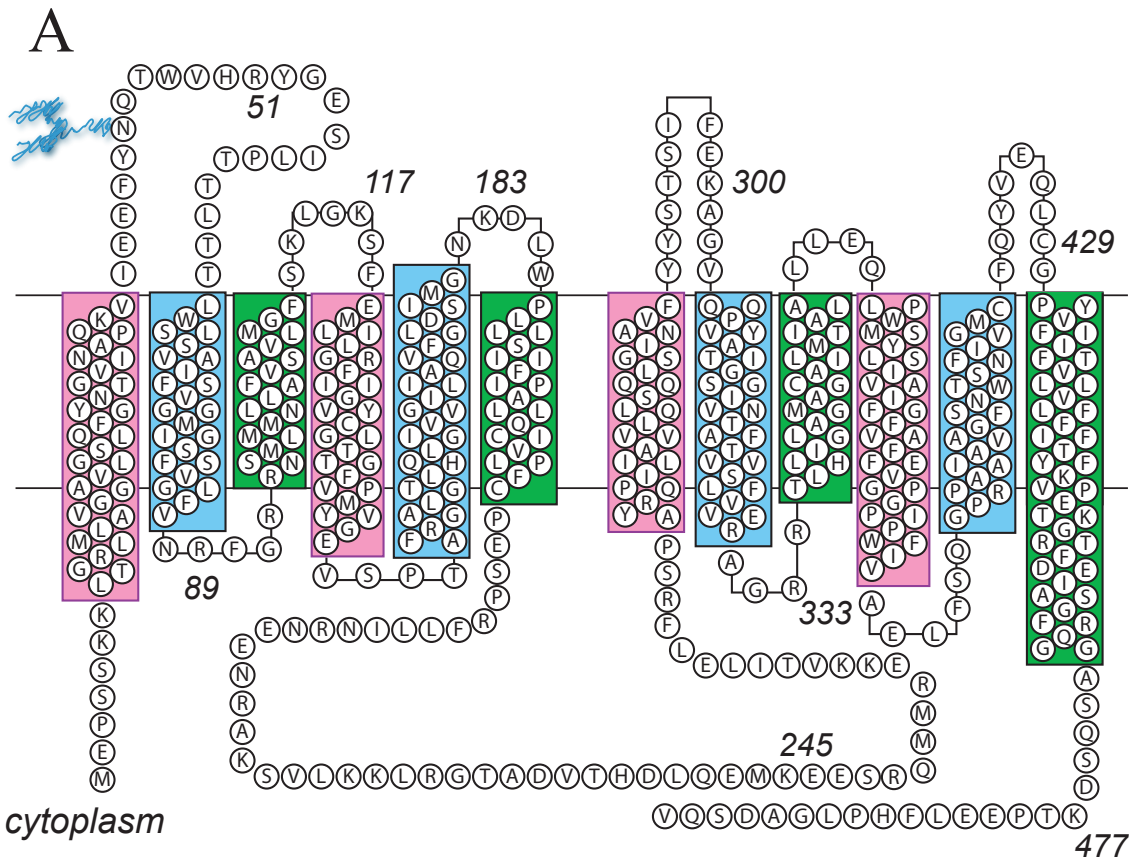
A
51
117
183
300
429
89
333
245
cytoplasm
477
B
C
N
1
2
3
4
5
6
7
8
9
10
11
12

Figure 3.1

(Figure 3.2A). Only R153 and K183, flanking TM5 and K451 at the C-terminal end of TM12 are inaccessible to trypsin digestion.

α-Chymotrypsin is a less specific protease, which we observe cleaves GLUT1, on a consistent and reproducible basis (as judged by the quality of MS/MS spectra), at the C-terminal end of phenylalanine, tyrosine, tryptophan, as well as leucine, alanine, methionine, and glutamic acid. These amino acid residues are found both in putative aqueous-accessible domains and in membrane-embedded protein domains. Although each putative transmembrane domain presents a minimum of 5 potential α-chymotrypsin cleavage sites, we detected variable levels of proteolysis (Figure 3.2B). All group 1 and 2 α-helices display at least one amino acid residue that is accessible to cleavage by α-chymotrypsin, whereas group 3 helices are completely resistant to proteolytic digestion.

Table 3.1 summarizes the results of GLUT1 proteolysis by α-helix classification and protein region. Overall, group 1 and group 2 α-helices demonstrate greater susceptibility to cleavage than group 3 α-helices (41% and 34% versus 2%, respectively). Group 1 TMs display the highest number of physically cleaved sites compared to group 2 and group 3 α-helices (15 to 10 to 1, respectively). The N- and C-termini, L1-2, and L6-7, which according to the model represent the largest regions of unstructured and flexible protein, are twice as susceptible to cleavage than the shorter loop regions [35]. Putative extra-membranous regions are two times more accessible to proteolysis than the membrane-embedded TM domains. Overall, 36% of all potential GLUT1 α-chymotrypsin cleavage sites are observed as actual sites with this reaction protocol.

**Figure 3.2 Topology representation of sites accessible to proteolytic enzymes.** Proteoliposome resident GLUT1 was digested with proteolytic enzymes (either trypsin or α-chymotrypsin) prior to separation and analysis by RP-HPLC and ESI-MS/MS. Peptides containing cleavage sites indicated in each graphic (adapted from the membrane topology model presented in Figure 3.1A) were positively identified by MS/MS. **(A)** GLUT1 contains 36 potential trypsin cleavage sites (16 lysine residues, 20 arginine residues) within its primary structure. 33 of the 36 potential sites are cleaved by trypsin. ☆ indicates cleaved lysine residues, ● represents inaccessible lysine residues, ◇ indicates cleaved arginine residues, and ◆ demonstrates intact arginine residues. R400 (grey ◆) is flanked by proline residues at its N- and C-termini and therefore is not a trypsin cleavage site. **(B)** GLUT1 contains 197 potential α-chymotrypsin cleavage sites (F, Y, W, L, M, A, E as identified in our MS/MS analyses) within its primary structure. ☆ indicates that 52 of these residues are accessible to proteolytic cleavage. Potential α-chymotrypsin cleavage sites appear in all TM domains, though no sites in TM α-helices 3, 6, 9, or 12 are accessible to α-chymotrypsin. Individual peptides and cleavage sites are listed in Appendix 1; Table A1.1.

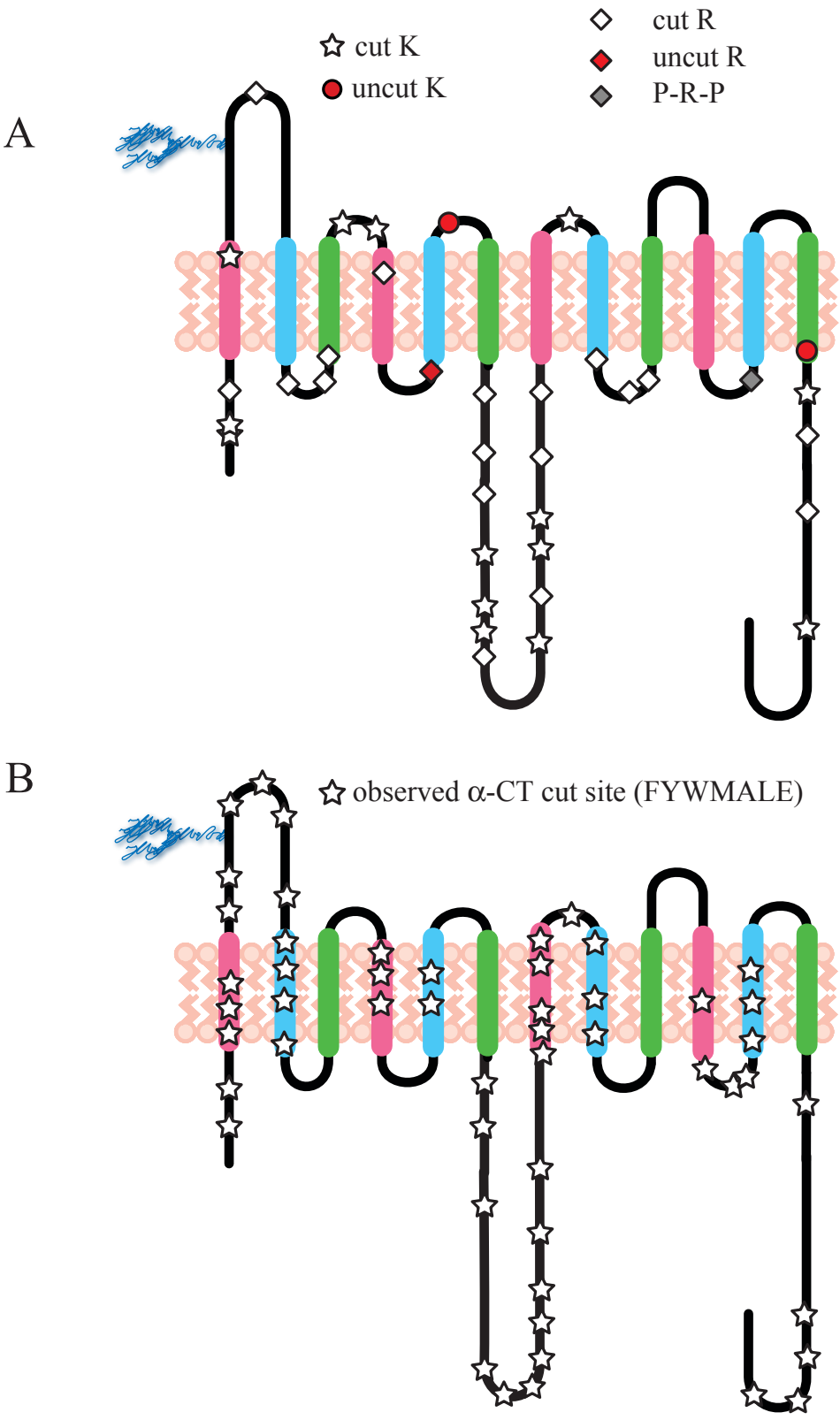
A
cut K
uncut K
cut R
uncut R
P-R-P
B
observed α-CT cut site (FYWMALE)

Figure 3.2

**Legend to Table 3.1 Analysis of GLUT1 accessibility to proteolytic digestion by trypsin and α-chymotrypsin.** The columns show the potential number of cleavage sites (TOTAL Sites), the number detected as susceptible to proteolysis (# Cleaved), and the percent accessibility of the region to proteolysis. Regions are delineated as: 1.) individual, membrane-embedded α-helices; 2.) helical grouping arrangements; 3.) loop, tail, and regions not embedded within the membrane; 4.) a summation of the individual membrane-embedded α-helices versus those regions not embedded within the membrane; 5.) the proteolytic susceptibility of the entire transport structure. A graphical representation is presented in Figure 3.3.

| Region | TOTAL Sites | # Cleaved | % Cleaved | % Cleaved | # Cleaved | TOTAL Sites | Region |
|---|---|---|---|---|---|---|---|
| ***TM1*** | 7 | 4 | 57% | 60% | 6 | 10 | ***TM7*** |
| ***TM2*** | 9 | 4 | 44% | 40% | 2 | 5 | ***TM8*** |
| ***TM3*** | 13 | 1 | 8% | 0% | 0 | 12 | ***TM9*** |
| ***TM4*** | 9 | 4 | 44% | 9% | 1 | 11 | ***TM10*** |
| ***TM5*** | 7 | 2 | 29% | 25% | 2 | 8 | ***TM11*** |
| ***TM6*** | 9 | 0 | 0% | 0% | 0 | 12 | ***TM12*** |
| ***Group 1*** | 37 | 15 | 41% | | | | |
| ***Group 2*** | 29 | 10 | 34% | | | | |
| ***Group 3*** | 46 | 1 | 2% | | | | |
| ***N-Term*** | 10 | 5 | 50% | | | | |
| ***L1-2*** | 10 | 7 | 70% | | | | |
| ***L6-7*** | 37 | 24 | 65% | | | | |
| ***C-Term*** | 19 | 10 | 53% | | | | |
| ***Total*** | 76 | 46 | 61% | | | | |
| ***Others*** | 46 | 13 | 28% | | | | |
| ***Membrane*** | 112 | 26 | 23% | | | | |
| ***Extramembrane*** | 122 | 59 | 48% | | | | |
| ***GLUT1 TOTAL*** | 234 | 85 | 36% | | | | |

Table 3.1

**Figure 3.3 Accessibility of each bilayer-embedded TM helix.** The X-axis shows each α-helix arranged according to its respective group classification (Group 1 includes TMs 1, 4, 7, 10). The Y-axis shows the fraction of potential proteolytic cleavage sites (trypsin or α-chymotrypsin) cleaved by proteolytic digestion for each α-helix.

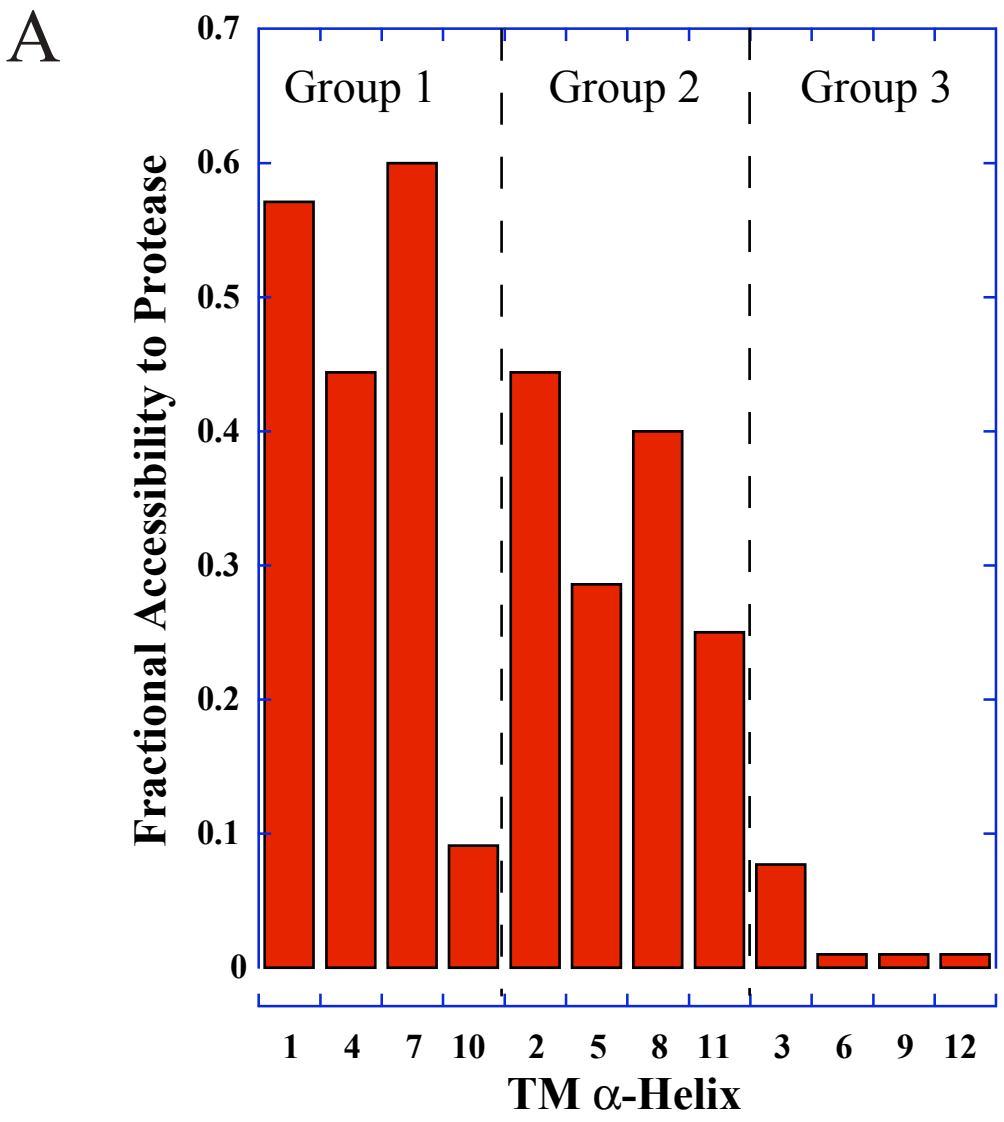
A
Group 1
Group 2
Group 3
Fractional Accessibility to Protease
0.7
0.6
0.5
0.4
0.3
0.2
0.1
0
1 4 7 10 2 5 8 11 3 6 9 12
TM α-Helix

Figure 3.3

Figure 3.3 represents these data graphically as the fractional proteolytic accessibility of each membrane-embedded α-helix according to group assignment. Group 1 and group 2 α-helices demonstrate similar accessibilities, however, the relative proteolysis patterns are distinct. TMs 1 and 7, which are characterized as helical symmetry pairs [56], demonstrate more than 50% accessibility to protease. TMs 4 and 10, also characterized as corresponding helices in the N- and C-terminal halves of the protein, do not share the same accessibility. Group 2 partners 2/8 and 5/11 as well as group 3 partners 3/9 and 6/12 demonstrate similar, but group specific, proteolysis patterns.

***GLUT1 Peptide Partitioning Behavior*** Following proteolytic digestion, GLUT1 peptides may be separated into aqueous- or membrane-associated fractions. Trypsin digestion releases the N- and C-termini, a portion of L1-2, and L6-7 in its entirety into the aqueous fraction. The L1-2 peptide is only detected following complete deglycosylation of GLUT1 catalyzed by PNGaseF. Full-length TM1, cleaved at intracellular R11 and extracellular K38 is also detected in the aqueous fraction (Figure 3.4A).

α-Chymotrypsin digestion releases a similar pattern of extra-membranous regions into the aqueous fraction including the N- and C-termini, a portion of L7-8, and L1-2, L6-7, and L10-11 in their entirety. The isolated aqueous fraction also contains TM1 in its entirety as well as outside facing portions of TM4, TM7, and TM8, inside facing peptides assigned to TM10 and TM11, and multiple faces of TM2 (Figure 3.4B).

When trypsin digestion was conducted in the presence of 10 μM cytochalasin B (CCB), a transport inhibitor that binds to the inward facing e1 GLUT1 conformation [136], TM8

**Figure 3.4 GLUT1 peptides released into the aqueous environment.** Proteoliposome-resident GLUT1 was digested by protease (trypsin or α-chymotrypsin), sedimented by high-speed centrifugation and the aqueous fraction collected and subjected to separation and analysis by RP-HPLC and ESI-MS/MS. **(A) & (B)** Peptides were positively identified using Bioworks Sequest version 3.2 database search program. Using the GLUT1 membrane topology map (from Figure 3.1A), those domains colored in black are detected in the aqueous fraction. **(A)** Trypsin digestion releases the N-terminus, TM1 in its entirety (cut at R11 and K38), a portion of L1-2, all of L6-7, and the C-terminus. If the digest occurs in the presence of 10 μM CCB or if the sedimented pellet is resuspended in 10μM CCB, TM8 (cleaved at K300 and R330) is released from the lipid region and is soluble in the aqueous fraction (area defined by the arrows). **(B)** α-chymotrypsin released fragments include the N-terminus, TM1, L1-2, portions of TM2, TM4, all of L6-7, portions of TM7, TM8, TM10, L10-11, TM11, and the C-terminus. The individual peptides are listed in Appendix 1; Table A1.2.

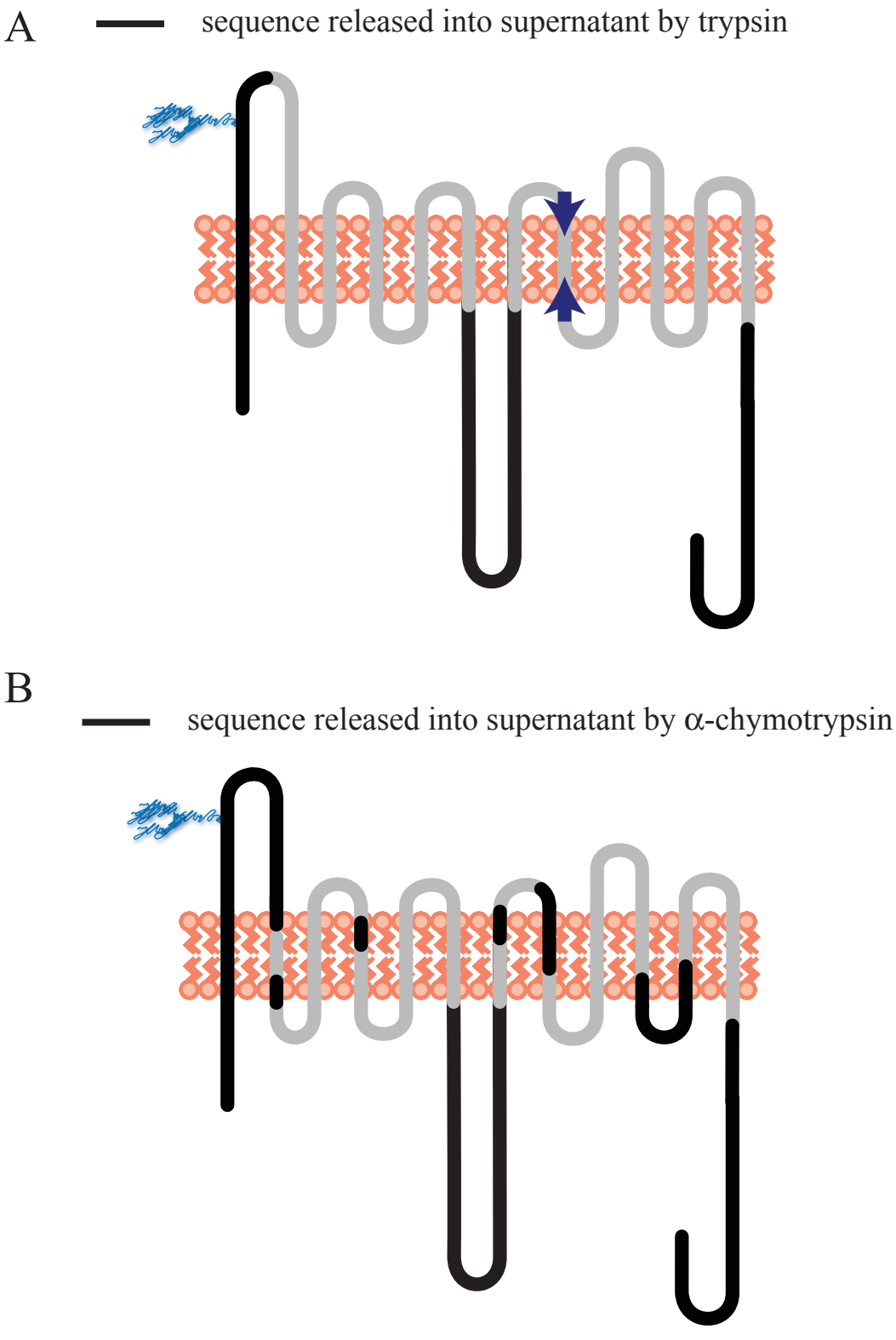
A
sequence released into supernatant by trypsin
B
sequence released into supernatant by α-chymotrypsin

Figure 3.4

**Figure 3.5 MS/MS spectrum CCB-released TM8.** The TM8 peptide is released upon CCB addition to GLUT1 during or following trypsin digestion. The amino acid sequence is K(300).AGVQQPVYATIGSGIVNTAFTVVSLFVVER(330).A, which corresponds to a portion of L7-8 and TM8 near the membrane/cytoplasm interface as predicted by the GlpT-homology model. The peptide elutes from the RP-HPLC column at 42.73 minutes, which corresponds to 43% organic solvent. The indicated y- (read C- to N-terminus, shown in blue) and b- (read N- to C-terminus, shown in red) ion series positively confirm the identity of this peptide with Sequest scoring parameters: XCorr: 5.53, Peptide Probability: $7.43 \times 10^{-8}$, $\Delta$Cn: 0.75, Preliminary Score: 1471.6.

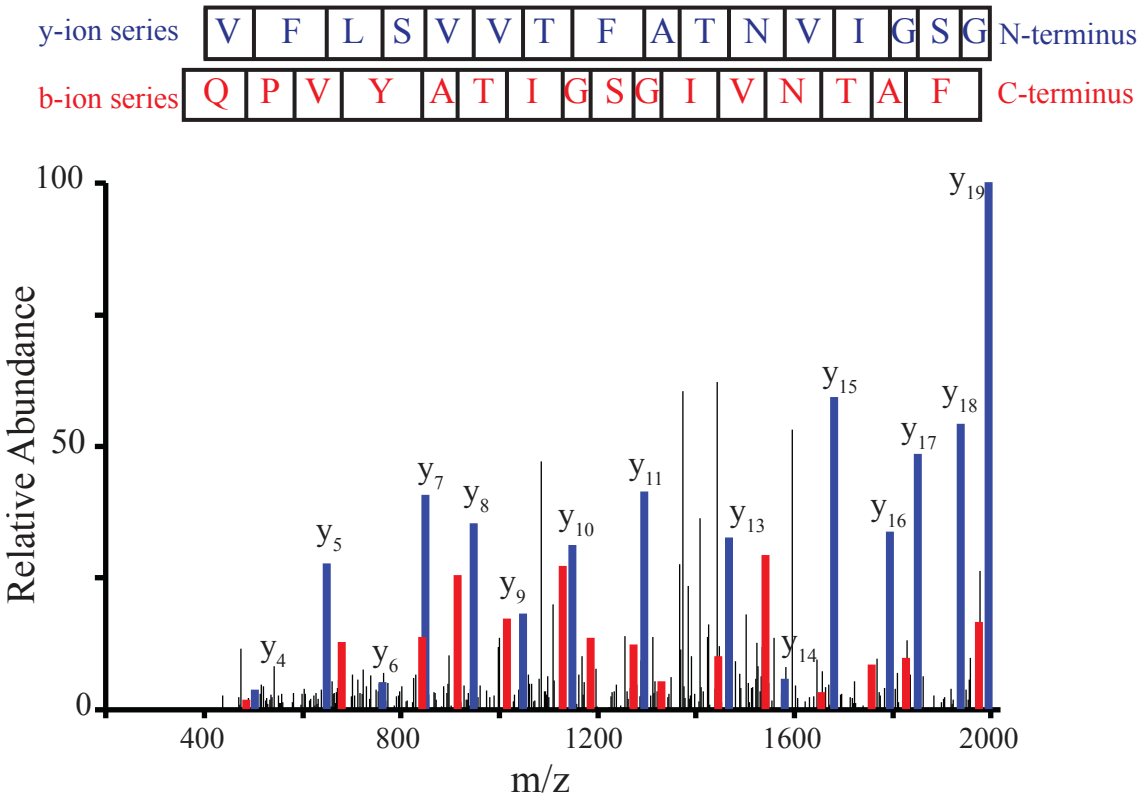
y-ion series
V F L S V V T F A T N V I G S G
N-terminus
b-ion series
Q P V Y A T I G S G I V N T A F
C-terminus
Relative Abundance
100
50
0
400
800
1200
1600
2000
m/z
y4
y5
y6
y7
y8
y9
y10
y11
y13
y14
y15
y16
y17
y18
y19

Figure 3.5

(cleaved after residues K300 and R330) is released into the aqueous fraction (Figure 3.5). The same CCB-specific response is observed when the trypsin-digested membrane-associated fraction is resuspended with CCB containing buffer. Resuspension of the membrane-associated fraction in medium containing cytochalasin D, DMSO, D-glucose, or maltose does not release TM8 or other trypsin-derived peptides.

***Covalent Modification of GLUT1 Lysine Residues*** In order to further investigate GLUT1 membrane topography and assignment of amino acid residues, we examined the accessibility of all 16 lysine residues to covalent modification by an aqueous soluble Sulfo-NHS-LC-Biotin probe. The reactive NHS ester specifically interacts with the primary amine on the lysine side chain forming a covalent amide bond that withstands MS/MS ionization. The GLUT1 modification reaction displays a pseudo-first-order rate constant that increases linearly with [Sulfo-NHS-LC-Biotin] (Figures 3.6A, 3.6B). The extent of modification saturates at probe to protein ratios above 200:1, and is half-maximal at a probe to protein ratio of (15.5 ± 3.2):1 (Figure 3.6B). CCB binding to GLUT1 proteoliposomes is competitively inhibited by GLUT1 biotinylation with half-maximal inhibition observed at a probe to protein ratio of 43 ± 17:1 (Figure 3.6C). Hence, ligand binding is not significantly altered at probe to protein ratios of less than 20:1 where 2.4 moles of probe incorporated per mole of GLUT1. At 20:1 and 200:1 probe to protein, all cytoplasmic lysine residues in L6-7 and the C-terminus are equally accessible (Figure 3.7). We identified modified GLUT1 peptides by accounting for a possible 339.16 Da adduct to lysine residues using the Sequest analysis program. Comparing the MS/MS spectra between unmodified (Figure 3.8A) and modified (Figure

**Figure 3.6 Kinetics of GLUT1 modification. (A)** Time course of GLUT1 labeling at 20ºC, pH 7.4 by sulfo-NHS-LC-biotin. Each data point represents the mean ± SEM of at least 4 separate measurements. The curves drawn through the points were computed using the Levenberg-Marquardt algorithm assuming a first order process described by: labeling = $B_0+B_\infty(1-e^{-k.t})$. **(B)** The results of Figure 3.6A were re-plotted as rate of GLUT1 modification versus [probe to protein molar ratio] or as equilibrium extent of GLUT1 labeling by biotin versus [probe to protein molar ratio]. The curves drawn through the points were computed using the Levenberg-Marquardt algorithm. The rate of labeling equation is described by: rate = $(2.92 \times 10^{-6} \pm 0.30 \times 10^{-6})x + (0.0021 \pm 0.0003$ $min^{-1})$, $R^2 = 0.984$. The extent of labeling was calculated using a modified Michaelis Menten equation: $B_{max} = (1.70 \pm 0.06)$ and $K_{½} = (15.5 \pm 3.2)$:1 , $\chi^2 = 1.9 \times 10^{-2}$. **(C)** Effect of GLUT1 modification on GLUT1 CCB binding. Ordinate: Biotinylated GLUT1 CCB binding capacity (●) or $K_{d(app)}$ (○) relative to untreated GLUT1; Abscissa: NHS-LC-biotin:GLUT1 molar ratio. Results are shown as mean ± SEM of 3 separate experiments in which CCB binding was measured over the [CCB] range of 0.05 to 25 μM in quadruplicate. Control GLUT1 is characterized by $B_{max}$ (capacity) and $K_{d(app)}$ of 0.45 ± 0.01 mol CCB/mol GLUT1 and 265 ± 16 nM respectively. The straight line drawn through the $K_{d(app)}$ data was computed by linear regression and extrapolates to a probe to protein molar ratio of 43 ± 17.

A

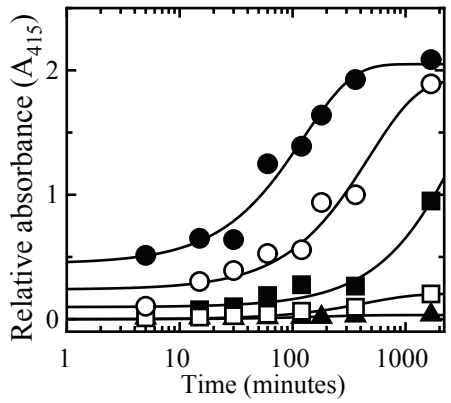


| | $B_0$ | $B_\infty$ | k ($min^{-1}$) | $\chi^2$ |
|---|---|---|---|---|
| ● 2000x | 0.45 ± 0.09 | 1.6 ± 0.1 | 0.008 ± 0.002 | 0.065 |
| ○ 200x | 0.24 ± 0.08 | 1.69 ± 0.002 | 0.0021 ± 0.0005 | 0.086 |
| ■ 20x | 0.04 ± 0.04 | 0.93 ± 0.02 | 0.0026 ± 0.0003 | 0.0006 |
| □ 2x | 0.020 ± 0.005 | 0.20 ± 0.01 | 0.0016 ± 0.0003 | 0.0003 |
| ▲ 0.2x | 0.008 ± 0.001 | 0.027 ± 0.002 | 0.0025 ± 0.0006 | 0.00002 |

B

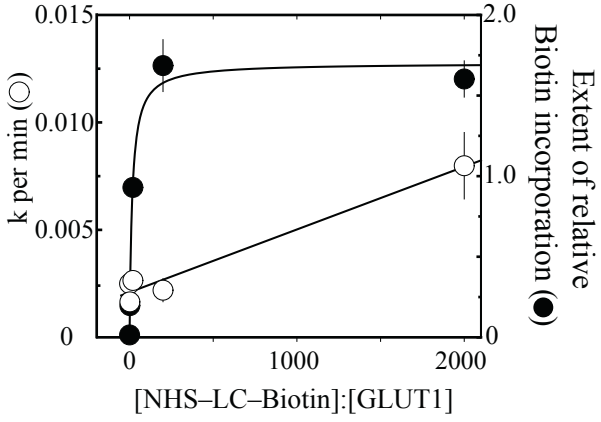


C

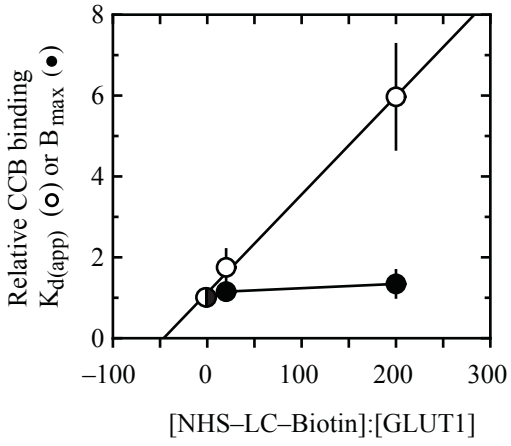


Figure 3.6

**Figure 3.7 Which GLUT1 cytoplasmic domains are most accessible to lysine-reactive probes?** Proteoliposome-resident GLUT1 was biotinylated by exposure to probe to protein molar ratios of 2, 20 or 200 for 1,000 min at 4ºC then treated with trypsin for 2 hr. Peptides retained within the lipid bilayer were removed by high speed sedimentation. Peptides (those released into the aqueous medium) were subjected to separation and analysis by RP-HPLC and ESI-MS/MS. This chart indicates the extent of biotinylation of L6-7 and CT peptides. L6-7 is divided into 3 domains - residues 224-232 (red bars), residues 233-249 (white bars) and residues 254-264 (light gray bars). The C-terminus (CT) domain comprises residues 469-492 (blue bars). Ordinate: fraction of pooled, biotinylated L6-7 & CT peptides observed as a biotinylated subdomain peptide. Abscissa: probe to protein molar ratio. Indicated above the bar chart is the percentage of total peptide (biotinylated and non biotinylated peptide ions) observed as biotinylated peptide. The extent of modification increases with probe to protein ratio.

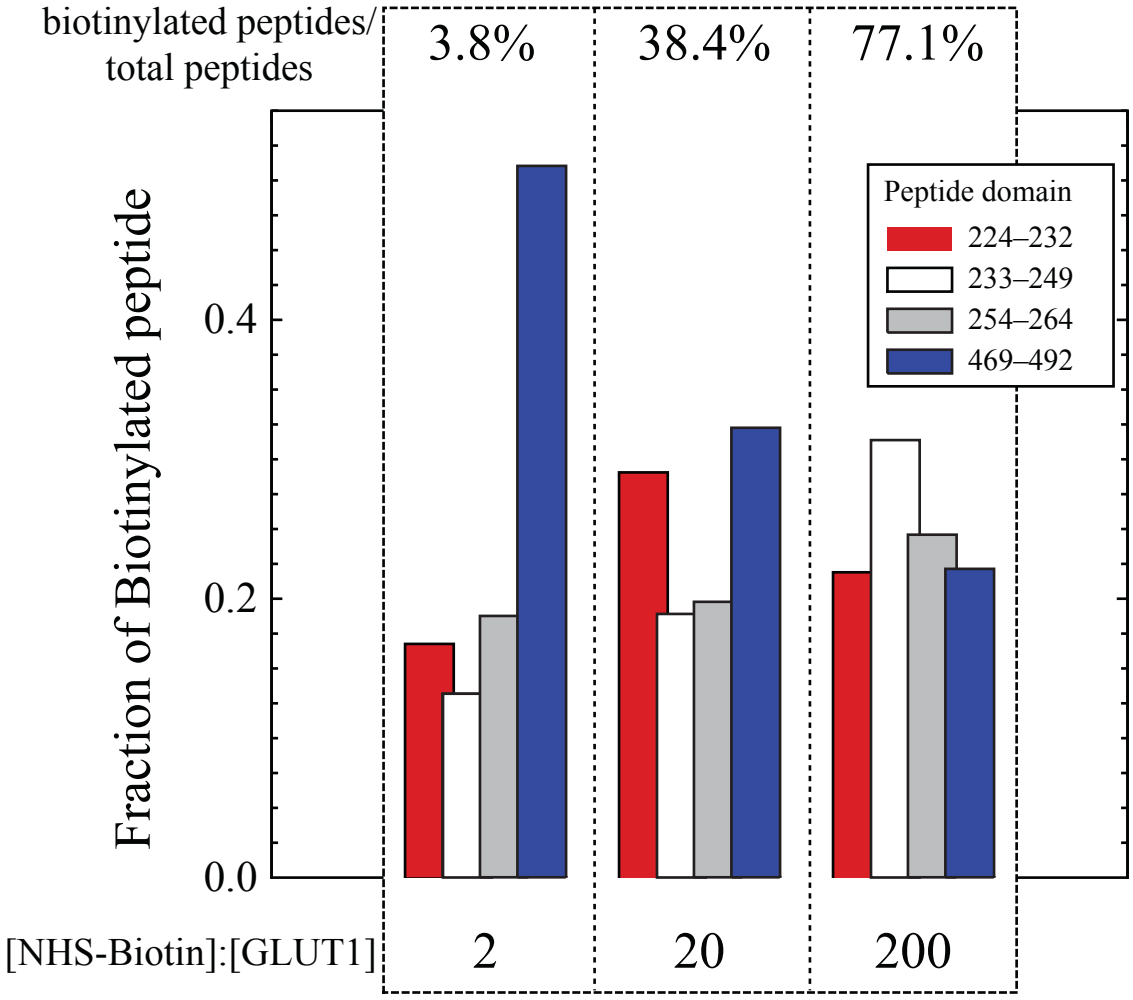
biotinylated peptides/
total peptides
3.8%
38.4%
77.1%
Fraction of Biotinylated peptide
0.0
0.2
0.4
Peptide domain
224–232
233–249
254–264
469–492
[NHS-Biotin]:[GLUT1]
2
20
200

Figure 3.7

**Figure 3.8 MS/MS spectra of GLUT1 peptide modified by Sulfo-NHS-LC-Biotin.** Lysine accessibility to an aqueous probe was monitored using Sulfo-NHS-LC-Biotin. The reactive NHS ester covalently modifies lysine side chain primary amines resulting in a net covalent mass addition of 339.16 Da, which are detected by Sequest analysis software. **(A)**: MS/MS spectrum of a GLUT1 peptide cleaved by trypsin at arginine 232 and arginine 249 with amino acid sequence R(232).GTADVTHDLQEMKEESR(249).Q corresponding to a portion of L6-7. The peptide eluted from the RP-HPLC column at 10.47 minutes, which corresponds to a 26% organic solvent. The y- and b-ion series (blue and red respectively) confirm the identity of this unmodified peptide: with Sequest scoring parameters of XCorr: 4.636, Peptide Probability: $3.4 \times 10^{-9}$, ΔCn: 0.740, Preliminary Score: 1975.5. **(B)**: The same peptide as in **(A)**, except modified at K245 by Sulfo-NHS-LC-Biotin. The modification can first be observed at $y_5$ and $b_{13}$, which show a 339.16 Da adduct to the lysine residue. All sequential ions in each series also represent this mass adduct. The modified peptide eluted from the RP-HPLC column at 19.64 minutes into the gradient, which corresponds to a 31% organic solvent. The MS/MS spectrum and the Sequest scoring parameters confirm its identification: XCorr: 4.652, Peptide Probability: $5 \times 10^{-9}$, ΔCn: 0.615, Preliminary Score: 1235.2.

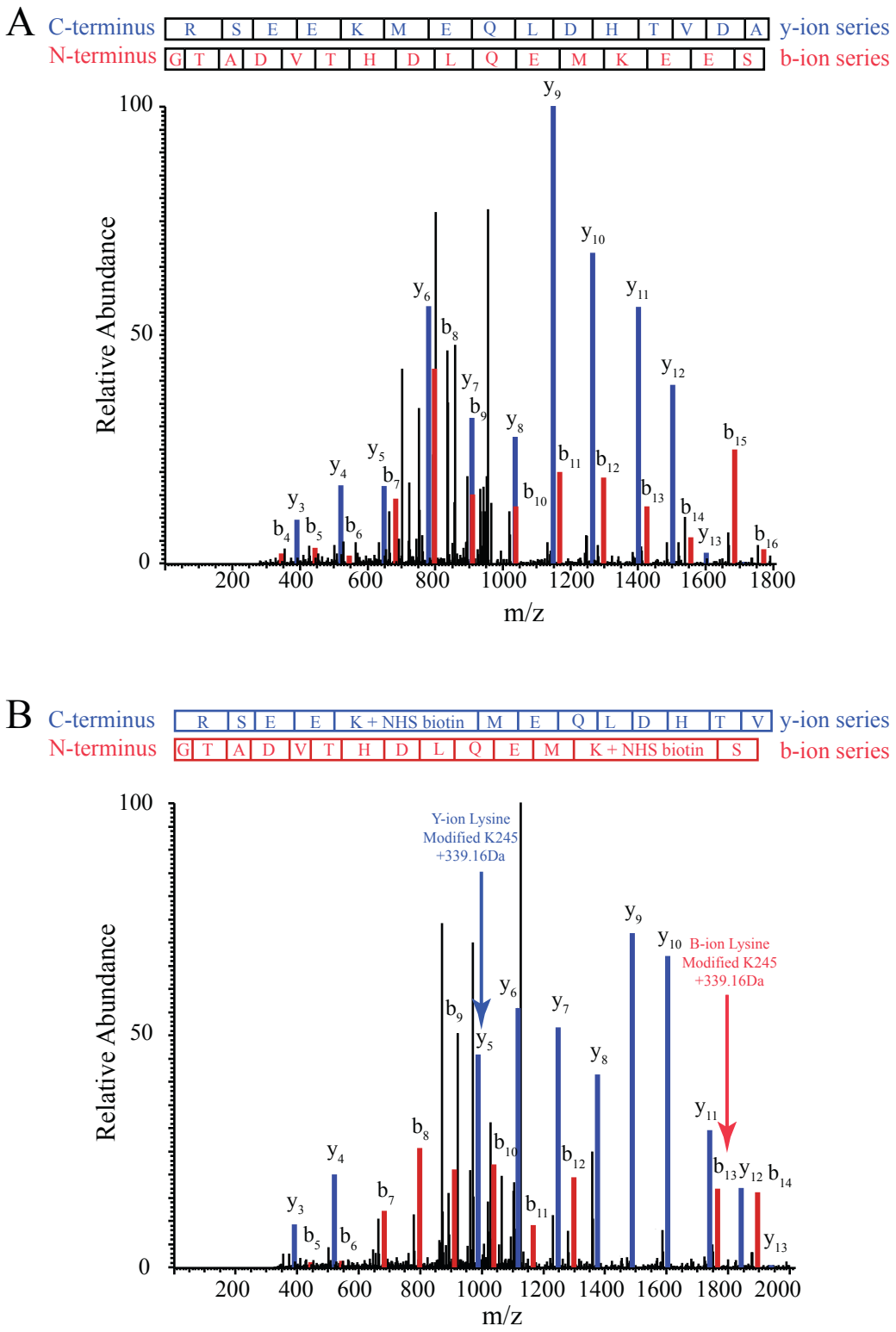
A
C-terminus
N-terminus
R S E E K M E Q L D H T V D A
G T A D V T H D L Q E M K E E S
y-ion series
b-ion series
Relative Abundance
m/z
B
C-terminus
N-terminus
R S E E K + NHS biotin M E Q L D H T V
G T A D V T H D L Q E M K + NHS biotin S
y-ion series
b-ion series
Y-ion Lysine
Modified K245
+339.16Da
B-ion Lysine
Modified K245
+339.16Da
Relative Abundance
m/z

Figure 3.8

3.8B) GLUT1 peptides containing K245 shows the *m/z* ratio difference in the b- and y-ion series peaks that correspond to unmodified and modified lysine residues.

Table 3.2 summarizes the putative location, susceptibility to trypsin proteolysis, and accessibility to covalent modification of GLUT1 lysine residues. The localization of lysine residues to the putative intra- and extracellular loops as well as at the membrane-aqueous interface made them ideal for assessing membrane topography. Of the 16 lysine residues, 14 residues are detected as actual tryptic cleavage sites. Only K183 and K451 are not detected as cleavage sites producing trypsin-specific GLUT1 peptides. Of the 14 trypsin accessible lysine residues, 12 are covalently modified by the Sulfo-NHS-LC-Biotin probe. K114 and K117 of extracellular L3-4 and K456 at the C-terminal end of TM12 are not detected as labeled amino acids. This could mean that these sites are not modified or that modification blocks trypsin cleavage and subsequently prevents production and detection of these peptides by MS/MS.

***Relative TM Hydrophobicity Calculations*** The reverse phase HPLC and ESI-MS/MS data analysis method provides the elution conditions and amino acid sequence of each GLUT1 peptide produced by proteolytic digestion. Using the sequence specific retention (SSR) calculator developed by the Manitoba Center for Proteomics [163], we compared the organic composition of the elution profile for each peptide (experimental peptide hydrophobicity) with the value obtained from entering the amino acid sequence into the SSR calculator (theoretical peptide hydrophobicity).

**Legend to Table 3.2 GLUT1 Lysine Accessibility.** GLUT1 lysine residues (column 1), their location within GLUT1 putative domains (column 2), their propensity to biotinylation by Sulfo-NHS-LC-biotin as detected by MS/MS (column 3) and their propensity to cleavage by trypsin as detected by MS/MS (column 4).

| Lysine Residue | Putative Location | Detected as Labeled | | | Detected as Cleaved |
|---|---|---|---|---|---|
| | | 2x | 20x | 200x | |
| K6 | N-Terminus | ■ | ■ | ■ | Yes |
| K7 | TM1 | | ■ | ■ | Yes |
| K38 | TM1 | | | ■ | Yes |
| K114 | TM3 | | | | Yes |
| K117 | L3-4 | | | ■ | Yes |
| *K183* | *L5-6* | | | | *No* |
| K225 | L6-7 | ■ | ■ | ■ | Yes |
| K229 | L6-7 | ■ | ■ | ■ | Yes |
| K230 | L6-7 | ■ | ■ | ■ | Yes |
| K245 | L6-7 | ■ | ■ | ■ | Yes |
| K255 | L6-7 | ■ | ■ | ■ | Yes |
| K256 | L6-7 | ■ | ■ | ■ | Yes |
| K300 | L7-8 | | ■ | ■ | Yes |
| *K451* | *TM12* | | | | *No* |
| K456 | C-Terminus | | | | Yes |
| K477 | C-Terminus | ■ | ■ | ■ | Yes |

Table 3.2

**Figure 3.9 Relative TM domain hydrophobicity.** Experimentally observed elution conditions were compared with the relative hydrophobicity as predicted by the Sequence Specific Retention (SSR) Calculator [163]. (**A**) Comparative analysis of how the predicted hydrophobicity corresponded to the actual measured elution conditions. Ordinate: the relative hydrophobicity of eluted peptides (Sequence Specific Retention score) calculated using the actual sequence and length of the eluted peptides. Abscissa: % Organic Solvent required for peptide elution. The straight line drawn through the points ($y = 0.65x + 12.62$; $R^2=0.947$) was computed by linear regression. **(B)** Relative theoretical hydrophobicity and order of elution for each membrane-embedded α-helix, L1-2, L6-7, and the C-terminus. The organic elution conditions (ordinate) were computed using the calculated, sequence-dependent SSR values. The SSR values (abscissa) were inserted into the standard curve obtained in **(A)**.

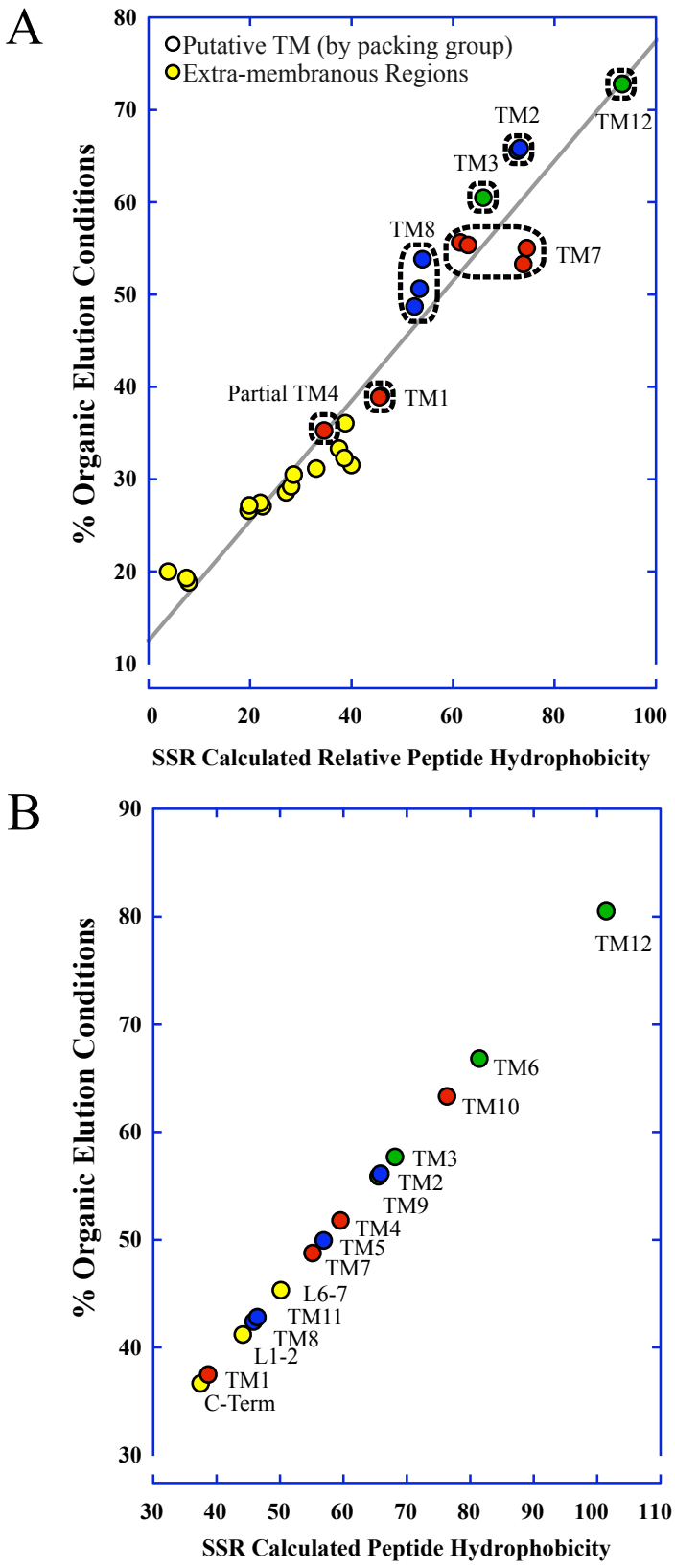
A
Putative TM (by packing group)
Extra-membranous Regions
TM2
TM12
TM3
TM8
TM7
Partial TM4
TM1
% Organic Elution Conditions
SSR Calculated Relative Peptide Hydrophobicity
B
TM12
TM6
TM10
TM3
TM2
TM9
TM4
TM5
TM7
L6-7
TM11
TM8
L1-2
TM1
C-Term
% Organic Elution Conditions
SSR Calculated Peptide Hydrophobicity

Figure 3.9

We first established a standard curve that plotted the elution conditions for trypsin derived peptide fragments versus the calculated SSR values for the exact sequence of the eluted peptide (Figure 3.9A). This plot shows a significant correlation between experimental and theoretical peptide hydrophobicity values ($R^2$ equals 0.94). We next used the standard curve and calculated SSR values to determine the experimental elution order for the membrane-embedded portion of each TM α-helix as described in the model presented by *Salas-Burgos et al* (Figure 3.9B). These results show that TM1 is the most hydrophilic and TM12 the most hydrophobic of all membrane-spanning domains. α-helices belonging to groups 1 and 2 show comparable average hydrophobicity values, whereas group 3 α-helices are approximately 30% more hydrophobic.

### *DISCUSSION*

The primary goal of this investigation was to experimentally unravel the structure of the mammalian facilitative glucose transporter GLUT1 from its innermost, aqueous, pore-forming α-helices to its outermost, lipid-embedded, scaffolding α-helices. To this end, we employed in-line RP-HPLC-ESI-MS/MS analysis to examine membrane-resident GLUT1 accessibility to water-soluble probes such as proteolytic enzymes and small molecules. This approach directly addresses the accessibility of individual transmembrane α-helices to solvent, the relative solubility of GLUT1 peptides in aqueous versus membrane environments, and the experimental hydrophobicity of individual TM α-helices. Although we use the MFS-homology predictions for GLUT1 helix packing as a guide, we present several observations that are inconsistent with the putative α-helical

arrangement and identify domains that potentially mediate conformational changes contributing to GLUT1 function as a carrier-protein [64]. We will discuss these results individually and then show how they support a new GLUT1 structural model.

Their positively charged nature suggests that lysine and arginine residues are located outside of the membrane [164]. Specific covalent modification of lysine side chains and the susceptibility of lysine and arginine residues to trypsin digestion address lysine and arginine topology relative to GLUT1 structure. Our results broadly support the modeling of lysine and arginine residues to either the intra- and extracellular regions corresponding to the N- and C-termini, loops connecting the TM α-helices, or the interface between the membrane-embedded protein and the aqueous environment. With the exception of three residues, we detect cleavage at all potential trypsin targets. All lysine residues detected as Sulfo-NHS-LC-Biotin reactive sites are also detected as cleavage sites. Additionally, lysine residues located in proposed intracellular L6-7 and the C-terminus (K225, K229, K230, K245, K255, K256, and K477) are equally accessible to covalent modification, which supports the depiction of these regions as unstructured and flexible within the cytoplasm [35]. R126 is the only potential trypsin cleavage site proposed to be located within the membrane bilayer. Despite this location, however, it is susceptible to proteolytic cleavage whereas putative loop residues R153, K183, and K451 are not detected as accessible sites. The locations of K183 (putative extracellular loop at the N-terminal end of TM6) and K451 (C-terminal end of the TM12 α-helix) are consistent with the proposed membrane insertion of these two regions.

α-Chymotrypsin accessibility studies and the identification of peptide fragments released into aqueous medium offer additional support for the proposed GLUT1 membrane topology. Similar to our results with trypsin, the N- and C-termini, L1-2, L6-7, L10-11, and a portion of L7-8 are accessible to α-chymotrypsin and released into the aqueous fraction. This is consistent with proposed assignments of extra-membranous residues. Interestingly, however, numerous α-helical fragments dissociate from the membrane-embedded region. Portions of TM2, TM4, TM7, TM8, TM10, and TM11 as well as TM1 in its entirety (from trypsin) or as individual fragments (from α-chymotrypsin) are found in the aqueous fraction following proteolytic digestion. Fragments from TMs 3, 5, 6, 9, and 12, if they are detectable at all, are only observed in the membrane-associated fraction.

Our results support the hypothesis that α-chymotrypsin-catalyzed proteolysis proceeds from the most aqueous portions of the protein toward more lipid-embedded regions. The loop and cytoplasmic terminal regions are highly accessible, as confirmed by lysine modification. We predict that α-chymotrypsin digestion and accessibility patterns reflect the extent to which each α-helix contributes to the aqueous translocation pore. TMs 1 and 7, which display the highest number of cleaved sites and protease accessibility (comparable to the termini and long transmembrane loops) likely comprise the innermost, aqueous-exposed α-helices. Cleavage susceptibility gradually decreases across TMs 2, 4, and 8, followed by TMs 5, 11, and 10, indicating further distance from or diminished interaction with the aqueous environment. The inner GLUT1 α-helices, therefore, show

characteristic contributions to the aqueous translocation pathway. The outer group 3 α-helices (3, 6, 9, and 12) are completely resistant to proteolysis (R93 in TM3 bridges the aqueous-lipid interface). Unlike their inner, pore-lining, variably accessible counterparts, these TMs are uniformly embedded within the membrane. According to the MFS model, they serve as scaffolding domains that keep the protein anchored within the membrane during conformational changes associated with transport. These observations are consistent with the model provided in Figure 3.1.

The release of small peptides from inner transmembrane α-helices into the aqueous fraction confirms their amphipathic nature and ability to interact with the aqueous environment and substrate. These interactions are fundamental to glucose-induced GLUT1 conformational changes and glucose translocation. TM1 is released from the membrane following trypsin digestion in a substrate-independent fashion. Previous studies demonstrated that CCB binds to proteolyzed GLUT1 proteoliposomes [87]. We hypothesized, therefore, that ligands and substrates might promote GLUT1 conformational changes that cause the release of additional transmembrane domains. Consistent with this proposal, we detect TM8 release from the membrane when 10 μM cytochalasin B is present during or following trypsin digestion of GLUT1 proteoliposomes. This result is CCB-specific, as D-glucose, maltose, and additional buffers do not alter TM8 release. This suggests that CCB binding to membrane-associated GLUT1 domains promotes a transporter conformational change. This could result from a physical interaction between TM8 and CCB or may be an indirect consequence of CCB binding to a distal region of the transporter. Peptide mapping

studies of CCB covalently photolabeled to GLUT1 indicate that TM10 forms a major site of GLUT1-CCB interaction [61].

The release of TM8 from the membrane indicates that the TM regions undergo a significant reorientation during the conformational changes that lock the transporter in the e1 orientation. The respective ability of each TM to leave the membrane bilayer and interact stably with the aqueous environment upon polypeptide backbone cleavage highlights their potential involvement in carrier conformational changes and is consistent with the high activation energies required for glucose sequestration within a translocation intermediate [87]. Crystallized EmrD [39] and OxlT [5,34] structures also suggest sequestration of substrates within the translocation pathway. These observations differ markedly from the protease resistance displayed by the less conformationally active cation translocation pathway of $K^+$-channels [52,165]. We propose that TMs 1 and 8 serve as key, structurally dynamic TMs, which, through the adoption of hydrophobic or hydrophilic conformations, mediate conformational changes associated with uniport and exchange transport function.

The close correspondence between calculated sequence specific retention (SSR; [163]) and the experimental elution profile of any given GLUT1 peptide from HPLC (Figure 3.9A), allows us to predict the relative hydrophobicity and elution conditions of full-length, membrane spanning α-helices (Figure 3.9B). In this work, we demonstrate that TM domains 1 and 8 are the most hydrophilic of all putative α-helices in terms of their minimally organic elution profile, favorable partitioning into the aqueous environment,

and low SSR score. Conversely, the group 3 α-helices are approximately 30% more hydrophobic than those associated with groups 1 and 2 and four of the six most hydrophobic TMs belong to group 3. This observation provides direct biochemical support for the idea that these TMs are completely embedded within the lipid bilayer and, therefore, are unlikely to present any interface with the aqueous environment.

*Mueckler et al.* have employed a scanning cysteine accessibility method (SCAM) to show that GLUT1 α-helices are amphipathic in nature and vary in accessibility to aqueous solvent. With the exception of TM 4 [49] and TM12 [74], the examined TMs show characteristic accessibility predicted by the emergent MFS helix-packing model [40,48,50,68-70,72]. They also support the idea that each pore forming α-helix presents differential accessibility patterns specific to the e2 or e1 protein configuration. TM5 and TM10 may be the most interesting in our studies because of their unique interaction with the aqueous environment. TM5 displays the same number of susceptible cleavage sites (two) as its helix-symmetry partner TM11, but all peptides remain tightly associated with the membrane. Conversely, unlike its helix symmetry partner TM4, TM10 only presents one susceptible cleavage site to digestion, but the C-terminal portion of this TM is released from the membrane-associated region.

We further note that the GlpT homology model does not account for the intramolecular disulfide bond proposed to link TMs 9 and 11 that promotes GLUT1 oligomerization observed in the plasma membrane [80,86]. As a result, it is likely that the MFS helix-packing model represents transporter proteins in the monomeric state. Given that our

studies were conducted on native protein, in non-reducing conditions, a disulfide bond between TMs 9 and 11 would change the helical tilts and relative orientation within the bilayer. This interaction would likely sequester TM10 from the aqueous translocation pathway reducing its accessibility to proteolytic digestion (Figure 3.10). The overall lack of accessibility to aqueous solvent demonstrated by TMs 3, 6, 9, and 12 may permit these α-helices to form the oligomerization interface.

**Figure 3.10 Model for GLUT1 α-helix packing arrangement.** TMs are numbered as presented in Figure 3.1B and colored according to their fractional protease accessibility. TMs 1, 2, 4, 5, 7, 8, 10, and 11 are proposed to form the glucose translocation pathway with variable degrees of interaction with aqueous solvent. TMs 3, 6, 9, and 12, which present no fractional accessibility to protease nor release any peptides into the aqueous fraction are deeply embedded within the membrane and have no contact with the aqueous solvent. We propose that the proposed disulfide bond between C3477 and C421 (found in TM9 and TM11, respectively) causes TM10 to be sequestered from the translocation pathway, thus reducing its fractional accessibility to protease.

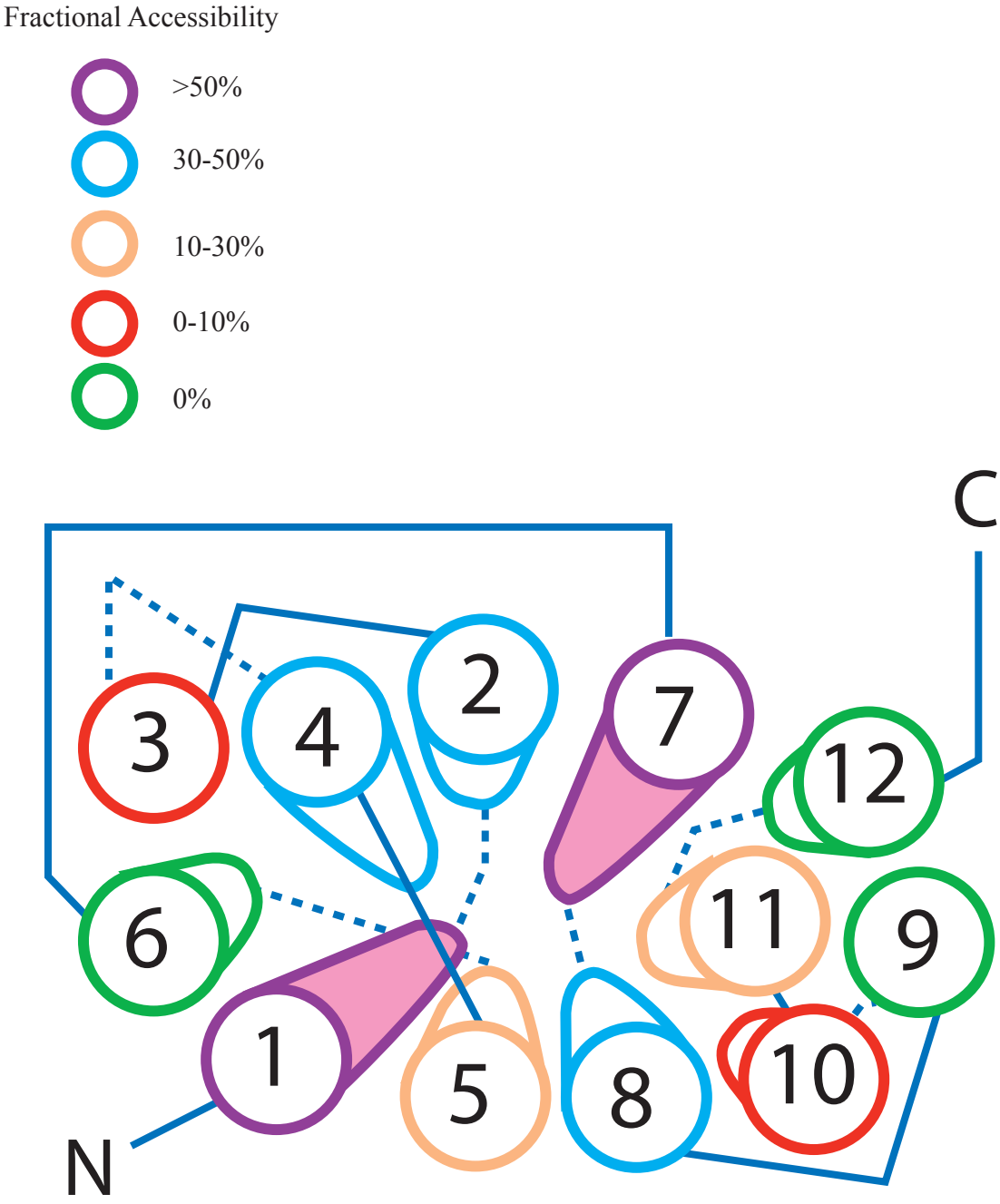
Fractional Accessibility
>50%
30-50%
10-30%
0-10%
0%
C
N
1
2
3
4
5
6
7
8
9
10
11
12

Figure 3.10

# CHAPTER IV

## CYTOPLASMIC REGIONS ARE RESPONSIBLE FOR ATP MODULATION OF GLUT1-MEDIATED SUGAR TRANSPORT

This chapter will be submitted as a manuscript in April of 2007.

**This work was supported by NIH grants DK 36081 and DK 44888 and by ADA grant ADA 1-06-IN-04 (Gail Patrick Innovation Award supported by a generous gift from the Estate of Gail Patrick)**

Data presented in this chapter found in Figures 4.1, 4.2, 4.3, and 4.4 were collected and analyzed by Julie A. K. DeZutter, PhD.

***ABSTRACT***

Cytoplasmic ATP regulates GLUT1-mediated sugar transport by reducing $K_m$ and $V_{max}$ for net sugar import and $K_m$ for exchange transport. We undertook an investigation of the mechanism of GLUT1-regulation by ATP by identifying GLUT1 domains that undergo significant conformational change upon GLUT1-ATP interaction. ATP (but not GTP) affords GLUT1 protection against tryptic digestion. Immunoblot analysis shows peptides released from the GLUT1 N-terminus, L6-7, L7-8 and the GLUT1 C-terminus are degraded less completely when tryptic digestions are carried out in the presence of ATP. ELISA assays of antibody binding to full-length GLUT1 show reduced binding of IgGs directed against L7-8 or the GLUT1 C-terminus when binding is performed in the presence of ATP. C-terminal antibody binding to wild-type GLUT1 expressed in HEK cells is inhibited by ATP but binding to a GLUT1-GLUT4 chimera in which L6-7 of GLUT1 is substituted with L6-7 of GLUT4 is unaffected by ATP. Sulfo-NHS-LC-Biotin GLUT1 labeling decreases in the presence of ATP. ESI-MS/MS studies show that labeling of lysine residues 245, 255, 256, and 477 is inhibited in the presence of ATP, whereas lysine residues 225, 229, and 230 demonstrate no change in labeling efficiency. These data suggest that the GLUT1 C-terminus interacts with the C-terminal half of L6-7 in an ATP-dependent manner, thereby reducing the efficiency of glucose transport.

## *INTRODUCTION*

Most eukaryotic cells import and export glucose via a saturable but passive transport process that, in the absence of sugar metabolism, leads to the equilibration of glucose between cell water and interstitium [2]. This sugar transport is catalyzed by a family of integral membrane proteins (GLUT1 - GLUT12 [115]) and is characterized by the catalytic mechanism of carrier-mediated, facilitated diffusion [2]. GLUT1 is expressed in most tissues but is especially abundant in erythrocytes [166], blood-tissue barriers (brain, retina, olfactory epithelium, inner ear, peripheral nerve and heart [167]), cardiomyocytes [168], vascular smooth muscle [167] and astrocytes [19]. While our studies specifically focus upon GLUT1 found in human erythrocyte, examining how GLUT1 catalyzes glucose transport and how this process is regulated should explain how this process is mediated and controlled at blood-tissue barriers.

Glucose uptake is rate-limiting for glucose utilization in cells with low glucose transport capacity relative to high rates of sugar metabolism (e.g. smooth, striated and cardiac muscle, adipose, nucleated erythrocytes and certain cultured cell lines). These cells characteristically display acute sugar transport regulation in which net sugar uptake is rapidly stimulated when glucose utilization is increased [169-173]. Sugar transport in muscle, nucleated erythrocytes and cultured cells is stimulated 3 to 50-fold by cellular metabolic depletion [170,172-174] while insulin produces an 8 to 40-fold stimulation of sugar transport in muscle and fat [175,176]. Many cells respond acutely to stimuli by

increasing cell surface sugar transporter content [176] while others respond with increased GLUT intrinsic activity [174].

The field has long held that sugar transport regulation is unnecessary in cells where transport is faster than metabolism [14,177]. This conclusion is, however, based on the assumption that the target served by the sugar transport activity of a cell is the metabolic machinery of that transporting cell. Would this conclusion still hold if the target were downstream from the transporting cell? In the brain, for example, glucose utilization by astrocytes and neurons is fed by glucose transport across the blood brain barrier. This barrier comprises endothelial cells which account for only 0.1% of the mass of the brain [178] but which must transport sugar for a significantly greater mass of metabolically active cells.

Several tissues are protected from direct access to serum-borne nutrients and electrolytes by blood-tissue barriers. The protected tissues include the brain, the retina, the olfactory epithelium, the inner ear, peripheral nerve and the heart [154,167]. The cells that form the blood-tissue barrier are normally endothelial cells sealed by tight junctions [154]. GLUT1 is expressed at high levels in these endothelial cells and constitutes the major pathway for glucose movement across these barriers via transcellular transport [154]. Glucose transport into brain, peripheral nerve and retina is especially important because glucose stores in these tissues are very small relative to glucose demand [179].

Erythrocytes and endothelial cells rapidly equilibrate with glucose indicating that their capacity to metabolize glucose is significantly less than their glucose transport capacity

[180]. Endothelial cell GLUT1 is functionally analogous to human red cell GLUT1 in that it displays similar substrate affinities, trans-acceleration of transport, and inhibitor sensitivities [181]. Human red cell GLUT1 and human GLUT1 heterologously expressed in CHO cells and HEK cells respond acutely to ATP-depletion with enhanced glucose import capacity [85,119,131,182,183].

Glucose transport measurements in human erythrocyte ghosts do not display the same characteristic transport asymmetry parameters observed in native human red cells. The removal of ATP from the cytosol is responsible for promotion of transport symmetry. In fact, ATP lowers $K_m$ and $V_{max}$ for net sugar import and lowers $K_m$ for exchange transport in human red cells [114,184]. This transport modulation reflects a direct action of ATP on GLUT1 [185], is competitively inhibited by AMP and ADP, and does not involve ATP hydrolysis [131]. At low temperatures (4ºC) where transport in human red cells is most easily measured, GLUT1 asymmetry is at least 20-fold [184]. At physiological temperature, asymmetry falls to 1.4 to 2-fold [116]. Thus the loss of transport asymmetry in the absence of ATP increases sugar uptake capacity at 4°C and 37°C by 20- and by 1.4 to 2-fold respectively.

GLUT1 is a nucleotide binding protein that directly interacts with ATP [135]. Peptide mapping studies suggest that ATP binds to GLUT1 between amino acid residues 301 to 364. This region comprises TM helices 8 and 9 and cytoplasmic loop 8-9. The primary sequence of this region displays 50% sequence identity with the ATP binding region of adenylate cyclase and further narrows the binding region to residues 332 to 343 [135].

The likely nucleotide-binding pocket, therefore, minimally contains L8-9 and the cytoplasmic half of TM9, however, the modulation mechanism (in terms of primary sequence) is likely distal to the physical binding site.

Our studies suggest that the GLUT1 C-terminus interacts with the cytoplasmic loop (L6-7) in an ATP-dependent manner thereby reducing the efficiency of transport. The overall modulation of erythrocyte GLUT1 by ATP may reflect a fundamental mechanism for GLUT1 regulation in other tissues. This chapter examines the biochemical basis of GLUT1 regulation by ATP through analysis of ATP-sensitive GLUT1 subdomains.

### *MATERIALS AND METHODS*

**Limited Proteolytic Digestion of Purified GLUT1** 10ug of purified GLUT1 was digested with a 20:1 (protein:enzyme) ratio of purified porcine trypsin (Princeton Separations) in 50 mM Tris-HCl (pH 7.5), 0.1% SDS, 5 mM $MgCl_2$, 4mM ATP (pH 7.5). Digestions were performed at 4°C for 60 minutes, or the indicated time period. Reactions were immediately loaded onto 15% SDS-PAGE.

**Western Blotting** Following SDS-PAGE, samples were transferred to nitrocellulose and blocked overnight in 25% nonfat dry milk/PBS/0.1%Tween-20. Primary antibody [C-Ab (1:15,000), L6-7-Ab (1:500), N-Ab (1:200), L2-3-Ab (1:200), L7-8-Ab (1:200)] was incubated in 3% nonfat dry milk/PBS/0.1% Tween-20 for 1 hour at room temperature. Blots were washed 3x with PBS/0.1% Tween-20. HRP conjugated goat anti-rabbit secondary antibody, diluted 1:5000, was incubated at room temperature for 1 hour. Blots

were washed 3x with PBS/0.1% Tween-20 followed by an additional 3 washes with PBS/0.2% Tween-20. Blots were developed using Pierce SuperSignal West Pico Chemiluminescent substrate and visualized by autoradiography.

**Differential Antibody binding: ELISA** 200 ng of purified GLUT1 in 1x PB buffer (20 mM $NaH_2PO_4$, 145 mM NaCl) was adsorbed to an ELISA plate for 2 hours at 37°C. Plates were blocked with PB buffer/3% BSA for 2 hours at 37°C. Primary antibody [C-Ab (1:15,000), L6-7-Ab (1:500), N-Ab (1:200), L2-3-Ab (1:200), L7-8-Ab (1:200)] was incubated in PB buffer/0.1% BSA for 2 hours. Plate was washed 5x with PB buffer. HRP-conjugated goat anti-rabbit secondary antibody, diluted 1:5000, was incubated for 1 hour at 37°C. Plate was washed 5x with PB buffer. ELISA was developed using 100 µl of 1-Step ABTS solution (Pierce). Extent of antibody binding was measured by quantitating OD (415nm).

**Construction of GLUT1-L6-7-GLUT4 Chimera** The human GLUT1chimera, which had the middle loop (L6-7) substituted with that from its counterpart from rat GLUT4, was constructed using a 6-step PCR protocol. In PCR 1A, a HindIII primer complimentary to the 5' end of human GLUT1 and a reverse primer complimentary to nucleotides (600-619) of GLUT1 and (667-685) of GLUT4 was used to generate a fragment containing TM 1-6 (nucleotides 1-620) of GLUT1. In a separate reaction, PCR1B, primer (TGCATCGTGCTGCCCTTCTGTCCTGAGAGCCCCCGA) containing sequence complimentary to nucleotides (600-619) of GLUT1 and (667-685) of GLUT4 (5'end of L6-7) and a reverse primer (containing a Not I restriction site) complimentary

to the 3' end of GLUT4 was used to generate a fragment containing the middle loop and TM 7-12 (nucleotides 667-1531) of GLUT4. In PCR2, the HindIII primer complimentary to the 5' end of human GLUT1 and the reverse primer (containing a Not I restriction site) complimentary to the 3' end of GLUT4 were used along with the products from PCR1A and B to generate an intermediate chimera containing sequence from nucleotides (1-620) of GLUT1 and (667- 1531) of GLUT4. This intermediate chimera contained TM 1-6 of GLUT1 in frame with L6-7 and TM 7-12 of GLUT4. In PCR 3A, the HindIII primer complimentary to the 5' end of human GLUT1 and a primer (CGCACCCAGGGGCAGCCTATCCTCATCGCTGTGGTC) complimentary to nucleotides (844-862) of GLUT4 and (815-829) of GLUT1 were used along with the product from PCR2 to generate a fragment containing TM 1-6 of GLUT1 (nucleotides 1-619) in frame with L6-7 (nucleotides 667-862) of GLUT4. In PCR 3B, a primer (CGCACCCAGGGGCAGCCTATCCTCATCGCTGTGGTC) complimentary to nucleotides (844-862) of GLUT4 and nucleotides (815-829) of GLUT1 were used with wild type GLUT1 plasmid as a template to generate a fragment containing TM 7-12 (nucleotides 815-1480) of GLUT1. In the final reaction, PCR 4, HindIII primer complimentary to the 5' end of human GLUT1 and the NotI primer complimentary to the 3' end of GLUT1 were used with the products of PCR 3A and B as a template generating the final product which contained TM 1-6 (nucleotides1-619) of GLUT1, followed by L6-7 of GLUT4 (nucleotides 667-862), followed by TM 7-12 (nucleotides 815-1480) of GLUT1. This PCR product was digested with HindIII and NotI and ligated into the mammalian expression vector pcDNA 3.1+, cut with the same enzymes. Sequences were

confirmed and the GLUT1-L6-7-GLUT4 chimera was shown transport glucose into HEK cells with kinetics similar to that seen for wt GLUT1.

Sulfo-NHS-LC-Biotin labeling, RP-HPLC, and ESI-MS/MS techniques are as described previously in Chapter III.

***RESULTS***

Purified human GLUT1 is reconstituted into unsealed proteoliposomes upon detergent removal [41,83,146] because the protein co-purifies with human red cell membrane lipids. If exogenous lipid is added to the protein/lipid/detergent mixture prior to detergent removal, the increased lipid:protein ratio causes sealed proteoliposomes, which contain GLUT1 in a random transmembrane orientation, to form [186-188]. These proteoliposomes are osmotically active and are suitable for sugar transport determinations. In the proteolysis and biotinylation experiments described below, we employed purified human GLUT1 in unsealed proteoliposomes to ensure that added reagent has access to both surfaces of the lipid bilayer and thus full access to exo- and endo-facial GLUT1 domains.

Exposure of GLUT1 proteoliposomes to trypsin (62.5:1 by mass) at 37ºC results in the rapid loss of intact GLUT1 as judged by silver-stain detection of peptides resolved by 10% SDS-PAGE (Figure 4.1A). The time course of GLUT1 proteolysis is biphasic, being characterized by a rapid burst phase of proteolysis in which approximately 30% of

**Figure 4.1 GLUT1 digestion by trypsin at 37ºC. (A)** GLUT1 (10 μg) was incubated with trypsin (0.16 μg) ± ATP (concentrations indicated) for 60 sec (panels **(A)** & **(C)**) or with 0 ATP, 4 mM ATP or 4 mM GTP for the times indicated **(B)**. GLUT1 was separated from proteolytic fragments by SDS-PAGE and the fraction of intact GLUT1 remaining quantitated by densitometry of silver-stained gels. The curves drawn through the data points assume two exponential phases of proteolysis. The fast phase accounts for 33% of GLUT1 proteolysis and has a first order rate constant of 0.056 ± 0.009 per sec (control) or 0.046 ± 0.018 per sec (GTP). The slow phase accounts for 66% of GLUT1 digestion and has a first order rate constant of 0.00036 ± 0.00003 per sec (control) or 0.00026 ± 0.00022 per sec (GTP). ATP reduces the magnitude of the fast phase to 22 ± 2% and slows the fast rate constant to 0.017 ± 0.003 per sec. Insufficient data exists to analyze slow phase kinetics in the presence of ATP. ATP protection of GLUT1 during fast phase proteolysis is half-maximal at 497 ± 148 μM ATP (panel C).

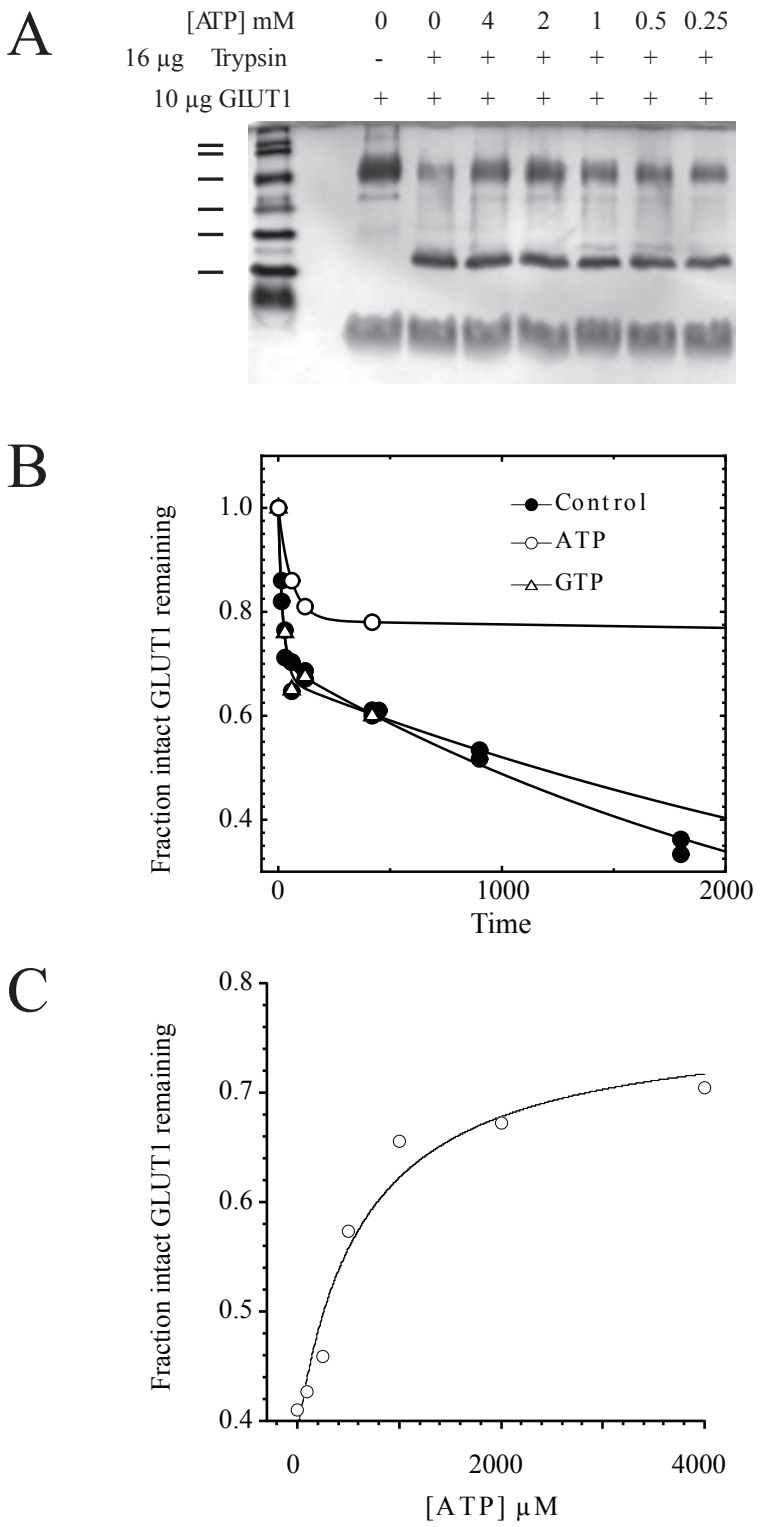
A
[ATP] mM 0 0 4 2 1 0.5 0.25
16 µg Trypsin - + + + + + +
10 µg GLUT1 + + + + + + +
B
Control
ATP
GTP
Fraction intact GLUT1 remaining
1.0
0.8
0.6
0.4
0
1000
2000
Time
C
Fraction intact GLUT1 remaining
0.8
0.7
0.6
0.5
0.4
0
2000
4000
[ATP] µM

Figure 4.1

GLUT1 is hydrolyzed with a tau of 4.5 sec and the remaining intact GLUT1 is proteolyzed with a tau of 2500 sec (Figure 4.1B).

***Specificity of nucleotides*** We first wanted to determine if the presence of nucleotides affects GLUT1 proteolysis by trypsin. Addition of 4 mM GTP is without effect on the time-course of GLUT1 proteolysis by trypsin (Figure 4.1B), however when 4 mM ATP is present in the digestion, the size and rate of the proteolysis burst phase are significantly reduced (extent = 22%, tau = 56 sec) (Figure 4.1B). Like GTP, unreactive nucleotides AMP, ADP, and CTP also do not affect the rate of trypsin-catalyzed GLUT1 proteolysis.

We further investigated ATP-suppression of GLUT1 trypsin digestion by measuring GLUT1 proteolysis at 60 seconds in the presence of increasing ATP concentrations. ATP inhibition of GLUT1 proteolysis shows a saturable dependence on [ATP] with 50% suppression of proteolysis observed at 627 ± 268 μM ATP (Figure 4.1C).

***Immunoblot Analysis*** We also examined GLUT1 fragmentation patterns by immunoblot analysis of GLUT1 digests using GLUT1 peptide-directed IgGs. These included N-Ab (directed against GLUT1 amino acid 1-13), L6-7-Ab (directed against GLUT1 amino acid 217-231), L7-8-Ab (directed against GLUT1 amino acid 299-311) and C-Ab (directed against GLUT1 amino acid 480-492). ATP (4 mM) reduces GLUT1 digestion efficiency (100:1 GLUT1:trypsin by mass; 20ºC; 30 min reaction) as detected by antibodies specific

to L7-8 and the C-terminus, see Figure 4.2A. Figure 4.2B aligns peptides with immunoblot analysis based upon peptide mass, location of trypsin-cleavage sites, and antibody reactivity to indicate potential assignments of ATP-protected peptides to GLUT1 sequence. To more closely examine the region specific concentration dependence of ATP-inhibition of trypsin-catalyzed GLUT1 proteolysis, we measured the retention of peptides recognized by carboxy terminal domain antibody (Figure 4.3). ATP-suppression of C-terminal digestion is half-maximal at approximately 400 μM ATP.

***Analysis of full-length GLUT1 accessibility to peptide directed IgGs*** We next examined if ATP induced global conformational changes to GLUT1 by using ELISA to monitor peptide-directed IgG binding to membrane-resident GLUT1. GLUT1 proteoliposomes were adsorbed to ELISA wells then incubated ± ATP and peptide-directed IgGs. As reported previously [185], ATP inhibits C-Ab binding to GLUT1 proteoliposomes (Figure 4.4A). This is also observed with C-Ab binding to red cell membrane fragments (Figure 4.4B) and in membranes isolated from HEK cells exogenously expressing wild-type human GLUT1 (Figure 4.4C). When HEK cells are transfected with a GLUT1-GLUT4 chimera in which the GLUT1 large middle loop (L6-7) is replaced by equivalent GLUT4 sequence (G1L4$_{6\text{-}7}$G1C1), ATP-inhibition of C-Ab binding to the chimera is lost. Despite the loss of ATP-modulation, this chimera is expressed at the cell surface and transports 2-deoxy-D-glucose as efficiently as does wild-type GLUT1.

We have also examined a wider array of peptide-directed IgG for ATP-inhibition of binding using this ELISA technique. Similar to the western blot analysis examining

**Figure 4.2 Immunoblot analysis of trypsin digested GLUT1 ± 4 mM ATP.** Purified GLUT1 was digested with limiting amounts of trypsin in the presence and absence of 4mM ATP. The resulting peptides were analyzed by Western Blot analysis using a panel of antibodies directed against specific GLUT1 domains: N-Ab (GLUT1 residues 1 - 13; L6-7-Ab (GLUT1 residues 217-231); L7-8-Ab (GLUT1 residues 299-311) and C-Ab (GLUT1 residues 480-492). The upper panels show western analysis of tryptic digests. The key indicates the presence (+) or absence (-) of trypsin or ATP (4 mM). The bars to the left of each blot show the mobility of molecular weight standards (kDa). The arrows to the right of each blot indicate peptides whose intensity is greater when digests are carried out in the presence of ATP. The lower panel represents GLUT1 in linear form and the open boxes show the locations of N-Ab, L6-7-Ab, L7-8-Ab and C-Ab directed IgG binding domains. The arrows above linearized GLUT1 indicate GLUT1 tryptic cleavage sites determined by MS/MS analysis of GLUT1 tryptic digests. The panels below indicate putative assignments of ATP-sensitive GLUT1 peptides detected by peptide-directed IgGs and their theoretical molecular weight (kDa).

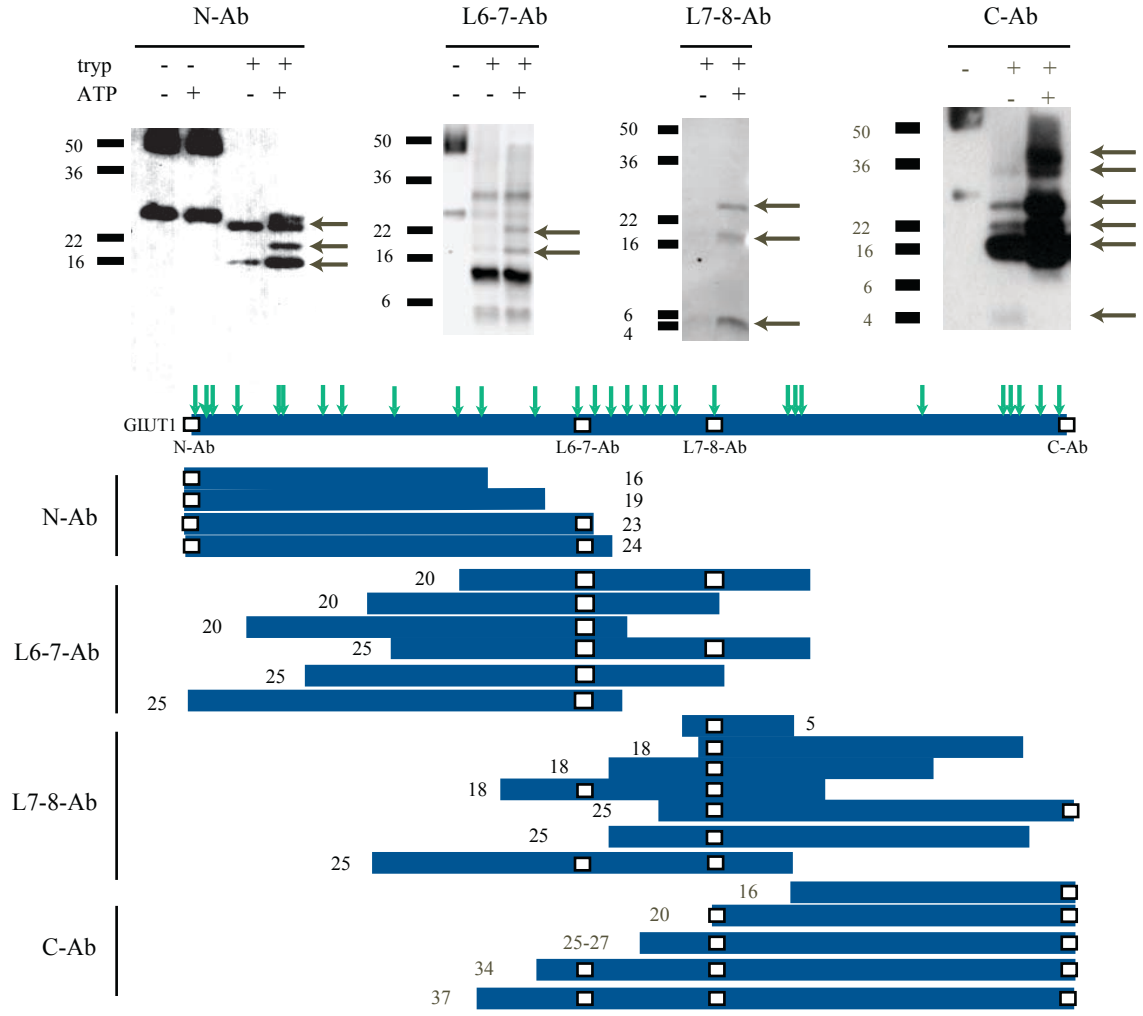
N-Ab
L6-7-Ab
L7-8-Ab
C-Ab
tryp
ATP
50
36
22
16
6
4
GLUT1
N-Ab
L6-7-Ab
L7-8-Ab
C-Ab
16
19
23
24
20
20
20
25
25
25
5
18
18
18
25
25
25
16
20
25-27
34
37

Figure 4.2

**Figure 4.3 [ATP] dose response to trypsin digestion.** Purified GLUT1 was digested with limiting amounts of trypsin in the presence of increasing amounts of ATP. The resulting peptides were analyzed by Western Blot analysis **(A)** using C-Ab (GLUT1 residues 480-492). The key indicates the concentration of ATP present during proteolysis. The lines to the left of the blot show the mobility of molecular weight standards (kDa). The arrows to the right of the blot indicate peptides (20 and 28 kDa) whose intensity was quantitated. **(B)** The relative intensities of 20 kDa (filled circles) and 28 kDa (open circles) peptides as [ATP] is increased during proteolysis. Peptide intensity (volume) was quantitated by densitometric analysis using the Image J software package and plotted as a function of [ATP]. The curves drawn through the points were computed by nonlinear regression assuming that intensity increases with [ATP] in a simple, saturable fashion. 20 kDa and 28 kDa peptides are half-maximally protected by ATP at (366 ± 202) and (440 ± 211) μM, respectively.

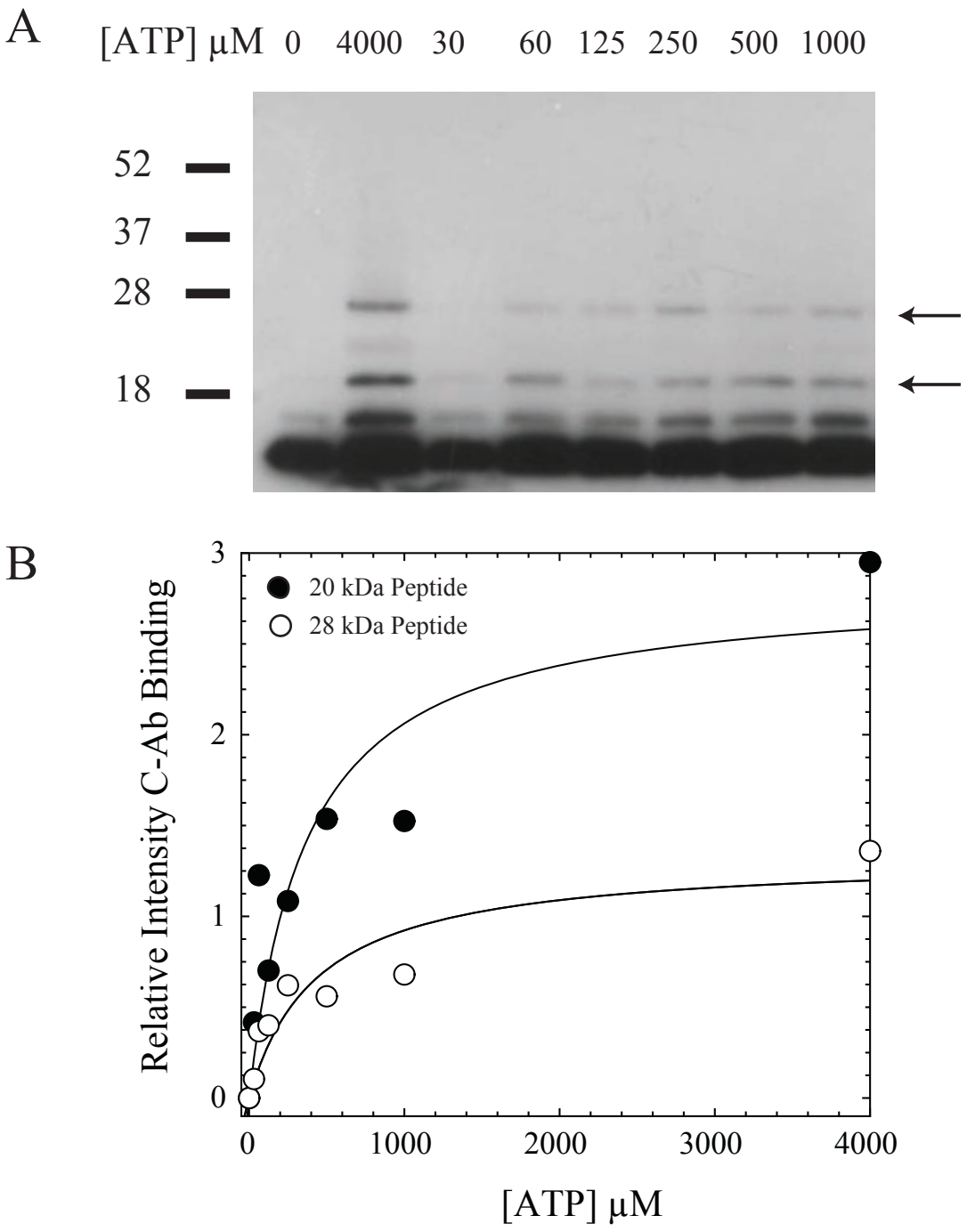
A
[ATP] μM 0 4000 30 60 125 250 500 1000
52
37
28
18
B
Relative Intensity C-Ab Binding
20 kDa Peptide
28 kDa Peptide
0
1
2
3
0
1000
2000
3000
4000
[ATP] μM

Figure 4.3

**Figure 4.4 Time course of C-Ab binding to ELISA dish-Immobilized GLUT1 proteoliposomes: (A)**, red cell membranes **(B)**, membranes from HEK cells expressing GLUT **(C)** and membranes from HEK cells expressing the GLUT1-GLUT4 chimera $G1L4_{6\text{-}7}G1C1$ in which GLUT1 L6-7 is substituted by GLUT4 L6-7 **(D)**. In each panel, the extent of C-Ab binding is read as $OD_{415\ nm}$ obtained upon addition of HRP substrate and using HRP-conjugated goat anti-rabbit IgG as the secondary antibody. The abscissa indicates the duration of C-Ab exposure to membranes prior to free C-Ab removal. Filled circles shown C-Ab binding in the presence of ATP (4 mM) and open circles show C-Ab binding in the absence of ATP. Results are shown as mean ± SEM of triplicate measurements. In all cases, results were analyzed assuming a single exponential phase of IgG binding described by $B_{max}(1\text{-}e^{-kt})$ where $B_{max}$ is equilibrium binding, k is the first order rate constant for binding and t is time. The following results were obtained: A, 0 ATP, $B_{max}$ = 0.65 ± 0.012, k = 0.13 ± 0.06 per min; + ATP, $B_{max}$ = 0.46 ± 0.02, k = 0.12 ± 0.01 per min. B, 0 ATP, $B_{max}$ = 0.84 ± 0.13, k = 0.10 ± 0.03 per min; + ATP, $B_{max}$ = 0.49 ± 0.05, k = 0.17 ± 0.05 per min. C, 0 ATP, $B_{max}$ = 0.67 ± 0.02, k = 0.11 ± 0.01 per min; + ATP, $B_{max}$ = 0.47 ± 0.03, k = 0.11 ± 0.01 per min. D, 0 ATP, $B_{max}$ = 0.63 ± 0.02, k = 0.14 ± 0.05 per min; + ATP, $B_{max}$ = 0.56 ± 0.04, k = 0.12 ± 0.01 per min.

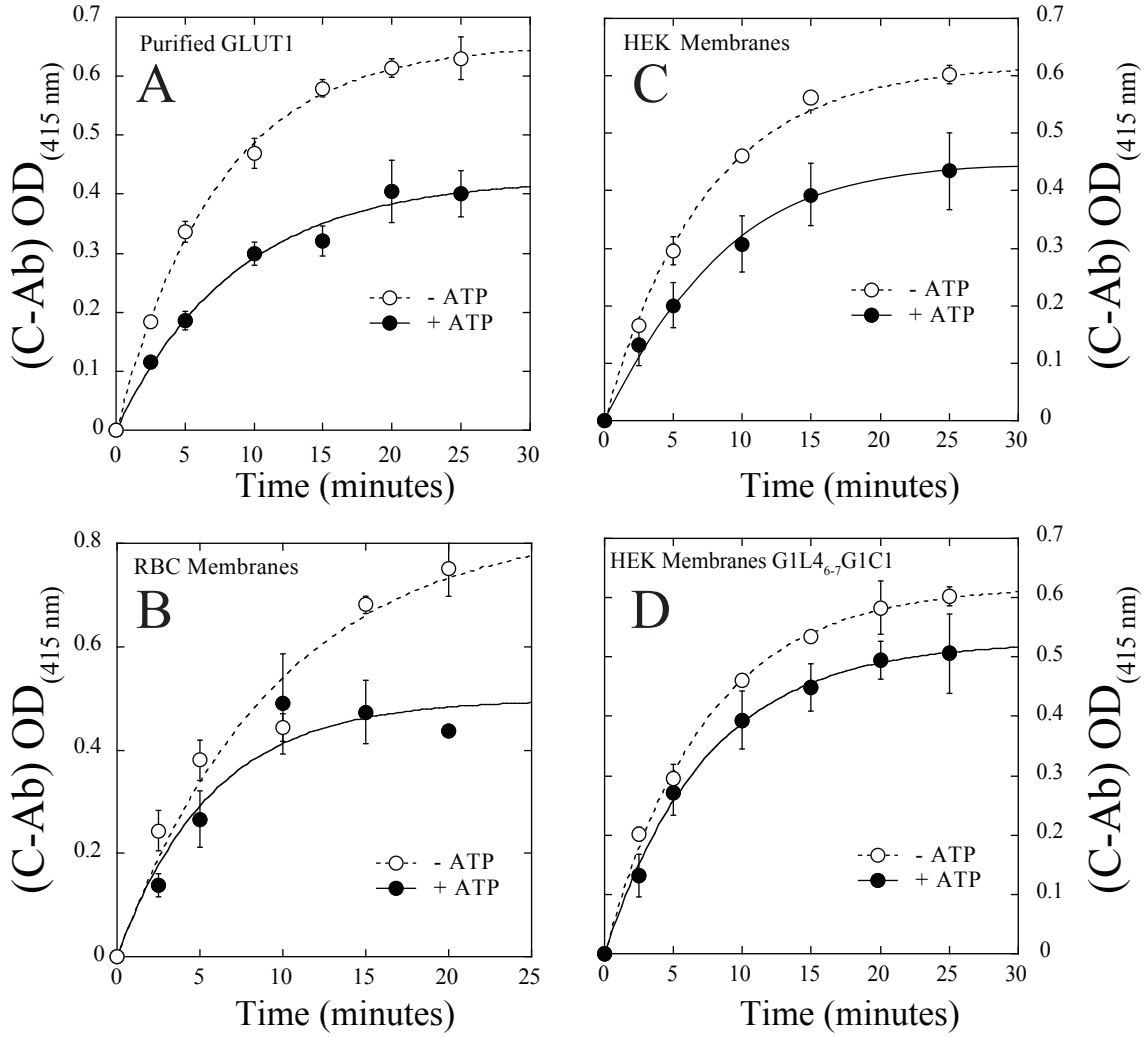
Purified GLUT1
A
HEK Membranes
C
RBC Membranes
B
HEK Membranes G1L4$_{6-7}$G1C1
D
- ATP
+ ATP
(C-Ab) OD$_{(415\ nm)}$
Time (minutes)

Figure 4.4

trypsin-derived peptides, ATP does not affect binding of L2-3-Ab or L6-7-Ab to membrane-resident GLUT1. ATP does, however, reduce L7-8-Ab and C-Ab binding to full-length GLUT1 proteoliposomes. N-Ab and L8-Ab do not bind appreciably to native GLUT1 structure.

***Analysis of GLUT1 biotinylation*** We have previously used ESI-MS/MS to show that biotin-conjugated N-hydroxysuccinimide esters (Sulfo-NHS-LC-Biotin) react with at least 12 of the 16 GLUT1 lysine side chains to form a covalent, MS/MS stable amide bond (see Chapter III). This probe is particularly useful for detecting differential side chain accessibility on both the global (western blot or ELISA using streptavidin-HRP) and local (MS/MS identifying the modified lysine) levels. In this study, monitoring GLUT1 labeling by these techniques provides the most specific method (in addition to the aforementioned observations from immunoblot and ELISA techniques) for probing the conformational dynamics displayed by GLUT1 in response to ATP modulation of glucose transport.

GLUT1 proteoliposomes were incubated at 4°C for 30 minutes with ATP (or control buffer environment) prior to adding a 20-fold molar excess of Sulfo-NHS-LC-Biotin to begin GLUT1 labeling. The reaction was quenched by exposure to 100 mM glycine, which neutralized remaining probe. Figure 4.5A shows the time course of GLUT1 labeling in the presence of 4 mM ATP. Compared to reaction conditions lacking nucleotide or containing non-inhibitory AMP (4 mM), the inclusion of ATP reduces total modification by approximately 40% (inset), without slowing the reaction rate.

By examining the extent of Sulfo-NHS-LC-Biotin incorporation in the presence of increasing ATP concentrations, we calculated the $K_i^{ATP}$ for ATP-inhibition of GLUT1 biotinylation to be 2.0 mM, (Figure 4.5B). AMP (0 to 4 mM) does not alter equilibrium GLUT1 labeling. The protection afforded GLUT1 from labeling occurs within the physiological concentration of ATP found in human erythrocytes. There is no change in the rate of biotinylation regardless of the concentration or type of nucleotide. When the same dose-response conditions were examined in the presence of 2 mM AMP, the $K_{i(app)}^{ATP}$ was 2-fold greater, at 3.8 mM. Assuming AMP competitively antagonizes ATP inhibition of biotinylation, we computed the $K_i^{AMP}$ for antagonism of ATP-inhibition of GLUT1 biotinylation to be 2.2 mM (see figure 4.5B). Although AMP binds to GLUT1 at the nucleotide-binding site, it does not alter GLUT1 accessibility to Sulfo-NHS-LC-Biotin, which appears to be an ATP specific response.

Equilibrium labeling studies performed at a 20 molar excess of Sulfo-NHS-LC-Biotin to GLUT1 proteoliposomes followed by trypsin digestion, isolation of soluble fragments, RP-HPLC separation, and subsequent ESI-MS/MS indicate that specific cytoplasmic loop regions and residues specifically display reduced accessibility to labeling reagent in the presence of 4 mM ATP. Cytoplasmic GLUT1 lysine residues may be grouped into four regions: region 1 contains K225, K229, and K230; region 2 is K245; region 3 is comprised of K255 and K256, all of which are found in L6-7; region 4 contains C-terminal K477.

**Figure 4.5 Analysis of ATP-dependence on lysine modification. (A)** Time course of GLUT1 labeling at 4°C, pH 7.4 by Sulfo-NHS-LC-Biotin (20:1 molar excess of probe to protein). GLUT1 proteoliposomes were pre-incubated for 30 minutes in Kaline, 4 mM AMP, or 4 mM ATP. Biotinylation kinetics are described by pseudo-first order kinetics where labeling equals $B_0 + B_\infty(1\text{-}e^{-kt})$. **Inset**: Average equilibrium labeling extent of at least three normalized labeling experiments done in triplicate ± SEM: Kaline, extent = 1.20 ± 0.03; 4 mM AMP extent = 1.28 ± 0.05; 4 mM ATP extent = 0.73 ± 0.03. **(B)** Effects of nucleotides on GLUT1 biotinylation. Biotin incorporation extent and labeling reaction rate were plotted versus [AMP] or [ATP] present during labeling. Linear regression analysis indicates no correlation between [AMP] and labeling extent ($R^2 = 0.31$), [AMP] and reaction rate ($R^2 = 0.29$), and [ATP] and reaction rate ($R^2 = 0.3$). Nonlinear regression using a modified Michaelis Menten equation provides the following labeling constants in the presence of variable [ATP]: labeling in the absence of ATP, $B_0 = 1.210 \pm 0.007$, maximum inhibition of labeling in the presence of saturating [ATP], $B_{min} = 0.72 \pm 0.04$ and [ATP] inhibits labeling half-maximally at $K_i = 2.0 \pm 0.3$ mM. ATP inhibition of labeling was measured in the presence of competing AMP. GLUT1 was labeled in the presence of increasing [ATP] at constant 2 mM [AMP]. Linear regression analysis shows no correlation between [ATP] and labeling rate ($R^2 = 0.014$). Modified Michaelis non-linear regression analysis provides: $B_0 = 0.9$, $B_{min} = 0.6$, and $K_i = 3.8 \pm 2$ mM. Assuming AMP competitively inhibits ATP modulation of labeling, $K_{i(app)}$ for AMP = 2.2 mM.

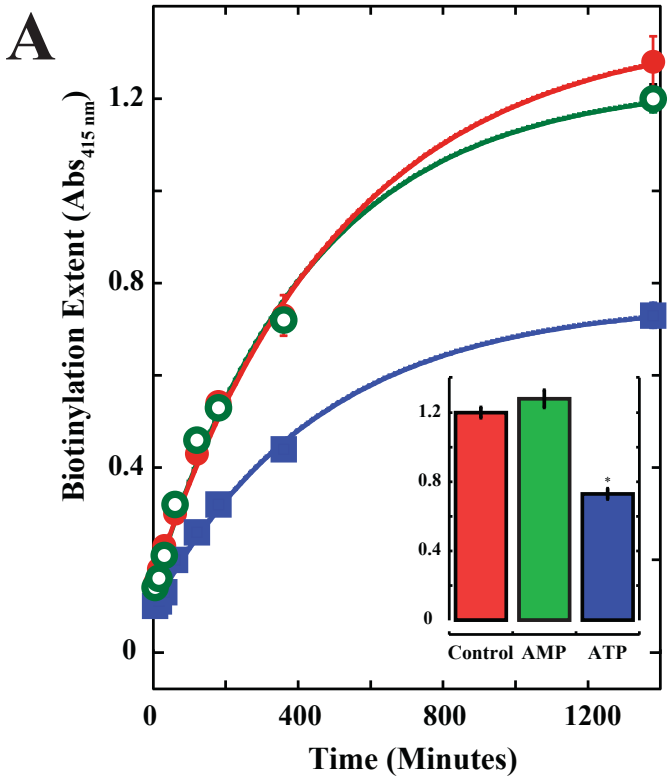


| Condition | $B_0$ | $B_\infty$ | k ($min^{-1}$) |
|---|---|---|---|
| Kaline | 0.15±0.02 | 1.09±0.05 | 0.0023±0.003 |
| 4 mM AMP | 0.16±0.01 | 1.20±0.03 | 0.0019±0.0001 |
| 4 mM ATP | 0.098±0.009 | 0.66±0.02 | 0.0022±0.0002 |

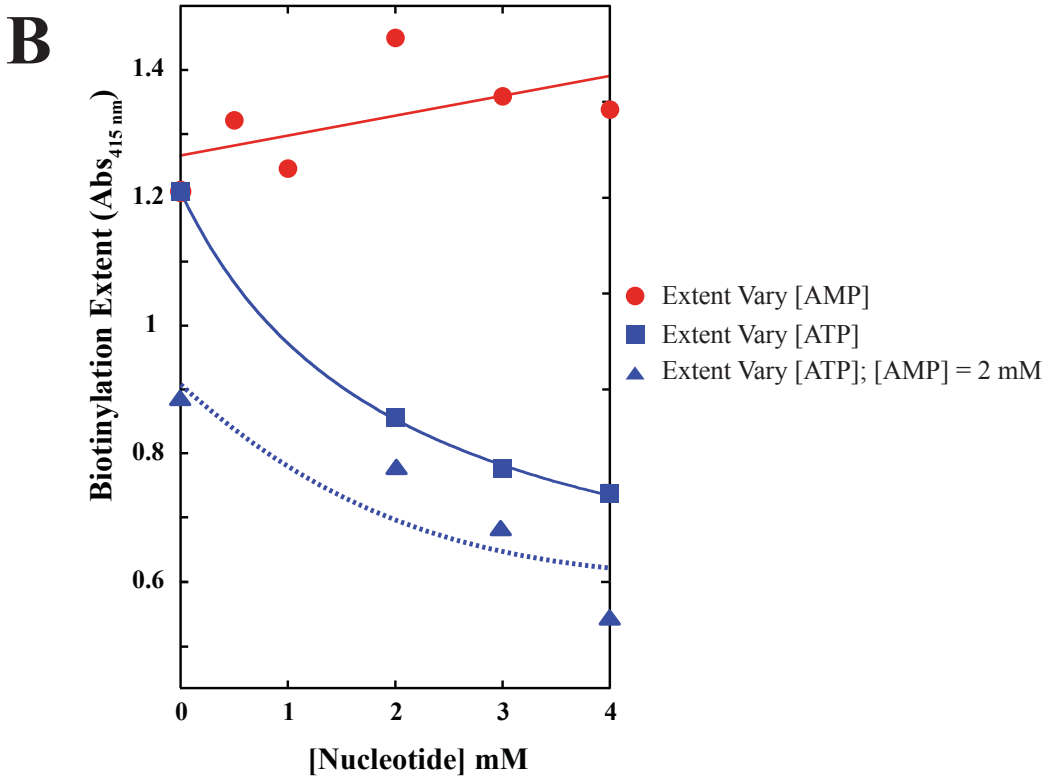


Figure 4.5

To examine localized changes in GLUT1 modification, we identified all peptides within a specific region that contain lysine residues, noted each *m/z* ratio, and isolated the intensity of each peak (area under the curve) using the Qual Browser program within X-Calibur for labeling reactions that took place in Kaline, 4 mM AMP, and 4 mM ATP. Next, we summed the total intensity for labeled peptides and divided this value by the total intensity for all peptides. The reported % difference in labeling intensity is relative to the ATP value.

Region 1 displayed no discernible change in the quantity of labeled peptide under any reaction conditions. Regions 2, 3, and 4, however, did display distinct decreases in lysine modification. K245 of region 2 displayed a 38% reduction in amount of labeled peptide detected (see Figure 4.6A (AMP) and 4.6B (ATP) for representative intensity and area images). Similarly region 3 displayed a 24% reduction and K477 of the C-terminal region 4 experienced a 26% decrease in labeling efficiency. Overall, the lysine residues found within the C-terminal half of L6-7 and the C-terminus of GLUT1 display a 20-25% reduction in labeling by Sulfo-NHS-LC-Biotin (Figure 4.7).

### *DISCUSSION*

ATP is the limiting reagent for primary active membrane transporters because the free energy released upon ATP hydrolysis is coupled to the movement of substrate against its concentration gradient as seen with proteins belonging to the ATP Binding Cassette (ABC) Superfamily [189]. Since GLUT1 is a passive glucose uniporter belonging to the Major Facilitator Superfamily (MFS), ATP hydrolysis is not necessary for solute

**Figure 4.6 ATP and differential K245 accessibility to biotin labeling.** GLUT1 was labeled to equilibrium by Sulfo-NHS-LC-Biotin in the presence of 4 mM AMP (A) or ATP (B). Proteoliposomes were digested with trypsin, and soluble peptides were examined by RP-HPLC-ESI-MS/MS. In each sample, two peptides containing K245 were isolated: the first (*m/z* = 1444.7 Da) with primary amino acid sequence R(232).GTADVTHDLQEM*K*(245).E, which was unlabeled and cleaved at K245 and the second (*m/z* = 2285.1 Da) with primary amino acid sequence R(232).GTADVTHDLQEM***K***EESR(249).Q, which was labeled (339.2 Da adduct covalently attached to K245) and cleaved at R249. The areas under each elution curve were obtained and analyzed as $\%\,\mathrm{mod}\,ified = \frac{area\,\mathrm{mod}\,ified}{\sum area K245\,peptides}$. **(A)** Labeling conducted in the presence of 4 mM AMP. Peptide 1 Area (●) = $5.54 \times 10^8$, Peptide 2 Area (■) = $1.15 \times 10^8$, % modified peptide = 17.24%. **(B)** Labeling conducted in the presence of 4 mM ATP. Peptide 1 Area (●) = $5.09 \times 10^8$, Peptide 2 Area (■) = $5.73 \times 10^7$, % modified peptide = 10.12%. 4 mM. K245 demonstrates a 41% decrease in labeling accessibility in the presence of 4 mM ATP.

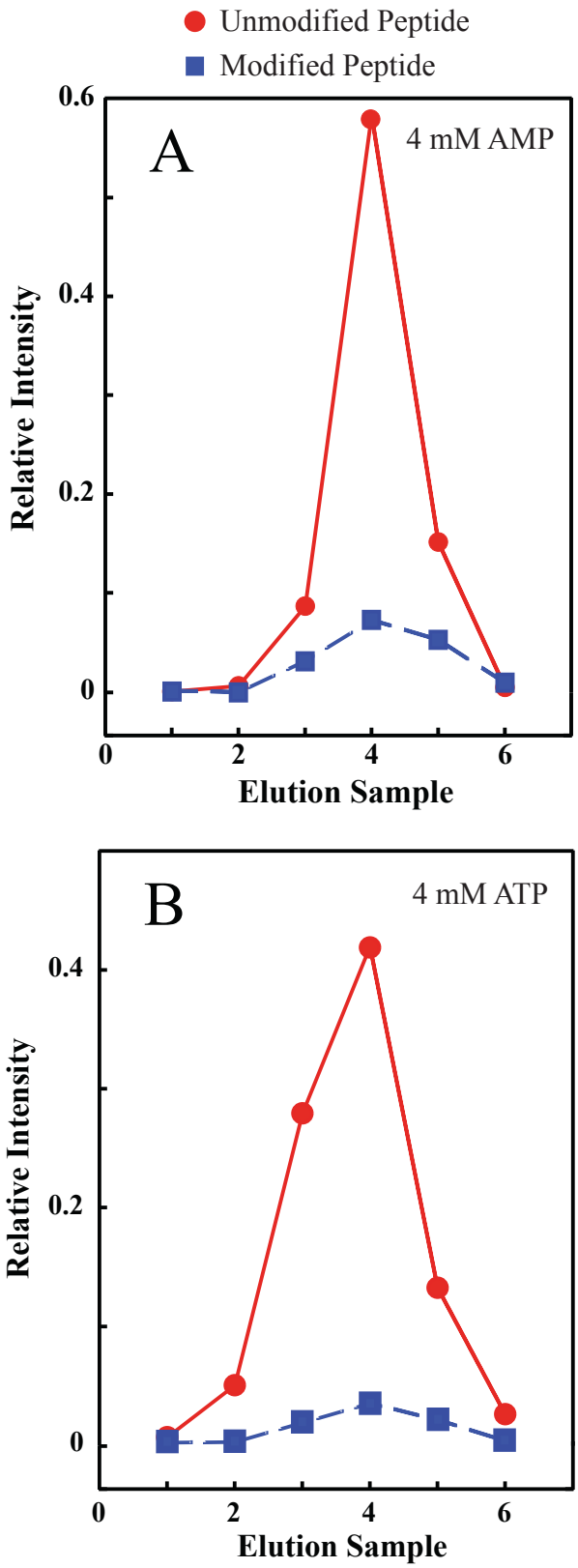
Unmodified Peptide
Modified Peptide
A
4 mM AMP
Relative Intensity
0.6
0.4
0.2
0
0
2
4
6
Elution Sample
B
4 mM ATP
Relative Intensity
0.4
0.2
0
0
2
4
6
Elution Sample

Figure 4.6

**Figure 4.7 Decrease in GLUT1 lysine modification in the presence of 4 mM ATP.** GLUT1 topography image to summarize all computations based upon the data isolated and analyzed as described in Figure 4.6. Region 1 (found on the N-terminal half of L6-7) considers lysine residues 225, 229, and 230; Regions 2 and 3 (found on the C-terminal half of L6-7) focuses on K245 and K255 and K256, respectively; Region 4 includes C-terminal K477. –Δ%ATP represents the decrease in labeled peptides (versus all peptides containing regional lysine residues) found when GLUT1 equilibrium labeling by Sulfo-NHS-LC-Biotin was conducted in the presence of 4 mM ATP. The –Δ%ATP ± SEM (four separate experiments) values for Region 1: 6.9 ± 3.4% (not significantly different ± 4 mM ATP); Region 2: 37.6 ± 5% (reported to 95% confidence interval); Region 3: 24.1 ± 5% (reported to 90% confidence interval); Region 4: 25.5 ± 4% (reported to 95% confidence interval).

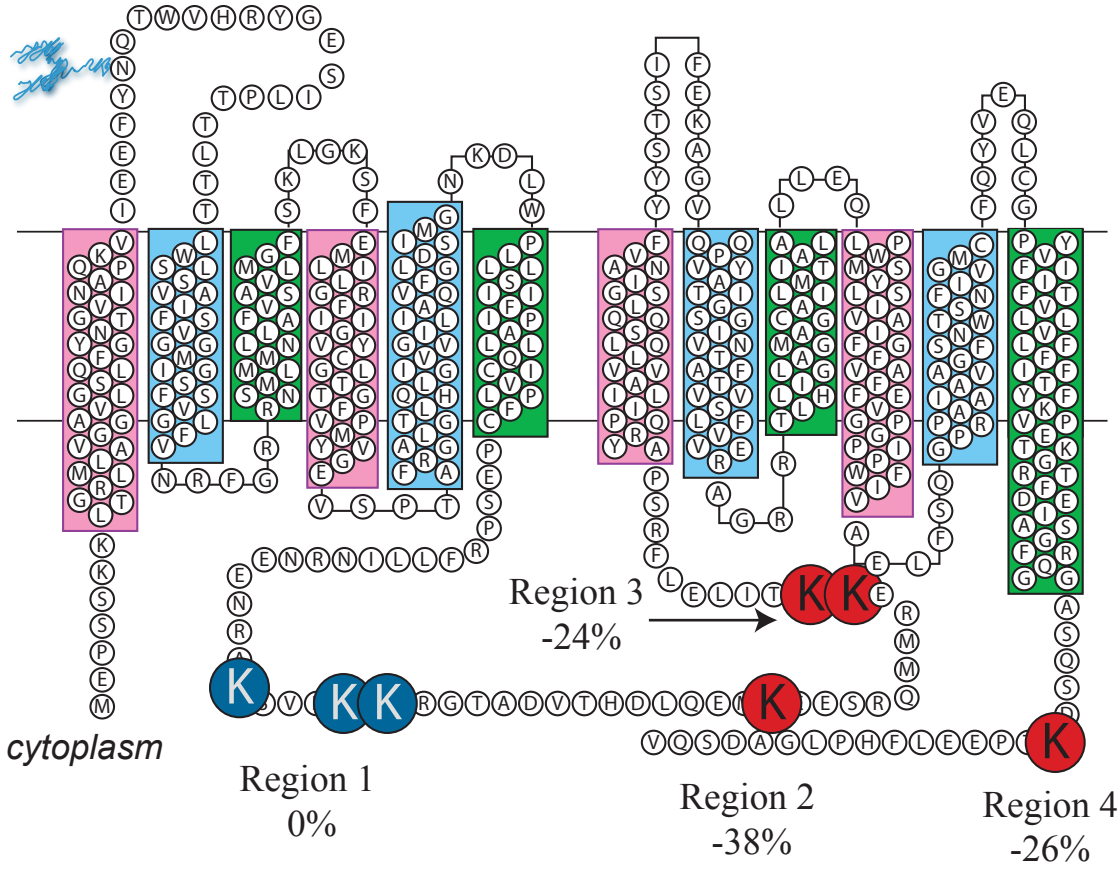


Figure 4.7

transport. The nucleotide, however, does play a significant role in regulating GLUT1-mediated glucose transport, especially as observed in the human erythrocyte. Glucose transport asymmetry in red blood cells is directly caused by cytoplasmic ATP, as evidenced by studies with erythrocyte ghosts in which those ghosts lacking ATP display transport symmetry while ghosts resealed with 4 mM ATP demonstrate normal transport asymmetry [184]. Further characterization of the ATP-dependent GLUT1-mediated transport modulation illustrates that ATP binds near putative L8-9 and TM9, which are located at the interface between the lipid bilayer and the cytoplasm [64,135]. Based upon our observations in this study, it does not appear that ATP binding at this site is sterically responsible for reducing the sugar carrying capacity of GLUT1. It is more likely that ATP induces global conformational changes that reduce $V_{max}$ and $K_m$ value for sugar import, thus resulting in the ATP-dependent regulation of GLUT1-mediated glucose transport.

GLUT1 has 36 potential trypsin cleavage sites that are conveniently distributed throughout the primary structure in both termini, multiple loops, and at the membrane-aqueous interface of many transmembrane α-helices [155]. These locations are useful for identifying the regions that display reduced susceptibility to trypsin proteolysis when ATP is present in the reaction sample. Gel electrophoresis clearly shows that trypsin adequately digests GLUT1 in buffer, but that the addition of ATP reduces digestion efficiency as the half-life of this reaction increases by 10-fold, in a concentration-dependent manner.

The global inhibition of trypsin digestion in the presence of 4 mM ATP manifests itself in the presence of more intense GLUT1 peptides arising from the N-terminus, the N-terminal half of L6-7, extracellular L7-8, and the intracellular C-terminus. The C-terminal half of the protein (which includes the nucleotide-binding pocket) demonstrates a greater overall decrease in complete proteolysis (+ATP) as evidenced by the C-Ab and L7-8-Ab blots, which display either a greater signal intensity or a unique signal for peptides not observed when proteolysis occurs in the absence of ATP. The L-6-7 and N-terminal antibodies also detect ATP-dependent peptides. These peptides, however, are more likely due to ATP protection of potential trypsin cleavage sites that fall within nonregulatory, ATP-binding motifs. These sites of likely steric interaction include exofacial Walker motif residues GFSKLGKS (containing two potential trypsin cleavage sites) and an internal adenylate kinase motif including residues KSVLK (containing two trypsin residues) [135].

We employed ELISA analyses to examine ATP-specific changes in IgG accessibility to full length GLUT1 protein. The results indicate that ATP inhibits the binding of the C-Ab and L7-8-Ab to full length GLUT1, while ATP does not antagonize GLUT1 recognition by antibodies recognizing the N-terminus or N-terminal half of L6-7. HEK cells can be transfected with wild type GLUT1 and isolated membranes display the same reduction in C-Ab binding observed in red cells, red cell membranes, and GLUT1 proteoliposomes. When the membranes from HEK cells expressing a GLUT1-GLUT4 chimera that replaces GLUT1 L6-7 with GLUT4 L6-7, but leaves the remainder of the membrane embedded $\alpha$-helices and interconnecting loops intact are isolated, the interaction with

GLUT1 C-Ab is equal in the presence or absence of ATP. Although HEK cells expressing this construct display normal levels of glucose transport and cell surface expression relative to control, it appears as if GLUT1 L6-7 is required to mediate the ATP-dependent response.

We pre-incubated GLUT1 with ATP prior to reaction with the NHS-biotin probe to determine if we could measure and localize ATP induced conformational changes to the transporter structure. GLUT1 displays a significant, global ATP-dependent decrease in lysine modification. We observed an approximately 40% decrease in GLUT1 NHS-biotin labeling efficiency when the reaction was carried out in 4mM ATP (versus competitive ATP antagonist AMP or kaline buffer). We were subsequently able to implicate specific ATP-sensitive GLUT1 lysine residues following trypsin-catalyzed proteolysis and ESI-MS/MS.

MS/MS quantitation studies show that K245, K255, K256, and K477 undergo a nucleotide-specific reduction in accessibility to NHS-biotin when labeled in the presence of 4mM ATP, whereas K225, K229, and K230 displayed no change in modification extent. The overall decrease in labeling as detected by quantitative mass spectrometry is approximately 25%. This implies that the majority of the global changes in accessibility can be attributed to these cytoplasmic residues, however, it is possible that additional changes are communicated to the extracellular loops or actual TM regions. Specifically, the L7-8 observations support ATP inhibition of K300 cleavage, however, this residue was difficult to isolate and quantify using the outlined MS technique.

Taking all of these observations together, it appears as if the GLUT1 C-terminus and the C-terminal half of L6-7 respond to ATP binding by undergoing a conformational change that reduces their respective accessibility to polar reagents. We propose a model where the GLUT1 C-terminal tail and L6-7 angle upward toward the cytoplasm-lipid bilayer interface, thereby modifying the translocation pathway. Figure 4.8 summarizes this idea by showing the putative locations of ATP-sensitive regions and residues that are protected from trypsin digestion (from Figure 4.2), antibody binding (from Figure 4.4), and covalent modification by Sulfo-NHS-LC-Biotin (from Figure 4.7).

ATP has been proposed to inhibit glucose transport by increasing transporter affinity for sugar and introducing an additional sugar binding or occlusion step within the protein, which reduces $V_{max}$ for sugar import [28,85,185]. We envision the following series of conformational changes that mediate this response: the C-terminal tail interacts with L6-7. The direct points of interaction likely include the primary sequence of at least K245-K256, but lack K230 and regions more N-terminal, as suggested by MS and antibody binding observations. This interaction creates a cage structure that effectively inhibits glucose release into the cytoplasm as a result of the GLUT1-ATP interaction, thus regulating glucose transport (Figure 4.8).

**Figure 4.8 Summary and model for ATP-mediated GLUT1 glucose transport regulation.** Using the GLUT1 putative topography [64], the ATP-responsive domains are highlighted and drawn to reflect the proposed mechanism of ATP modulation. In the presence of AMP (left topography), all trypsin cleavage sites (○) and sites of antibody recognition sequence (colored rectangles; grey represents sites where IgG recognition was not detected; blue represents sites where IgG recognition was detected) are indicated with cytoplasmic L6-7 and the C-terminus extended into the cytosol. In the presence of ATP (right topography), the putative locations of ATP-sensitive regions and residues are highlighted: (grey ●) represents cleavage sites protected from trypsin digestion (from Figure 4.2), colored rectangles: (green represents sites where IgG binding is unaffected by ATP and red represents sites where IgG binding is affected by ATP binding) represent changes in antibody binding (from Figure 4.4), and (red ●) represents sites of decreased covalent modification by Sulfo-NHS-LC-Biotin (from Table 4.1). Taking all of these observations together, it appears that the GLUT1 C-terminus and the C-terminal half of L6-7 respond to ATP binding by undergoing a conformational change that reduces their respective accessibility to polar reagents. We propose a model where the GLUT1 C-terminal tail (from K477 to the end) and L6-7 (all regions C-terminal to K245) interact by angling upward toward the cytoplasm-lipid bilayer interface, thereby modifying the translocation pathway. This model provides biochemical support for the observation that ATP inhibits glucose transport by introducing an additional sugar binding or occlusion step within the protein, which reduces $V_{max}$ for sugar import [28,85,185]. This interaction is proposed to create a cage that slows glucose release into the cytoplasm.

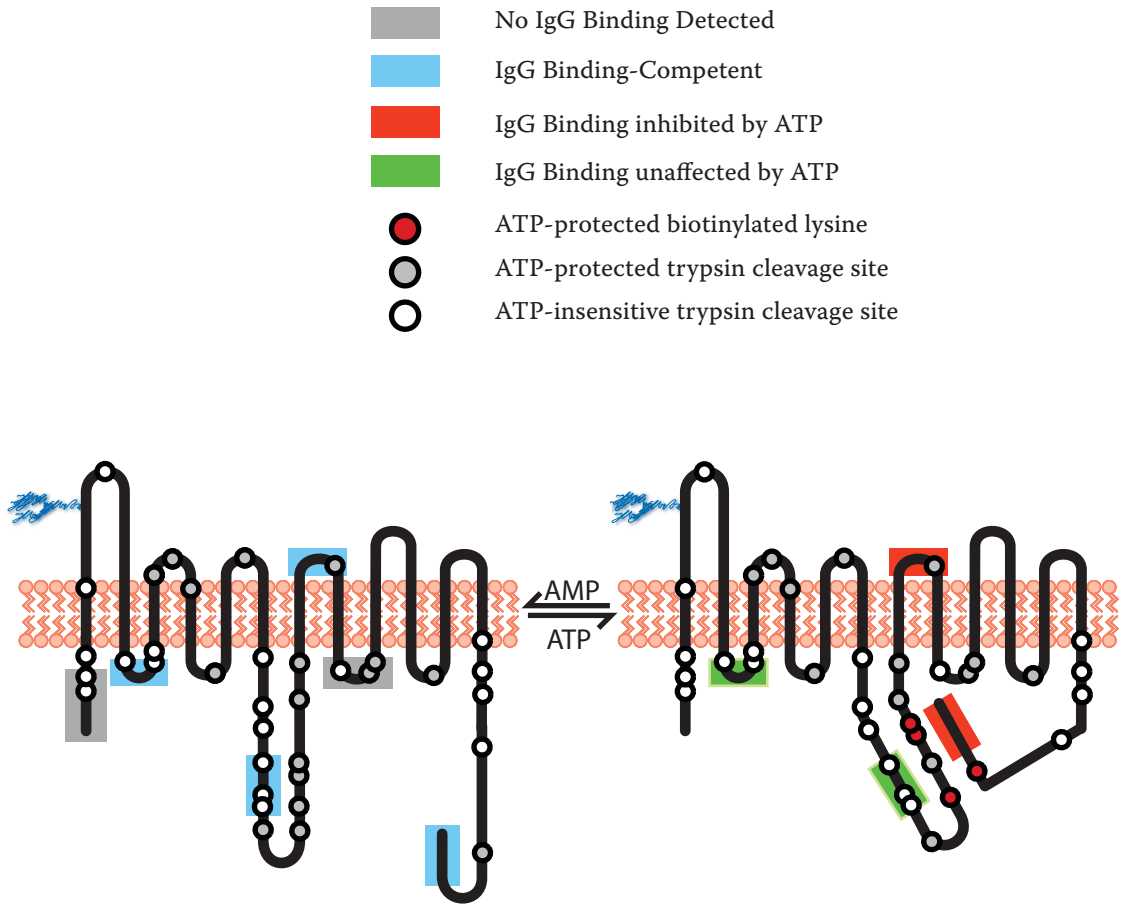
No IgG Binding Detected
IgG Binding-Competent
IgG Binding inhibited by ATP
IgG Binding unaffected by ATP
ATP-protected biotinylated lysine
ATP-protected trypsin cleavage site
ATP-insensitive trypsin cleavage site
AMP
ATP

Figure 4.8

# CHAPTER V

## HUMAN TYPE 1 FACILITATIVE GLUCOSE TRANSPORT PROTEIN PRESENTS REDUCTANT-SENSITIVE CONFORMERS

**This work was supported by NIH grants DK 36081 and DK 44888 and by ADA grant ADA 1-06-IN-04 (Gail Patrick Innovation Award supported by a generous gift from the Estate of Gail Patrick)**

Data presented in this chapter found in Figures 5.1, 5.2, and 5.3 and tables 5.1 and 5.2 were collected and analyzed with Christopher A. Graybill, PhD.

***ABSTRACT***

The human type 1 facilitative glucose transport protein (GLUT1) displays cell-specific transport behavior, conformational states and electrophoretic mobilities. We investigated populations of GLUT1 conformational states and mobilities by gel electrophoresis and Mass Spectrometry (MS). GLUT1 was purified from human erythrocytes and deglycosylated using PNGaseF to produce two peptides that migrate as 49 and 41 kDa species upon SDS-PAGE. Both peptides cross-react with GLUT1 amino- and carboxy-terminal peptide-directed IgGs and retain significant α-helical structure upon gel-elution as judged by circular dichroism. Mass analysis of 49 and 41 kDa peptides by MS results in mass recordings of 54 kDa. MS/MS sequence analysis of tryptic-, α-chymotryptic- or CNBr-digests of gel-eluted GLUT1 yields 90% sequence coverage. GLUT1 contains 6 cysteine residues but none is fatty-acylated. Three cysteine residues (C133, C201, and C429) are alkylated by iodoacetamide in membrane-resident, non-reduced GLUT1. Two additional residues (C207 and C421) are alkylated following GLUT1-reduction. Nonreduced, alkylated, deglycosylated GLUT1 migrates as a 49 kDa peptide upon nonreducing SDS-PAGE whereas reduction/alkylation produces 49 and 41 kDa peptides. We conclude that C207, C421 and possibly C347 assume a primary role in GLUT1 intra-chain folding by forming internal- or mixed-disulfides that promote the "49 kDa peptide" fold and the reductant-sensitive GLUT1 conformation.

## *INTRODUCTION*

The Type 1 glucose transport protein (GLUT1) is a 54 kDa, Major Facilitator Superfamily (MFS) transport protein [189] expressed in the endothelial cells of the blood brain barrier [190,191], the perineurium [192] and the blood heart barrier [167,168]. GLUT1 is also expressed in astrocytes [191], cardiomyocytes [168,193] and erythrocytes [194] where it catalyzes passive uniport of pentose and hexose sugars [117]. GLUT1 thus assumes a principal role in cellular glucose import and glucose delivery to the brain, peripheral nerve and myocardium [167,195,196].

This central physiological function in combination with accessibility to biochemical [166,197] and molecular manipulation [49,155,190] has stimulated a significant body of work investigating GLUT1 higher order structure and transport mechanism. At this time, however, GLUT1 structure and mechanism are only partially understood [43,48,64,80,116,182,198-200]. Difficulties in characterizing GLUT1 function arise in part because GLUT1 catalytic behavior is cell-specific. For example, GLUT1 displays accelerated exchange transport and asymmetric net fluxes in human red cells [125] but net fluxes are symmetric in rabbit and rat erythrocytes [201,202] while accelerated exchange transport is absent when human GLUT1 is expressed in *Saccharomyces cerevisiae* [182]. Do cell-specific environmental factors or post-translational modifications influence GLUT1 function? Erythrocyte GLUT1 is a recognized substrate for serine-phosphorylation [203] and thiol-fatty-acylation [204]. Where examined, however, GLUT1 phosphorylation appears to be physiologically silent [203] and thiol-

acylation is significantly sub-stoichiometric [204] suggesting that neither modification can account for variations in GLUT1 function.

GLUT1 is glycosylated at Asn45 [45] and shows cell-specific glycosylation. Human red cell GLUT1 resolves as a diffuse protein band of $M_r$ = 50-65 kDa upon SDS-PAGE which collapses to a 46 kDa species following deglycosylation [205]. Rat brain capillary GLUT1 and astrocytic GLUT1 resolve as 55 and 45 kDa species respectively [206]. Heterologously expressed human GLUT1 resolves as 52 and 49 kDa species in *Saccharomyces* [182] and as a 48 kDa species in *Xenopus* oocytes where it collapses to a 39 kDa species following deglycosylation [45]. It appears, therefore, that both glycosylated and deglycosylated GLUT1 display cell-specific electrophoretic mobility. Anomalous electrophoretic behavior ($M_{rapp}$ < theoretical $M_r$) may result in part from GLUT1 hydrophobicity causing the protein to oligomerize in sample buffer [182] and may increase GLUT1 SDS binding capacity. However, this cannot explain the different electrophoretic mobilities of deglycosylated human GLUT1 observed upon SDS-PAGE of erythrocyte and oocyte extracts.

One factor that could contribute to cell-specific anomalies in GLUT1 SDS-PAGE mobility is GLUT1 redox state. Purified, nonreduced human GLUT1 forms noncovalent tetramers in non-denaturing detergents whereas reduced GLUT1 forms monomers and dimers [80,84,86,207]. Freeze-fracture EM analysis of membrane bilayer resident native and reduced GLUT1 reveals integral membrane particles of average diameter 10 and 6 nm respectively [80,194]. GLUT1-sensitivity to reductant has been proposed to result

from a single intramolecular disulfide bridge between C347 and C421 leading to GLUT1 oligomerization [86]. The results of some studies, however, question the functional significance of reductant sensitive, GLUT1 oligomers because wild-type- and cys-less GLUT1 catalyze similar rates of reductant-insensitive sugar transport when heterologously expressed in *Xenopus* oocytes [66].

The present study investigates the electrophoretic mobility of reduced and nonreduced deglycosylated GLUT1 and examines the accessibility of membrane-resident GLUT1 cysteine sulfhydryl groups by mass spectrometric analysis of differentially alkylated GLUT1. We demonstrate the presence of reductant-sensitive GLUT1 folding states and show that specific intra-chain folds are associated with the accessibility of specific GLUT1 cysteine sulfhydryl groups.

## *MATERIALS AND METHODS*

***Materials*** Fresh, de-identified human blood was purchased from Biological Specialties Corporation (Colmar, PA). Protein determination assays, Pro Blue coomassie stain and Supersignal chemiluminescence kits were from Pierce (Rockford, IL). Glycerol-free endoglycosidase peptide-N-glycosidase F (PNGaseF) was purchased from New England Biolabs (Ipswich, MA). Nitrocellulose and Immobilon-P were purchased from Fisher Scientific (Hampton, NH). Purified rabbit anti-GLUT1 antibody (C-Ab) raised against a synthetic cytoplasmic carboxyl-terminal peptide of human GLUT1 (residues 480-492) was obtained from Animal Pharm Services, Inc. (Healdsburg, CA). Abgent, Inc. (San Diego, CA) produced two rabbit anti-GLUT1 antibodies, N-Ab and L7-Ab, raised against

synthetic peptides representing intracellular residues 1-13 and exofacial residues surrounding 299-311, respectively. Anti-GLUT1 antisera (δ-Ab) was raised against intact GLUT1 and exclusively recognizes exofacial epitopes [208]. All other reagents were purchased from Sigma-Aldrich (St. Louis, MO).

***Solutions*** Saline consisted of 150 mM NaCl, 10 mM Tris-HCL, and 0.5 mM EDTA, pH 7.4. Lysis medium contained 10 mM Tris-HCl and 0.2 mM EDTA, pH 7.2. K-medium comprised 150 mM KCl, 10 mM Tris-HCL, and 0.5 mM EDTA, pH 7.4. Stripping solution contained 2 mM EDTA, 15.2 mM NaOH, pH 12. Tris medium contained 50 mM Tris-HCL, pH 7.4. Ammonium bicarbonate was 0.5% (63 mM), pH 9.0. Phosphate-buffered saline containing Tween (PBS-T) comprised 140 mM NaCl, 10 mM Na2HPO4, 3.4 mM KCl, 1.84 mM KH2PO4, 0.1% Tween, pH 7.3.

***Glucose transport protein purified from human erythrocytes*** Glucose transporter and endogenous lipids were purified from human erythrocyte membranes in the absence of reductant [84]. Purified, proteoliposome-resident GLUT1 was stored at -80ºC. Protein purity was assessed by SDS-PAGE, and function assayed by determination of GLUT1 binding capacity for the transport inhibitor cytochalasin B (CCB).

***Gel Electrophoresis and Western Blotting*** GLUT1 protein was resolved on 8% polyacrylamide gels as described by Laemmli [162]. Immunoblot analysis using C-Ab (at 1:10,000 dilution); N-Ab (1:250); L7-Ab (1:250) or δ-Ab (1:1,000) was as previously described [182].

***GLUT1 Deglycosylation*** Aliquots of 50 μL purified GLUT1 (1 mg/mL in buffer) were incubated with 3 μL (1,500 activity units) PNGaseF for 1 hr at 37ºC. Deglycosylated GLUT1 was resolved using 8% SDS-PAGE.

***Sample Preparation for Mass Spectrometry Analysis*** Purified GLUT1 protein was separated from bulk, erythrocyte lipids using 8% SDS-PAGE. Coomassie-stained gel lanes guided protein band excision from unstained lanes. Gel slices were homogenized and incubated 16-72 hrs at 25ºC in HPLC grade $H_2O$ containing 0, 2, 4 % SDS or (4% SDS; 8% βME). GLUT1-containing supernatant was collected and GLUT1 isolated by chloroform/methanol/water precipitation [209]. Briefly, 300μL methanol, 100μL chloroform, and 200μL $H_2O$ were sequentially added to 100 μL of GLUT1-containing supernatant. The suspension was centrifuged (13,000 rpm; 10 min) to produce two phases with protein precipitate at the interface. The upper phase was aspirated and 200 μL methanol added to bottom phase to form a single phase. GLUT1 precipitate was sedimented by centrifugation (13,000 rpm; 5 min), the supernatant aspirated, and the pellet dried under nitrogen. Protein was resuspended to 1-5 mg/mL in 90% formic acid for MALDI-TOF-MS and LC-MS.

***Mass Spectrometry Data Collection*** For MALDI-TOF, the sample was applied to a 96 well MALDI plate using a modified thin-layer technique. Samples were dried at ambient temperatures and pressures. All spectra were acquired using a Waters MALDI LR MALDI-TOF mass spectrometer in linear mode for intact protein samples. Pulse voltage, matrix suppression delay, and laser energy were adjusted to maximize resolution and to

minimize the signal-to-noise ratio. Spectra from 75 individual laser shots were averaged and smoothed using MassLynx 4.0 software. For LC-MS, 50-100 μg of sample in 90% formic acid was subjected to size exclusion chromatography (TSK-gel SW2000; 4 μm, 125Å; 4.6 mm ID x 30 cm) using an isocratic gradient of chloroform:methanol:1% formic acid (4:4:1). Column eluant was injected into the mass spectrometer and the resulting spectra were deconvoluted using Waters MaxEnt 1 software. MALDI-TOF mass spectra were calibrated using the standards BSA (double and single charge states), aldolase and apomyoglobin. For each deglycosylated GLUT1 peptide spectrum, the $M_w$ range of detected ions prior to smoothing is 54,174 - 54,667 and 27,083 - 27,319 for singly and doubly charged species respectively. The average ratio of singly to doubly charged species is thus 2.00029 ± 0.00041 (n = 19) indicating that mass analysis is consistent to within 0.015%. HPLC-ESI-MS $M_w$ assignment was verified using purified commercial bacteriorhodopsin (BR) haloprotein yielding an $M_{obs}$ of 26,784 ($M_{theory}$ = 26,784) [210]. Commercial BR haloprotein is contaminated with trace bacteriorhodopsin apoprotein, detected as species with $M_{obs}$ of 27,051, ($M_{theory}$ = 27,051).

***Preparation of Tryptic and α-Chymotryptic Digested GLUT1 Peptides*** Reduction and alkylation of membrane resident GLUT1 thiol groups was achieved using 10 mM dithiothreitol (DTT; 120 minutes at 37°C) followed by 54 mM iodoacetamide (60 minutes at 20°C in the dark as described previously [86]). Unmodified or PNGase F treated (deglycosylated), reduced and alkylated GLUT1 proteoliposomes or gel-eluted protein were resuspended in K-medium (0.5 mg/mL, 55μL total reaction volume) or

water and digested with trypsin or α-chymotrypsin at a 10:1 ratio (GLUT1:enzyme, by mass) for 120 min at 30°C.

***HPLC Separation and Electrospray Ionization MS/MS*** Reverse Phase HPLC-ESI-MS/MS analysis of fragmented GLUT1 was performed as described in Chapter III.

***Circular Dichroism*** Deglycosylated, purified GLUT1 was resolved using 8% SDS-PAGE, and protein bands were eluted as previously described. Spectra were collected at room temperature using a Jasco J-810 spectropolarimeter from 300-180 nm at 20 nm/min with a data pitch of 0.5 nm. A 0.01 cm path length cuvette was used. Six spectra were averaged and control baselines subtracted.

***Determination of GLUT1 Free Sulfhydryl Content*** Reduced and nonreduced, purified GLUT1 (each at 100 μg/mL in 1 mL and exhaustively dialyzed to remove traces of DTT) were resuspended in TrisHCL medium or denatured in 0.5% SDS in 50 mM Tris-HC1, 3 mM EDTA, pH 8.0, for 30 min. Solubilized, denatured protein was collected as supernatant by centrifugation (100,000 x g for 1 h at 4ºC) and quantitated. The free sulfhydryl contents of reduced and nonreduced GLUT1 were determined by using Ellman's reagent [211]. The reaction was initiated by addition of 100μL of freshly prepared 10 mM 5,5'-dithiobis-(2-nitrobenzoic acid) (DTNB). The course of the reaction at room temperature was recorded as the increase in absorbance at 412 nm. An extinction coefficient of 13,600 $M^{-1}.cm^{-1}$ at 412 nm for 2-nitro-5-thiobenzoic acid (NTB) was used to quantitate both reactions. All NTSB assays included the parallel, internal controls of

porcine insulin (three disulfides per molecule) and oxidized glutathione (one disulfide per molecule).

***RESULTS***

***GLUT1 cysteine accessibility*** GLUT1 contains 6 cysteine residues (positions 133, 201, 207, 347, 421 and 429; (14)). Native, proteoliposome-resident GLUT1 exposes 3.13 ± 0.2 free thiol groups per GLUT1 monomer as assayed by DTNB (Ellman's reagent) accessibility. Treatment with 50 mM DTT increases proteoliposomal GLUT1 free thiol content to 4.33 ± 0.4 thiols per GLUT1 monomer. By contrast, SDS-unfolded, non-reduced GLUT1 exposes 2.8 ± 0.3 thiols per GLUT1 molecule while reduced and SDS-denatured GLUT1 exposes 6.7 ± 0.4 thiols per monomer indicating that all cysteine residues are accessible to DTNB.

***GLUT1 electrophoretic mobility*** GLUT1 is glycosylated at asparagine 45 [45] causing the transport protein to smear as a diffuse band of molecular weight 50 to 65 kDa upon SDS-PAGE (see Figure 5.1A, lanes 1, 2 and 3). GLUT1-deglycosylation using N-glycosidase F (PNGaseF) hydrolyzes the polysaccharide chain at the polypeptide backbone asparagine. Following PNGase treatment GLUT1 resolves as two distinct species on SDS-PAGE (Figure 5.1A, lanes 4 - 8). In Figure 5.1A, these peptides comprise a mobile band of 40 kDa, and a less mobile band of 47 kDa. In 9 separate experiments, the computed mass of the mobile band ranges from 36.5 to 43.9 kDa (mean ± SEM = 40.7 ± 0.5 kDa) while the mass of the less mobile species ranges from 45.3 to

**Figure 5.1 Effects of sulfhydryl chemistry on GLUT1 deglycosylation. (A)** Deglycosylation in the presence of SDS & βME. SDS and βME were present during deglycosylation and concentrations are reported as % (v:v). Control lanes 1, 2, & 3 contain glycosylated GLUT1 incubated in the absence of PNGaseF but at [SDS] and [βME] (%) of (0; 0), (0.5; 1), and (4; 8), respectively. Lanes 4 & 5 contain SDS (0.5 and 4% respectively)-denatured GLUT1 exposed to PNGaseF. Lane 6 contains proteoliposome-resident GLUT1. The deglycosylation reaction of lane 6 was divided and each aliquot subsequently incubated with either (0%, 0%; lane 7) or (4%; 8%; lane 8). **(B)** Effect of SDS on the relative proportions of 41 (squares) and 49 (circles) kDa species observed upon GLUT1 deglycosylation. Deglycosylations were performed at fixed βME (1% - open symbols; 8% closed symbols) as described in Methods with increasing [SDS]. Ordinate: fraction of deglycosylated GLUT1; Abscissa: [SDS] in %. Lines drawn through the 1% βME data were computed by linear regression and have the following constants: 41 kDa species, y = (0.47 ± 0.02) - (0.02 ± 0.01)[SDS], $R^2$ = 0.687; 49 kDa species, y = (0.53 ± 0.02) - (0.02 ± 0.01)[SDS], $R^2$ = 0.687. Curves drawn through the 8% βME data were computed by nonlinear regression assuming that relative content increases or decreases in a saturable manner according to the expression: y = $f_0$ + $f_\Delta$ [SDS]/(K+[SDS]) where $f_0$ is relative content at [SDS] = 0, $f_\Delta$ is relative content at saturating [SDS] and K is that [SDS] where y = $f_0$ + 0.5$f_\Delta$. The following results were obtained: 41 kDa peptide (filled squares), $f_0$ = 0.46 ± 0.05, $f_\Delta$ = 0.38 ± 0.08 K = 0.39 ± 0.29; 49 kDa peptide (filled circles), $f_0$ = 0.54 ± 0.05, $f_\Delta$ = -0.38 ± 0.08, K = 0.39 ± 0.29. **(C)** Effect of βME on the relative proportions of 41 and 49 kDa species observed upon

**Figure 5.1 (continued)** GLUT1 deglycosylation. Deglycosylations were performed at fixed [SDS] (0.5% - open symbols; 4% closed symbols) with increasing [βME]. Ordinate: fraction of deglycosylated GLUT1; Abscissa: [βME] in %. Curves drawn through the data were computed by nonlinear regression assuming that relative content increases or decreases in a saturable manner according to the expression: y = $f_0$ + $f_\Delta$ [βME]/(K+[βME]) where $f_0$ is relative content at [βME] = 0, $f_\Delta$ is relative content at saturating [βME] and K is that [βME] where y = $f_0$ + 0.5$f_\Delta$. The following results were obtained: **0.5% SDS,** 41 kDa peptide (open squares), $f_0$ = 0.40 ± 0.01, $f_\Delta$ = 0.61 ± 0.04 K = 9.0 ± 1.2; 49 kDa peptide (open circles), $f_0$ = 0.60 ± 0.01, $f_\Delta$ = -0.61 ± 0.04, K = 9.0 ± 1.2. **4% SDS,** 41 kDa peptide (filled squares), $f_0$ = 0.30 ± 0.01, $f_\Delta$ = 0.70 ± 0.17 K = 10.9 ± 3.1; 49 kDa peptide (filled circles), $f_0$ = 0.70 ± 0.01, $f_\Delta$ = -0.70 ± 0.17, K = 10.9 ± 3.1.

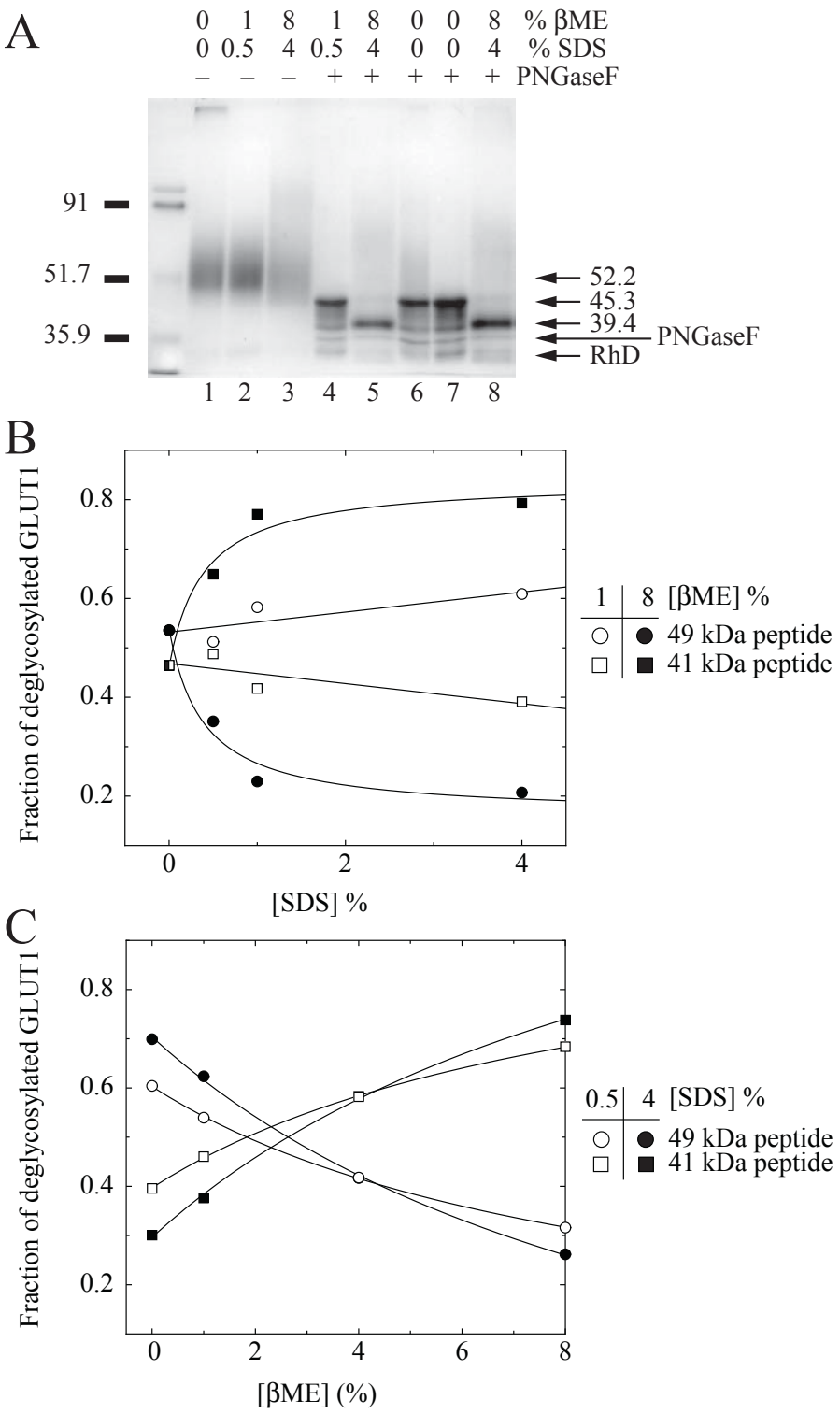
A
0 1 8 1 8 0 0 8 % βME
0 0.5 4 0.5 4 0 0 4 % SDS
– – – + + + + + PNGaseF
91
51.7
35.9
52.2
45.3
39.4
PNGaseF
RhD
1 2 3 4 5 6 7 8
B
Fraction of deglycosylated GLUT1
0.8
0.6
0.4
0.2
0
2
4
[SDS] %
1 8 [βME] %
49 kDa peptide
41 kDa peptide
C
Fraction of deglycosylated GLUT1
0.8
0.6
0.4
0.2
0
2
4
6
8
[βME] (%)
0.5 4 [SDS] %
49 kDa peptide
41 kDa peptide

Figure 5.1

52.9 kDa (mean ± SEM = 48.6 ± 0.9 kDa). Henceforth, we refer to the mobile and less mobile species as 41 and 49 kDa proteins, respectively.

Glycosylated GLUT1 electrophoretic mobility shows no significant change in the presence of low SDS (0.5%) or βME (1%), but displays increased mobility of leading edge peptides and more diffuse staining in the presence of 4% SDS and 8% βME (Figure 5.1A, lanes 1-3). Deglycosylated GLUT1 was exposed to low and high SDS/βME concentrations either during (Figure 5.1A lanes 4-6) or following (Figure 5.1A lanes 7-8) deglycosylation. Increased SDS and βME cause a mobility shift favoring the 41 kDa peptide over the 49 kDa peptide. At 1% [βME] (open symbols Figure 5.1B), deglycosylated peptide mobility is independent of [SDS]. At 8% [βME] (Figure 5.1B, filled symbols), the 49 kDa species is reduced to a 41 kDa peptide in a saturable manner with increasing [SDS]. At low [SDS] (0.5%, Figure 5.1C, open symbols) or high [SDS] (4%, Figure 5.1C, filled symbols), the 49 kDa deglycosylated species is converted to the 41 kDa form in a saturable manner with increasing [βME].

Deglycosylated GLUT1 was subjected to SDS-PAGE, the 49 kDa species was excised from the gel, eluted into 0%, 2%, and 4% SDS plus 4% and 8% SDS/βME to generate 41, 49, 49, and 41 kDa species respectively (see Figure 5.2A) and the resulting samples were subjected to analysis by circular dichroism (Figure 5.2B). Samples eluted into 2% and 4% SDS exhibit spectral qualities consistent with the presence of α-helical content. Specifically, these include signal minima at 208 and 222 nm and a molar elipticity ratio value (195:222 nm) greater than 2.1 (Figure 5.2B; ([212])). Samples eluted into 0% SDS

**Figure 5.2 GLUT1 secondary structure analyses by CD. (A)** Deglycosylated purified GLUT1 was resolved using 8% SDS-PAGE, and excised protein bands were eluted into buffer containing 0% (lane 2), 2% (lane 3), 4% (lane 4) SDS and into 4% SDS + 8% βME (lane 5). **(B)** CD Spectra were recorded as described in the methods. Ordinate: mean residue elipticity in degree.cm$^2$.dmol$^{-1}$ x 10$^{-3}$. Abscissa: wavelength, nm. Spectra of peptides eluted from lanes 2, 3 and 4 are indicated.

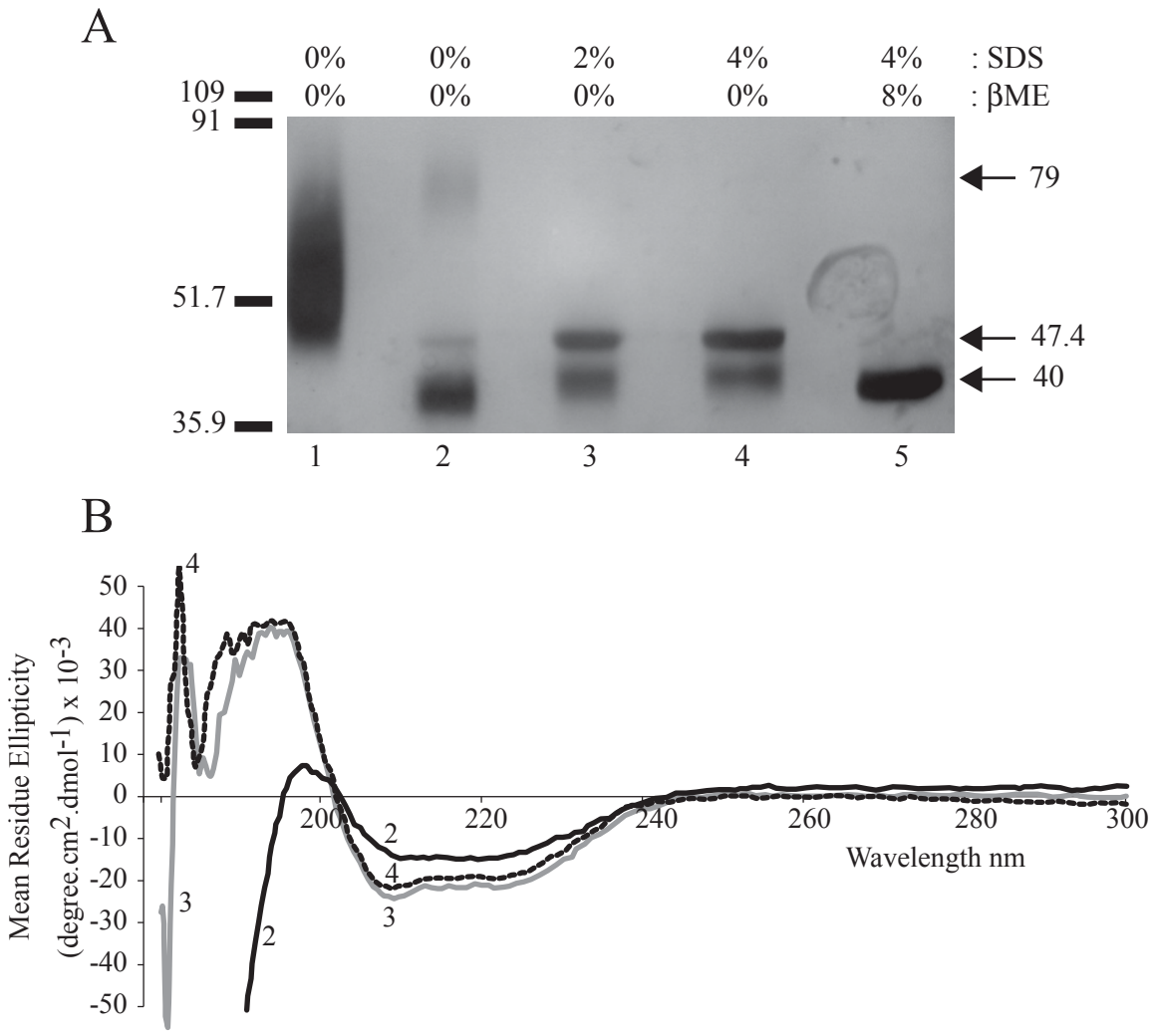
A
0%
0%
2%
4%
4%
: SDS
0%
0%
0%
0%
8%
: βME
109
91
51.7
35.9
79
47.4
40
1
2
3
4
5
B
Mean Residue Ellipticity
(degree.cm2.dmol-1) x 10-3
50
40
30
20
10
0
-10
-20
-30
-40
-50
200
220
240
260
280
300
Wavelength nm
2
3
4

Figure 5.2

do not display these α-helical characteristics as prominently. CD spectra of samples eluted into 4% SDS and 8% βME were uninterpretable owing to the high concentration of reductant in the sample.

***Identity of deglycosylated species*** Multiple deglycosylation products could result from GLUT1 proteolysis, physiologic covalent modification, artifactual covalent modifications or multiple intra-chain folds of identical molecular species. Deglycosylation in the presence of serine protease inhibitors does not alter the appearance of 49 kDa and 41 kDa peptides (data not shown). PNGase F concentration, total reaction time, and reaction temperature were each adjusted without effect on the multiple banding. Calf alkaline phosphatase (CAP), which alters the mobility of phosphorylated proteins by catalyzing their dephosphorylation and thereby altering protein mass/charge ratio and SDS binding [213,214], is without effect on GLUT1 electrophoretic mobility (data not shown). Gas chromatography-mass spectrometry (GC-MS) of deglycosylated GLUT1 does not detect significant GLUT1 fatty acyl chain modifications (GLUT1:long chain fatty acid molar ratios observed = 1:0.03). These results suggest that 41 and 49 kDa GLUT1 deglycosylation products do not result from GLUT1 proteolysis, phosphorylation/dephosphorylation or thiol fatty acylation.

Immunoblot analysis of deglycosylated GLUT1 suggests that 49 kDa and 41 kDa GLUT1 bands represent identical molecular species. The antibodies tested were: N-Ab, directed against GLUT1 residues 1-13; L7-Ab, directed against GLUT1 residues 299-311 (putative extracellular loop 7); δ-Ab, directed against nonreduced, nondenatured GLUT1

and which recognizes exofacial GLUT1 epitopes [208]; and C-Ab, directed against GLUT1 residues 480-492 (Figure 5.3). All 4 antibodies recognize the 49 and 41 kDa peptides suggesting that full-length GLUT1 is present in both bands. In these experiments and those of Figure 5.2, the 41 kDa peptide appears to be the major deglycosylation product.

Glycosylated GLUT1 and the 49 kDa and 41 kDa GLUT1 deglycosylated species display nearly identical amino acid compositions that are also consistent with the predicted amino acid composition of intact GLUT1 (Table 5.1). The unexpectedly high glycine and tyrosine contents of 41 and 49 kDa peptides respectively likely result from the use of glycine-containing buffers during gel electrophoresis and from TRIS contamination which produces a large artifact peak that co-elutes with tyrosine on the amino acid analyzer [215,216].

***Mass Spectrometry of GLUT1*** The theoretical $M_w$ of deglycosylated, full length GLUT1 is 54,118. Analysis of gel-eluted 49 and 41 kDa GLUT1 peptide mass by MS yields $M_w$ values of 54,440 and 54,435 respectively (Table 5.2). Experimental mass (accurate to at least 0.015%) therefore exceeds GLUT1 theoretical mass by as much as 322 Da (0.59%). If the 49 and 41 kDa species are derived from GLUT1 - a hypothesis supported by immunoblot and amino acid analyses - what is the origin of the extra mass associated with GLUT1 peptides?

Tables A2.1 and A2.2 summarize the results of HPLC MS/MS sequence analysis of tryptic and α-chymotryptic fragments of gel-eluted GLUT1 respectively. GLUT1

**Figure 5.3 Immunoblot analysis of intact and deglycosylated GLUT1.** Panels **(A)**, **(B)**, **(C)**, & **(D)** represent immunoblots using C-Ab, N-Ab, L7-Ab, and δ-Ab, respectively. Lane 1 is glycosylated GLUT1 and lane 2 is GLUT1 deglycosylated under denaturing conditions (0.5% SDS, 1% NP-40, and 1% βME). The mobility of molecular weight standards is indicated to the left of each blot. The computed mass (kDa) of selected peptides and their mobilities are indicated in italics and by arrows respectively at the right of each blot.

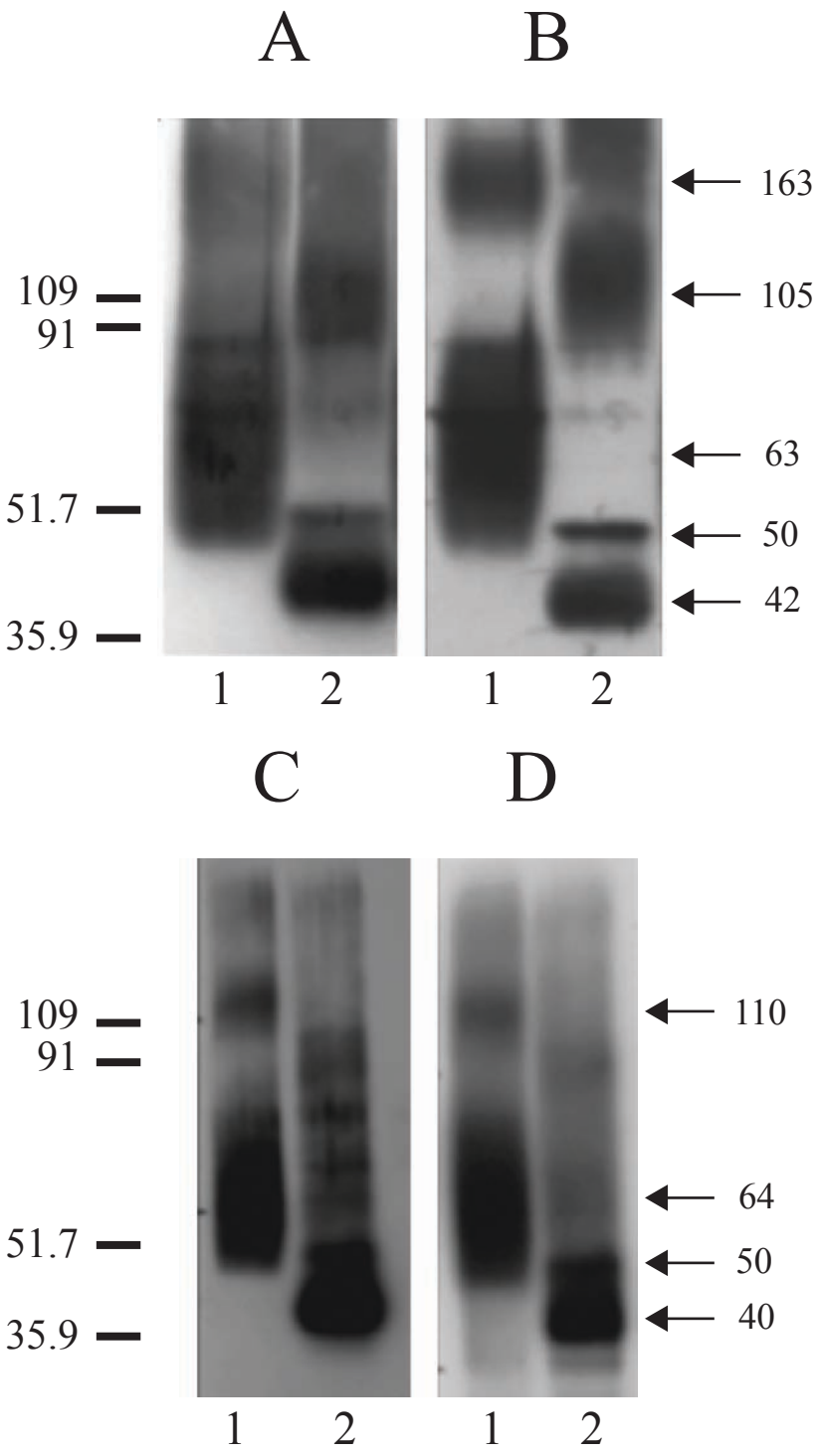
A
B
109
91
51.7
35.9
163
105
63
50
42
1
2
1
2
C
D
109
91
51.7
35.9
110
64
50
40
1
2
1
2

Figure 5.3

**Legend for Table 5.1 Amino acid analysis of intact and deglycosylated GLUT1.** Deglycosylated, eluted GLUT1 was separated on 8% SDS-PAGE and electrophoretically transferred to a PVDF membrane. Peptides were stained using amido black then 49 kDa and 41 kDa deglycosylated peptides and glycosylated GLUT1 were excised for amino acid analysis (Harvard Microchemistry and Proteomics Facility, Cambridge, MA). Peptides (2.4-7.6 pmol) were hydrolyzed in 6N HCL and derivatized to phenylthiocarbamyl (PTC)-amino acids for analysis using an Applied Biosystems 420A Amino Acid Analyzer. The table displays the amount of amino acid present in each sample relative to the total amino acid composition of the sample (% of total). Results are shown for: [a]predicted amino acid content of GLUT1; [b]amino acid content of glycosylated GLUT1; [c]amino acid content of the 41 kDa deglycosylation product; [d]amino acid content of the 49 kDa deglycosylation product. Glycine and tyrosine contents may be elevated in some samples owing to the glycine and Tris contents of the various buffers employed.

| amino acid | [a]theory | [b]GLUT1 | [c]41 kDa | [d]49 kDa |
|---|---|---|---|---|
| ala | 7.1% | 9.3% | 8.4% | 8.6% |
| arg | 4.4% | 6.1% | 5.5% | 5.6% |
| asx | 4.4% | 5.8% | 5.5% | 6.0% |
| glx | 9.4% | 4.6% | 5.9% | 6.2% |
| gly | 9.6% | 9.5% | 18.7% | 8.5% |
| his | 1.0% | 1.5% | 1.4% | 1.4% |
| ile | 7.7% | 6.9% | 6.0% | 6.2% |
| leu | 12.1% | 13.1% | 11.1% | 11.8% |
| lys | 3.3% | 5.4% | 4.7% | 4.8% |
| met | 3.5% | 2.2% | 2.2% | 2.2% |
| phe | 8.1% | 7.2% | 6.1% | 6.1% |
| pro | 4.8% | 4.8% | 4.2% | 4.1% |
| ser | 7.3% | 7.4% | 6.4% | 7.5% |
| thr | 5.4% | 4.3% | 4.0% | 3.8% |
| tyr | 2.7% | 2.8% | 1.9% | 9.2% |
| val | 9.2% | 9.1% | 8.0% | 7.9% |

Table 5.1

**Legend for Table 5.2 Full-length deglycosylated GLUT1 mass as detected by Mass Spectrometry.** [a]$M_w$ was measured by MALDI-TOF or by ESI-MS analysis. [b]The more mobile, 41 kDa deglycosylated GLUT1 peptide was obtained by eluting the 49 kDa species into SDS- and βME-free $ddH_2O$. [c]The less mobile, 49 kDa deglycosylated GLUT1 peptide was obtained by eluting the 49 kDa species into $ddH_2O$ containing 2% SDS. [d]41 and 49 kDa species were mixed in equal proportions for MALDI-TOF. [e]GLUT1 was eluted into SDS (4%) + βME (8%) for ESI-MS measurements. Results are shown as the mean ± SEM.

| | Peptide Species | | |
|---|---|---|---|
| [a]Method | [b]41 kDa | [c]49 kDa | [d]mixture or [e]reduced |
| MALDI-TOF | 54,401 ± 94 | 54,353 ± 81 | 54,457 ± 101 |
| ESI-MS | 54,465 ± 10 | 54,526 ± 12 | 54,524 ± 11 |

Table 5.2

sequence coverage is extensive, corresponding to 59% (tryptic digests) and 71% (α–chymotryptic digests) yielding combined sequence coverage of 90%. Five of six total cysteine residues (C201, C207, C347, C421 and C429) are resolved in these analyses (cysteine 133 was not detected) and, with the exception of C347, each is observed both as unmodified cysteine and as a cysteine-acrylamide adduct (cys-S-β-propionamide or Cys-S-Pam). C347 alone was observed as unmodified cysteine. Thus any specific GLUT1 molecule in the sample could contain as many as 4 modified cysteine residues or as few as zero. CNBr digestion of formic acid dissolved, eluted GLUT1 provides less extensive (20%) sequence coverage by MS/MS (Table A2.3). This may result from the great length of several GLUT1 CNBr fragments that complicates MS/MS sequence analysis. CNBr sequence coverage includes GLUT1 peptide 121 – 142, containing cysteine residue 133 in both unmodified and cys-S-β-propionamide forms. Hence all GLUT1 cysteine residues barring C347 may be observed as unmodified cysteine and as a modified cysteine containing an acrylamide adduct. Furthermore, of the 9 serine residues detected in CNBr fragments, 7 serine residues are observed both as unmodified and formylated residues. Hence electrophoresis and formic acid exposure can result in variable GLUT1 mass additions within any given sample ranging from 0 to as great as 1,363 Da (36 formylations + 5 acrylamide adducts; see Table 5.3). This may explain the divergence between experimental and predicted GLUT1 masses obtained upon MALDI-TOF and ESI-MS analysis of full-length GLUT1.

***Are deglycosylated GLUT1 species and cysteine classes related?*** We subjected GLUT1 to alkylation and or reduction/alkylation prior to gel electrophoresis to avoid variable

**Legend for Table 5.3 Summary of GLUT1 ESI-MS/MS sequence coverage (trypsin and α-chymotrypsin, CNBr digests) and covalent modification to gel-eluted GLUT1.** [a]Indicates the N-terminal cleavage site. [b]Indicates the C-terminal cleavage site. Total indicates the number of residues sequenced in the peptide. [c]Indicates the total sequence coverage that is also expressed as % coverage assuming human GLUT1 comprises 492 residues. [d]Indicates a compilation of cysteine residues identified in tryptic and α-chymotryptic digests (Column 1) or in CNBr digests (column 2) of GLUT1 and whether the cysteine is resolved as [e]free cysteine or as [f]acrylamide-modified cysteine. ND indicates that the residue was not detected. [g]Indicates serine or threonine residues detected in CNBr digests of GLUT1 and whether the residue is resolved as an unmodified amino acid or as a formylated amino acid. ND indicates that the residue was not detected. [h]Indicates total GLUT1 sequence coverage obtained from tryptic, chymotryptic and CNBr digests of GLUT1.

| Trypsin | | |
|---|---|---|
| [a]Start | [b]End | Total |
| 11 | 126 | 115 |
| 153 | 183 | 30 |
| 212 | 218 | 6 |
| 225 | 229 | 4 |
| 232 | 333 | 101 |
| 458 | 492 | 34 |
| [c]Total | | 290 |
| % Coverage | | 59% |

| α-chymotrypsin | | |
|---|---|---|
| [a]Start | [b]End | Total |
| 8 | 26 | 18 |
| 48 | 61 | 13 |
| 72 | 86 | 14 |
| 90 | 115 | 25 |
| 127 | 132 | 5 |
| 152 | 214 | 62 |
| 215 | 228 | 13 |
| 231 | 251 | 20 |
| 278 | 291 | 13 |
| 292 | 320 | 28 |
| 336 | 363 | 27 |
| 373 | 409 | 36 |
| 416 | 492 | 76 |
| [c]Total | | 350 |
| % Coverage | | 71% |

| [d]Cysteine Residues | [e]Cys-SH | [f]Cys-S-Pam |
|---|---|---|
| 133 | ND | ND |
| 201 | Yes | Yes |
| 207 | Yes | Yes |
| 347 | ND | Yes |
| 421 | Yes | ND |
| 429 | Yes | Yes |

| CNBr | | |
|---|---|---|
| [a]Start | [b]End | Total |
| 1 | 13 | 12 |
| 77 | 142 | 65 |
| 244 | 251 | 7 |
| 351 | 364 | 13 |
| [c]Total | | 97 |
| % Coverage | | 20% |

| | Unmodified | Modified |
|---|---|---|
| S4 | Yes | Yes |
| S5 | Yes | Yes |
| T9 | Yes | yes |
| S80 | Yes | Yes |
| S82 | Yes | ND |
| S95 | Yes | ND |
| S106 | Yes | Yes |
| S113 | Yes | Yes |
| S118 | Yes | Yes |
| T136 | Yes | ND |
| T137 | Yes | ND |
| S248 | Yes | Yes |
| T352 | Yes | ND |

| Cysteine residues | [e]Cys-SH | [f]Cys-S-Pam |
|---|---|---|
| C133 | Yes | Yes |

[h]CNBr, Trypsin, and α-Chymotrypsin

| [a]Start | [b]End | Total |
|---|---|---|
| 1 | 142 | 141 |
| 152 | 229 | 77 |
| 231 | 333 | 102 |
| 336 | 364 | 28 |
| 373 | 409 | 36 |
| 416 | 492 | 76 |
| [c]Total | | 460 |
| % Coverage | | 93% |

Table 5.3

blocking of free thiols by acrylamide. GLUT1 was treated ± reductant (10 mM DTT, 2 hr at 37ºC), washed in reductant free medium then alkylated using 54 mM iodoacetamide (60 minutes at 20°C in the dark). Iodoacetamide-reactive GLUT1 thiols were identified by MS/MS sequence analysis of tryptic and α-chymotryptic digests of iodoacetamide-alkylated, proteoliposomal GLUT1 (Table 5.4; Figure 5.4). Alkylated cysteine residues C133, C201 and C429 are detected in nonreduced GLUT1 but alkylated C207, C347 and C421 are not detected. Following GLUT1 reduction by DTT and subsequent alkylation, 5 of the 6 total GLUT1 cysteine residues are resolved as alkylated species (Figure 5.4, Table 5.4; only C347 is not observed). Unmodified cysteine residues were not detected in GLUT1 proteoliposome samples. Peptides containing alkylated histidine, methionine or tyrosine residues were not detected.

Is GLUT1 SH-group availability associated with specific GLUT1 electrophoretic mobility? GLUT1 was deglycosylated then either: 1) processed no further; 2) reduced, 3) alkylated without reduction or 4) reduced and alkylated. Following these treatments, deglycosylated GLUT1 was subjected to reducing and nonreducing SDS-PAGE (Figure 5.5). The result is the generation of two peptides that migrate with $M_{rapp}$ 49 and 41 kDa upon reducing SDS-PAGE. The 49 kDa peptide dominates under nonreducing SDS-PAGE unless deglycosylated GLUT1 is first reduced then alkylated in which case both 49 and 41 kDa species are observed. This suggests that alkylation of reductant-sensitive GLUT1 cysteine residues C207 and C421 prevents their re-oxidation upon nonreducing electrophoresis.

**Figure 5.4 MS/MS analysis of accessible GLUT1 thiols.** Sequential trypsin and α-chymotrypsin (10:1 protein:enzyme) digests of alkylated **(A)** or reduced and alkylated **(B)** GLUT1 proteoliposomes. Boxed residues indicate the identity of the N-terminal amino acid and match the y-ion series peaks (blue peaks) in the spectrum below. **(A)** Alkylated peptide from nonreduced GLUT1 containing cysteine 429. Doubly charged ion MS/MS spectrum of this triply charged ion with a precursor mass of 4162.3 Da. The sequence includes residues 423-456 with cleavage sites at F422 and K456 (F.QYVEQLCGPYVFIIFTVLLVLFFIFTYFKVPETK.G) and a +57 Da adduct at cysteine 429. Retention time = 41.98 minutes; MS/MS Scores: XCorr = 5.561, ΔCn = 0.622, Sp = 942.2, and RSp = 1. **(B)** Alkylated peptide from reduced GLUT1 containing cysteine 421. MS/MS spectrum of the singly charged ion with a precursor mass of 726.3 Da. The sequence includes residues 417-422 with cleavage sites at F416 and F422 (F.IVGMCF.Q) with a +57 Da adduct on the cysteine residue. Retention time = 11.10 minutes; MS/MS Scores: XCorr = 1.542, ΔCn = 0.434, Sp = 399.3, and RSp = 1.

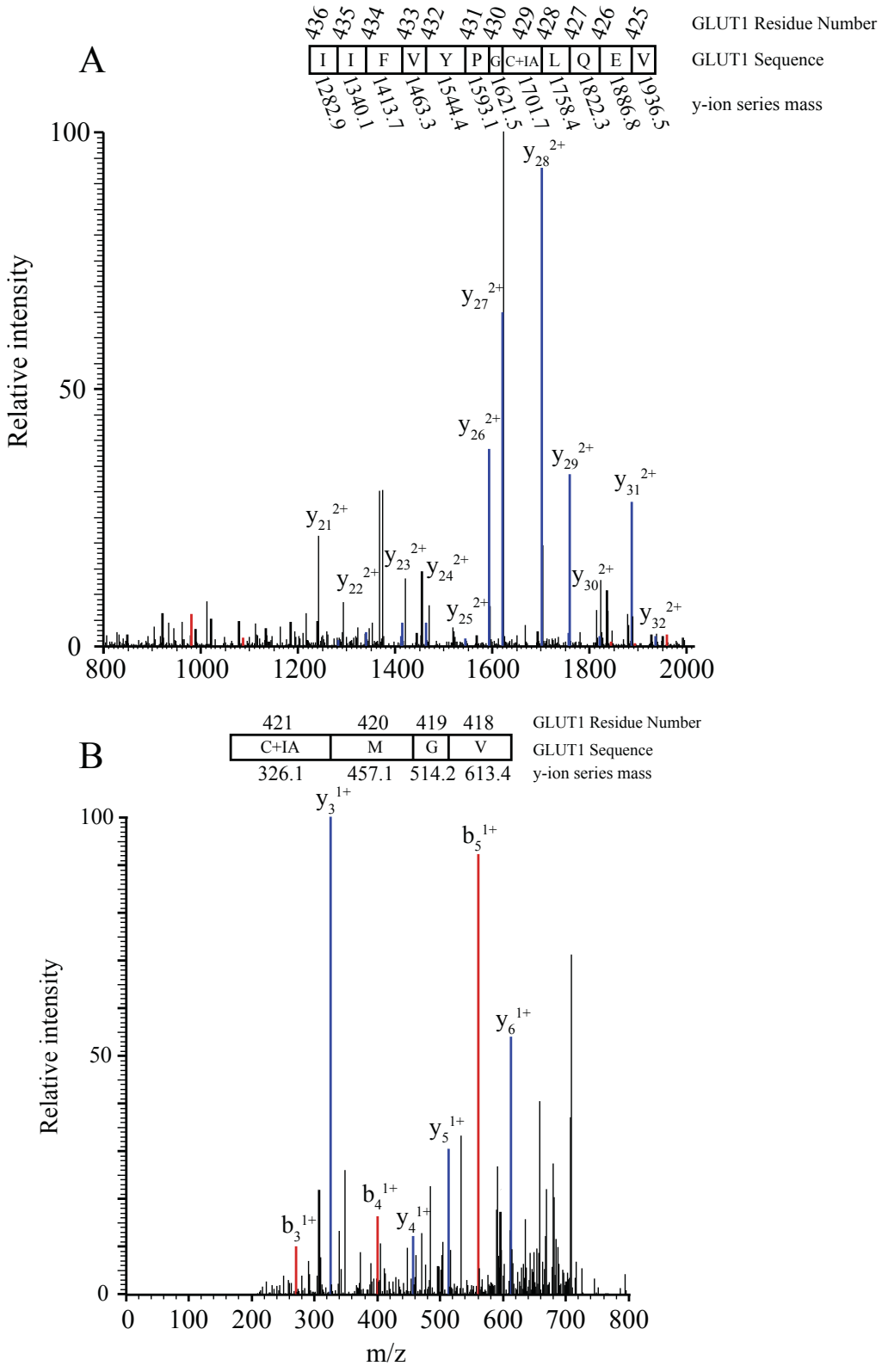
A
436 435 434 433 432 431 430 429 428 427 426 425
GLUT1 Residue Number
I I F V Y P G C+IA L Q E V
GLUT1 Sequence
1282.9 1340.1 1413.7 1463.3 1544.4 1593.1 1621.5 1701.7 1758.4 1822.3 1886.8 1936.5
y-ion series mass
Relative intensity
100
50
0
800 1000 1200 1400 1600 1800 2000
y28 2+
y27 2+
y26 2+
y29 2+
y31 2+
y21 2+
y23 2+
y24 2+
y22 2+
y30 2+
y25 2+
y32 2+
B
421 420 419 418
GLUT1 Residue Number
C+IA M G V
GLUT1 Sequence
326.1 457.1 514.2 613.4
y-ion series mass
Relative intensity
100
50
0
0 100 200 300 400 500 600 700 800
m/z
y3 1+
b5 1+
y6 1+
y5 1+
b4 1+
y4 1+
b3 1+

Figure 5.4

**Legend for Table 5.4 MS/MS analysis of cysteine accessibility to iodoacetamide in GLUT1 proteoliposomes.** [a]GLUT1 was deglycosylated and subjected to sequence analysis by α-chymotryptic digestion, HPLC- separation of proteolytic fragments and subsequent MS-MS analysis. Prior to proteolysis, GLUT1 and alkylation, GLUT1 was treated [b]without our [c]with DTT reduction (see methods). Samples were then alkylated with iodoacetamide and subjected to proteolysis/MS-MS analysis. [d]The table illustrates whether each specific GLUT1 cysteine residue is not detected (ND), detectable as an alkylated (yes) species or as a free sulfhydryl (no).

| GLUT1 Cysteine Residue | [a]Non-reduced GLUT1 | [b]Reduced GLUT1 |
|---|---|---|
| 133 | [c]yes | yes |
| 201 | no | yes |
| 207 | yes | yes |
| 347 | ND | ND |
| 421 | no | yes |
| 429 | yes | yes |

Table 5.4

**Figure 5.5 Effects of alkylation/reduction on degylcosylated GLUT1 mobility.** Lanes 1 through 5 were resolved under reducing conditions (sample buffer contained 3.65% βME). Lanes 6 through 9 were resolved under nonreducing conditions. **Lane 1** contains glycosylated GLUT1. GLUT1 was deglycosylated then treated the following treatments were made: **lanes 2 & 6 -** Kaline for 2 hr at 37ºC followed by 1 hr at 20ºC with Kaline; lanes **3 & 7 -** 10 mM DTT for 2 hr at 37ºC followed by 1 hr at 20 ºC with Kaline; **lanes 4 & 8 -** Kaline for 2 hr at 37ºC followed by 1 hr at 20ºC with 54 mM iodoacetamide; **lanes 5 & 9 -** 10 mM DTT for 2 hr at 37ºC followed by 1 hr at 20ºC with 54 mM iodoacetamide. The mobility of molecular weight markers (kDa) is indicated at the left. The calculated mass of GLUT1 peptides is indicated at the right of the gel. Locations of PNGaseF and RhD peptides are also indicated.

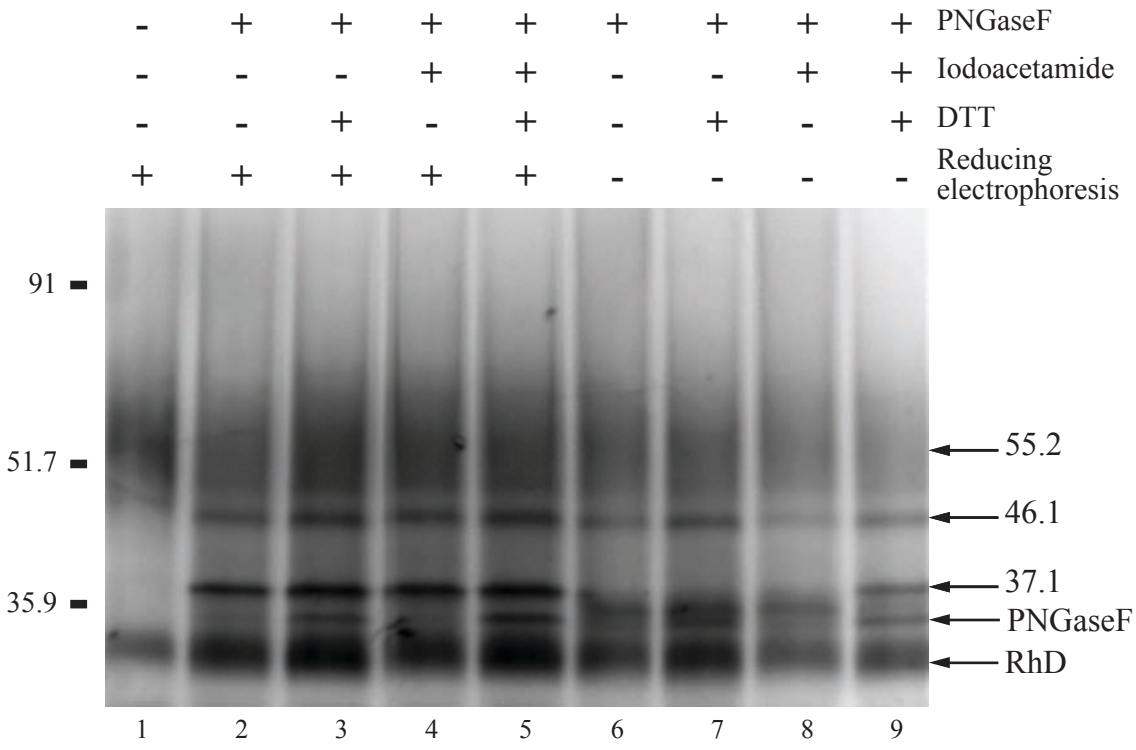
- + + + + + + + + PNGaseF
- - - + + - - + + Iodoacetamide
- - + - + - + - + DTT
+ + + + + - - - - Reducing electrophoresis
91
51.7
35.9
55.2
46.1
37.1
PNGaseF
RhD
1 2 3 4 5 6 7 8 9

Figure 5.5

## *DISCUSSION*

The human type 1 facilitative glucose transport protein displays cell-specific transport behavior [182], conformational states [86,191] and electrophoretic mobilities [191] suggesting that cell-specific environmental factors or post-translational modifications influence GLUT1 folding and function. Recognized GLUT1 post-translational modifications include serine-phosphorylation [203] and thiol-fatty-acylation [204]. GLUT1 phosphorylation appears to be physiologically silent [203] and thiol-acylation is significantly sub-stoichiometric [204] suggesting that neither modification accounts for variations in GLUT1 function. GLUT1 sugar transport capacity and oligomeric state are reduced in red cells by reductants [86,217] and GLUT1-mediated sugar transport is inhibited by thiol-reactive compounds such as pCMBS and N-ethylmaleimide [66] suggesting that GLUT1 redox state affects GLUT1 structure and function.

Membrane proteins often retain intra- and inter-chain structures in SDS that cause anomalous electrophoretic mobility [218]. Hemagglutinin (HA) ectodomain folding requires formation of six intra-chain disulfide bonds. Intermediate forms of HA containing fewer than 6 disulfides can be resolved by SDS-PAGE indicating that intra-chain disulfides affect the compactness and/or SDS binding capacity of polypeptides, which, in turn, alters polypeptide electrophoretic mobility [219]. Lemmon et al [220] have demonstrated that dimerization of the glycophorin A (GpA) transmembrane α-helix during SDS-PAGE is spontaneous and highly specific and exploited this behavior to establish the sequence and structural determinants of the dimerization interface. NMR

studies confirm that the alpha-helical structure of the GpA transmembrane domain is retained in SDS [221] and the conclusions of these studies were later affirmed by the TOXCAT system in which determinants of transmembrane helix-helix oligomerization in a natural membrane environment were studied by a recombinant approach [222].

The goal of the present study was to determine whether reductant-sensitive GLUT1 oligomeric structures and transport function are also associated with specific intra-chain folds. Our approach was to ask whether GLUT1 displays altered mobility upon reducing/nonreducing SDS-PAGE. Erythrocyte GLUT1 glycosylation is so heterogeneous, however, that the protein smears broadly during SDS-PAGE [166,197]. We therefore deglycosylated purified GLUT1 by use of PNGaseF which cleaves between the innermost GlcNAc and asparagine residues of high mannose oligosaccharides from N-linked glycoproteins [223]. This generates two peptides that migrate with $M_{rapp}$ 49 and 41 kDa upon reducing SDS-PAGE. The 49 kDa peptide is the major species observed during nonreducing electrophoresis. When deglycosylated GLUT1 is reduced then alkylated, both 49 and 41 kDa species are observed upon SDS-PAGE.

Immunoblot and MALDI-TOF analyses confirm that both peptides are full-length GLUT1. MALDI-TOF analysis indicates that the peptides have near identical $M_w$ values of 54,440. This $M_w$ is significantly greater than the theoretical mass of deglycosylated GLUT1 (54,118) but MS/MS sequence analysis of tryptic, $\alpha$–chymotryptic or CNBr digests of GLUT1 demonstrates that the additional mass results from formylation of serine and threonine residues during exposure to formic acid and from alkylation of

cysteine residues by free acrylamide during PAGE. Moreover, any given GLUT1 sample demonstrates both modified and unmodified amino acids at any specific serine, threonine or cysteine resulting in significant, internal sample mass heterogeneity.

GLUT1 contains two classes of cysteine residues. The accessible class (C133, C201 and C429) presents sulfhydryl groups for alkylation by iodoacetamide whether GLUT1 is folded and fully functional in the lipid bilayer or unfolded in SDS. The inaccessible class (C207 and C421) is reactive only following GLUT1 reduction by DTT or βME. Although DTT and iodoacetamide react with the inaccessible cysteine residues in folded, membrane-resident GLUT1, Ellman's reagent (DTNB) is unable to react with all GLUT1 cysteine residues unless the transporter is first unfolded in SDS and reduced. This may result from the significantly greater van der Waal's volume of DTNB (199 $cm^3$/mol) versus iodoacetamide (53.5 $cm^3$/mol) or DTT (74.7 $cm^3$/mol), which might limit DTNB access to occluded cysteine residues in native GLUT1. Neither unmodified nor iodoacetamide-alkylated C347 were detected in ESI-MS/MS studies of proteoliposomal GLUT1 although this residue was detected with and without an acrylamide adduct following reducing SDS-PAGE, gel elution and CNBr digestion. C207 (not C201) presents the pCMBS-sensitive intracellular thiol when GLUT1 is heterologously expressed in *Xenopus* oocytes [66]. The present study, however, suggests that C207 is inaccessible without prior reduction whereas C201 is accessible.

These observations support the hypothesis that the 41 kDa deglycosylated GLUT1 peptide represents maximally-alkylated GLUT1 whereas the 49 kDa species contains

only alkylated C133, C201 and C429. We further suggest that the oxidation state of C207, C421 and possibly C347 are causally linked to GLUT1 electrophoretic mobility. When expressed in *Xenopus* oocytes, both wild-type and cys-less GLUT1 resolve as two peptides upon immunoblot analysis [68] - a 55 kDa species and a more mobile 45 kDa peptide. These may represent two glycosylated forms of GLUT1 as suggested by the authors. Wild-type GLUT1, however, resolves largely as the 55 kDa species whereas cys-less GLUT1 resolves predominantly as the 45 kDa peptide. Reintroduction of a single cysteine residue at specific locations in GLUT1 membrane spanning helix (TM) 5 increases the amount of 55 kDa peptide relative to 45 kDa peptide. These results are also consistent with the hypothesis that the electrophoretic mobilities of cys-less GLUT1 and fully alkylated GLUT1 are equivalent. What roles might C207, C347 and C421 play in GLUT1 intra-chain folding? Several possibilities exist. 1) Two of these residues form an internal disulfide bridge. 2) All 3 residues form mixed disulfides with other molecular species. 3) These cysteine residues are thiol-acylated by myristic or palmitic acid. While cysteine 207 is topographically well suited for thiol-fatty-acylation [48,64], the extent of GLUT1 modification is sub-stoichiometric (see [204] and here). Earlier peptide mapping studies have indicated that a disulfide bridge does not link GLUT1 amino- and carboxy-terminal halves [86]. These observations suggest that GLUT1 cysteine residues C207, C347 and C421 form mixed disulfides with low molecular weight species (e.g. glutathione) or that C347 and C421 form a disulfide and C207 forms a mixed disulfide.

# CHAPTER VI

# DISCUSSION AND FUTURE DIRECTIONS

## *INTRODUCTION*

Advanced research technology provides new tools to probe and explain complex biological systems. We have employed two such advances over the course of this research. First, we utilized a rapid quench flow device to measure the earliest stages of GLUT1-mediated glucose transport in red blood cells. Second, we developed and applied a mass spectrometry based technique to an experimentally difficult family of molecules, the integral membrane transport proteins. We used MS to provide optimal sequence coverage, peptide separation, and the ability to detect single amino acid modifications. Our findings first demonstrate that carriers form conformationally dynamic structures unlike their channel counterparts [52,165] and second, that the structural organization of GLUT1 presents distinct features that do not completely mimic the consensus helix packing model obtained by X-ray diffraction analysis of crystallized, but distantly related bacterial MFS transporters [5,33-35,39]. The techniques we have developed should allow us to answer more difficult and specific questions related to the structure-function relationship of carrier-mediated transport.

## *GLUT1-MEDIATED TRANSPORT: "THE RAPID PHASE"*

Previous works have examined the rapid kinetics of glucose transport in erythrocytes [224]. These studies primarily focused on the half-turnover time for a single glucose transport event where the transporter converted from the e1 to e2 conformation and determining the number of GLUT1 molecules present per red cell [41,46]. We have extended these studies to consider the entire glucose transport import process [87,132].

We were able to isolate a previously unidentified rapid phase of transport that precedes the fast and slow phases of glucose uptake into the erythrocyte. This rapid phase is a first order reaction, is protein-mediated (it is impeded by e1- and e2-inhibitors CCB and phloretin, respectively), and is completely independent of ATP modulating effects. Additionally, sugar transport measurements in unsealed red blood cells ghosts, previously treated with trypsin to remove cytoplasmic portions, and quenched by e2- and e1-inhibitors phloretin and CCB showed substrate specific trapping of glucose within the membrane bound transporter. By observing glucose uptake rates at multiple temperatures, we were able to obtain the activation energies for each step. Tremendous conformational dynamics are required to mediate conversion from e2.S through the intermediate e(S) to e1.S, the sugar translocation steps. We propose that the rapid phase, whose kinetics we have measured and that we have trapped with inhibitors, represents the intermediate step in the e2-e1 conversion and may be schematically represented as e2+S2→e(S)→e1+S1. Recent crystallographic evidence showing MFS transporters locked in this arrangement have been observed for OxlT and EmrD, thereby offering support to the occlusion state model [5,34,39].

### *THE TRANSPORTER STRUCTURE-FUNCTION RELATIONSHIP*

These findings prompted the literature review presented in Chapter I to determine if there was a common structural basis for the functional mechanism observed among transport proteins. The structural and corresponding functional characteristics observed in crystallized membrane transport proteins illustrate that there are numerous ways to

catalyze substrate transport across the plasma membrane. The most common structural feature is the predominantly α-helical nature of each transmembrane domain. Although not all families have twelve transmembrane spanning helices like MFS transporters, the secondary structure and role of the α-helices in forming the pore pathway are quite similar. For many of these transporters, the general transport mechanism follows the Albers-Post model that describes MFS-mediated transport. The proteins present an outward facing, e2-like, substrate binding site that undergoes a series of conformational changes to eventually present the opposite, inward facing, e1-like conformation. Despite these similarities in basic transport mechanism, P-type ATPase and ABC transporters rely heavily on cytoplasmic domains and ATP binding to induce the conformational changes that catalyze transport. ABC transporters catalyze only unidirectional substrate transport, MCF transporters must exist as a dimer to undergo conformational changes, and CPA transporters minimize the extent of conformational changes required for substrate translocation, markedly increasing the turnover rate. It appears as if the structure function relationship is highly dependent upon cellular environments. Reviewing each mechanism with relation to the MFS transporters reveals why the study of GLUT1 by mass spectrometry provides a bridge for understanding MFS carrier-mediated transport.

### *APPLYING MASS SPECTROMETRY TO THE STRUCTURE-FUNCTION RELATIONSHIP*

Recent success in analysis of membrane transport proteins is not limited to the application of three-dimensional crystallography. Mass spectrometry of membrane proteins is yielding increasingly useful results. It has become the primary technique for

proteomics studies attempting to identify all proteins within a given cell type or organism, or when comparing the appearance or quantity of specific proteins in healthy versus diseased cells [225]. As with crystallography, mass spectrometry has been more successfully applied to the study of hydrophilic proteins than to analysis of membrane embedded proteins such as transporters [106,107]. Successful identification of integral membrane proteins is lacking in many proteomics studies. Additionally, MS studies that focus upon the relationship between integral membrane protein structure and function are also limited. The extremely hydrophobic nature of the transmembrane domains, the tendency of these peptides to aggregate during HPLC separation, the presence of reactive cysteine residues, and the overabundance of contaminating soluble proteins found in cellular samples contribute to these problems [107]. A comprehensive literature review reveals that eukaryotic Aquaporin 0 and Band 3 (the erythrocyte anion transporter) and prokaryotic LacY, EmrE, and MOMP are the only integral membrane proteins for which intensive mass spectrometry experiments have been conducted [108-113]. Each of these studies has contributed in one way or another to improving MS techniques applied to integral membrane proteins. We will consider the findings of this thesis in terms of how much we have learned about GLUT1 in light of each of these previous studies.

### *AQUAPORIN AND SEQUENCE COVERAGE*

Aquaporin 0 (AQP0) is an integral membrane protein containing 263 amino acids that comprise six transmembrane spanning domains with N and C-termini exposed to the cytoplasm. It functions as a water channel within the plasma membrane of mammalian

lens cells. By supplementing standard tryptic digests with pepsin digests at highly acidic pH values, AQP0 was sequenced in its entirety [109]. The utilization of pepsin digestion permitted the sequencing of large tryptic fragments that were previously identified only by the MALDI and LC-MS recorded *m/z* values. Complete sequence coverage is significant because all amino acid residues can potentially be studied for post-translational or experimental modifications. We have achieved greater than 85% GLUT1 sequence coverage by trypsin, α-chymotrypsin, and cyanogen bromide catalyzed proteolysis. This analysis covered all GLUT1 domains including intra- and extracellular loop regions, the amino and carboxy termini, and entire transmembrane helices. This provided us with the ability to study all regions of the protein and established a means to examining the GLUT1 structure function relationship.

### *ANION TRANSPORTER AND COVALENT MODIFICATIONS*

The anion transporter (Band 3; AE1) exchanges chloride and bicarbonate ions across the human erythrocyte plasma membrane. AE1 has two distinct functional regions: a cytoplasmic N-terminal portion and a 55 kDa membrane spanning C-terminal domain that includes fourteen membrane-embedded segments, which are necessary and sufficient for functionality. Tryptic fragments of the entire 551 amino acid transmembrane region were observed through MALDI and LC-MS output as confirmed by MS/MS spectra for small peptides and *m/z* values plus N-terminal sequencing for larger peptides [108]. Previous studies had shown that AE1 contained reactive and accessible lysine residues. The separation protocol and MS techniques developed by *Abe et al.* combined with

peptide mapping and supplemental cyanogen bromide (CNBr) digests, resulted in the significant finding that identified specific lysine residues as the actual modified amino acid residues [108]. N-terminal sequencing and mass analysis of the modified peptides were employed to support these findings, but MS/MS spectra were lacking. We have succeeded in identifying specific GLUT1 lysine residues modified by Sulfo-NHS-LC-biotin using MS/MS spectra that show the mass shift.

### *MOMP AND SURFACE EXPOSED RESIDUES AND DISULFIDE BONDS*

The MS studies of human AQP0 and Band 3 mirror those performed on prokaryotic integral membrane proteins. Major outer membrane protein (MOMP) of *Chlamydia trachomatis* serovar F spans the outer bacterial membrane and functions as a simple diffusion porin [110]. Through digestion with trypsin, Glu-C, and Asp-N, the authors developed a new model for which residues were surface exposed versus buried within the β-sheet transmembrane region. Additionally, the cysteine residues were examined to show which formed disulfide bonds versus those that were reactive, and therefore unbound, prior to reduction. Peptide mass fingerprinting was used to identify the presence of two disulfide bridges, a finding that along with the discovery of previously undetermined surface exposed residues altered the previous membrane topology model. We were able to distinguish between surface exposed and membrane embedded GLUT1 peptides as well as identify which cysteine residues are exposed under native versus reducing conditions. Unfortunately, we were unable to positively confirm the existence of a disulfide bond.

### *EmrE and LacY and Monitoring Conformational Changes*

*Escherichia coli* multidrug resistance protein (EmrE) and lactose permease (LacY) have also been subjected to MS analysis. EmrE is a small 110 amino acid protein with four membrane spanning domains and cytoplasmic terminal ends whose function is to exchange positively charged drugs for protons, thus granting these cells drug-resistance. LacY is a standard model for the major facilitator superfamily (MFS) of integral membrane proteins. This 417 amino acid protein has twelve membrane spanning α-helices and the carrier exploits a favorable electrochemical proton gradient to catalyze net movement of D-galactopyranosides against a concentration gradient. Similar to AQP0 and AE1, the entire sequence of LacY has been observed through either LC-MS/MS sequence identification or LC-MS peptide mass fingerprinting of peptides produced from a CNBr digest [113]. Of greater interest with regard to EmrE and LacY, however, are the observations that specific amino acid residues demonstrate altered accessibility to chemical modification either in the presence of substrate or with the introduction of point mutations within the binding cavity. By quantifying the percentage of modification of a particular residue in the presence or absence of substrates, it can be determined whether the residue of interest displays increased, decreased, or the same accessibility to the modifying agent [111-113]. These types of experiments cast light on both potential substrate binding sites and conformational changes that can occur as a result of the transport mechanism. We were able to identify specific GLUT1 cytoplasmic residues that were differentially modified in the presence of sugar transport modulator ATP.

### *APPLICATION OF MASS SPECTROMETRY TO GLUT1*

Our experiments using native GLUT1 proteoliposomes accomplished many of the aforementioned results, by using a single protein. These findings provided details supporting the general membrane topology predicted by homology modeling and cysteine scanning mutagenesis. More specifically, these data described the relative accessibility and solvent exposure of amino acid residues within each GLUT1 α–helix and allowed comparison with the helix packing motifs observed for crystallized MFS transporters LacY, GlpT, OxlT, and EmrD [5,33-35,39,64,74].

Specifically, we could determine how the transmembrane helices were related in terms of experimental hydrophobicity. The high frequency of trypsin cleavage sites at membrane/aqueous solvent interfaces permitted isolation of many individual TMs. These observations allowed us to determine the likely role for each helix and provided a useful method for testing the helix-packing hypothesis. The transmembrane α–helices that were generally the most hydrophobic and the least accessible to protease (TMs 3, 6, 9, and 12) are likely tightly associated with the lipid bilayer. Those α–helices that are generally less hydrophobic, and more accessible to proteolysis (TMs 1, 2, 4, 5, 7, 8, 10, and 11) likely display variable degrees of interaction with the aqueous translocation pathway and the lipid bilayer.

The organization of MFS transport proteins is proposed to have arisen from a gene duplication event [56]. This hypothesis speculates that the original precursor was an integral membrane protein with six membrane-spanning domains that presumably

functioned as a dimer. Upon gene duplication, the transport protein possessed twelve transmembrane domains. The N-terminal half of the protein (TMs 1-6) is linked to the C-terminal half (TMs 7-12) by a large intracellular loop, known as L6-7. In essence the C-terminal half serves as a mirror image of the N-terminal half, where TM1 is the structurally symmetric equivalent to TM7 and TM6 is the structurally symmetric partner of TM12. Additionally, many primary structure signature sequences, such as the RXGRR motif complementarily found in L2-3 and L8-9, support the gene duplication hypothesis.

Although our results examining TM accessibility to proteolytic cleavage generally support the internal symmetry hypothesis, we observe phenomena inconsistent with this idea. First, TM4 and its proposed structurally symmetric $\alpha$–helix partner TM10 demonstrate drastically different accessibility to proteolytic digestion: TM4 has 4 susceptible cleavage sites and 44% overall protease accessibility whereas TM10 only presents 1 susceptible cleavage site for 9% overall protease accessibility. We hypothesize that the arrangement of TM10 within each subunit of the membrane-resident GLUT1 tetramer differs from the model due to a potential disulfide bond between TM9 and TM11 that would force TM10 away from the aqueous pore. Second, a portion of TM11 is released into aqueous solvent following proteolysis and sedimentation of the membrane-associated fraction. Conversely, all peptides from the putative structurally symmetric partner TM5 remain associated with the membrane. This again could be the result of the alternative fold TM11 demonstrates due to the disulfide bond thus granting it a higher degree of interaction with the aqueous environment than its partner. Third, TM1 is released into the aqueous fraction following trypsin digestion, however its C-terminal

equivalent TM7 remains embedded within the membrane. TM1 and TM7 also fundamentally differ in that TM1 is associated with the small N-terminal tail whereas TM7 is located within the middle of the protein, surrounded by two TM connecting loop regions. Fourth, there appears to be minimal correlation between the relative hydrophobicity values (SSR) for each symmetry partner. One partner is generally more hydrophobic than the other despite their proposed reflective arrangement within the bilayer. Although many α–helix partners demonstrate similar digestion, solvent exposure, and peptide release patterns, there are clear examples of transmembrane domains that do not share characteristics reproduced across the N- and C-terminal halves of the protein.

We did attempt to study GLUT1 proteolytic accessibility in its native environment using human erythrocytes and alkaline-washed erythrocyte ghost membranes. Human red cells were digested for 15-120 minutes with α-chymotrypsin, sedimented, and the aqueous fraction was examined using RP-HPLC-ESI-MS/MS. Unfortunately, some red cells lysed and released intracellular hemoglobin into the aqueous fraction. The large amount of contaminating hemoglobin peptides overwhelmed those surface-exposed GLUT1 peptides presumably produced by α-chymotrypsin and prevented this analysis. When we performed the same studies using erythrocyte membranes, the anion exchange protein (AE1) contaminated much of the data acquisition. Our best results were obtained if we first lysed erythrocytes, performed limited trypsin proteolysis to remove the cytoplasmic, N-terminal AE1 domain, washed the ghosts in high alkaline medium, and then resuspended them in digestion buffer. Subsequent trypsin and α-chymotrypsin digestion

provided limited resolution of GLUT1 peptides that was far less comprehensive than the proteoliposome studies. We obtained a great deal of AE1 sequence coverage within these fractions. This provided evidence that membrane-embedded amino acid residues found in the α-helices of another mammalian transport protein interacted with the aqueous environment and were susceptible to proteolysis (Appendix 3; Figure A3.1 and Table A3.1).

Under conditions where e1-binding transport inhibitor cytochalasin B is added to the digest buffer or when the insoluble fraction is resuspended in CCB, followed by a second sedimentation step, TM8 becomes released into the aqueous solvent fraction. Currently, however, we are unable to determine if the addition of 10 μM CCB releases all of TM8 from the lipid bilayer, if TM8 release into the aqueous fraction is [CCB]-dependent, or if the majority of it remains embedded within the membrane. Unlike cytoplasmic peptides, which are present in large quantities, resolve very well, and are easily amenable to analysis by mass spectrometry, transmembrane proteins are more difficult to quantify. The LCQ mass spectrometer has served as a great instrument for quantifying peptide amount, but is less equipped for the rapid identification of multiple peptides. The LTQ, which scans peptide samples 10-100x faster than the LCQ, is far superior in peptide identification by MS/MS, but is less adept at quantifying peptide amounts in our hands. Resolving this problem may enhance our ability to grasp the greater details that these studies could provide.

### *COVALENT MODIFICATION*

To further assess GLUT1 accessibility and exploit the developed mass spectrometry technique, we employed a covalent NHS-ester biotin conjugate probe to study lysine accessibility. This was a particularly fortuitous choice because GLUT1 has 16 lysine residues distributed throughout the protein at the bilayer interface (at the terminal ends and loop regions of TM helices 1, 3, 5, 7, 12), in the N-terminus, in the C-terminus, and within the N- and C-terminal halves of L6-7 [24]. We employed a Sulfo-NHS-LC-Biotin tag that specifically modified the primary amine group found on the lysine side chain.

The Sulfo-NHS-LC-Biotin probe has multiple advantages upon which we capitalized throughout these experiments (Figure 6.1). First, the Sulfo group causes the probe to fully dissolve in aqueous buffer eliminating the need to introduce organic solvents, thus maintaining native experimental conditions. Second, the NHS reaction with the lysine primary amine forms a covalent amide bond that is much stronger than the thiourea linkage formed by fellow lysine reactive probe fluorescein isothiocyanate. This is an important distinction because the bond formed by FITC was unable to withstand the ionization energy of the mass spectrometer, and it was not possible to identify specific lysine residues that were modified. Third, a covalent modification to a lysine residue adds a distinguishable 339.16 Da mass adduct. Within the same run, therefore, we could identify modified and unmodified lysine containing peptides. We used mass spectrometry software to quantify the intensity of each peptide to determine the ratio of lysine modification under varying labeling conditions. Fourth, the LC-linker region separates

**Figure 6.1** Biotin labeling chemistry. The water-soluble Sulfo-NHS-LC-Biotin probe, manufactured by Pierce, was used to monitor lysine accessibility in GLUT1 proteoliposomes. As described in the text, Sulfo-NHS-LC-Biotin was chosen because GLUT1 has sixteen lysine residues, the reaction chemistry produces a covalent MS/MS stable bond, and the reactive group (a N-Hydroxysuccinimide (NHS) ester) functions at neutral pH and is soluble under aqueous conditions to preserve physiological conditions. The majority of reactions used a 10 mM concentration of NHS-LC-Biotin dissolved in water that presented a 20-fold molar excess of probe:protein. The NHS ester covalently modifies the lysine side chain primary amine resulting in a covalent mass net addition of 339.16 Da. Thus, a modified lysine residue registers as 467 Da versus 127.9 Da for unmodified lysine on an MS/MS spectrum. The confirmed reaction chemistry and mass addition facilitated identification of modified peptides.

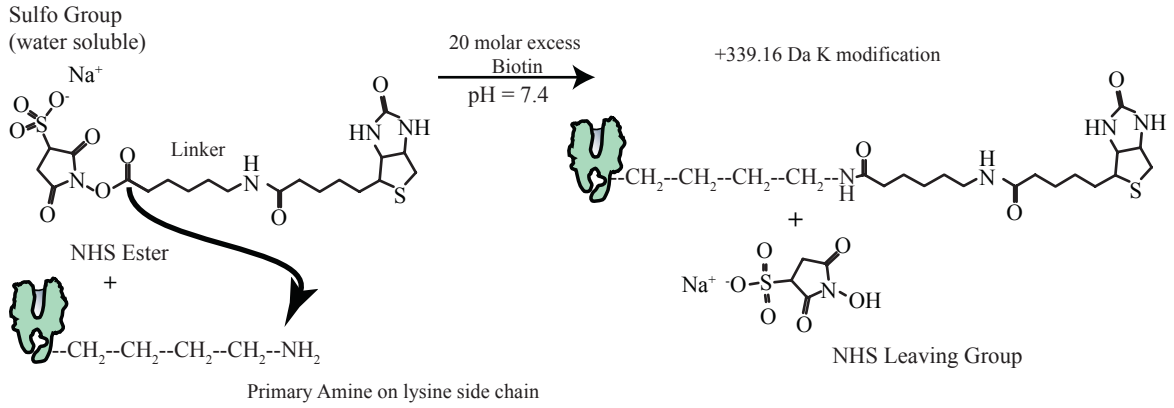
Sulfo Group
(water soluble)
Na+
Linker
NHS Ester
+
--CH2--CH2--CH2--CH2--NH2
Primary Amine on lysine side chain
20 molar excess
Biotin
pH = 7.4
+339.16 Da K modification
--CH2--CH2--CH2--CH2--
+
Na+
OH
NHS Leaving Group

Figure 6.1

the biotin reporter molecule from the reactive NHS ester, reducing steric hindrance that would inhibit labeling. We were able to take advantage of this feature when determining the differential labeling pattern of lysine residues found within the cytoplasm. Fifth, the biotin tag itself was a useful reporter molecule that could be detected by a streptavidin antibody conjugated to horseradish peroxidase using ELISA and western blots.

We detected a preferential order of addition or extent of modification among the lysine residues found in the cytoplasmic aqueous fraction (K225, K229, K230, K245, K255, K256, K477). Under simple kaline buffer conditions, the C-terminus was most accessible, while the C-terminal half of L6-7 was least accessible when the concentration of labeling reagent was limiting. At saturating levels of probe, however, all lysine residues were equally labeled throughout the protein. Under native conditions, therefore, the C-terminus may be the most flexible and solvent-exposed of the cytoplasmic portions, but with enough reagent, all cytoplasmic regions are labeled to the same extent. This observation suggests that there is some degree of organization among these domains, but overall, they demonstrate a high degree of flexibility and interaction with the aqueous intracellular environment. Overall all of these findings encouraged us to examine the dynamic response of GLUT1 to different substrates, inhibitors, or modulators on the global (ELISA or western blot) and local (MS/MS) levels.

We pre-incubated GLUT1 with D-glucose substrate (Appendix 3; Figure A3.2), CCB inhibitor (Appendix 3; Figure A3.3), and ATP modulator (Chapter IV) prior to reaction with the NHS-biotin probe to determine if these molecules induced conformational

changes within the transporter that would enhance or inhibit covalent modification. GLUT1 displayed a global increase in NHS-biotin labeling in a D-glucose specific manner, a minor change in labeling in the presence of CCB, and a sharp ATP-specific decrease in lysine modification. In contrast to D-glucose and CCB, we have observed residue and region specific changes in GLUT1 when ATP is added to these reaction mixtures. Our results suggest that in the presence of ATP, L6-7 and the C-terminus interact to reduce overall GLUT1 sugar carrying capacity. The fact that our proposed model is supported by three independent techniques, requires the GLUT1 L6-7 primary sequence, and provides MS data implicating exact residues that undergo changes in labeling efficiency is entirely consistent with transport observations and offer a plausible molecular mechanism by which these kinetic finding can be explained.

Using mass spectrometry techniques coupled with traditional biochemistry approaches, we have conclusively shown that GLUT1 is a conformationally dynamic protein that responds globally to substrate, ligand, or modulator interactions. The similarities between the GLUT1 responses to CCB and ATP binding are of particular interest because they demonstrate a communication between distal protein domains. In Chapter III we discussed how trypsin digests conducted in the presence of CCB or when the membrane fraction is resuspended with CCB result in TM8 release from the membrane-embedded protein domains. Since CCB is proposed to bind to GLUT1 in the TM10-TM11 region [61] the release of TM8 indicates that these conformational dynamics are communicated to other parts of the protein. ATP is proposed to bind a nucleotide binding pocket that includes, but is not limited to the L8-9-TM9 region [135]. As we showed in Chapter IV,

ATP interaction with GLUT1 causes domains, separated by 100 amino acids of primary structure, to interact with one another thereby regulating the overall transport function. Our observations of global changes in lysine accessibility in the presence of D-glucose and CCB and overall accessibility of transmembrane regions to proteolytic agents support the hypothesis that GLUT1 undergoes a wide range of conformational changes to mediate glucose transport across the plasma membrane.

### *How Thiol Chemistry Affects GLUT1 Structure*

Before examining cysteine accessibility by mass spectrometry, we conducted a thorough analysis of glucose transport protein electrophoretic behavior. After deglycosylating GLUT1 with PNGaseF to improve GLUT1 resolution on reducing SDS-PAGE, we resolved two species of GLUT1 in the gel. We found the pattern of GLUT1 resolution to be dependent upon the presence of reducing agents such as DTT and βME. Further analysis showed that the less mobile species was nonreduced while the more mobile species was completely reduced. This demonstrates that membrane resident GLUT1 is sensitive to reductant and that thiol chemistry likely plays an important role in determining or mediating its folding pattern.

We further explored the accessibility of the six GLUT1 cysteine residues (C133, C201, C207, C347, C421, and C429) using mass spectrometry to determine how reductant affected the number and availability of reactive thiol side chains. According to *Zottola et al.* [86], GLUT1 may contain an internal disulfide bridge. If correct, we should have isolated a disulfide bond and confirmed its identity by mass and amino acid sequence by

this technique. If a GLUT1 intramolecular disulfide does exist, our lack of detection may result from insufficient resolution or the propensity of α-chymotrypsin to create multiple peptides containing the disulfide bond, thus preventing its quantitation. Our observations and previous findings, however, support the existence of a disulfide bond between C347 and C421 [80,84,86]. When GLUT1 was alkylated in the absence of reductant, we detected far fewer peptides with cysteine modifications. C133, C207, and C429 are accessible to iodoacetamide regardless of whether or not the protein has been previously reduced. This observation indicates that these cysteine side chains are not involved in any thiol-mediated interactions, essentially eliminating them from participating in disulfide forming side chains. C201 and C421, however, are only detectable as modified residues following GLUT1 reduction and C347 is completely undetectable by this technique. Although we were unable to categorically identify the C347-C421 disulfide bond, our findings are consistent with its existence and role within controlling GLUT1 oligomerization.

### *FUTURE DIRECTIONS*

This discussion has offered our interpretation of the data collected, analyzed, and presented within this thesis. After considering these findings and the associated commentary, specific observations merit further consideration if we are to continue to improve our comprehension of carrier-mediated transport. In particular, the MS technique provides an avenue to investigate very specific questions relating to GLUT1-mediated

glucose transport and broad questions concerning how the structure-function relationship mediates the molecular workings of facilitated diffusion.

The most interesting fundamental questions are – where do glucose, ATP, and CCB bind? Upon identifying the static binding site, the next question asks how binding influences transporter conformational states? It is conceivably possible to envision reactions that link these molecules to their respective binding sites within the transporter, followed by digestion, and identification of the substrate binding site. Biotinylated (glucose and ATP) and radiolabeled (CCB) molecules do in fact exist to examine this inquiry. Covalent probes with refined chemistries that have a predictable and preferential side chain reaction and mass addition would simplify this project and enable more computer and database searching. In the absence of these reagents (remember NHS-biotin labels any lysine residue with an available primary amine), the suggested probes allow definition of the elution conditions required to observe the reporter molecule-peptide conjugate, and thus help identify the modified peptides and its reported mass. The MS spectra can then be carefully reviewed to identify the peptide of interest and the MS/MS spectra can be combed to determine the modified amino acids. Once we gather where a substrate binds, we can more accurately model the substrate binding pocket by molecular docking procedures using three-dimensional homology models [226].

These findings will help us to understand how basal glucose transport is catalyzed in all cell types. Furthermore, molecular structure-function relationships obtained with GLUT1 could be applied to other transporters. It is possible to envision experiments that offer

biochemical clues for intelligent drug design preventing export from diseased cells or promoting targeted and specific uptake.

Our studies provided biochemical details comparing the structural arrangement of GLUT1 transmembrane α-helices with the MFS helix-packing model. TM embedded helices 3, 6, 9, and 12 were almost completely resistant to proteolytic digestion. This is entirely consistent with a model that buries each helix, peptide backbone and side chain, in the lipid bilayer, completely isolating them from aqueous solvent except for the loops connecting them to the other TMs. All other lipid embedded TMs are predicted, in some form or another, to line the aqueous translocation pathway, and as a result the side chains directly interact with water, thus explaining their susceptibility to proteolytic enzymes. Proteolytic enzymes only have the capability of cleaving after certain side chains (as we have discussed trypsin specificity for peptide bonds following lysine and arginine residues). Even though each α-helix has ample potential cleavage sites, this restriction limits the ability of this technique to report back on each residue within the entire helix.

Hydrogen-deuterium exchange studies coupled with mass spectrometry are seemingly the next step to define the translocation pathway and delineate the differences between residues exposed to the aqueous solvent in the e2, e( ), and e1 conformations. This technique takes advantage of differences in proton exchange rates based on location within the protein. Solvent exposed protons exchange at a much faster rate than those buried within the lipid membrane or involved in protein secondary structure [227]. Jung has shown that deuterium does exchange with upwards of 80% of peptide backbone

hydrogen molecules in GLUT1 [67]. This observation provides a solid basis for trying to identify and determine which residues in each TM are easily exchanged versus those which are resistant. Given our high degree of sequence coverage, we should be able to detect deuterium exchange based upon the 1 Da mass adducts for each hydrogen replaced. This type of experiment will further solidify the helix packing hypothesis. By examining deuterium exchange profiles in the presence of glucose, CCB, phloretin, or maltose, we can understand which residues of particular regions are directly or indirectly involved in dynamic changes and which portions form each conformation.

We can further probe the GLUT1 residues directly involved in ATP modulation of glucose transport. In particular, it would be interesting to determine the precise amino acids that mediate the proposed interaction between L6-7 and the C-terminus. We can approach this question in two ways. First, we can create point mutations within GLUT1, which correspond to primary structure residues that fall between K245 and K256 or surrounding K477 in the C-terminus, and express these constructs in HEK cells. Transport assays, limited proteolysis, and IgG accessibility in the presence of ATP will more directly implicate the residues involved in this interaction. Second, we can test if K245, K255, K256, and K477 directly interact by using NHS reactive chemical crosslinkers of various linker lengths. Following this reaction, we would subject GLUT1 to proteolysis and RP-HPLC-ESI-MS/MS to identify uniquely linked peptides. Lysine residues would be a starting point for the crosslinking reactions before branching out to test other reaction chemistries.

Finally, we would like to identify the disulfide bond proposed to exist between C347 and C421 using tandem mass spectrometry. This may be accomplished by using more specific proteolytic agents, more limited proteolysis, or a disulfide isolation technique to assist in identifying this bond and the residues involved in its formation. This idea would promote the formation of specific peptides (unlike what α-chymotrypsin produces) that would appear in a non-reduced sample, but disappear in a reduced sample. We would like to examine proteolysis patterns when GLUT1 is in its native tetrameric form and following reduction to determine if overall aqueous accessibility (particularly for TM10) changes when the putative disulfide bond is removed. Furthermore, we could apply isobaric tags for relative and absolute quantitation (iTRAQ) technology [228] to better quantify the cleavage susceptibility patterns in the presence and absence of reductant. These studies would provide direct experimental evidence to support the existence of the disulfide bond and would explain the diminished exposure of TM10 to the aqueous environment.

### *FINAL CONCLUSIONS*

This thesis has strengthened the GLUT1 structure-function relationship and provided a new technique to further this investigation and to approach additional questions in the membrane transport field. The main discoveries included kinetically isolating a protein intermediate between the import and export conformational changes, strengthening the role of intramolecular bonds in controlling transporter structure and function, and

defining membrane topography and solvent accessibility demonstrated by the GLUT1 α-helices.

The future directions discuss how we may extend these findings to improve and enhance our understanding of how the structure-function relationship governs carrier-mediated transport. Integral membrane proteins, which comprise approximately 20% of the proteins coded for by the human genome, have distinct and necessary functions in all cell types. Their role in regulating interactions between the intra- and extracellular environments is absolutely vital for homeostasis and cellular survival. The pathophysiology of carrier-mediated diseases and the degree to which the total body suffers due to these conditions clearly illustrates the importance transmembrane proteins assume in ensuring a properly functioning system. We mentioned cystic fibrosis, GLUT1-deficiency syndrome, diabetes, drug addiction, and resistance to drug treatments as direct examples of how individual transporters establish and sustain homeostasis. The first step to addressing carrier pathophysiology is to understand how protein structure governs function, and in this regard, how diseases and other ailments interrupt this condition at the molecular level. This thesis presents techniques and findings that offer broad solutions to address these issues.

***REFERENCES***

1. Rabilloud T (2003) Membrane proteins ride shotgun. Nat Biotechnol S 21: 508-510.

2. Stein WD (1986) Transport and diffusion across cell membranes. New York: Academic Press.

3. Singer SJ, Nicolson GL (1972) The fluid mosaic model of the structure of cell membranes. Science 175: 720-731.

4. Verkman AS (2002) Aquaporin water channels and endothelial cell function. J Anat 200: 617-627.

5. Hirai T, Subramaniam S (2004) Structure and transport mechanism of the bacterial oxalate transporter OxlT. Biophys J 87: 3600-3607.

6. Abramson J, Iwata S, Kaback HR (2004) Lactose permease as a paradigm for membrane transport proteins (Review). Mol Membr Biol 21: 227-236.

7. Kasho VN, Smirnova IN, Kaback HR (2006) Sequence alignment and homology threading reveals prokaryotic and eukaryotic proteins similar to lactose permease. J Mol Biol S 358: 1060-1070.

8. Lander ES, Linton LM, Birren B, Nusbaum C, Zody MC, et al. (2001) Initial sequencing and analysis of the human genome. Nature 409: 860-921.

9. Venter JC, Adams MD, Myers EW, Li PW, Mural RJ, et al. (2001) The sequence of the human genome. Science 291: 1304-1351.

10. Klepper J, Wang D, Fischbarg J, Vera JC, Jarjour IT, et al. (1999) Defective glucose transport across brain tissue barriers: a newly recognized neurological syndrome. Neurochem Res 24: 587-594.

11. Klepper J, Voit T (2002) Facilitated glucose transporter protein type 1 (GLUT1) deficiency syndrome: impaired glucose transport into brain-- a review. Eur J Pediatr 161: 295-304.

12. Skach WR (2006) CFTR: New Members Join the Fold. Cell 127: 673-675.

13. Bryant NJ, Govers R, James DE (2002) Regulated transport of the glucose transporter GLUT4. Nat Rev Mol Cell Biol 3: 267-277.

14. Carruthers A (1990) Facilitated diffusion of glucose. Physiol Rev 70: 1135-1176.

15. Sharom FJ, Lugo MR, Eckford PD (2005) New insights into the drug binding, transport and lipid flippase activities of the p-glycoprotein multidrug transporter. J Bioenerg Biomembr S 37: 481-487.

16. Surratt CK, Ukairo OT, Ramanujapuram S (2005) Recognition of psychostimulants, antidepressants, and other inhibitors of synaptic neurotransmitter uptake by the plasma membrane monoamine transporters. AAPS J 7: E739-51.

17. Wang W, Sonders MS, Ukairo OT, Scott H, Kloetzel MK, et al. (2003) Dissociation of high-affinity cocaine analog binding and dopamine uptake inhibition at the dopamine transporter. Mol Pharmacol 64: 430-439.

18. Kreek MJ, Bart G, Lilly C, LaForge KS, Nielsen DA (2005) Pharmacogenetics and human molecular genetics of opiate and cocaine addictions and their treatments. Pharmacol Rev 57: 1-26.

19. Vannucci SJ, Maher F, Simpson IA (1997) Glucose transporter proteins in brain: delivery of glucose to neurons and glia. Glia 21: 2-21.

20. De Feo P, Di Loreto C, Lucidi P, Murdolo G, Parlanti N, et al. (2003) Metabolic response to exercise. J Endocrinol Invest 26: 851-854.

21. Aubert A, Costalat R, Magistretti PJ, Pellerin L (2005) Brain lactate kinetics: Modeling evidence for neuronal lactate uptake upon activation. Proc Natl Acad Sci U S A S 102: 16448-16453.

22. Wood IS, Trayhurn P (2003) Glucose transporters (GLUT and SGLT): expanded families of sugar transport proteins. Br J Nutr 89: 3-9.

23. Joost HG, Thorens B (2001) The extended GLUT-family of sugar/polyol transport facilitators: nomenclature, sequence characteristics, and potential function of its novel members (review). Mol Membr Biol 18: 247-256.

24. Mueckler M, Caruso C, Baldwin SA, Panico M, Blench I, et al. (1985) Sequence and structure of a human glucose transporter. Science 229: 941-945.

25. Leturque A, Brot-Laroche E, Le Gall M, Stolarczyk E, Tobin V (2005) The role of GLUT2 in dietary sugar handling. J Physiol Biochem 61: 529-537.

26. Bernhardt I, Hall AC, Ellory JC (1991) Effects of low ionic strength media on passive human red cell monovalent cation transport. J Physiol 434: 489-506.

27. Kakhniashvili DG, Bulla LAJ, Goodman SR (2004) The human erythrocyte proteome: analysis by ion trap mass spectrometry. Mol Cell Proteomics 3: 501-509.

28. Cloherty EK, Levine KB, Graybill C, Carruthers A (2002) Cooperative nucleotide binding to the human erythrocyte sugar transporter. Biochemistry 41: 12639-12651.

29. Hatanaka M (1974) Transport of sugars in tumor cell membranes. Biochim Biophys Acta 355: 77-104.

30. McAllister MS, Krizanac-Bengez L, Macchia F, Naftalin RJ, Pedley KC, et al. (2001) Mechanisms of glucose transport at the blood-brain barrier: an in vitro study. Brain Res 904: 20-30.

31. Guo X, Geng M, Du G (2005) Glucose transporter 1, distribution in the brain and in neural disorders: its relationship with transport of neuroactive drugs through the blood-brain barrier. Biochem Genet 43: 175-187.

32. Macheda ML, Rogers S, Best JD (2005) Molecular and cellular regulation of glucose transporter (GLUT) proteins in cancer. J Cell Physiol 202: 654-662.

33. Abramson J, Smirnova I, Kasho V, Verner G, Kaback HR, et al. (2003) Structure and mechanism of the lactose permease of Escherichia coli. Science 301: 610-615.

34. Hirai T, Heymann JA, Shi D, Sarker R, Maloney PC, et al. (2002) Three-dimensional structure of a bacterial oxalate transporter. Nat Struct Biol 9: 597-600.

35. Huang Y, Lemieux MJ, Song J, Auer M, Wang DN (2003) Structure and mechanism of the glycerol-3-phosphate transporter from Escherichia coli. Science 301: 616-620.

36. Jung CY (1971) Permeability of bimolecular membranes made from lipid extracts of human red cells to sugar. J Memb Biol 5: 2300–2314.

37. Jung CY, Carlson LM, Whaley DA (1971) Glucose transport carrier activities in extensively washed human red cell ghosts. Biochim Biophys Acta 241: 613–627.

38. Widdas WF (1952) Inability of diffusion to account for placental glucose transfer in the sheep and consideration of the kinetics of a possible carrier transfer. J Physiol (London) 118: 23–39.

39. Yin Y, He X, Szewczyk P, Nguyen T, Chang G (2006) Structure of the multidrug transporter EmrD from Escherichia coli. Science 312: 741-744.

40. Alisio A, Mueckler M (2004) Relative proximity and orientation of helices 4 and 8 of the GLUT1 glucose transporter. J Biol Chem 279: 26540-26545.

41. Appleman JR, Lienhard GE (1985) Rapid kinetics of the glucose transporter from human erythrocytes. Detection and measurement of a half-turnover of the purified transporter. J Biol Chem 260: 4575-4578.

42. Carruthers A (1991) Mechanisms for the facilitated diffusion of substrates across cell membranes. Biochemistry 30: 3898-3906.

43. Cloherty EK, Heard KS, Carruthers A (1996) Human erythrocyte sugar transport is incompatible with available carrier models. Biochemistry 35: 10411-10421.

44. Due AD, Cook JA, Fletcher SJ, Qu ZC, Powers AC, et al. (1995) A "cysteineless" GLUT1 glucose transporter has normal function when expressed in Xenopus oocytes. Biochem Biophys Res Commun 208: 590-596.

45. Hresko RC, Kruse M, Strube M, Mueckler M (1994) Topology of the Glut 1 glucose transporter deduced from glycosylation scanning mutagenesis. J Biol Chem 269: 20482-20488.

46. Lowe AG, Walmsley AR (1987) A single half-turnover of the glucose carrier of the human erythrocyte. Biochim Biophys Acta 903: 547-550.

47. Monden I, Olsowski A, Krause G, Keller K (2001) The large cytoplasmic loop of the glucose transporter GLUT1 is an essential structural element for function. Biol Chem 382: 1551-1558.

48. Mueckler M, Makepeace C (2004) Analysis of transmembrane segment 8 of the GLUT1 glucose transporter by cysteine-scanning mutagenesis and substituted cysteine accessibility. J Biol Chem 279: 10494-10499.

49. Mueckler M, Makepeace C (2005) Cysteine-scanning mutagenesis and substituted cysteine accessibility analysis of transmembrane segment 4 of the Glut1 glucose transporter. J Biol Chem 280: 39562-39568.

50. Mueckler M, Roach W, Makepeace C (2004) Transmembrane segment 3 of the Glut1 glucose transporter is an outer helix. J Biol Chem S 279: 46876-46881.

51. Wellner M, Monden I, Keller K (1995) From triple cysteine mutants to the cysteine-less glucose transporter GLUT1: a functional analysis. FEBS Lett 370: 19-22.

52. Doyle DA, Morais Cabral J, Pfuetzner RA, Kuo A, Gulbis JM, et al. (1998) The structure of the potassium channel: molecular basis of K+ conduction and selectivity. Science 280: 69-77.

53. Toyoshima C, Nakasako M, Nomura H, Ogawa H (2000) Crystal structure of the calcium pump of sarcoplasmic reticulum at 2.6 A resolution. Nature 405: 647-655.

54. Guan L, Kaback HR (2006) Lessons from lactose permease. Annu Rev Biophys Biomol Struct 35: 67-91.

55. Barrett MP, Walmsley AR, Gould GW (1999) Structure and function of facilitative sugar transporters. Curr Opin Cell Biol 11: 496-502.

56. Saier MH, Jr., Beatty JT, Goffeau A, Harley KT, Heijne WH, et al. (1999) The major facilitator superfamily. J Mol Microbiol Biotechnol 1: 257-279.

57. Pao SS, Paulsen IT, Saier MH, Jr. (1998) Major facilitator superfamily. Microbiol Mol Biol Rev 62: 1-34.

58. Huggett AS, Warren FL, Warren NV (1951) The origin of the blood fructose of the foetal sheep. J Physiol 113: 258-275.

59. LeFevre PG (1948) Evidence of active transfer of certain non-electrocytes across the human red cell membrane. J. Gen. Physiol. 31, 405.:

60. Cairns MT, Alvarez J, Panico M, Gibbs AF, Morris HR, et al. (1987) Investigation of the structure and function of the human erythrocyte glucose transporter by proteolytic dissection. Biochim Biophys Acta 905: 295-310.

61. Hruz PW, Mueckler MM (2001) Structural analysis of the GLUT1 facilitative glucose transporter (review). Mol Membr Biol 18: 183-193.

62. Pawagi AB, Deber CM (1987) D-glucose binding increases secondary structure of human erythrocyte monosaccharide transport protein. Biochem Biophys Res Commun 145: 1087-1091.

63. Holyoake J, Caulfeild V, Baldwin SA, Sansom MS (2006) Modeling, docking, and simulation of the major facilitator superfamily. Biophys J S 91: L84-6.

64. Salas-Burgos A, Iserovich P, Zuniga F, Vera JC, Fischbarg J (2004) Predicting the three-dimensional structure of the human facilitative glucose transporter glut1 by a novel evolutionary homology strategy: insights on the molecular mechanism of substrate migration, and binding sites for glucose and inhibitory molecules. Biophys J 87: 2990-2999.

65. Preston RA, Baldwin SA (1993) GLUT 1: identification of exofacial lysine-residues. Biochem Soc Trans 21: 309-312.

66. Wellner M, Monden I, Keller K (1994) The role of cysteine residues in glucose-transporter-GLUT1-mediated transport and transport inhibition. Biochem J 299: 813-817.

67. Jung EK, Chin JJ, Jung CY (1986) Structural basis of human erythrocyte glucose transporter function in reconstituted system. Hydrogen exchange. J Biol Chem 261: 9155-9160.

68. Mueckler M, Makepeace C (1999) Transmembrane segment 5 of the Glut1 glucose transporter is an amphipathic helix that forms part of the sugar permeation pathway. J Biol Chem 274: 10923-10926.

69. Hruz PW, Mueckler MM (1999) Cysteine-scanning mutagenesis of transmembrane segment 7 of the GLUT1 glucose transporter. J Biol Chem 274: 36176-36180.

70. Hruz PW, Mueckler MM (2000) Cysteine-scanning mutagenesis of transmembrane segment 11 of the GLUT1 facilitative glucose transporter. Biochemistry 39: 9367-9372.

71. Olsowski A, Monden I, Krause G, Keller K (2000) Cysteine scanning mutagenesis of helices 2 and 7 in GLUT1 identifies an exofacial cleft in both transmembrane segments. Biochemistry 39: 2469-2474.

72. Mueckler M, Makepeace C (2002) Analysis of transmembrane segment 10 of the Glut1 glucose transporter by cysteine-scanning mutagenesis and substituted cysteine accessibility. J Biol Chem 277: 3498-3503.

73. Heinze M, Monden I, Keller K (2004) Cysteine-scanning mutagenesis of transmembrane segment 1 of glucose transporter GLUT1: extracellular accessibility of helix positions. Biochemistry 43: 931-936.

74. Mueckler M, Makepeace C (2006) Transmembrane segment 12 of the glut1 glucose transporter is an outer helix and is not directly involved in the transport mechanism. J Biol Chem 281: 36993-36998.

75. Sato M, Mueckler M (1999) A conserved amino acid motif (R-X-G-R-R) in the glut1 glucose transporter is an important determinant of membrane topology [In Process Citation]. J Biol Chem 274: 24721-24725.

76. Gould GW, Holman GD (1993) The glucose transporter family: structure, function and tissue-specific expression. Biochem J 295: 329-341.

77. Doege H, Schurmann A, Ohnimus H, Monser V, Holman GD, et al. (1998) Serine-294 and threonine-295 in the exofacial loop domain between helices 7 and 8 of glucose transporters (GLUT) are involved in the conformational alterations during the transport process. Biochem J 329: 289-293.

78. Seatter MJ, De la Rue SA, Porter LM, Gould GW (1998) QLS motif in transmembrane helix VII of the glucose transporter family interacts with the C-1 position of D-glucose and is involved in substrate selection at the exofacial binding site. Biochemistry 37: 1322-1326.

79. Inukai K, Asano T, Katagiri H, Anai M, Funaki M, et al. (1994) Replacement of both tryptophan residues at 388 and 412 completely abolished cytochalasin B photolabelling of the GLUT1 glucose transporter. Biochem J 302: 355-361.

80. Graybill C, van Hoek AN, Desai D, Carruthers AM, Carruthers A (2006) Ultrastructure of Human Erythrocyte GLUT1. Biochemistry 45: 8096-8107.

81. Levine KB, Carruthers A (2004) Regulation of carrier-mediated sugar transport by transporter quaternary structure. In: Boles E k, R K, editors. Topics in Current Genetics Molecular mechanisms controlling transmembrane transport(9). pp. 67 – 694.

82. Naftalin RJ, Smith PM, Roselaar SE (1985) Evidence for non-uniform distribution of D-glucose within human red cells during net exit and counterflow. Biochim Biophys Acta 820: 235-249.

83. Sultzman LA, Carruthers A (1999) Stop-flow analysis of cooperative interactions between GLUT1 sugar import and export sites. Biochemistry Biochemistry 38: 6640-6650.

84. Hebert DN, Carruthers A (1992) Glucose transporter oligomeric structure determines transporter function. Reversible redox-dependent interconversions of tetrameric and dimeric GLUT1. J Biol Chem 267: 23829-23838.

85. Levine KB, Cloherty EK, Hamill S, Carruthers A (2002) Molecular determinants of sugar transport regulation by ATP. Biochemistry 41: 12629-12638.

86. Zottola RJ, Cloherty EK, Coderre PE, Hansen A, Hebert DN, et al. (1995) Glucose transporter function is controlled by transporter oligomeric structure. A single, intramolecular disulfide promotes GLUT1 tetramerization. Biochemistry 34: 9734-9747.

87. Blodgett DM, Carruthers A (2005) Quench-Flow Analysis Reveals Multiple Phases of GluT1-Mediated Sugar Transport. Biochemistry 44: 2650-2660.

88. Kubala M (2006) ATP-binding to P-type ATPases as revealed by biochemical, spectroscopic, and crystallographic experiments. Proteins 64: 1-12.

89. Toyoshima C, Mizutani T (2004) Crystal structure of the calcium pump with a bound ATP analogue. Nature 430: 529-535.

90. Toyoshima C, Nomura H (2002) Structural changes in the calcium pump accompanying the dissociation of calcium. Nature 418: 605-611.

91. Dawson RJ, Locher KP (2006) Structure of a bacterial multidrug ABC transporter. Nature 443: 180-185.

92. Karpowich NK, Huang HH, Smith PC, Hunt JF (2003) Crystal structures of the BtuF periplasmic-binding protein for vitamin B12 suggest a functionally important reduction in protein mobility upon ligand binding. J Biol Chem 278: 8429-8434.

93. Linton KJ, Higgins CF (2006) Structure and function of ABC transporters: the ATP switch provides flexible control. Pflugers Arch

94. Locher KP, Borths E (2004) ABC transporter architecture and mechanism: implications from the crystal structures of BtuCD and BtuF. FEBS Lett 564: 264-268.

95. Locher KP, Lee AT, Rees DC (2002) The E. coli BtuCD structure: a framework for ABC transporter architecture and mechanism. Science 296: 1091-1098.

96. Hunte C, Screpanti E, Venturi M, Rimon A, Padan E, et al. (2005) Structure of a Na+/H+ antiporter and insights into mechanism of action and regulation by pH. Nature 435: 1197-1202.

97. Murakami S, Nakashima R, Yamashita E, Matsumoto T, Yamaguchi A (2006) Crystal structures of a multidrug transporter reveal a functionally rotating mechanism. Nature 443: 173-179.

98. Schuldiner S (2006) Structural biology: the ins and outs of drug transport. Nature 443: 156-157.

99. Seeger MA, Schiefner A, Eicher T, Verrey F, Diederichs K, et al. (2006) Structural asymmetry of AcrB trimer suggests a peristaltic pump mechanism. Science 313: 1295-1298.

100. Pebay-Peyroula E, Dahout-Gonzalez C, Kahn R, Trezeguet V, Lauquin GJ, et al. (2003) Structure of mitochondrial ADP/ATP carrier in complex with carboxyatractyloside. Nature 426: 39-44.

101. Kuhlbrandt W, Zeelen J, Dietrich J (2002) Structure, mechanism, and regulation of the Neurospora plasma membrane H+-ATPase. Science 297: 1692-1696.

102. Taglicht D, Padan E, Schuldiner S (1991) Overproduction and purification of a functional Na+/H+ antiporter coded by nhaA (ant) from Escherichia coli. J Biol Chem 266: 11289-11294.

103. Viitanen P, Garcia ML, Kaback HR (1984) Purified reconstituted lac carrier protein from Escherichia coli is fully functional. Proc Natl Acad Sci U S A 81: 1629-1633.

104. Klingenberg M (1985) The ADP/ATP Carrier in Mitochondrial Membranes. New York: Plenun.

105. Auer M, Kim MJ, Lemieux MJ, Villa A, Song J, et al. (2001) High-yield expression and functional analysis of Escherichia coli glycerol-3-phosphate transporter. Biochemistry 40: 6628-6635.

106. Domon B, Aebersold R (2006) Mass spectrometry and protein analysis. Science 312: 212-217.

107. Whitelegge JP, Laganowsky A, Nishio J, Souda P, Zhang H, et al. (2006) Sequencing covalent modifications of membrane proteins. J Exp Bot 57: 1515-1522.

108. Abe Y, Chaen T, Jin XR, Hamasaki T, Hamasaki N (2004) Massspectrometric analyses of transmembrane proteins in human erythrocyte membrane. J Biochem (Tokyo) S 136: 97-106.

109. Han J, Schey KL (2004) Proteolysis and mass spectrometric analysis of an integral membrane: aquaporin 0. J Proteome Res 3: 807-812.

110. Wang Y, Berg EA, Feng X, Shen L, Smith T, et al. (2006) Identification of surface-exposed components of MOMP of Chlamydia trachomatis serovar F. Protein Sci 15: 122-134.

111. Weinglass A, Whitelegge JP, Faull KF, Kaback HR (2004) Monitoring conformational rearrangements in the substrate-binding site of a membrane transport protein by mass spectrometry. J Biol Chem 279: 41858-41865.

112. Weinglass AB, Soskine M, Vazquez-Ibar JL, Whitelegge JP, Faull KF, et al. (2005) Exploring the role of a unique carboxyl residue in EmrE by mass spectrometry. J Biol Chem 280: 7487-7492.

113. Weinglass AB, Whitelegge JP, Hu Y, Verner GE, Faull KF, et al. (2003) Elucidation of substrate binding interactions in a membrane transport protein by mass spectrometry. Embo J 22: 1467-1477.

114. Cloherty EK, Diamond DL, Heard KS, Carruthers A (1996) Regulation of GLUT1-mediated sugar transport by an antiport/uniport switch mechanism. Biochemistry 35: 13231-13239.

115. Joost HG, Bell GI, Best JD, Birnbaum MJ, Charron MJ, et al. (2002) Nomenclature of the GLUT/SLC2A family of sugar/polyol transport facilitators. Am J Physiol Endocrinol Metab 282: E974-6.

116. Lowe AG, Walmsley AR (1986) The kinetics of glucose transport in human red blood cells. Biochim Biophys Acta 857: 146-154.

117. Naftalin RJ, Holman GD (1977) Transport of sugars in human red cells. In: Ellory JC, Lew VL, editors. Membrane transport in red cells. New York: Academic Press. pp. 257-300.

118. Helgerson AL, Carruthers A (1987) Equilibrium ligand binding to the human erythrocyte sugar transporter. Evidence for two sugar-binding sites per carrier. J Biol Chem 262: 5464-5475.

119. Carruthers A, Zottola RJ (1996) Erythrocyte sugar transport. In: W.N. Konings HRKJSL, editor. Handbook of Biological Physics. "*Transport Processes in Eukaryotic and Prokaryotic Organisms*".*(2)*. Elsevier. pp. pp 311-342.

120. Naftalin RJ, Smith PM, Roselaar SE (1985) Evidence for non–uniform distribution of D–glucose within human red cells during net exit and counterflow. Biochim Biophys Acta 820: 235–249.

121. Cloherty EK, Sultzman LA, Zottola RJ, Carruthers A (1995) Net sugar transport is a multistep process. Evidence for cytosolic sugar binding sites in erythrocytes. Biochemistry 34: 15395-15406.

122. Kaback HR, Voss J, Wu J (1997) Helix packing in polytopic membrane proteins: the lactose permease of Escherichia coli. Current Opinion in Structural Biology 7: 537-542.

123. Baker PF, Carruthers A (1981) Sugar transport in giant axons of Loligo. J Physiol (Lond) 316: 481-502.

124. Lemieux MJ, Song J, Kim MJ, Huang Y, Villa A, et al. (2003) Three-dimensional crystallization of the Escherichia coli glycerol-3-phosphate transporter: A member of the major facilitator superfamily. Protein Sci 12: 2748-2756.

125. Baker GF, Naftalin RJ (1979) Evidence of multiple operational affinities for D-glucose inside the human erythrocyte membrane. Biochim Biophys Acta 550: 474-484.

126. Lieb WR, Stein WD (1974) Testing and characterizing the simpler pore. Biochim Biophys Acta 373: 165-177.

127. Ginsburg H (1978) Galactose transport in human erythrocytes. The transport mechanism is resolved into two simple asymmetric antiparallel carriers. Biochim Biophys Acta 506: 119-135.

128. Karlish SJD, Lieb WR, Ram D, Stein WD (1972) Kinetic Parameters of glucose efflux from human red blood cells under zero-trans conditions. Biochim Biophys Acta 255: 126-132.

129. Miller DM (1968) The kinetics of selective biological transport. IV. Assessment of three carrier systems using the erythrocyte-monosaccharide transport data. Biophys J 8: 1339-1352.

130. Hebert DN, Carruthers A (1991) Uniporters and anion antiporters. Curr Opin Cell Biol 3: 702-709.

131. Heard KS, Fidyk N, Carruthers A (2000) ATP-dependent substrate occlusion by the human erythrocyte sugar transporter. Biochemistry 39: 3005-3014.

132. Blodgett DM, Carruthers A (2004) Conventional transport assays underestimate sugar transport rates in human red cells. Blood Cells Mol Dis 32: 401-407.

133. Gutfreund H (1969) Rapid mixing: Continuous flow. Methods in Enzymology 16: 229-249.

134. Coderre PE, Cloherty EK, Zottola RJ, Carruthers A (1995) Rapid substrate translocation by the multisubunit, erythroid glucose transporter requires subunit associations but not cooperative ligand binding. Biochemistry 34: 9762-9773.

135. Levine KB, Cloherty EK, Fidyk NJ, Carruthers A (1998) Structural and physiologic determinants of human erythrocyte sugar transport regulation by adenosine triphosphate. Biochemistry 37: 12221-12232.

136. Carruthers A, Helgerson AL (1991) Inhibitions of sugar transport produced by ligands binding at opposite sides of the membrane. Evidence for simultaneous occupation of the carrier by maltose and cytochalasin B. Biochemistry 30: 3907-3915.

137. Hamill S, Cloherty EK, Carruthers A (1999) The human erythrocyte sugar transporter presents two sugar import sites. Biochemistry 38: 16974-16983.

138. Carruthers A (1986) ATP regulation of the human red cell sugar transporter. J Biol Chem 261: 11028-11037.

139. Mercer RW, Dunham PB (1981) Membrane-bound ATP fuels the Na/K pump. Studies on membrane-bound glycolytic enzymes on inside-out vesicles from human red cell membranes. J Gen Physiol 78: 547-568.

140. Singh R, Barden A, Mori T, Beilin L (2001) Advanced glycation end-products: a review. Diabetologia 44: 129-146.

141. Carruthers A, Melchior DL (1985) Transport of a- and b-D-glucose by the intact human red cell. Biochemistry 24: 4244-4250.

142. Pessino A, Hebert DN, Woon CW, Harrison SA, Clancy BM, et al. (1991) Evidence that functional erythrocyte-type glucose transporters are oligomers. J Biol Chem 266: 20213-20217.

143. Masiak SJ, LeFevre PG (1977) Glucose transport inhibition by proteolytic degradation of the human erythrocyte membrane inner surface. Biochim Biophys Acta S 465: 371-377.

144. Naftalin RJ, Arain M (1999) Interactions of sodium pentobarbital with D-glucose and L-sorbose transport in human red cells. Biochim Biophys Acta 1419: 78-88.

145. Afzal I, Cunningham P, Naftalin RJ (2002) Interactions of ATP, oestradiol, genistein and the anti-oestrogens, faslodex (ICI 182780) and tamoxifen, with the human erythrocyte glucose transporter, GLUT1. Biochem J 365: 707-719.

146. Baldwin SA, Baldwin JM, Gorga FR, Lienhard GE (1979) Purification of the cytochalasin B binding component of the human erythrocyte monosaccharide transport system. Biochim Biophys Acta 552: 183-188.

147. Appleman JR, Lienhard GE (1989) Kinetics of the purified glucose transporter. Direct measurement of the rates of interconversion of transporter conformers. Biochemistry 28: 8221-8227.

148. Connolly TJ, Carruthers A, Melchior DL (1985) Effects of bilayer cholesterol on human erythrocyte hexose transport protein activity in synthetic lecithin bilayers. Biochemistry 24: 2865-2873.

149. Connolly TJ, Carruthers A, Melchior DL (1985) Effect of bilayer cholesterol content on reconstituted human erythrocyte sugar transporter activity. J Biol Chem 260: 2617-2620.

150. Carruthers A, Melchior DL (1984) Human erythrocyte hexose transporter activity is governed by bilayer lipid composition in reconstituted vesicles. Biochemistry 23: 6901-6911.

151. Glynn IM, Hara Y, Richards DE (1984) The occlusion of sodium ions within the mammalian sodium-potassium pump: its role in sodium transport. J Physiol (Lond) 351: 531-547.

152. Glynn IM, Richards DE (1982) Occlusion of rubidium ions by the sodium-potassium pump: Its implications for the mechanism of potassium transport,. J Physiol (Lond) 330: 17-43.

153. Mueckler M (1994) Facilitative glucose transporters. Eur J Biochem 219: 713-725.

154. Takata K, Hirano H, Kasahara M (1997) Transport of glucose across the blood-tissue barriers. Int Rev Cytol S 172: 1-53.

155. Mueckler M, Caruso C, Baldwin SA, Panico M, Blench I, et al. (1985) Sequence and structure of a human glucose transporter. Science 229: 941-945.

156. Dahl SG, Sylte I, Ravna AW (2004) Structures and models of transporter proteins. J Pharmacol Exp Ther S 309: 853-860.

157. Dwyer DS (2001) Model of the 3-D structure of the GLUT3 glucose transporter and molecular dynamics simulation of glucose transport. Proteins 42: 531-541.

158. Hirai T, Heymann JA, Maloney PC, Subramaniam S (2003) Structural model for 12-helix transporters belonging to the major facilitator superfamily. J Bacteriol S 185: 1712-1718.

159. Zuniga FA, Shi G, Haller JF, Rubashkin A, Flynn DR, et al. (2001) A three-dimensional model of the human facilitative glucose transporter Glut1. J Biol Chem S 276: 44970-44975.

160. Zeng H, Parthasarathy R, Rampal AL, Jung CY (1996) Proposed structure of putative glucose channel in GLUT1 facilitative glucose transporter. Biophys J S 70: 14-21.

161. Steck TL, Yu J (1973) Selective solubilization of proteins from red blood cell membranes by protein perturbants. J Supramol Struct 1: 220-232.

162. Laemmli UK (1970) Cleavage of structural proteins during the assembly of the head of bacteriophage T4. Nature 227: 680-685.

163. Krokhin OV, Craig R, Spicer V, Ens W, Standing KG, et al. (2004) An improved model for prediction of retention times of tryptic peptides in ion pair reversed-phase HPLC: its application to protein peptide mapping by off-line HPLC-MALDI MS. Mol Cell Proteomics S 3: 908-919.

164. Tusnady GE, Simon I (1998) Principles governing amino acid composition of integral membrane proteins: application to topology prediction. J Mol Biol S 283: 489-506.

165. Molina ML, Encinar JA, Barrera FN, Fernandez-Ballester G, Riquelme G, et al. (2004) Influence of C-terminal protein domains and protein-lipid interactions on tetramerization and stability of the potassium channel KcsA. Biochemistry S 43: 14924-14931.

166. Zoccoli MA, Baldwin SA, Lienhard GE (1978) The monosaccharide transport system of the human erythrocyte. Solubilization and characterization on the basis of cytochalasin B binding. J Biol Chem 253: 6923-6930.

167. Mann GE, Yudilevich DL, Sobrevia L (2003) Regulation of amino acid and glucose transporters in endothelial and smooth muscle cells. Physiol Rev S 83: 183-252.

168. Davey KA, Garlick PB, Warley A, Southworth R (2006) An immunogold labelling study of the distribution of GLUT 1 & GLUT 4 in cardiac tissue following stimulation by insulin or ischemia. Am J Physiol Heart Circ Physiol S

169. Cooper DR, Khalakdina A, Watson JE (1993) Chronic effects of glucose on insulin signaling in A-10 vascular smooth muscle cells. Archives of Biochemistry & Biophysics 302: 490-498.

170. Haworth RA, Berkoff HA (1986) The control of sugar uptake by metabolic demand in isolated heart cells. Circ Res 58: 157-165.

171. Holloszy JO, Narahara HT (1975) Studies on tissue permeability. X. Changes in permeability to 3-O-methylglucose associated with contraction in frog muscle. J Biol Chem 240: 349-355.

172. Holman GD, Kozka IJ, Clark AE, Flower CJ, Saltis J, et al. (1990) Cell surface labeling of glucose transporter isoform GLUT4 by bis- mannose photolabel. Correlation with stimulation of glucose transport in rat adipose cells by insulin and phorbol ester. J Biol Chem 265: 18172-18179.

173. Shetty M, Loeb JN, Vikstrom K, Ismail BF (1993) Rapid activation of GLUT-1 glucose transporter following inhibition of oxidative phosphorylation in clone 9 cells. Journal of Biological Chemistry 268: 17225-17232.

174. Diamond D, Carruthers A (1993) Metabolic control of sugar transport by derepression of cell surface glucose transporters: an insulin-independent, recruitment-independent mechanism of regulation. J Biol Chem 268: 6437-6444.

175. Wilson CM, Cushman SW (1994) Insulin stimulation of glucose transport activity in rat skeletal muscle: increase in cell surface GLUT4 as assessed by photolabelling. Biochem J 755-759.

176. Simpson IA, Cushman SW (1986) Hormonal regulation of mammalian glucose transport. Ann Rev Biochem 55: 1059-1089.

177. Elbrink J, Bihler I (1975) Membrane transport. Its relation to cellular metabolic rates. Science 188: 1177–1184.

178. Harik SI (1992) Changes in the glucose transporter of brain capillaries. Can J Physiol Pharmacol 70: S113-7.

179. Kumagai AK (1999) Glucose transport in brain and retina: implications in the management and complications of diabetes. Diabetes Metab Res Rev 15: 261-273.

180. Gerritsen ME, Burke TM, Allen LA (1988) Glucose starvation is required for insulin stimulation of glucose uptake and metabolism in cultured microvascular endothelial cells. Microvasc Res S 35: 153-166.

181. Takakura Y, Kuentzel SL, Raub TJ, Davies A, Baldwin SA, et al. (1991) Hexose uptake in primary cultures of bovine brain microvessel endothelial cells. I. Basic characteristics and effects of D-glucose and insulin. Biochimica et Biophysica Acta 1070: 1-10.

182. Levine KB, Robichaud TK, Hamill S, Sultzman LA, Carruthers A (2005) Properties of the human erythrocyte glucose transport protein are determined by cellular context. Biochemistry 44: 5606-5616.

183. Leitch JM, Carruthers A (2007) ATP-dependent sugar transport complexity in human erythrocytes. Am J Physiol Cell Physiol S 292: C974-86.

184. Helgerson AL, Hebert DN, Naderi S, Carruthers A (1989) Characterization of two independent modes of action of ATP on human erythrocyte sugar transport. Biochemistry 28: 6410-6417.

185. Carruthers A, Helgerson AL (1989) The human erythrocyte sugar transporter is also a nucleotide binding protein. Biochemistry 28: 8337-8346.

186. Baldwin SA, Baldwin JM, Lienhard GE (1982) The monosaccharide transporter of the human erythrocyte. Characterization of an improved preparation. Biochemistry 21: 3836–3842.

187. Carruthers A, Melchior DL (1984) A rapid method of reconstituting human erythrocyte sugar transport proteins. Biochemistry 23: 2712-2718.

188. Zeidel ML, Albalak A, Grossman E, Carruthers A (1992) Role of glucose carrier in human erythrocyte water permeability. Biochemistry 31: 589-596.

189. Saier MH, Jr. (2000) Families of transmembrane sugar transport proteins. Mol Microbiol 35: 699-710.

190. Birnbaum MJ, Haspel HC, Rosen OM (1986) Cloning and characterization of a cDNA encoding the rat brain glucose- transporter protein. Proc Natl Acad Sci USA 83: 5784-5788.

191. Vannucci SJ, Clark RR, Koehler-Stec E, Li K, Smith CB, et al. (1998) Glucose transporter expression in brain: relationship to cerebral glucose utilization. Dev Neurosci 20: 369-379.

192. Tserentsoodol N, Shin BC, Koyama H, Suzuki T, Takata K (1999) Immunolocalization of tight junction proteins, occludin and ZO-1, and glucose transporter GLUT1 in the cells of the blood-nerve barrier. Arch Histol Cytol S 62: 459-469.

193. Doria MC, Lund DD, Pasley A, Sandra A, Sivitz WI (1993) Immunolocalization of GLUT-1 glucose transporter in rat skeletal muscle and in normal and hypoxic cardiac tissue. American Journal of Physiology 265: E454-E464.

194. Sogin DC, Hinkle PC (1978) Characterization of the glucose transporter from human erythrocytes. J Supramolec Struct 8: 447-453.

195. Dwyer DS, Vannucci SJ, Simpson IA (2002) Expression, regulation, and functional role of glucose transporters (GLUTs) in brain. Int Rev Neurobiol 51: 159-188.

196. Kennergren C, Mantovani V, Strindberg L, Berglin E, Hamberger A, et al. (2003) Myocardial interstitial glucose and lactate before, during, and after cardioplegic heart arrest. Am J Physiol Endocrinol Metab S 284: E788-94.

197. Kasahara M, Hinkle PC (1977) Reconstitution and purification of the D-glucose transporter from human erythrocytes. J Biol Chem 253: 7384-7390.

198. Leitch J, Carruthers A (2006) ATP-dependent sugar transport complexity in human erythrocytes. Am J Physiol Cell Physiol

199. Naftalin RJ (1997) Evidence from studies of temperature-dependent changes of D-glucose, D- mannose and L-sorbose permeability that different states of activation of the human erythrocyte hexose transporter exist for good and bad substrates. Biochim Biophys Acta 1328: 13-29.

200. Naftalin RJ (1988) Pre-steady-state uptake of D-glucose is inconsistent with a circulating carrier mechanism. Biochim Biophys Acta 946: 431-438.

201. Helgerson AL, Carruthers A (1989) Analysis of protein-mediated 3-O-methylglucose transport in rat erythrocytes: rejection of the alternating conformation carrier model for sugar transport. Biochemistry 28: 4580-4594.

202. Regen DM, Morgan HE (1964) Studies of the glucose-transport system in the rabbit erythrocyte. Biochim Biophys Acta 79: 151-166.

203. Witters LA, Vater CA, Lienhard GE (1985) Phosphorylation of the glucose transporter in vitro and in vivo by protein kinase C. Nature 315: 777-778.

204. May JM (1990) Thiol-fatty acylation of the glucose transport protein of human erythrocytes. FEBS Lett 274: 119-121.

205. Lienhard GE, Crabb JH, Ransome KJ (1984) Endoglycosidase F cleaves the oligosaccharides from the glucose transporter of the human erythrocyte. Biochimica et Biophysica Acta (BBA) - Biomembranes 769: 404-410.

206. Vannucci SJ, Simpson IA (2003) Developmental switch in brain nutrient transporter expression in the rat. Am J Physiol Endocrinol Metab 285: E1127-34.

207. Haneskog L, Andersson L, Brekkan E, Englund AK, Kameyama K, et al. (1996) Monomeric human red cell glucose transporter (Glut1) in non-ionic detergent solution and a semi-elliptical torus model for detergent binding to membrane proteins. Biochim Biophys Acta 1282: 39-47.

208. Harrison SA, Buxton JM, Helgerson AL, MacDonald RG, Chlapowski FJ, et al. (1990) Insulin action on activity and cell surface disposition of human HepG2 glucose transporters expressed in Chinese hamster ovary cells. Journal of Biological Chemistry 265: 5793-5801.

209. Bligh EG, Dyer WJ (1959) A rapid method of total lipid extraction and purification. Can J Med Sci 37: 911-917.

210. Whitelegge JP, Gundersen CB, Faull KF (1998) Electrospray-ionization mass spectrometry of intact intrinsic membrane proteins. Protein Sci 7: 1423-1430.

211. Rao US, Scarborough GA (1980) Chemical state of the cysteine residues in the Neurospora crasa plasma membrane H+-ATPase. J Biol Chem 265: 7227-7235.

212. Hunt JF, Earnest TN, Bousche O, Kalghatgi K, Reilly K, et al. (1997) A biophysical study of integral membrane protein folding. Biochemistry 36: 15156-15176.

213. Kethidi DR, Li Y, Palli SR (2006) Protein kinase C mediated phosphorylation blocks juvenile hormone action. Mol Cell Endocrinol 247: 127-134.

214. Tang M, Mazella J, Gao J, Tseng L (2002) Progesterone receptor activates its promoter activity in human endometrial stromal cells. Mol Cell Endocrinol 192: 45-53.

215. Cohen SA, Strydom DJ (1988) Amino acid analysis utilizing phenylisothiocyanate derivatives. Anal Biochem 174: 1-16.

216. Strydom DJ, Cohen SA (1994) Comparison of amino acid analyses by phenylisothiocyanate and 6-aminoquinolyl-N-hydroxysuccinimidyl carbamate precolumn derivatization. Anal Biochem 222: 19-28.

217. Wood RE, Morgan HE (1969) Regulation of sugar transport in avian erythrocytes. J Biol Chem 244: 1451-1460.

218. Schagger H (2006) Tricine-SDS-PAGE. Nat Protocols 1: 16-22.

219. Marquardt T, Hebert DN, Helenius A (1993) Post-translational folding of influenza hemagglutinin in isolated endoplasmic reticulum-derived microsomes. J Biol Chem 268: 19618-19625.

220. Lemmon MA, Flanagan JM, Treutlein HR, Zhang J, Engelman DM (1992) Sequence specificity in the dimerization of transmembrane alpha-helices. Biochemistry 31: 12719-12725.

221. MacKenzie KR, Prestegard JH, Engelman DM (1997) A transmembrane helix dimer: structure and implications. Science 276: 131-133.

222. Russ WP, Engelman DM (1999) TOXCAT: a measure of transmembrane helix association in a biological membrane. Proc Natl Acad Sci U S A 96: 863-868.

223. Nunez E, Aragon C (1994) Structural analysis and functional role of the carbohydrate component of glycine transporter. J Biol Chem 269: 16920-16924.

224. Lowe AG, Walmsley AR (1985) A quenched-flow technique for the measurement of glucose influx into human red blood cells. Anal Biochem 144: 385-389.

225. Azad NS, Rasool N, Annunziata CM, Minasian L, Whiteley G, et al. (2006) Proteomics in clinical trials and practice: present uses and future promise. Mol Cell Proteomics S 5: 1819-1829.

226. Cunningham P, Afzal-Ahmed I, Naftalin RJ (2006) Docking studies show that D-glucose and quercetin slide through the transporter GLUT1. J Biol Chem S 281: 5797-5803.

227. Kheterpal I, Wetzel R (2006) Hydrogen/deuterium exchange mass spectrometry--a window into amyloid structure. Acc Chem Res S 39: 584-593.

228. Ross PL, Huang YN, Marchese JN, Williamson B, Parker K, et al. (2004) Multiplexed protein quantitation in Saccharomyces cerevisiae using amine-reactive isobaric tagging reagents. Mol Cell Proteomics S 3: 1154-1169.

# APPENDIX A1

## SUPPLEMENTARY MATERIAL FOR CHAPTER III

## HUMAN ERYTHROCYTE GLUCOSE TRANSPORT PROTEIN TOPOLOGY AND HELIX PACKING

**Legend to Table A1.1 Trypsin and α-chymotrypsin cleavage sites and full-length GLUT1 peptides.** For each proteolytic fragment of GLUT1, columns 1 through 8 indicate: the N-terminal amino acid preceding the N-terminal cut site, its residue number in GLUT1 sequence, its location in GLUT1 putative domain structure, the N-terminal amino acid preceding the C-terminal cut site, its residue number in GLUT1 sequence, its location in GLUT1 putative domain structure, the peptide sequence confirmed by MS/MS and the mass of the peptide respectively.

| Cut 1 | AA# | [a]Topology | Cut 2 | AA# | [a]Topology | Sequence | Mass (MH+) |
|---|---|---|---|---|---|---|---|
| start | 1 | N-Terminus | K | 6 | N-terminus | -.MEPSSK.K | 678.31 |
| start | 1 | N-Terminus | K | 7 | H1 | -.MEPSSKK.L | 806.38 |
| K | 6 | N-Terminus | R | 11 | H1 | K.KLTGR.L | 574.37 |
| K | 6 | N-Terminus | K | 38 | TM1 | K.KLTGRLMLAVGGAVLGSLQFGYNTGVINAPQK.V | 3273.81 |
| R | 11 | H1 | K | 38 | TM1 | R.LMLAVGGAVLGSLQFGYNTGVINAPQK.V | 2718.46 |
| K | 38 | TM1 | R | 51 | L1-2 | K.VIEEFYN^QTWVHR.Y | 1721.84 |
| R | 51 | L1-2 | R | 89 | L2-3 | R.YGESILPTTLTTLWSLSVAIFSVGGMIGSFSVGLFVNR.F | 4020.12 |
| R | 51 | L1-2 | R | 92 | L2-3 | R.YGESILPTTLTTLWSLSVAIFSVGGMIGSFSVGLFVNRFGR.R | 4380.31 |
| R | 93 | TM3 | K | 114 | L3-4 | R.NSMLMMNLLAFVSAVLMGFSK.L | 2304.16 |
| K | 117 | L3-4 | R | 126 | TM4 | K.SFEMLILGR.F | 1065.58 |
| R | 212 | L6-7 | R | 218 | L6-7 | R.FLLINR.N | 775.48 |
| R | 218 | L6-7 | R | 223 | L6-7 | R.NEENR.A | 661.27 |
| K | 225 | L6-7 | K | 229 | L6-7 | K.SVLK.K | 446.30 |
| K | 230 | L6-7 | K | 245 | L6-7 | K.LRGTADVTHDLQEMK.E | 1713.86 |
| K | 230 | L6-7 | R | 249 | L6-7 | K.LRGTADVTHDLQEMKEESR.Q | 2215.08 |
| R | 232 | L6-7 | K | 245 | L6-7 | R.GTADVTHDLQEMK.E | 1444.67 |
| R | 232 | L6-7 | R | 249 | L6-7 | R.GTADVTHDLQEMKEESR.Q | 1945.89 |
| R | 249 | L6-7 | R | 253 | L6-7 | R.QMMR.E | 565.26 |
| R | 253 | L6-7 | R | 264 | L6-7 | R.EKKVTILELFR.S | 1375.83 |
| K | 255 | L6-7 | R | 264 | L6-7 | K.KVTILELFR.S | 1118.69 |
| K | 255 | L6-7 | K | 300 | L7-8 | K.KVTILELFRSPAYRQPILIAVVLQLSQQLSGINAVFYYSTSIFEK.A | 5143.86 |
| K | 256 | L6-7 | R | 264 | L6-7 | K.VTILELFR.S | 990.60 |
| K | 256 | L6-7 | K | 300 | L7-8 | K.VTILELFRSPAYRQPILIAVVLQLSQQLSGINAVFYYSTSIFEK.A | 5015.76 |
| R | 264 | L6-7 | K | 300 | L7-8 | R.SPAYRQPILIAVVLQLSQQLSGINAVFYYSTSIFEK.A | 4044.18 |
| R | 269 | TM7 | K | 300 | L7-8 | R.QPILIAVVLQLSQQLSGINAVFYYSTSIFEK.A | 3469.90 |
| K | 300 | L7-8 | R | 330 | H8 | K.AGVQQPVYATIGSGIVNTAFTVVSLFVVER.A | 3122.69 |
| K | 300 | L7-8 | R | 333 | L8-9 | K.AGVQQPVYATIGSGIVNTAFTVVSLFVVERAGR.R | 3406.85 |
| K | 300 | L7-8 | R | 334 | L8-9 | K.AGVQQPVYATIGSGIVNTAFTVVSLFVVERAGRR.T | 3562.95 |
| K | 456 | H12 | R | 468 | H12 | K.GRTFDEIASGFR.Q | 1355.65 |
| R | 458 | H12 | R | 468 | H12 | R.TFDEIASGFR.Q | 1142.55 |
| R | 458 | H12 | end | no cut | C-Terminus | R.TFDEIASGFRQGGASQSDKTPEELFHPLGADSQV.- | 3621.71 |
| R | 468 | H12 | end | no cut | C-Terminus | R.QGGASQSDKTPEELFHPLGADSQV.- | 2498.18 |
| K | 477 | C-Terminus | end | no cut | C-Terminus | K.TPEELFHPLGADSQV.- | 1639.80 |

Table A1.1

| Cut 1 | AA# | [a]Topology | Cut 2 | AA# | [a]Topology | Sequence | Mass (MH+) |
|---|---|---|---|---|---|---|---|
| L | 8 | H1 | M | 13 | H1 | L.TGRLM.L | 577.31 |
| M | 13 | H1 | L | 21 | TM1 | M.LAVGGAVL.G | 699.44 |
| L | 21 | TM1 | F | 26 | TM1 | L.GSLQF.G | 551.28 |
| Y | 28 | TM1 | E | 42 | L1-2 | Y.NTGVINAPQKVIEE.F | 1511.81 |
| Y | 28 | TM1 | Y | 44 | L1-2 | Y.NTGVINAPQKVIEEFY.N | 1821.94 |
| W | 48 | L1-2 | L | 61 | L1-2 | W.VHRYGESILPTTL.T | 1485.81 |
| Y | 52 | L1-2 | L | 61 | L1-2 | Y.GESILPTTL.T | 930.51 |
| E | 54 | L1-2 | L | 61 | L1-2 | E.SILPTTL.T | 744.45 |
| W | 65 | TM2 | F | 72 | TM2 | W.SLSVAIF.S | 736.42 |
| F | 72 | TM2 | F | 81 | TM2 | F.SVGGMIGSF.S | 854.41 |
| F | 81 | TM2 | F | 86 | TM2 | F.SVGLF.V | 522.29 |
| L | 122 | TM4 | F | 127 | TM4 | L.ILGRF.I | 605.38 |
| F | 127 | TM4 | Y | 132 | TM4 | F.IIGVY.C | 564.34 |
| L | 162 | TM5 | L | 169 | TM5 | L.GIVVGIL.I | 670.45 |
| L | 214 | L6-7 | E | 220 | L6-7 | L.LINRNEE.N | 887.46 |
| L | 231 | L6-7 | L | 241 | L6-7 | L.RGTADVTHDL.Q | 1084.54 |
| L | 231 | L6-7 | E | 243 | L6-7 | L.RGTADVTHDLQE.M | 1341.64 |
| L | 231 | L6-7 | M | 244 | L6-7 | L.RGTADVTHDLQEM.K | 1472.68 |
| L | 231 | L6-7 | E | 247 | L6-7 | L.RGTADVTHDLQEMKEE.S | 1858.86 |
| E | 247 | L6-7 | M | 251 | L6-7 | E.SRQM.M | 521.25 |
| M | 252 | L6-7 | F | 263 | L6-7 | M.REKKVTILELF.R | 1375.83 |
| M | 252 | L6-7 | L | 260 | L6-7 | M.REKKVTIL.E | 986.64 |
| F | 263 | L6-7 | Y | 268 | TM7 | F.RSPAY.R | 593.30 |
| Y | 268 | TM7 | L | 273 | TM7 | Y.RQPIL.I | 626.40 |
| L | 273 | TM7 | L | 278 | TM7 | L.IAVVL.Q | 514.36 |
| L | 278 | TM7 | L | 284 | TM7 | L.QLSQQL.S | 716.39 |
| L | 284 | TM7 | F | 291 | TM7 | L.SGINAVF.Y | 707.37 |
| F | 298 | L7-8 | Y | 308 | TM8 | F.EKAGVQQPVY.A | 1118.58 |
| Y | 308 | TM8 | F | 320 | TM8 | Y.ATIGSGIVNTAF.T | 1150.61 |
| F | 320 | TM8 | F | 326 | H8 | F.TVVSLF.V | 665.39 |
| F | 379 | TM10 | W | 388 | H10 | F.EVGPGPIPW.F | 951.49 |
| W | 388 | H10 | E | 393 | L10-11 | W.FIVAE.L | 578.32 |
| W | 388 | H10 | F | 395 | L10-11 | W.FIVAELF.S | 838.47 |
| F | 395 | L10-11 | F | 409 | TM11 | F.SQGPRPAAIAVAGF.S | 1341.73 |
| A | 402 | TM11 | F | 409 | TM11 | A.AIAVAGF.S | 648.37 |
| F | 460 | H12 | F | 467 | H12 | F.DEIASGF.R | 738.33 |
| F | 467 | H12 | E | 480 | C-Terminus | F.RQGGASQSDKTPE.E | 1360.65 |
| F | 467 | H12 | L | 482 | C-Terminus | F.RQGGASQSDKTPEEL.F | 1602.77 |
| F | 467 | H12 | F | 483 | C-Terminus | F.RQGGASQSDKTPEELF.H | 1749.84 |
| F | 467 | H12 | L | 486 | C-Terminus | F.RQGGASQSDKTPEELFHPL.G | 2097.04 |
| F | 483 | C-Terminus | end | no cut | C-Terminus | F.HPLGADSQV.- | 923.46 |
| L | 486 | C-Terminus | end | no cut | C-Terminus | L.GADSQV.- | 576.26 |

Table A1.1 (continued)

**Legend to Table A1.2 Trypsin and α-chymotrypsin derived GLUT1 peptides released into supernatant.** The columns indicate: the N-terminal amino acid preceding the N-terminal cut site, its residue number in GLUT1 sequence, its location in GLUT1 putative domain structure, the N-terminal amino acid preceding the C-terminal cut site, its residue number in GLUT1 sequence, its location in GLUT1 putative domain structure, the peptide sequence confirmed by MS/MS and the mass of the peptide respectively.

| Cut 1 | AA# | [a]Topology | Cut 2 | AA# | [a]Topology | Sequence | Mass (MH+) |
|---|---|---|---|---|---|---|---|
| start | 1 | N-Terminus | K | 6 | N-terminus | -.MEPSSK.K | 678.31 |
| start | 1 | N-Terminus | K | 7 | H1 | -.MEPSSKK.L | 806.38 |
| K | 6 | N-Terminus | R | 11 | H1 | K.KLTGR.L | 574.37 |
| L | 8 | H1 | M | 13 | H1 | L.TGRLM.L | 577.31 |
| R | 11 | H1 | K | 38 | TM1 | R.LMLAVGGAVLGSLQFGYNTGVINAPQK.V | 2718.46 |
| M | 13 | H1 | L | 21 | TM1 | M.LAVGGAVL.G | 699.44 |
| L | 21 | TM1 | F | 26 | TM1 | L.GSLQF.G | 551.28 |
| Y | 28 | TM1 | Y | 44 | L1-2 | Y.NTGVINAPQKVIEEFY.N | 1821.94 |
| Y | 28 | TM1 | W | 48 | L1-2 | Y.NTGVINAPQKVIEEFYNQTW.V | 2351.17 |
| K | 38 | TM1 | R | 51 | L1-2 | K.VIEEFYN^QTWVHR.Y | 1721.84 |
| W | 48 | L1-2 | L | 61 | L1-2 | W.VHRYGESILPTTL.T | 1485.81 |
| Y | 52 | L1-2 | L | 61 | L1-2 | Y.GESILPTTL.T | 930.51 |
| W | 65 | TM2 | F | 72 | TM2 | W.SLSVAIF.S | 736.42 |
| F | 81 | TM2 | F | 86 | TM2 | F.SVGLF.V | 522.29 |
| L | 122 | TM4 | F | 127 | TM4 | L.ILGRF.I | 605.38 |
| R | 212 | L6-7 | R | 218 | L6-7 | R.FLLINR.N | 775.48 |
| R | 218 | L6-7 | R | 223 | L6-7 | R.NEENR.A | 661.27 |
| K | 225 | L6-7 | K | 229 | L6-7 | K.SVLK.K | 446.30 |
| K | 230 | L6-7 | K | 245 | L6-7 | K.LRGTADVTHDLQEMK.E | 1713.86 |
| K | 230 | L6-7 | R | 249 | L6-7 | K.LRGTADVTHDLQEMKEESR.Q | 2215.08 |
| L | 231 | L6-7 | E | 243 | L6-7 | L.RGTADVTHDLQE.M | 1341.64 |
| L | 231 | L6-7 | M | 244 | L6-7 | L.RGTADVTHDLQEM.K | 1472.68 |
| L | 231 | L6-7 | E | 247 | L6-7 | L.RGTADVTHDLQEMKEE.S | 1858.86 |
| R | 232 | L6-7 | K | 245 | L6-7 | R.GTADVTHDLQEMK.E | 1444.67 |
| R | 232 | L6-7 | R | 249 | L6-7 | R.GTADVTHDLQEMKEESR.Q | 1945.89 |
| R | 249 | L6-7 | R | 253 | L6-7 | R.QMMR.E | 565.26 |

Table A1.2

| Cut 1 | AA# | [a]Topology | Cut 2 | AA# | [a]Topology | Sequence | Mass (MH+) |
|---|---|---|---|---|---|---|---|
| M | 252 | L6-7 | F | 263 | L6-7 | M.REKKVTILELF.R | 1375.83 |
| M | 252 | L6-7 | L | 260 | L6-7 | M.REKKVTIL.E | 986.64 |
| R | 253 | L6-7 | R | 264 | L6-7 | R.EKKVTILELFR.S | 1375.83 |
| K | 255 | L6-7 | R | 264 | L6-7 | K.KVTILELFR.S | 1118.69 |
| K | 256 | L6-7 | R | 264 | L6-7 | K.VTILELFR.S | 990.60 |
| F | 263 | L6-7 | Y | 268 | TM7 | F.RSPAY.R | 593.30 |
| L | 278 | TM7 | L | 284 | TM7 | L.QLSQQL.S | 716.39 |
| L | 284 | TM7 | F | 291 | TM7 | L.SGINAVF.Y | 707.37 |
| F | 298 | L7-8 | Y | 308 | TM8 | F.EKAGVQQPVY.A | 1118.58 |
| *K* | *300* | *L7-8* | *R* | *330* | *H8* | *K.AGVQQPVYATIGSGIVNTAFTVVSLFVVER.A*** | *3122.69* |
| Y | 308 | TM8 | F | 320 | TM8 | Y.ATIGSGIVNTAF.T | 1150.61 |
| F | 379 | TM10 | W | 388 | H10 | F.EVGPGPIPW.F | 951.49 |
| W | 388 | H10 | F | 395 | L10-11 | W.FIVAELF.S | 838.47 |
| F | 395 | L10-11 | F | 409 | TM11 | F.SQGPRPAAIAVAGF.S | 1341.73 |
| K | 456 | H12 | R | 468 | H12 | K.GRTFDEIASGFR.Q | 1355.65 |
| R | 458 | H12 | R | 468 | H12 | R.TFDEIASGFR.Q | 1142.55 |
| R | 458 | H12 | end | no cut | C-Terminus | R.TFDEIASGFRQGGASQSDKTPEELFHPLGADSQV.- | 3621.71 |
| F | 467 | H12 | L | 482 | C-Terminus | F.RQGGASQSDKTPEEL.F | 1602.77 |
| F | 467 | H12 | F | 483 | C-Terminus | F.RQGGASQSDKTPEELF.H | 1749.84 |
| F | 467 | H12 | L | 486 | C-Terminus | F.RQGGASQSDKTPEELFHPL.G | 2097.04 |
| R | 468 | H12 | end | no cut | C-Terminus | R.QGGASQSDKTPEELFHPLGADSQV.- | 2498.18 |
| K | 477 | C-Terminus | end | no cut | C-Terminus | K.TPEELFHPLGADSQV.- | 1639.80 |
| F | 483 | C-Terminus | end | no cut | C-Terminus | F.HPLGADSQV.- | 923.46 |
| L | 486 | C-Terminus | end | no cut | C-Terminus | L.GADSQV.- | 576.26 |
| F | 483 | C-Terminus | end | no cut | C-Terminus | F.HPLGADSQV.- | 923.46 |
| L | 486 | C-Terminus | end | no cut | C-Terminus | L.GADSQV.- | 576.26 |

Table A1.2 (continued)

# APPENDIX A2

## SUPPLEMENTARY MATERIAL FOR CHAPTER V

## HUMAN TYPE 1 FACILITATIVE GLUCOSE TRANSPORT PROTEIN PRESENTS REDUCTANT-SENSITIVE CONFORMERS

**Legend for Table A2.1 Trypsin digest of gel-eluted GLUT1 as detected by ESI-MS/MS.** [a]GLUT1 was gel-eluted and subjected to trypsin digestion followed by definitive sequence analysis by MS/MS. M* indicates an oxidized methionine residue (+15.99 Da). [b]*m/z* is the mass to charge ratio of the isolated peptide prior to fragmentation. [c]Tryptic site indicates the amino acid at the N-terminal tryptic cleavage site. [d]Residue # 1 indicates the specific GLUT1 residue at the N-terminal tryptic cleavage site. [e]Tryptic site 2 indicates the amino acid at the C-terminal tryptic cleavage site. [f]Residue # 2 indicates the specific GLUT1 residue at the C-terminal tryptic cleavage site. [g]This peptide is detected only in deglycosylated GLUT1.

| [a]Tryptic Peptides | [b]m/z | [c]Tryptic Site 1 | [d]Residue #1 | [e]Tryptic Site 2 | [f]Residue #2 |
|---|---|---|---|---|---|
| R.LMLAVGGAVLGSLQFGYNTGVINAPQK.V | 2718.46 | R | 11 | K | 38 |
| [g]K.VIEEFYNQTWVHR.Y | 1720.84 | K | 38 | R | 51 |
| R.YGESILPTTLTTLWSLSVAIFSVGGMIGSFSVGLFVNR.F | 4020.12 | R | 51 | R | 89 |
| R.YGESILPTTLTTLWSLSVAIFSVGGMIGSFSVGLFVNRFGR.R | 4380.31 | R | 51 | R | 92 |
| R.YGESILPTTLTTLWSLSVAIFSVGGMIGSFSVGLFVNRFGRR.N | 4536.41 | R | 51 | R | 93 |
| R.RNSMLMMNLLAFVSAVLMGFSK.L | 2460.26 | R | 92 | K | 114 |
| R.RNSM*LMMNLLAFVSAVLMGFSK.L | 2476.26 | R | 92 | K | 114 |
| R.NSMLMMNLLAFVSAVLMGFSK.L | 2304.16 | R | 93 | K | 114 |
| R.NSM*LMMNLLAFVSAVLMGFSK.L | 2320.16 | R | 93 | K | 114 |
| R.NSMLMMNLLAFVSAVLMGFSK.L | 2304.16 | R | 93 | K | 114 |
| R.NSMLMMNLLAFVSAVLM*GFSK.L | 2320.16 | R | 93 | K | 114 |
| R.NSMLM*MNLLAFVSAVLM*GFSK.L | 2336.15 | R | 93 | K | 114 |
| R.NSMLMMNLLAFVSAVLMGFSKLGK.S | 2602.36 | R | 93 | K | 117 |
| R.NSMLMMNLLAFVSAVLMGFSKLGKSFEMLILGR.F | 3648.92 | R | 93 | R | 126 |
| R.GALGTLHQLGIVVGILIAQVFGLDSIMGNK.D | 3034.71 | R | 153 | K | 183 |
| R.FLLINR.N | 775.48 | R | 212 | R | 218 |
| K.SVLK.K | 446.30 | K | 225 | R | 229 |
| R.GTADVTHDLQEMK.E | 1444.67 | R | 232 | K | 245 |
| R.GTADVTHDLQEM*K.E | 1460.67 | R | 232 | K | 245 |
| R.GTADVTHDLQEMKEESR.Q | 1945.89 | R | 232 | R | 249 |
| R.GTADVTHDLQEM*KEESR.Q | 1961.89 | R | 232 | R | 249 |
| R.QMMR.E | 565.26 | R | 249 | R | 253 |
| R.EKKVTILELFRSPAYRQPILIAVVLQLSQQLSGINAVFYYSTSIFEK.A | 5401.00 | R | 253 | K | 300 |
| K.KVTILELFRSPAYRQPILIAVVLQLSQQLSGINAVFYYSTSIFEK.A | 5143.86 | K | 255 | K | 300 |
| K.VTILELFRSPAYRQPILIAVVLQLSQQLSGINAVFYYSTSIFEK.A | 5015.76 | K | 256 | K | 300 |
| R.SPAYR.Q | 593.30 | R | 264 | R | 269 |
| R.SPAYRQPILIAVVLQLSQQLSGINAVFYYSTSIFEK.A | 4044.18 | R | 264 | K | 300 |
| R.QPILIAVVLQLSQQLSGINAVFYYSTSIFEK.A | 3469.90 | R | 269 | K | 300 |
| K.AGVQQPVYATIGSGIVNTAFTVVSLFVVER.A | 3122.69 | K | 300 | R | 330 |
| K.AGVQQPVYATIGSGIVNTAFTVVSLFVVERAGR.R | 3406.85 | K | 300 | R | 333 |
| R.TFDEIASGFR.Q | 1142.55 | R | 458 | R | 468 |
| R.QGGASQSDKTPEELFHPLGADSQV.- | 2498.18 | R | 468 | end | 492 |

Table A2.1

**Legend for Table A2.2 α-Chymotrypsin digest of gel-eluted GLUT1 as detected by ESI-MS/MS.** [a]GLUT1 was gel-eluted and subjected to alpha-chymotrypsin digestion followed by definitive sequence analysis by MS/MS. M* indicates an oxidized methionine residue (+15.99 Da). C# indicates a Cys-S-Pam residue (cysteine with an acrylamide adduct; +57 Da). [b]*m/z* is the mass to charge ratio of the isolated peptide prior to fragmentation. [c]α-Chymo site indicates the amino acid at the N-terminal tryptic cleavage site. [d]Residue # 1 indicates the specific GLUT1 residue at the N-terminal chymotryptic cleavage site. [e]α-Chymo site 2 indicates the amino acid at the C-terminal tryptic cleavage site. [f]Residue # 2 indicates the specific GLUT1 residue at the C-terminal α-chymotryptic cleavage site.

| [a]α-Chymotryptic Peptides | [b]m/z | [c]α-Chymo Site 1 | [d]Residue #1 | [c]α-Chymo Site 2 | [f]Residue #2 |
|---|---|---|---|---|---|
| L.TGRLMLAVGGAVLGSLQF.G | 1790.00 | L | 8 | F | 26 |
| M.LAVGGAVL.G | 699.44 | M | 13 | L | 21 |
| W.VHRYGESILPTTL.T | 1485.81 | W | 48 | L | 61 |
| Y.GESILPTTL.T | 930.51 | Y | 52 | L | 61 |
| F.SVGGMIGSF.S | 854.41 | F | 72 | F | 81 |
| F.SVGLF.V | 522.29 | F | 81 | F | 86 |
| F.GRRNSMLMMNLLAFVSAVLMGFSKL.G | 2786.47 | F | 90 | L | 115 |
| N.SMLMMNLLAFVSAVLMGFSKL.G | 2303.20 | N | 94 | L | 115 |
| F.IIGVY.C | 564.34 | F | 127 | Y | 132 |
| F.RGALGTLHQLGIVVGILIAQVF.G | 2275.36 | F | 152 | F | 174 |
| L.SIIFIPALL.Q | 986.63 | L | 167 | L | 199 |
| F.GLDSIMGNKDLWPLLLSIIFIPALL.Q | 2752.57 | F | 174 | L | 199 |
| F.GLDSIMGNKDLWPLLLSIIFIPALLQCIVLPFCPESPRF.L | 4369.36 | F | 174 | F | 213 |
| L.QC#IVLPFC#PESPRFL.L | 1890.89 | L | 199 | L | 214 |
| F.C#PESPRFL.L | 1019.46 | F | 206 | L | 214 |
| L.INRNEENRAKSVL.K | 1542.83 | L | 215 | L | 228 |
| L.RGTADVTHDLQEMKEESRQM.M | 2361.09 | L | 231 | M | 251 |
| L.QLSQQL.S | 716.39 | L | 278 | L | 284 |
| L.QLSQQLSGINAVF.Y | 1404.75 | L | 278 | F | 291 |
| Y.YSTSIFEKAGVQQPVY.A | 1816.91 | Y | 292 | Y | 308 |
| Y.STSIFEKAGVQQPVY.A | 1653.85 | Y | 293 | Y | 308 |
| F.EKAGVQQPVY.A | 1118.58 | F | 298 | Y | 308 |
| F.EKAGVQQPVYATIGSGIVNTAF.T | 2250.18 | F | 298 | F | 320 |
| Y.ATIGSGIVNTAF.T | 1150.61 | Y | 308 | F | 320 |
| L.HLIGLAGMAGC#AILMTIALALLEQLPW.M | 2890.54 | L | 336 | W | 363 |
| F.GFVAFFEVGPGPIPW.F | 1619.83 | F | 373 | W | 388 |
| F.EVGPGPIPW.F | 951.49 | F | 379 | W | 388 |
| W.FIVAELF.S | 838.47 | W | 388 | F | 395 |
| F.SQGPRPAAIAVAGF.S | 1341.73 | F | 395 | F | 409 |
| F.IVGM*CFQYVEQLCGPYVFIIFTVLLVLFFIFTYFKVPETKGRTF.D | 5232.75 | F | 416 | F | 460 |
| F.QYVEQLCGPYVFIIFTVLLVLFFIFTYFKVPETKGRTF.D | 4566.46 | F | 422 | F | 460 |
| F.QYVEQLC#GPYVFIIFTVLLVLFFIFTYFKVPETKGRTF.D | 4637.46 | F | 422 | F | 460 |
| F.DEIASGF.R | 738.33 | F | 460 | F | 467 |
| F.RQGGASQSDKTPEELFHPLGADSQV.- | 2654.28 | F | 467 | end | 492 |

Table A2.2

**Legend for Table A2.3 Cyanogen bromide digest of gel-eluted GLUT1 as detected by ESI-MS/MS.** [a]GLUT1 gel-eluted GLUT1 was dissolved in formic acid and subjected to CNBr digestion followed by definitive sequence analysis by MS/MS. M. indicates the N-terminal cleavage site. M@ indicates a homoserine lactone at the C-terminal methionine cleavage site (-48.1 Da). M~ indicates a homoserine at the C-terminal methionine cleavage site (-30.1 Da). S^ indicates a formylated serine residue (+28 Da). T^ indicates a formylated threonine residue. C# indicates a cys-S-Pam residue (cysteine with an acrylamide adduct; + 71 Da). [b]*m/z* is the mass to charge ratio of the isolated peptide prior to fragmentation. [c]Residue # 1 indicates the specific GLUT1 residue at the N-terminal CNBr cleavage site. [d]Residue # 2 indicates the specific GLUT1 residue at the C-terminal CNBr cleavage site. [e]Modification indicates the formylated or acrylamide-modified residue. [f]The sequence of this peptide was confirmed from partial b and y ion series spectra but the peptide mass indicates an unknown modification.

| [a]CNBR Peptide | [b]m/z | [c]Residue #1 | [d]Residue #2 | [e]Modification |
|---|---|---|---|---|
| M.EPSSKKLTGRLM@.L | 1298.75 | 1 | 13 | 0 |
| M.EPSSKKLTGRLM~.L | 1316.75 | 1 | 13 | 0 |
| M.EPSS^KKLTGRLM@.L | 1326.75 | 1 | 13 | S5 |
| M.EPS^SKKLTGRLM@.L | 1326.75 | 1 | 13 | S4 |
| M.EPSSKKLT^GRLM@.L | 1326.75 | 1 | 13 | T9 |
| M.EPS^S^KKLTGRLM@.L | 1354.75 | 1 | 13 | S4, S5 |
| M.IGSFSVGLFVNRFGRRNSM@.L | 2096.12 | 77 | 96 | 0 |
| M.IGS^FSVGLFVNRFGRRNSM@.L | 2124.12 | 77 | 96 | S80 |
| M.LM*MNLLAFVSAVLM~.G | 1538.82 | 96 | 110 | 0 |
| M.M*NLLAFVSAVLM@.G | 1276.70 | 98 | 110 | 0 |
| M.M*NLLAFVS^AVLM@.G | 1304.70 | 98 | 110 | S106 |
| M.NLLAFVSAVLM@.G | 1129.66 | 99 | 110 | 0 |
| M.NLLAFVS^AVLM@.G | 1157.66 | 99 | 110 | S106 |
| M.NLLAFVSAVLMGFS^KLGKSFEM@.L | 2369.27 | 99 | 121 | S113 |
| M.GFSKLGKSFEM@.L | 1182.62 | 110 | 121 | 0 |
| M.GFSKLGKSFEM~.L | 1200.62 | 110 | 121 | 0 |
| M.GFSKLGKS^FEM@.L | 1210.62 | 110 | 121 | S118 |
| M.GFS^KLGKSFEM@.L | 1210.62 | 110 | 121 | S113 |
| M.GFS^KLGKS^FEM@.L | 1238.62 | 110 | 121 | S113, S118 |
| [f]M.LILGRFIIGVYCGLTTGFVPM.Y | 2270.24 | 121 | 142 | 0 |
| M.LILGRFIIGVYC#GLTTGFVPM@.Y | 2293.29 | 121 | 142 | C133 |
| M.KEESRQM@.M | 859.43 | 244 | 251 | 0 |
| M.KEES^RQM@.M | 887.43 | 244 | 251 | S248 |
| M.TIALALLEQLPWM@.S | 1450.83 | 351 | 364 | 0 |

Table A2.3

# APPENDIX A3

## SUPPLEMENTARY MATERIAL FOR CHAPTER VI

## DISCUSSION AND FUTURE DIRECTIONS

**Figure A3.1 AE1 accessibility to proteolytic cleavage (putative topography and graphic from [176]).** Human red blood cells were washed, lysed, digested with trypsin to remove the cytoplasmic N-terminal domain (amino acids 1-358), reduced (10 mM DTT), alkylated (50 mM iodoacetamide), and digested with either trypsin or α-chymotrypsin. The entire ghost digest was subjected to RP-HPLC and ESI-MS/MS using the LTQ as described for GLUT1 proteolipsome analysis. The cleavage sites (represented by an X) indicate amino acids within the AE1 C-terminal domain that are accessible to proteolytic cleavage by trypsin or α-chymotrypsin, see Table A1.3 for further details.

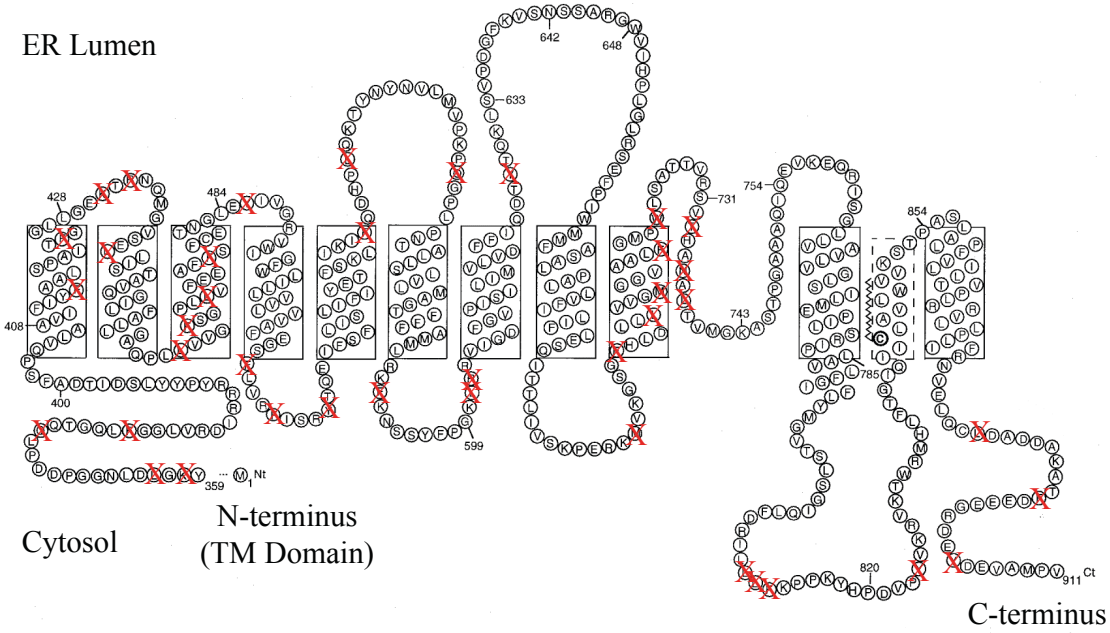


Figure A3.1

**Legend to Table A3.1 Trypsin and α-chymotrypsin digest of anion exchange protein 1 (AE1).** Columns indicate the location (within the C-terminal, membrane-embedded portion of the protein, amino acids 359-911) where the peptide can be found, the peptide sequence including the residues after which it was cleaved, and a description of where the cleavage sites are located: cytosolic, internal TM, interface (location where the lipid bilayer, the TM domain, and aqueous environment directly interact), lumen, and entire TM (indicating that the cleavage sites were in the cytosolic and lumenal regions and produced a peptide that included the entire TM).

| Region | Detected Sequence | Comments |
|---|---|---|
| N-TERM | Y.KGLDLNGGPDDPLQQTGQLF.G | Cytosolic |
| N-TERM | L.DLNGGPDDPLQQTGQLF.G | Cytosolic |
| N-TERM | LDLNGGPDDPLQQTGQ.L | Cytosolic |
| N-TERM | K.GLDLNGGPDDPLQQTGQLF.G | Cytosolic |
| N-TERM | K.GLDLNGGPDDPLQ.Q | Cytosolic |
| N-TERM | L.DLNGGPDDPLQQTGQLF.G | Cytosolic |
| TM1 | F.AALSPAITF.G | Internal TM |
| L1-2 | F.GGLLGEF.T | Interface and Lumen |
| L1-2 | F.NQMGVSEL.L | Lumen and Interface |
| TM3 | L.VVGF.S | Internal TM |
| TM3 | L.VFEEAFF.S | Internal TM |
| TM4 | Y.IVGRVWIGFWLILLVVLVVAFEGSF.L | Entire TM |
| TM5 | Y.TQEIFSFLISLIFIYETFSKLIKIFQDHPL.Q | Entire TM |
| TM5 | F.ISRYTQEIFSFLISLIFIYETFSKLIKIF.Q | Entire TM |
| TM6 | Q.GPLPNTALLSLVLMAGTFFFAMMLRKF.K | Entire TM |
| TM7 | L.RRVIGDFGVPISILIMVLVDFFIQDTY.T | Entire TM |
| TM7 | R.RVIGDFGVPISILIMVLVDFFIQDTY.T | Entire TM |
| TM9 | M.VKGSGFHLDLLLVVGMGGVAALFGMPWLSATTVRSVT.H | Entire TM |
| TM9 | F.HLDLLLVVGMGGVAAL.F | Interface and Internal TM |
| TM9 | F.HLDLLLVVGM.G | Interface and Internal TM |
| TM9, L9-10 | F.GMPWLSATTVRSVTHANAL.T | Internal TM and Lumen |
| TM9, L9-10 | L.VVGMGGVAALFGMPWLSATTVRSVTHAN.A | Internal TM and Lumen |
| L9-10 | W.LSATTVRSVTHANAL.T | Interface and Lumen |
| L10-11 | L.FKPPKYHPDVPY.V | Cytosolic |
| L10-11 | L.LFKPPKYHPDVPY.V | Cytosolic |
| C-TERM | L.DADDAKATF.D | Cytosolic |
| C-TERM | F.DEEEGRDEY.D | Cytosolic |
| C-TERM | F.DEEEGRDEYDEVAMPV- | Cytosolic |

Table A3.1

Despite the global observations for D-glucose, we were unable to identify the specific residues responsible for displaying the global increase in lysine modification (see Figure A3.2). We focused on lysine residues found in L6-7 (K225, K229, K230, K245, K255, and K256) and the C-terminal tail (K477). It is unknown if the change in labeling was due to enhanced accessibility of one residue, multiple residues, or if some residues demonstrated enhanced labeling, while others became less available for modification. Additionally, one or multiple residues found at the extracellular TM interface, which are generally more difficult to quantitatively detect by mass spectrometry, may be responsible for the global labeling changes.

The lack of detectable labeling variation in the presence of CCB may not be terribly surprising (Figure A3.3). We have previously noted that CCB is hypothesized to interact with GLUT1 at a site in between TM10 and TM11 [61, 79]. Furthermore, we have observed that TM8 is released from the membrane bilayer when the protein is digested in the presence of CCB. Although lysine 300 forms one of the cleavage sites responsible for TM8 release, there are no other lysine residues in this entire C-terminal region until K451 found at the cytoplasmic end of TM12. It is possible that CCB binding does not affect the conformational dynamics of L6-7 or the C-terminus, and as a result, the absence of global labeling changes could be consistent with the current hypothesis for localized CCB binding. Undertaking residue specific studies or antibody binding experiments within the TM8-TM11 $\alpha$-helical regions could determine if more localized conformational changes occur, if any enhancements within one region are offset by inhibition in a corresponding region, or if there are no conformational changes as a result of CCB binding.

**Figure A3.2 Extent of GLUT1 lysine modification in the presence of sugars.** Final extent of GLUT1 labeling by Sulfo-NHS-LC-Biotin (20:1 molar excess of probe to protein) at 4°C, pH 7.4 in the presence of sugars. GLUT1 proteoliposomes were pre-incubated for 30 minutes in Kaline (red), 50 mM Mannitol (maroon), 50 mM D-Glucose (blue), or 50 mM Maltose (green) prior to labeling. The average equilibrium labeling extent of at least three normalized labeling experiments done in triplicate ± SEM: Kaline, extent = 1.02 ± 0.04; 50 mM Mannitol extent = 1.05 ± 0.05; 50 mM D-Glucose extent = 1.33 ± 0.04; 50 mM Maltose extent = 1.19 ± 0.04.

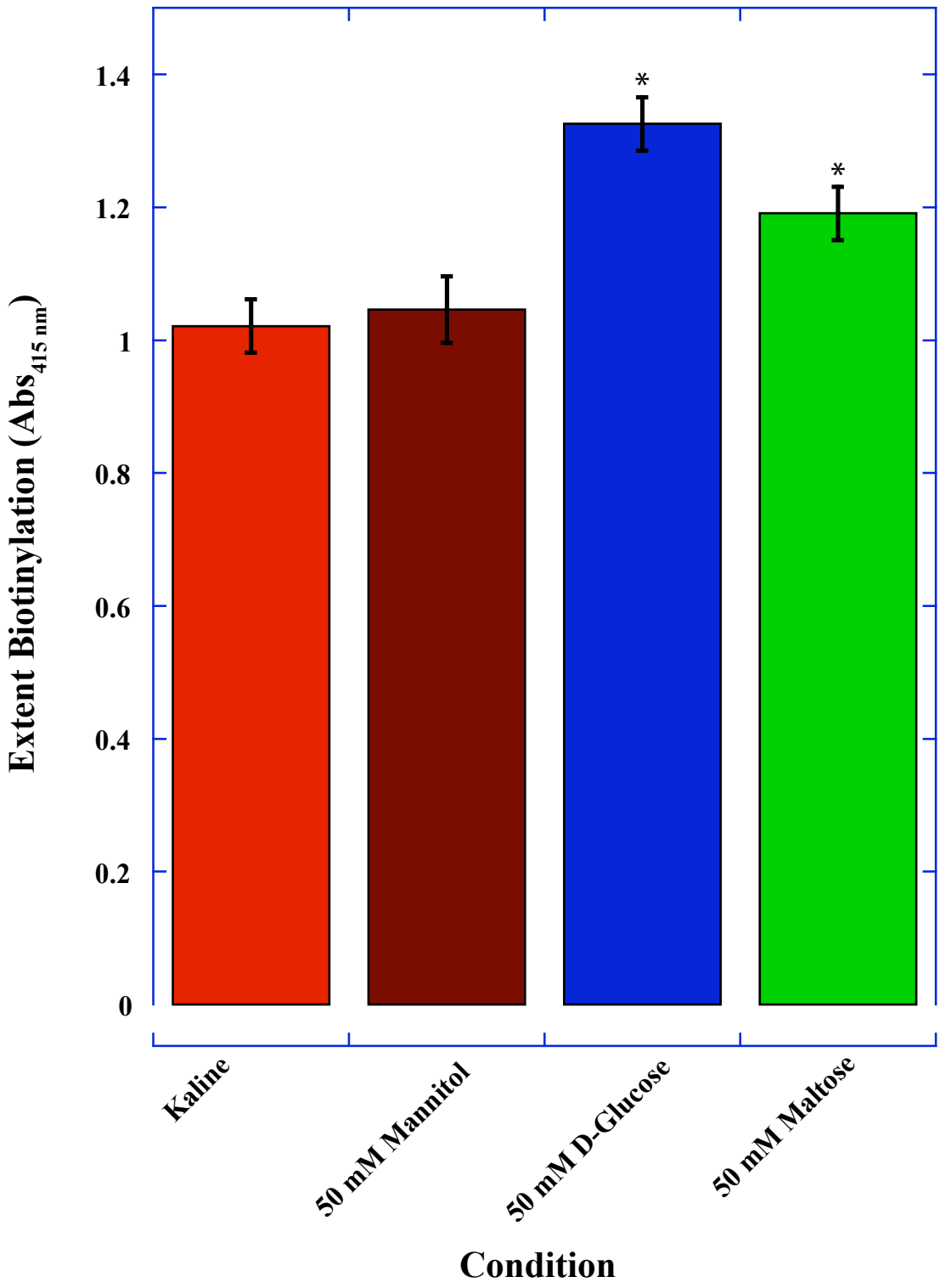
1.4
1.2
1
0.8
0.6
0.4
0.2
0
Extent Biotinylation (Abs415 nm)
*
*
Kaline
50 mM Mannitol
50 mM D-Glucose
50 mM Maltose
Condition

Figure A3.2

**Figure A3.3 Extent of GLUT1 lysine modification in the presence of cytochalasin B.** Final extent of GLUT1 labeling by Sulfo-NHS-LC-Biotin (20:1 molar excess of probe to protein) at 4°C, pH 7.4 in the presence of cytochalasin. GLUT1 proteoliposomes were pre-incubated for 30 minutes in Kaline (red), 10 μM CCB (blue), 0.2% DMSO (green) prior to labeling. The average equilibrium labeling extent of at least three normalized labeling experiments done in triplicate ± SEM: Kaline, extent = 1.02 ± 0.04; 10 μM CCB extent = 0.97 ± 0.05; 0.2% DMSO extent = 0.93 ± 0.03.

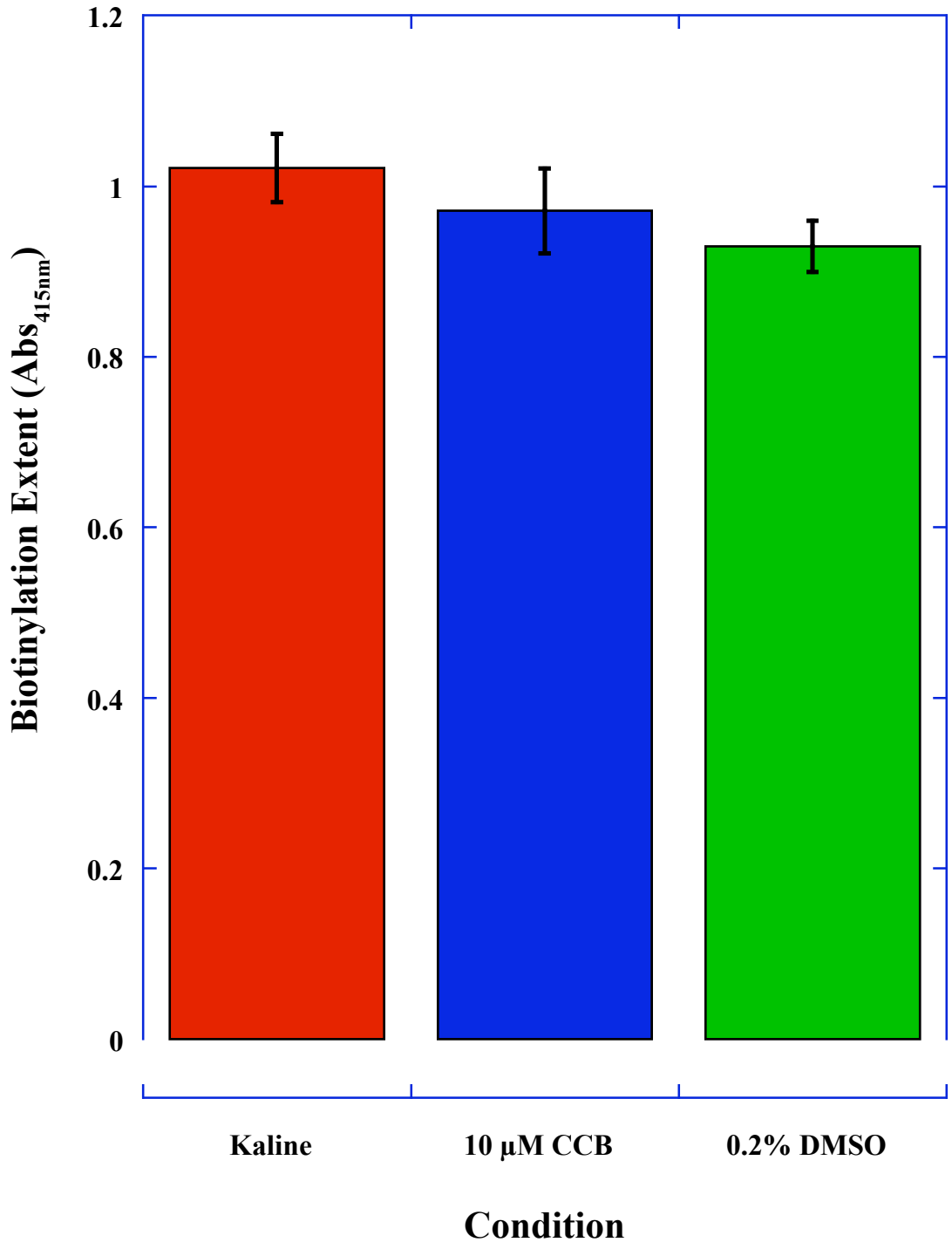
1.2
1
0.8
0.6
0.4
0.2
0
Biotinylation Extent (Abs415nm)
Kaline
10 µM CCB
0.2% DMSO
Condition

Figure A3.3